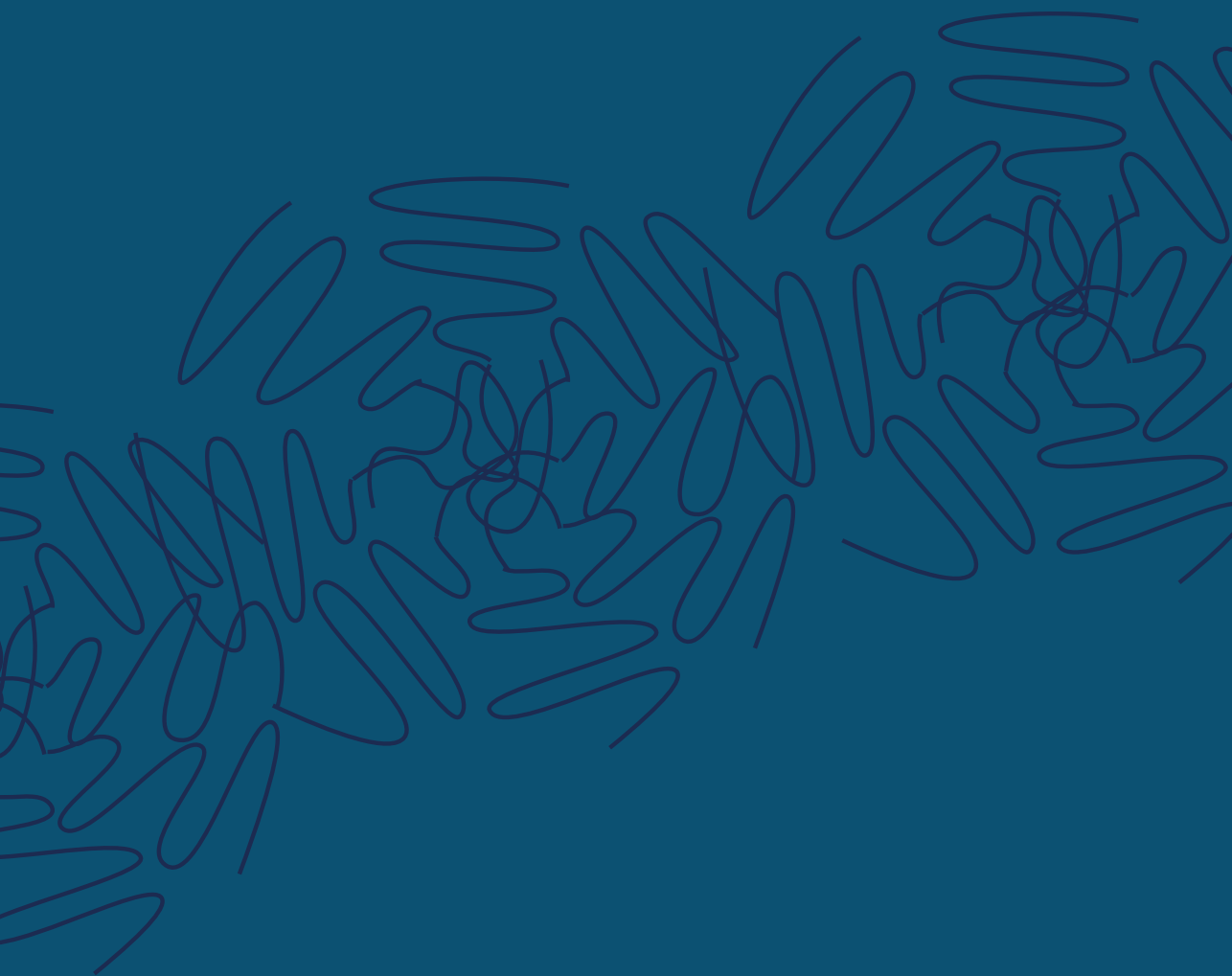# Temperature Responsive Polyelectrolyte Complexes
Bio-Inspired Wet-Adhesives

Ilse Adriënne van Hees

Propositions

1. Oppositely charged polyelectrolyte block copolymers with poly(N-isopropylacrylamide) provide strong reversible underwater adhesion. (this thesis)

2. Ion specific effects on the characteristics of responsive polyelectrolyte complexes are too strong to be ignored. (this thesis)

3. Biomedical applications are misused to obtain funding for fundamental research.

4. Bachelor and master thesis students must receive active coaching on general scientific skills.

5. The size of burgers should be decreased.

6. Everyone should learn to play a musical instrument.

Propositions belonging to the thesis entitled:

TEMPERATURE RESPONSIVE POLYELECTROLYTE
COMPLEXES
BIO-INSPIRED WET-ADHESIVES

Ilse Adriënne van Hees
Wageningen, 15 November 2019

Temperature Responsive Polyelectrolyte Complexes

Bio-Inspired Wet-Adhesives

Ilse Adriënne van Hees

Thesis committee

Promotors
Prof. Dr Jasper van der Gucht
Professor of Physical Chemistry and Soft Matter
Wageningen University & Research

Prof. Dr Marleen Kamperman
Professor of Polymer Science
University of Groningen

Other members
Prof. Dr Harry Bitter, Wageningen University & Research
Prof. Dr Alla Synytska, Leibniz Institute of Polymer Research Dresden, Germany
Dr Tina Vermonden, Utrecht University
Dr Wiebe de Vos, University of Twente

Temperature Responsive Polyelectrolyte Complexes

Bio-Inspired Wet-Adhesives

Ilse Adriënne van Hees

Contents

Introduction

<div style="text-align: right">I</div>

Biomedical wet-adhesives

Sutures and clamps are commonly used tools for wound closure.[1, 2, 3] However, these methods face drawbacks, such as fluid leakage, inconvenience of handling and a high risk of infection.[1, 2, 4] These disadvantages could be circumvented by using adhesives for wound closure.[1, 2, 3] However, adhesives are not yet commonly used in internal medicine as many of the available products adhere weakly to wet surfaces.[3, 5] Moreover, some available adhesives for wet conditions are toxic and others have a weak cohesive performance.[6] Here, we investigate a new alternative system for improved underwater adhesion: Bioinspired temperature responsive polyelectrolytes.

Adhesion

Adhesive performance is characterized by the balance between adhesion and cohesion. The strength of the interactions between the adhesive and the surface of the substrate defines adhesion, while the interactions within the adhesive define cohesion. Adhesion can be achieved by interactions between the adhesive and the substrate, for which intimate contact and a large contact area are crucial. A large contact area may be achieved by the adhesive flowing into small pores or gaps of the substrate, which is promoted by good surface wetting, i.e. a low interfacial tension, and by a low viscosity.[4] After application, adhesives are solidified by a chemical reaction, by evaporation of solvent, or by altering environmental conditions, such as temperature for hot melt adhesives. The hardened material should be strong enough to maintain the position of the substrates, while dissipating the energy from applied forces.

Biomedical adhesives for internal application

In internal medicine, adhesion is complicated by fluids in the body, such as blood and mucus. These fluids form a layer on the tissue which hinders the formation of strong, adhesive interactions.[2, 4, 6] Moreover, most available medical wet-adhesives display poor cohesion.[6] Therefore, new medical wet-adhesives should remove or absorb the fluid layer for proper adhesion, and have an improved cohesion. In addition, several other conditions have to be met to approve internal application of new materials. Most importantly, the adhesive should be harmless to the patient. Therefore, the adhesive, i.e. its components, precursors, and possible degradation products, should be non-toxic.[3, 4, 5, 6] Moreover, the adhesive and/or possible degradation products should be soluble in aqueous solvents to ensure secretion from the body and to prevent local accumulation of possible toxins.[5] Moreover, the adhesive should not cause any blood borne diseases, such as HIV and hepatitis, which may be transferred by materials from animals, such as collagen or fibrinogen.[5] Finally, the stiffness of the adhesive should be comparable and adapted to the rigidity of the tissue. Adhesive joints that are stiffer than the tissue will be uncomfortable to patients and may cause rupture of the substrate.[1, 5, 7]

Several adhesives were developed for internal biomedical application and most of these materials are produced for bleeding control. Bioglue® is an adhesive used for the sealing of large blood vessels and is prepared from bovine serum albumin and glutaraldehyde.[5, 8] The aldehyde groups bind covalently with amines present on tissue and bovine serum albumin, resulting in strong adhesive and cohesive bonds. However, glutaraldehyde may be toxic and consequently clinical use is restricted to the bonding of blood vessels, as approved alternatives were unavailable so far.[8, 5] Similarly, Setalium™ is used for sealing blood vessels and was recently approved for clinical application in Europe.[6, 9, 10] The biodegradable adhesive is prepared from hydrophobic poly(glycerol sebacate acrylate) (PGSA) and is not flushed away by body fluids before solidification. Injectability is achieved by stabilising PGSA nanoparticles with anionic alginate. Upon injecting polycations, the nanoparticles are destabilized resulting in a viscous glue. Setalium flows into the small pores of the tissue, and becomes soft and flexible after a quick UV induced solidification. UV light should be applied briefly as it can harm tissue by heating or DNA mutations in cells.[3, 7] Furthermore, Hemcon® was reported to reduce a liver bleed and is composed of a blend mixture of catechol modified chitosan and temperature responsive thiol-terminated Pluronic F-127, i.e. PEG-*b*-poly(propylene glycol)-*b*-PEG.[6, 11] Solidification of the adhesive is obtained instantly through heating, followed by oxidation of the catechol moieties. As a result, covalent bonds are formed between catechol and the amino groups on chitosan, as well as with the thiol moieties of Pluronic, leading to strong cohesion. Finally, in Chapter 2, a few more adhesives for internal applications are reported. These adhesives are based on electrostatic interactions and were successfully applied for fetal surgery or bone graft binding. However, these materials are not approved for clinical use as far as the author is aware.

To date, the number of approved and well-functioning adhesives for internal ap-

plications is limited due to the presence of fluids. Therefore, we investigate an alternative approach for preparing wet-adhesives by mixing oppositely charged temperature responsive polyelectrolytes in aqueous solution. At room temperature, the mixture is fluid, while a gel is formed at body temperature. Consequently, the adhesive can easily be injected and sets quickly after application, which prevents solvation of the adhesive by body fluids. Accordingly, the setting mechanism is easy and harmless as it does not require a chemical reaction or UV light. Moreover, fluid polyelectrolyte complexes display a low interfacial tension, which promotes adhesive interactions.[12, 13] Consequently, we believe that temperature responsive polyelectrolytes are promising compounds for wet-adhesives.

Complex coacervation

Complex coacervation is an associative liquid-liquid phase separation of oppositely charged macro-ions, such as polyelectrolytes, in aqueous solution, Figure 1.1.[14] Complex coacervates are fluid like materials with a low interfacial tension, and are insoluble in water despite the high water content.[15] In the following sections we describe the driving forces for complex coacervation and discuss the influence of salt, which is used as a tool to tune the material properties.

Thermodynamics

The driving force for complex coacervation is mostly entropic and induced by the release of counterions. In solution, macro-ions are surrounded by an electrical double layer of counterions. Upon complexation, the charges of the macro-ion are neutralized, leading to the release of the counter-ions which subsequently gain entropy. In addition, complexation of the macro-ions can either be exothermic or endothermic. At low salt concentrations, large Debye screening lengths are found and the electrostatic energy is significantly decreased upon complexation of the macro-ions, resulting in an exothermic process. At high salt concentrations, however, small Debye screening lengths are found, resulting in a lower energy gain upon macro-ion complexation. Therefore, the energy cost of counterion release exceeds the energy gain of complexation, resulting in an endothermic process. Before the energy cost becomes too large and prevents complexation, a regime is found where complexation is solely driven by entropy, because of the endothermic enthalpy.[13]

Salt response

Complex coacervation is salt dependent as increasing salt concentrations lower the entropic and enthalpic gain of complexation.[13] As a result, complexation can be prevented at high salt concentrations, i.e. when the critical salt concentration, $c_{s,cr}$, is
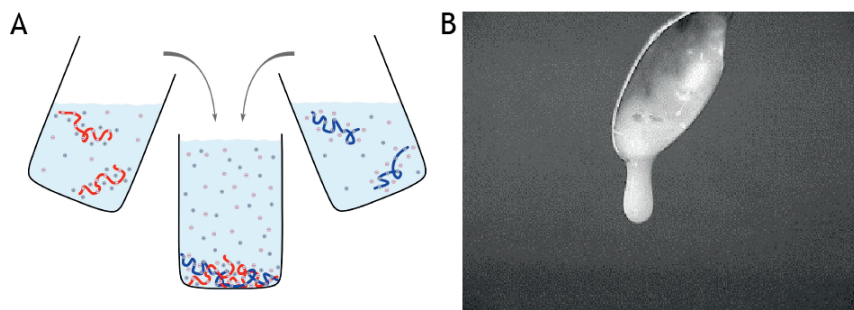
Figure 1.1 – A Upon mixing solutions with oppositely charged polyelectrolytes, phase separation occurs and a polymer rich coacervate phase coexists with a dilute solvent phase that mainly contains ions. Reprinted from reference 13 with permission from Elsevier. **B** A complex coacervate is shown to flow from a spoon, illustrating the fluid-like nature of the coacervate phase. Besides, complex coacervates are usually turbid. Reprinted from reference 16 with permission from Elsevier.

exceeded.[12] The height of $c_{s,cr}$ depends on several factors such as polymer chemistry, polymer length, degree of ionization, the salt type and temperature. More hydrophobic polymers show a higher $c_{s,cr}$ because ions are more depleted from the coacervate. As a result, higher salt concentrations are needed in the dilute phase to push sufficient ions into the coacervate, to disrupt the electrostatic interactions between the macro-ions.[13, 17] The polymer chemistry, i.e. the molecular architecture, influences the ion pair energy, which determines the strength of the electrostatic interaction. The stronger this interaction, the higher the enthalpic gain of complexation, and thus the higher $c_{s,cr}$ will be.[13] However, when the interactions are too strong, solid precipitates are formed, instead of fluid-like coacervates. Furthermore, higher $c_{s,cr}$ are found for longer polymers as more interactions have to be disrupted per chain to prevent or undo complexation.[13] Accordingly, a higher degree of ionization leads to an elevated $c_{s,cr}$ also. Moreover, $c_{s,cr}$ was shown to alter upon adding different types of ions, which enables tuning of $c_{s,cr}$.[17] Finally, elevated temperatures increase the energy gain of complexation, which rises $c_{s,cr}$. Besides influencing $c_{s,cr}$, increasing salt concentrations also lower the interfacial tension of the complex coacervate, which can be used as a tool in the development of adhesives.[13]

PNIPAM

Thermodynamics

Complex coacervates have convenient properties for adhesion, such as a low interfacial tension and good fluidity.[12, 13] However, the adhesive performance is greatly improved upon solidification, which is achieved by preparing block copoly-

mers with thermo-responsive poly(*N*-isopropylacrylamide) (PNIPAM), Figure 3.2A. PNIPAM is a thermo-responsive polymer displaying a lower critical solution temperature (LCST), meaning that the polymer is soluble in aqueous solutions at temperatures below the LCST, but becomes insoluble at higher temperatures.[18] Below the LCST, the hydrophilic amide group of NIPAM can form hydrogen bonds within the polymer or with the water molecules, which is an exothermic process.[18] The hydrophobic isopropyl group, on the other hand, is solubilized by ordering water molecules in a specific way around the tail, which reduces the entropy.[19] Therefore, solubilisation of PNIPAM at low temperatures is driven by the enthalpy gain of hydrogen bonding. At higher temperatures, however, the hydrogen bonds are disrupted, and the entropic contribution to the free energy of mixing increases.[18, 20] As a result, it becomes more favourable to reduce the order of the water molecules surrounding the isopropyl group which increases the entropy.[19] Consequently, the isopropyl groups are no longer dissolved and the PNIPAM chains collapse, leading to aggregation of the polymer. This coil to globule transition is a reversible process, and therefore cooling will dissolve PNIPAM again.[18, 20]

Salt response

The LCST of PNIPAM is found at approximately 32 °C for homopolymers in water, which makes PNIPAM an interesting polymer for biomedical applications. Moreover, the LCST can be altered by adding different types of salts, as well as by copolymerizing PNIPAM with electrolytes or hydrophobic monomers.[18, 19, 20, 21, 22, 23] Salts can both increase and decrease the LCST depending on the ion hydration. Strongly hydrated ions promote a rearrangement of water molecules, and therewith these ions compete with the water that surrounds the polymer. As a result, strongly hydrated salts decrease the solubility of polymers and therefore lower the LCST. Weakly hydrated salts, by contrast, favour interactions with the polymer, which improves the solubility and increases the LCST.[19] Besides, salts seem to slightly reduce the hydration of PNIPAM below LCST, which may influence rheological properties.[19]

Polymer assembly

Micelles

Well-defined structures can be obtained by self-assembly of block-copolymers that are composed of monomers with dissimilar characteristics.[24, 25] In solution, block-copolymers can assemble when the solvent is bad for one block, while it is a good solvent for the other block. The insoluble block of the polymer will collapse and try to minimize interactions with the solvent. As a result, polymers with small soluble blocks will precipitate, while polymers with larger soluble blocks form micelles. To

avoid unfavourable interactions, the core of the micelles is formed by the insoluble polymer block, while the corona is formed by the soluble part. Depending on the block-copolymer composition, different types of micelles can be obtained. For shorter soluble blocks, crew-cut micelles are observed, while for large soluble blocks, star-like micelles are found.[13] Besides, also worm-like micelles can be obtained.[26] In case the soluble blocks are too short to efficiently stabilize the micelles, sedimentation can occur over time.[27] A specific type of micelles are complex coacervate core micelles (C3M).[27, 28] These micelles exist of oppositely charged block-copolymers that contain a polyelectrolyte and a hydrophilic block, and occur in aqueous solutions. As contact between the insoluble complex coacervate and the solvent is unfavourable, the coacervate will form the core of the micelle, while the corona is formed by the hydrophilic block. In this thesis, it is shown that temperature responsive polyelectrolytes form C3Ms with a PNIPAM corona at low salt concentrations and temperatures, Figure 3.2B. In addition, it is shown that the micelles can be inverted at high salt concentrations, Figure 3.2C. This is caused by exceeding $c_{s,cr}$ which makes the polyelectrolytes soluble, while the PNIPAM becomes insoluble due to a severely lowered LCST, Chapter 4.

Outline

The use of temperature responsive polyelectrolytes for underwater adhesion was bioinspired and therefore we present a literature review in Chapter 2. Here, the natural wet-adhesives made by sandcastle worms and mussels are discussed, as well as (wet-)adhesives based on electrostatic interactions.[29] Subsequently, RAFT polymerization and the preparation of temperature responsive polyelectrolytes are described in Chapter 3.[30] In this thesis, polyelectrolytes with both low and high PNIPAM contents were prepared and investigated. Chapter 4 describes the assembly of polyelectrolytes with low amounts of PNIPAM in dilute conditions. We show that micelles are formed at room temperature, which phase separate upon increasing the temperature. By adjusting the salt concentration, the core and corona of the micelles can be inverted. Namely, below $c_{s,cr}$, C3Ms with a PNIPAM corona are observed, while PNIPAM cored micelles (PCM) are found above $c_{s,cr}$. The PCMs are stabilized by the polyelectrolytes, that no longer form complexes at room temperature because of the high salt concentration. Moreover, as complex coacervation is temperature responsive, PCMs phase separate upon temperature increase as well as C3Ms.

Polymer mixtures with a high PNIPAM content are investigated in concentrated conditions using NaCl, Chapter 5, or guanidinium thiocyanate (GndSCN), Chapter 6. At low temperature, a concentrated C3M solution is found and a PNIPAM-induced solidification occurs upon crossing the gelation temperature, T_{gel}, Figure 3.2D. The resulting TERPOC does not phase separate, which shows that the water content remains unchanged upon gelation. Furthermore, charge neutraliz-
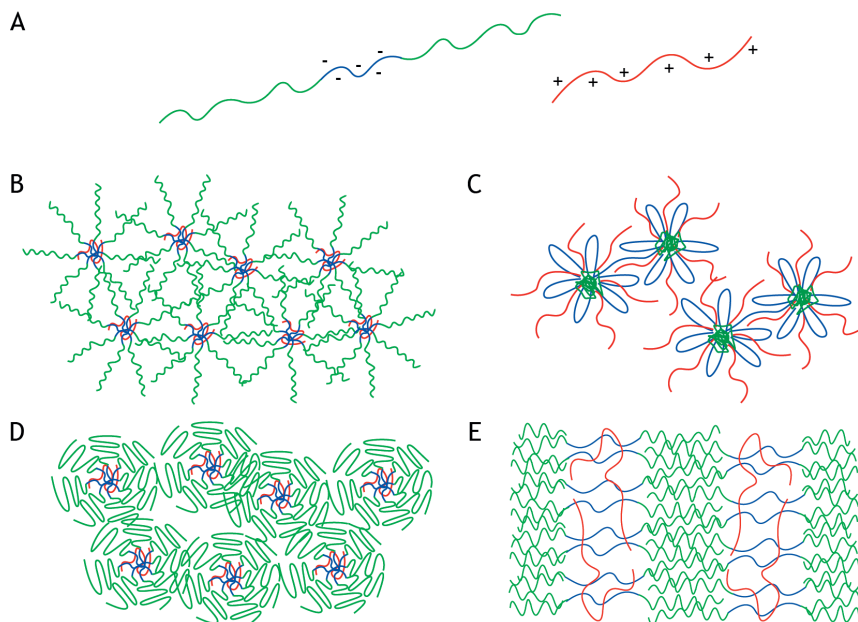
Figure 1.2 – Schematic representation of **A** the polymers, and their assemblies at different conditions. The green polymer blocks represent the PNIPAM, while the blue polymer block is the polyanion, and the red polymer is the polycation. Below T_{gel} **B** C3Ms are found below $c_{s,cr}$, while **C** PCMs are found above $c_{s,cr}$. Moreover, above T_{gel} and below $c_{s,cr}$, the PNIPAM chains collapse leading to solidification of the micelle solutions. **D** For NaCl, an undefined morphology is found, while **E** for samples with guanidinium thiocyanate lamellae are observed.

ation is required for strong gelation. By altering the salt and polymer concentrations, the T_{gel}, storage modulus (G'), and work of adhesion, W_{adh}, could be adjusted. For NaCl containing samples, the lowest T_{gel} and strongest gel was found for high salt and polymer concentrations. Moreover, a satisfying adhesion to glass was found for fully submerged TERPOCs. A maximum W_{adh} is observed at a high polymer concentration and slightly lower salt concentration. Finally, by using GndSCN, it is shown that various salt concentrations and temperatures result in different polymer assemblies. For TERPOCs, lamellae are found below $c_{s,cr}$, while rods seem present at higher GndSCN concentrations, Figure 3.2E. Furthermore, the addition of GndSCN leads to much weaker gels than the addition of NaCl. Therefore, the type of salt, and the salt and polymer concentrations are important tools for adjusting the characteristics of TERPOCs. To conclude the thesis, a general discussion is provided in Chapter 7 which considers the used approach for making underwater adhesives, and the results that are obtained by using temperature responsive polyelectrolytes.

Bibliography

[1] L. P. Bre, Y. Zheng, A. P. Pego, and W. X. Wang. Taking tissue adhesives to the future: from traditional synthetic to new biomimetic approaches. *Biomaterials Science*, 1(3):239–253, 2013.

[2] S. Khanlari and M. A. Dube. Bioadhesives: A review. *Macromolecular Reaction Engineering*, 7(11):573–587, 2013.

[3] A. Lauto, D. Mawad, and L. J. R. Foster. Adhesive biomaterials for tissue reconstruction. *Journal of Chemical Technology and Biotechnology*, 83(4):464–472, 2008.

[4] M. Mehdizadeh and J. Yang. Design strategies and applications of tissue bioadhesives. *Macromolecular Bioscience*, 13(3):271–288, 2013.

[5] W. Z. Zhu, Y. J. Chuah, and D. A. Wang. Bioadhesives for internal medical applications: A review. *Acta Biomaterialia*, 74:1–16, 2018.

[6] D. W. R. Balkenende, S. M. Winkler, and P. B. Messersmith. Marine-inspired polymers in medical adhesion. *European Polymer Journal*, 116:134–143, 2019.

[7] R. Pinnaratip, M. S. A. Bhuiyan, K. Meyers, R. M. Rajachar, and B. P. Lee. Multifunctional biomedical adhesives. *Advanced Healthcare Materials*, 8(11), 2019.

[8] W. D. Spotnitz and S. Burks. Hemostats, sealants, and adhesives: components of the surgical toolbox. *Transfusion*, 48(7):1502–1516, 2008.

[9] N. Lang, M. J. Pereira, Y. Lee, I. Friehs, N. V. Vasilyev, E. N. Feins, K. Ablasser, E. D. O'Cearbhaill, C. J. Xu, A. Fabozzo, R. Padera, S. Wasserman, F. Freudenthal, L. S. Ferreira, R. Langer, J. M. Karp, and P. J. del Nido. A blood-resistant surgical glue for minimally invasive repair of vessels and heart defects. *Science Translational Medicine*, 6(218), 2014.

[10] Y. Lee, C. J. Xu, M. Sebastin, A. Lee, N. Holwell, C. V. Xu, D. M. Nieves, L. Y. Mu, R. S. Langer, C. P. Lin, and J. M. Karp. Bioinspired nanoparticulate medical glues for minimally invasive tissue repair. *Advanced Healthcare Materials*, 4(16):2587–2596, 2015.

[11] J. H. Ryu, Y. Lee, W. H. Kong, T. G. Kim, T. G. Park, and H. Lee. Catechol-functionalized chitosan/pluronic hydrogels for tissue adhesives and hemostatic materials. *Biomacromolecules*, 12(7):2653–2659, 2011.

[12] E. Spruijt, A. H. Westphal, J. W. Borst, M. A. C. Stuart, and J. van der Gucht. Binodal compositions of polyeleetrolyte complexes. *Macromolecules*, 43(15):6476–6484, 2010.

[13] J. van der Gucht, E. Spruijt, M. Lemmers, and M. A. C. Stuart. Polyelectrolyte complexes: Bulk phases and colloidal systems. *Journal of Colloid and Interface Science*, 361(2):407–422, 2011.

[14] E. Spruijt, J. Sprakel, M. A. C. Stuart, and J. van der Gucht. Interfacial tension between a complex coacervate phase and its coexisting aqueous phase. *Soft Matter*, 6(1):172–178, 2010.

[15] R. J. Stewart, C. S. Wang, and H. Shao. Complex coacervates as a foundation for synthetic underwater adhesives. *Advances in Colloid and Interface Science*, 167(1-2):85–93, 2011.

[16] C. G. de Kruif, F. Weinbreck, and R. de Vries. Complex coacervation of proteins and anionic polysaccharides. *Current Opinion in Colloid & Interface Science*, 9(5):340–349, 2004.

[17] E. Spruijt. *Strength, structure and stability of polyelectrolyte complex coacervates*. Wageningen University, Wageningen, 2012.

[18] H. G. Schild. Poly (n-isopropylacrylamide) - experiment, theory and application. *Progress in Polymer Science*, 17(2):163–249, 1992.

[19] M. C. M. Costa, S. M. C. Silva, and F. E. Antunes. Adjusting the low critical solution temperature of poly(n-isopropyl acrylamide) solutions by salts, ionic surfactants and solvents: A rheological study. *Journal of Molecular Liquids*, 210:113–118, 2015.

[20] T. Patel, G. Ghosh, S. Yusa, and P. Bahadur. Solution behavior of poly(n-isopropylacrylamide) in water: Effect of additives. *Journal of Dispersion Science and Technology*, 32(8):1111–1118, 2011.

[21] H. Feil, Y. H. Bae, J. Feijen, and S. W. Kim. Effect of comonomer hydrophilicity and ionization on the lower critical solution temperature of n-isopropylacrylamide copolymers. *Macromolecules*, 26(10):2496–2500, 1993.

[22] M. Hahn, E. Gornitz, and H. Dautzenberg. Synthesis and properties of ionically modified polymers with lcst behavior. *Macromolecules*, 31(17):5616–5623, 1998.

[23] Y. J. Zhang, S. Furyk, D. E. Bergbreiter, and P. S. Cremer. Specific ion effects on the water solubility of macromolecules: Pnipam and the hofmeister series. *Journal of the American Chemical Society*, 127(41):14505–14510, 2005.

[24] K. Kataoka, A. Harada, and Y. Nagasaki. Block copolymer micelles for drug delivery: Design, characterization and biological significance. *Advanced Drug Delivery Reviews*, 64:37–48, 2012.

[25] G. Riess. Micellization of block copolymers. *Progress in Polymer Science*, 28(7):1107–1170, 2003.

[26] C. A. Dreiss. Wormlike micelles: where do we stand? recent developments, linear rheology and scattering techniques. *Soft Matter*, 3(8):956–970, 2007.

[27] I. A. Van Hees, P.J.M. Swinkels, R.G. Fokkink, A.H. Velders, I. K. Voets, J. Van der Gucht, and M. Kamperman. Self-assembly of oppositely charged polyelectrolyte block copolymers containing short thermoresponsive blocks. *Polymer Chemistry*, 2019.

[28] I. K. Voets, A. de Keizer, and M. A. C. Stuart. Complex coacervate core micelles. *Advances in Colloid and Interface Science*, 147-48:300–318, 2009.

[29] A. H. Hofman, I. A. van Hees, J. Yang, and M. Kamperman. Bioinspired underwater adhesives by using the supramolecular toolbox. *Advanced Materials*, 30(19), 2018.

[30] A. D. Filippov, I. A. van Hees, R. Fokkink, I. K. Voets, and M. Kamperman. Rapid and quantitative de-tert-butylation for poly(acrylic acid) block copolymers and influence on relaxation of thermoassociated transient networks. *Macromolecules*, 51(20):8316–8323, 2018.

Wet adhesion in nature and polyelectrolyte based underwater adhesives

2

Nature has developed protein-based adhesives whose underwater performance has attracted much research attention over the last decades. The adhesive proteins are rich in catechols combined with amphiphilic and ionic features. This combination of features constitutes a supramolecular toolbox, to provide stimuli-responsive processing of the adhesive, to secure strong adhesion to a variety of surfaces, and to control the cohesive properties of the material. In this chapter, the versatile interactions used in the adhesives secreted by sandcastle worms and mussels are discussed. Subsequently, we consider adhesive systems based on electrostatic interactions.

Introduction

Adhesives developed by marine organisms have been the focus of a great number of studies over the last two decades. These organisms are able to bond materials underwater using protein-based adhesives: barnacles use secretions to glue calcareous base plates to rocks, mussels use a network of threads to attach their soft invertebrate body to hard surfaces, and both sandcastle worms and caddisfly larvae assemble a protective tubular shell by gluing together sand grains or stones.[1, 2, 3] It is well-known that the adhesive abilities of the sandcastle worm and mussel both involve post-translational modifications of the adhesive proteins. Hydroxylated tyrosine, known as L-3,4-dihydroxyphenylalanine (DOPA), and phosphorylated serine are common adhesion promoters.[4, 5, 6, 7, 8] The importance and use of DOPA in synthetic mimics has been reviewed extensively in several excellent reviews.[9, 10, 11, 12] Moreover, it was emphasized by Waite that catechol moieties alone are insufficient to ensure proper underwater adhesion and that the performance is a complex interplay between DOPA and its local environment.[13] Therefore, attention is shifting to include other (non-covalent) interactions used in these natural glues to obtain underwater adhesives. In addition, much progress has been made in understanding both the performance and delivery process of natural underwater adhesives.[14]

Wet adhesion in nature

In the upcoming sections, we will discuss the features and mechanisms of adhesion by sandcastle worms and mussels. Even though there are large differences between the organisms, the adhesive chemistries also show similarities. Therefore, at the end of this chapter, a concise overview of the important chemical interactions for both adhesion and cohesion is given.

Sandcastle worms

Sandcastle worms, *Phragmatopoma californica* (Figure 2.1a), are marine organisms that live in colonies along the coast of North America. These worms build protective shells which are formed from minerals found in their surroundings. The mineral particles, such as sand grains or pieces of shell, are glued together underwater with a bioadhesive packaged in granules that are secreted from adhesive glands.[14] After an initial curing period of less than 30 seconds, the adhesive is strong enough to hold the particles in place. In the next hours, a second curing step follows which darkens the
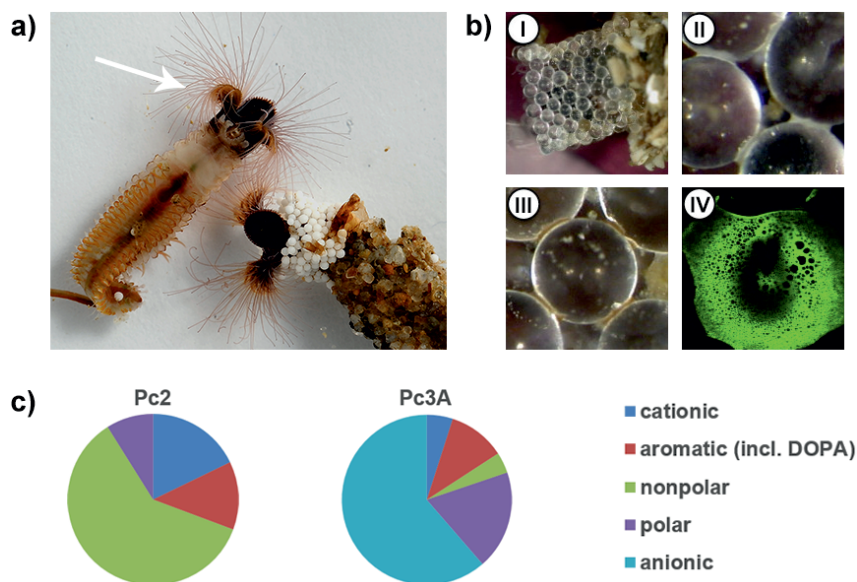
Figure 2.1 – a) Image of sandcastle worms, *Phragmatopoma californica*; the worms are depicted in- and outside their protective shell. New particles are placed onto the shell by its ciliated tentacles (white arrow). The shells in the picture were partially built in a laboratory environment, explaining the different colors of the ceramic particles. **b)** Glass beads can also be used by the worms for building shells (I). The adhesive was only applied around the contacts of the beads, and spread over the surface which suggests a low interfacial tension (II). After protein secretion, the initially white glue turned brownish in a few hours as a result of DOPA oxidation (III). The final adhesive has a porous, foam-like structure (IV). Reprinted from Ref. [15], copyright 2011, with permission from Elsevier. **c)** An overview of the chemical characteristics of the amino acids present in cationic Pc2 and anionic Pc3A. Pc2 is used as representative for all cationic Pc proteins. Data derived from Refs. 14 and 16.

color. The resulting cement is a porous solid with the pores being filled with liquid (Figure 2.1b).[17]

Adhesive composition

The main constituents of the sandcastle glue are six different types of adhesive proteins, sulfated polysaccharides, and magnesium ions. The proteins can roughly be divided into two groups: anionic proteins and cationic proteins (Figure 2.1c). The two anionic proteins are referred to as Pc3A and Pc3B, after *Phragmatopoma californica* (Pc). These proteins contain large quantities of phosphorylated serine, thereby introducing negative charges into the protein.[18] Pc1, Pc2, Pc4 and Pc5 are cationic proteins that are rich in the nonpolar amino acid glycine, with an exception of Pc5, which contains a mixture of several nonpolar amino acids. The positive charges on these proteins originate from quaternized histidine and lysine residues, which represent 5-18% of the total amino acid content.[16] In addition, all six proteins contain at least 10% aromatic amino acids.[16, 18] These aromatic residues include tyrosine
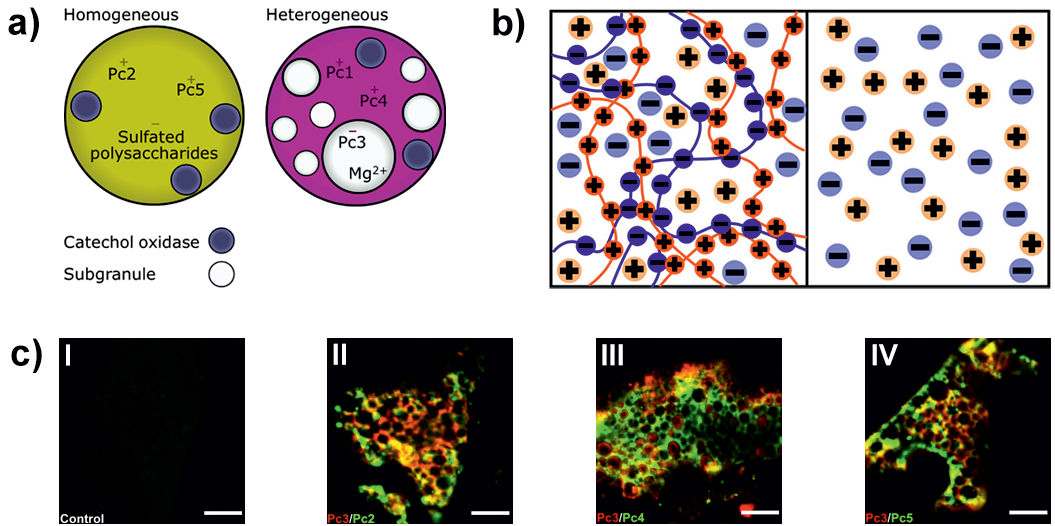
Figure 2.2 – a) The adhesive proteins of the sandcastle worm are secreted from two types of granules (homogeneous and heterogeneous granules) that both contain catechol oxidase. Besides a main compartment, the heterogeneous granules also contain subgranules. The main compartment contains cationic Pc1 and Pc4, mixed with catechol oxidase. The subgranules contain anionic Pc3, mixed with Mg^{2+} (adapted from Wang et al.[19]). **b)** Complex coacervates are formed when oppositely charged polyelectrolytes complex and release their counterions. Two phases coexist; a concentrated coacervate phase (left) and a dilute phase (right). Reprinted with permission from Ref. 20. Copyright 2015 American Chemical Society. **c)** The different sandcastle worm proteins were imaged by fluorescence microscopy after immunological labelling. The cationic proteins (Pc2, Pc4 and Pc5) were labelled green and Pc3 was labelled red. Hardly any overlap (yellow) of the cationic and anionic proteins was visible. (I) Negative control (without any labelling), (II) Pc2 and Pc3, (III) Pc4 and Pc3, (IV) Pc5 and Pc3 were labelled. Scale bars are 20 μm. Reproduced with permission, Journal of Experimental Biology.[21]

and DOPA. DOPA originates from the posttranslational modification of tyrosine by tyrosinase[18] and is considered to be an important feature for underwater adhesion, because it forms interactions through a high variety of chemistries, as will be discussed in section 2.2.2.[11, 13]

Adhesive storage

The adhesive proteins are stored in two different types of secretory granules inside the adhesive glands, i.e. the homogeneous and heterogeneous granules (Figure 2.2a). The homogeneous granule contains cationic Pc2 and Pc5 proteins together with sulfated polysaccharides.[19, 21] The heterogeneous granules contain two separate domains each with a different content. The main domain encloses cationic Pc1 and Pc4,[21] whereas the subgranules contain anionic Pc3A and Pc3B proteins together with cationic magnesium ions.[22] The fluid, yet concentrated character of the adhesive before secretion is likely explained by complex coacervation.[19]

Complex coacervation is the association of oppositely charged polyelectrolytes res-

ulting in liquid-liquid phase separation (Figure 2.2b).[23] This process is often driven by electrostatic interactions, but may involve other types of interactions. The combination of oppositely charged compounds in both the homogeneous and the subgranules suggests that complex coacervates are formed in the granule. The use of coacervation is advantageous for storage and application because it enables surface wetting through low interfacial tension and it concentrates the materials, while maintaining the fluid-like properties.[24] Besides electrostatic interactions, additional interactions, such as hydrophobic, cation-π, or π-π interactions may take place.[25] These interactions have not been identified in the adhesive of sandcastle worms, but hydrophobic interactions may increase the driving force for coacervation, and cation-π interactions may relate to the cationic character of Pc1 and Pc4, which remains unexplained so far.[14, 26]

Adhesive application and curing mechanisms

The sandcastle worm applies its adhesive onto the mineral particle from pores in the surface of the building organ. These pores are close together and it is suggested that each pore secretes a particular granule, i.e., homogeneous or heterogeneous granules.[14] After granule rupture, the fluid-like granule contents fuse together into a single heterogeneous material without extensive mixing of the anionic and cationic proteins (Figure 2.2c).[21] Because it is not clear whether specific proteins are solely located at the adhesive interface,[4] it is also not clear which specific interactions are responsible for adhesion. However, based on similarities between the proteins of the sandcastle worm and mussel, it is expected that comparable mechanisms are involved. Both the sandcastle worm cement and the mussel plaque are rich in phosphate and catechol groups, i.e. DOPA, that are known adhesion promotors. Surface interactions of DOPA are discussed in section 2.2.2, because in literature they are mainly associated with mussel adhesion.

Several toughening and curing mechanisms start to play a role after application. First there is a change from acidic pH in the gland to the slightly basic pH of seawater.[18] The increase in pH solidifies the Mg^{2+}/sulfated Pc3 bonds that are present in the heterogeneous subgranules. [15, 18] Second, the metal ion content in the adhesive changes. While before secretion the granules solely contain Mg^{2+}, significant amounts of Ca^{2+} were detected in the cured adhesive, that were presumably extracted from the seawater.[4, 14] Besides magnesium and calcium, also iron, manganese and zinc were detected in the secreted adhesive material. These ions might cause complexation, by forming ionic bonds or coordinating to DOPA. As a result they can contribute to the solidification process and act as physical crosslinks.[4, 27, 28]

At last, the adhesive changes color from off-white to reddish-brown while curing (Figure 2.1b). This color change occurs over a time span of several hours to days and is caused by the oxidation of DOPA. The enzyme catechol oxidase is enclosed in both adhesive granules (Figure 2.2a) and oxidizes DOPA into DOPA-quinone (Figure 2.3), subsequently leading to the formation of covalent bonds that contribute to the cohesion of the adhesive.[19, 29]

Structural characteristics of the adhesive

The adhesive that is formed after curing has an open and foam-like structure, similar to mussel plaque (Figure 2.1b, IV).[17] Different hypotheses exist about the formation of these porous structures. As Pc3 proteins were solely found at the pore walls, it is hypothesized that the pores in sandcastle adhesives are caused by swelling of the subgranules and subsequent phase inversion. The other proteins from the heterogeneous granule form a matrix closely around the subgranules, which is expected to limit pore growth by providing a counter pressure. Also, this pressure balance on the pore walls might provide mechanical stability to the adhesive after curing.[14, 21] Additionally, the sandcastle worm adhesive has a porosity gradient from small pores at the interface of the joint to larger pores inside the joint. Efficiently, high amounts of material are present at highly stressed spots, while only little material is located at spots with low stress.[3, 17]

Mussels

Mussels are extensively studied marine organisms that stick to surfaces using their byssal threads (Figure 2.4a). These threads consist of three parts: the adhesive plaque, the rigid distal thread and the flexible proximal thread, that are all coated by cuticle (Figure 2.4c).[13, 30, 31] The byssal thread is formed by the mussel foot (Figure 2.4b), a flexible organ that is pressed against the surface that the mussel aims to adhere to. The byssal thread proteins are secreted in the ventral groove that is isolated from the environment. Three glands were found in the mussel foot: the phenol gland, the collagen gland and the accessory gland, each secreting granules that contain proteins for different parts of the thread (Figure 2.4c). After all proteins have been secreted, the mussel retracts its foot and the byssal thread can obtain its final properties through equilibration with the environment.[2, 13, 31, 32, 33, 34]

Byssus thread proteins

So far, 25 to 30 different mussel foot proteins (mfps) have been identified, of which only five types are found in the plaque.[35] These five protein types can be roughly
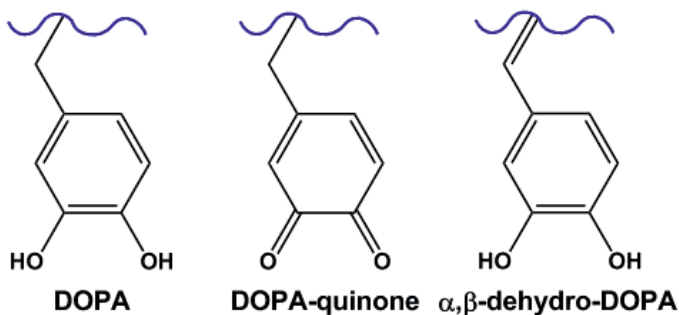

Figure 2.3 – Chemical structures of DOPA, its oxidized form (DOPA-quinone) and the tautomerized form of DOPA-quinone (α, β-dehydro-DOPA).
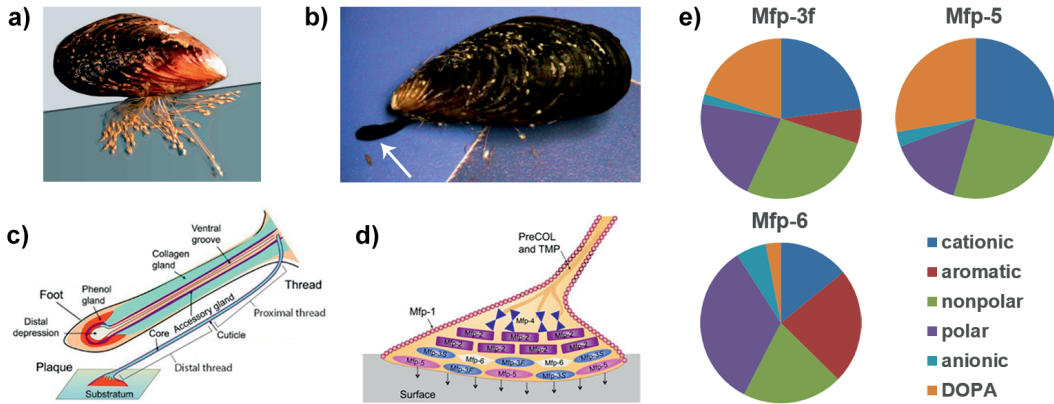
Figure 2.4 – a) Image of an adult mussel, *Mytilus californianus*, that secreted multiple byssal threads from **b)** the mussel foot (white arrow). The foot is extended from the shell and attaches to the surface before protein secretion. **c)** Firm attachment to the surface takes place by lifting the ceiling of the distal depression; then, the byssus proteins are secreted into the ventral groove. The phenol gland (red) secretes the proteins that form the plaque (red). The proteins secreted from the collagen gland (green) form the core of the thread (green). The accessory gland (purple) secretes mfp-1 proteins for the cuticle (purple). **d)** After protein secretion, the mussel foot retracts, leaving the byssus behind in which the proteins are highly organized. The adhesive and DOPA-rich mfp-5 and mfp-3 are located at the bottom of the plaque. Above these, the cohesive mfp-6, mfp-2 and mfp-4 are located. Mfp-4 facilitates attachment of the plaque to the thread that is made from collagen (PreCOL) and thread matrix protein (TMP). Mfp-1 covers the byssus as a cuticle. Reproduced with permission, Journal of Experimental Biology.[13] **e)** An overview of the chemical characteristics of the amino acids present in the mussel foot. Data derived from Ref.35.

divided into two groups, i.e. the DOPA-rich mfp-3 and mfp-5 proteins at the surface, and the mfp-6, mfp-2 and mfp-4 proteins that are located higher in the plaque (Figure 2.4d).[35] Mfp-3 is a polymorphous polar protein, meaning that there are many variations of this type, originating from posttranslational modifications,[35] for example through conversion of tyrosine into DOPA and conversion of arginine into 4-hydroxyarginine.[36] The mfp-3 variants are subdivided into two groups, mfp-3 fast (mfp-3f) and mfp-3 slow (mfp-3s), based on their distinct elution in electrophoretic analysis. Both groups are rich in nonpolar glycine and polar asparagine, but differ substantially in their DOPA and cationic residue contents. Mfp-3f contains a significant amount of DOPA, while mfp-3s only has half of this amount in favor of other aromatic residues. Furthermore, the cationic residue content, mostly protonated 4-hydroxyarginine, is almost twice as high in mfp-3f as in mfp-3s.[37] Mfp-5 is very similar to mfp-3 but is larger (9 kDa vs 6 kDa), and contains significant amounts of cationic lysine instead of arginine. Furthermore, the conversion of tyrosine into DOPA in mfp-5 is almost complete and also comparable between the mfp-5 proteins (Figure 2.4e). In addition to the posttranslational conversions mentioned above, anionic groups are introduced in mfp-5 by phosphorylation of serine.[35, 38]

Mfp-6 can be found further away from the surface. Similar to mfp-3 and mfp-5, mfp-6 is rich in glycine and aromatic residues, although a much lower amount of

tyrosine is converted into DOPA and also fewer cationic groups are present.[35, 39] Above the mfp-5/mfp-3/mfp-6 layer, mfp-2 can be found which covers 25% of the total protein content in the plaque. The DOPA content in mfp-2 is low and part of the cysteine residues is crosslinked by disulfide bonds as a result of oxidation.[31, 35, 40] At the very top, hydrophobic and cationic mfp-4 can be found that is rich in copper-binding histidine. In contrast to all other adhesive mussel proteins, mfp-4 is poor in aromatic amino acids as it only contains trace amounts of DOPA.[35, 37]

Besides these five plaque proteins, thread and cuticle proteins are important in byssus formation as well. The thread is attached to the top of the plaque and contains both aligned collagen and thread matrix proteins. The structure of the collagen is as found in other animals $[GX_1X_2]_n$, i.e. a repeated amino acid sequence starting with glycine followed by two varied amino acids in the second and third position. As a result of the repetitive amino acid sequence, protein domains with a semicrystalline structure of beta-sheets are formed. The crystallinity, and thus the stiffness of the thread, is determined by the variation of the amino acids in the second and third position and is therefore different in distal and proximal byssal regions (see Figure 2.4c). Final alignment of the semicrystalline domains is likely a result of contraction of the mussel foot during thread formation.[13, 31] The thread matrix protein, tmp-1, is rich in hydrophobic glycine and tyrosine residues, but the conversion of tyrosine into DOPA is low in contrast to mfp-3f and mfp-5. Finally, mfp-1 is used to coat the mussel byssus thread with cuticle, and thus resides at the water/byssus interface.[13] Mfp-1 has equal amounts of DOPA and cations, and contains many uncharged polar residues, while the amount of nonpolar residues is limited.[15, 31, 35]

Adhesion

Mfp-3 and mfp-5 are mainly responsible for adhesion of the plaque to the surface. More specifically, DOPA is thought to play a dominant role in both dehydration of, and binding to the surface. A submerged hydrophilic surface is generally covered by a layer of ions, water and several other compounds.[13] For proper adhesion, this layer first has to be removed. For several mimics, it was shown that DOPA efficiently dehydrated surfaces, while tyrosine was inefficient. These experiments also revealed that dehydration was enhanced when DOPA was in the proximity of cationic lysine, or incorporated into a coacervate of polyampholytic peptides.[13, 34, 41, 42] After dehydration, DOPA adheres to a surface by using different mechanisms such as hydrogen bonding, metal oxide coordination or cation-π interactions (Figure 2.5), as will be discussed more extensively in Chapter 3.[11, 13, 35, 42] Other amino acids of mfp-3 and mfp-5 may contribute to adhesion by electrostatic or hydrophobic interactions.[13]

In seawater, DOPA is readily oxidized to DOPA-quinone, which can subsequently be converted to α, β-dehydro-DOPA through tautomerization (Figure 2.3). Both DOPA and α, β-dehydro-DOPA can form hydrogen bonds with the surface, but DOPA-quinone cannot.[32] For this reason, DOPA-quinone tautomerization seems an easy approach to maintain the adhesive abilities. Furthermore, in the mussel proteins, except for mfp-1, and also in the sandcastle worm proteins, the nonpolar amino

acid glycine is mostly located next to DOPA. [16] From synthetic polymers, and from comparing hydrophilic mfp-3f and hydrophobic mfp-3s, it was shown that nonpolar groups inhibit oxidation of DOPA when located in close proximity, hypothetically through hydrophobic or electrostatic shielding of the DOPA moiety.[43, 44] Therefore, glycine likely controls the degree of DOPA oxidation in the adhesive proteins of sandcastle worms and mussels. Additionally, a special feature in the mussel plaque is the reducing ability of mfp-6 that is located in the proximity of mfp-3 and mfp-5. It was shown that both cysteine and DOPA residues in mfp-6 contribute to the reduction of the radical scavenger 2,2-diphenyl-1-picryl hydrazyl and are thus expected to reduce DOPA-quinone in the mussel plaque.[11, 13, 35, 45, 46] At neutral pH, however, thiols show high reactivity towards quinones and a cysteine-DOPA adduct is formed. This adduct has a slightly lowered oxidation potential compared to DOPA, but is still a strong reducing agent.[29, 46] At last, DOPA oxidation can be controlled by careful tuning of the conditions in the ventral groove of the mussel foot. While seawater has a pH of 8.2, the pH in the groove is acidic which severely limits both auto-oxidation and enzymatic oxidation. Catechol oxidase is co-secreted with the mfps and has an optimal activity at pH 8. As a result, the activity of catechol oxidase is minimal at acidic pH.[11, 13]

Processing of the adhesive

While complex coacervation is expected to concentrate the adhesive proteins of the sandcastle worm before secretion, complex coacervation in the mussel adhesive is unlikely because so far no oppositely charged molecules have been found to complex with the cationic mfps. Alternatively, concentration of the adhesive is hypothesized to take place through coacervation. Coacervation differs from complex coacervation because it involves a liquid-liquid phase separation in a system containing one type of macromolecules, instead of two. From the mfps, mfp-3s was shown to coacervate before full charge neutralization was obtained,[47] suggesting that ionic coacervation of mfp-3s is enhanced by additional interactions such as hydrophobic, cation-π, or π-π interactions.[11, 13, 47, 48] Cation-π interactions were shown to induce a liquid-liquid phase separation of recombinant mfp-1 from solution.[26] At constant pH (7.2), phase separation was induced by increasing the salt concentration till 0.7 M, which is equal to the salt concentration in seawater. As mfp-1 lacks anionic amino acids, cation-π induced coacervation is a plausible mechanism for concentrating mfps.

Toughening and curing mechanisms

The mfps are in a fluid state during secretion, and therefore have to solidify and cure afterwards, which can be induced by the addition of metal ions, or by increasing the pH and ionic strength.[13, 31, 34] For example, DOPA is able to form metal coordination bonds, such as occur between Fe^{3+} and mfp-1, and between Fe^{3+} and mfp-2. These metal ions change to a higher stoichiometry (i.e., number of catechol groups per metal ion) with increasing pH, resulting in stronger binding. However, depend-

ing on the amino acids that surround DOPA, the pH at which this strengthening occurs varies.[11, 13, 31, 34, 40, 49] In addition, pH increase leads to both auto- and enzyme-induced oxidation of DOPA, that is similar in the DOPA-containing proteins of sandcastle worms.[4, 11, 13]

Besides DOPA, additional functional groups were found to be responsible for so-lidification and hardening of the byssal thread. For example, proteinaceous phosphate groups, e.g. in mfp-5, complex with calcium or magnesium ions that were added to the adhesive, post secretion. Upon pH increase, these ionic complexes insolubilize.[13, 18, 31] Similar insolubilization was identified in the collagen thread; at pH values above six, histidine's imidazolium side group is able to form coordination bonds with zinc and copper ions, resulting in additional toughening of the byssal thread.[13]

Exposure to seawater may also result in changes at the interface. For metal ox-ide surfaces, such as rock, hydrogen bonds between the surface and catechols are weakened by increasing the ionic strength, due to deprotonation of the hydroxyl groups. Upon sufficient increase of the pH, formation of stronger coordination bonds with the metal oxide groups compensates for this weakening, resulting in improved adhesion.[13, 49]

Plaque characteristics

After curing, the adhesive plaque has a porous structure that is similar to sandcastle glue. Priemel et al. revealed by Raman spectroscopy that the environment of the tyr-osine moieties in the byssal thread proteins changes from hydrophobic to hydrophilic during thread formation. This observation suggests that the transition from a fluid to a foam-like structure of the plaque coexists with a conformational change of the proteins.[31] However, this technique did not reveal the mechanism for foam forma-tion. Phase inversion might be an explanation for pore formation in both the mussel plaque and sandcastle worm cement (section 2.1.4), since phase inversion of complex coacervates led to similar porous structures in synthetic systems.[13, 34]

Adhesion and cohesion of adhesives from sandcastle worms and mussels

Even though the sandcastle worm and the mussel adhesives have different characterist-ics, several strategies seem to be used by both organisms. Figure 2.5 summarizes all dif-ferent interactions that have been identified in either the sandcastle worm or the mus-sel. The adhesive compounds of the sandcastle worms are rich in nonpolar and ionic groups.[16, 18] Enhanced by nonpolar amino acids, complex coacervates and metal ion-polyelectrolyte complexes are formed from oppositely charged compounds.[14, 19] As a result of complexation, which is a cohesive feature, the adhesive material is concentrated and insoluble in water.[13, 14] In addition to the ionic groups, sand-castle worm glue contains moderate amounts of DOPA, which is abundantly present in mfps.[13, 16, 18] DOPA can interact noncovalently with both the surface, and other

Figure 2.5 – Overview of the different adhesive and cohesive interactions as found in or hypothesized for wet adhesion by sandcastle worms and mussels.
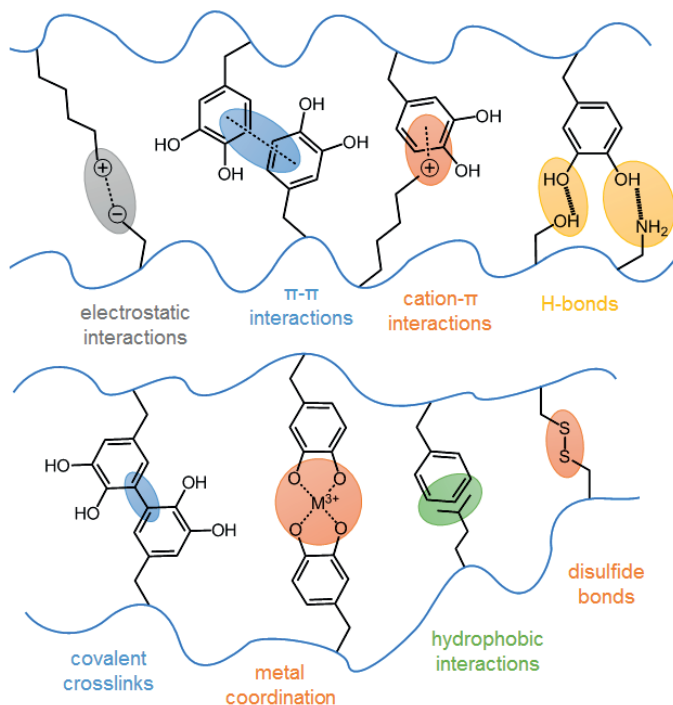
moieties inside the glue through multiple mechanisms, i.e. H-bonds, metal(oxide) coordination bonds, cation-π and π-π interactions (Figure 2.5).[11, 13, 50] Both organisms co-secrete catechol oxidase with their proteins, resulting in the conversion of DOPA into DOPA-quinone.[13, 19] Consequently, covalent bonds are formed between DOPA-quinone groups or other amino acids that promote cohesion, such as cysteine or lysine.[11, 13, 35] This variety of interactions and possible chemical reactions have been used either separately or combined in the development of improved underwater adhesives, as will be described in the following chapters.

Adhesives based on electrostatic interactions

Several research groups have been inspired to develop adhesive materials based on electrostatic interactions, because these interactions play an important role in the adhesive processing and performance of sandcastle worms and mussels. The strength of electrostatic interactions can be controlled by varying the ionic strength or pH, and can thus be used to tune the mechanical properties. In this chapter, materials based on electrostatic interactions will be discussed, including (complex) coacervation (Figure 2.2b)

and ion-based crosslinking, of either recombinant proteins or synthetic materials. We will also highlight work where (complex) coacervation is used as a delivery tool for underwater adhesives. Table 2.1 and Table 2.2 provide an overview of the adhesive strengths as measured by SFA and lap shear testing, respectively.

Protein-based (complex) coacervate adhesives

Natural mussel foot proteins

The most obvious approach to obtain underwater adhesive properties is to use the adhesive proteins from the marine animals themselves. To this end, Wei et al. isolated mfp-3s from the mussel plaque, which is so far the only natural mussel foot protein that has been shown to phase separate by coacervation at low salt concentrations.[44, 47] Coacervation usually occurs when the proteins carry equal amounts of positive and negative charges, which is at pH > 7.5 for mfp-3s. Here, phase separation occurred at lower pH values (pH = 5.5), which suggested that additional interactions between the now net-charged proteins enhanced electrostatically-driven coacervation. Adhesion was determined by both SFA (Table 2.1) and quartz crystal microbalance dissipation (QCM-D). Optimal adhesion to hydroxyapatite (QCM-D) was obtained in a buffer at pH 5.5, which was the condition that resulted in the most fluid-like material. Wei et al. speculated that the mfp-3s coacervate in optimal conditions is able to dissipate the energy of deformation which results in improved adhesion compared to mfp-3s coacervates at different pH.

Recombinant mussel foot proteins

Unlike Wei et al., Choi and coworkers did not isolate proteins from the mussel glue but produced natural mfp-5 protein from recombinant E. coli.[51] However, since these bacteria are not able to convert tyrosine into DOPA, because they lack the tyrosinase enzyme of mussels, mushroom tyrosinase was added to the protein solution after purification. Adhesion of recombinant mfp-5 was investigated by lap shear tests. Adhesive strengths of 1.11 MPa to aluminum were measured after incubation with tyrosinase for 4 hours at 37 °C (Table 2.2). Since complexation with a polyanion was shown to further improve adhesion of mussel foot proteins,[52] a complex coacervate (Figure 2.2b) was formed by mixing cationic mfp-5 with hyaluronic acid, an anionic polyelectrolyte commonly present in the human body.[6, 53, 52] After complexation, the shear strength increased to 1.73 MPa and could compete with values previously reported for recombinant mimics of mussel adhesive proteins that were also complexed into coacervates.[51, 52, 54]

An example of a protein mimic is mfp-151, developed by Hwang et al.[54] Mfp-151 is composed of an mfp-5 protein sequence in the middle of the protein, flanked by six repeats of an mfp-1 sequence on both sides. The protein was post-translationally exposed to tyrosinase to obtain DOPA, and subsequently complexed to hyaluronic acid.[24] The adhesive showed immediate surface wetting because of the low inter-

facial tension with water that is typical for complex coacervates, and shear thinning enabled facile application through a syringe. In addition, for the coacervates high friction coefficients of 1.2-1.4 were obtained and were independent of the degree of coacervation, and therefore presumably caused by the presence of DOPA in mfp-151.

In subsequent work, Lim et al. tested the adhesion of hyaluronic acid complexed to mfp-151 and mfp-131 (mfp-3 flanked by six mfp-1 repeats), which were treated with tyrosinase to acquire DOPA.[52] This work demonstrated that complexed recombinant mfps may acquire stronger adhesion than complexed natural mfp-5 (Table 2.2).[51] In addition to adhesion, Lim et al. also investigated the formation of microcapsules from these recombinant mfp-based complex coacervates.[52] They found that red pepper seed oil was completely taken up by the coacervate droplets. This finding illustrates the opportunities for employing complex coacervates in medicine, for example as drug carrier.

The water-insoluble mfp-151/hyaluronic acid complex was applied as medical adhesive for urinary fistula sealing and bone graft binding by Kim et al.[6, 53] For urinary fistula sealing, the adhesive was covalently cured by oxidizing DOPA with sodium periodate (12 h, 37 °C) after application to the surface. Subsequently, the wet shear strength of the cured complex was investigated under physiological conditions and compared to conventional medical glues. On the one hand, adhesion of the material to metal oxide surfaces was only half as strong as adhesion of conventional cyanoacrylate, while on the other hand, wet adhesion to porcine skin appeared to be four times stronger. This difference in adhesion was attributed to the presence of surface-bound nucleophilic groups (e.g. hydroxyl groups) on the porcine skin that form covalent bonds with DOPA, but not with acrylates.[6] In the second application, an unmodified, so DOPA-free, mfp-151/hyaluronic acid complex enriched with deproteinized bovine bone minerals was applied as bone graft binder.[53] Complex coacervation was required to avoid dispersion of the protein by blood. Without curing, the bovine-enriched complex coacervate displayed improved resistance to uniaxial compression, and improved bone regeneration with 50%, at 8 weeks post-surgery.[53] These two examples indicate that complex coacervates of recombinant adhesive proteins are promising materials for medical applications, irrespective of the DOPA content.

Synthetic adhesives with opposite charges

Polyelectrolytes

In contrast to the protein-based adhesives discussed in the previous section, Zhao and co-workers designed a fully synthetic underwater adhesive that was applied to a water immersed surface via solvent exchange.[55] The adhesive consisted of oppositely charged polymers: a random copolyanion containing anionic acrylic acid and catechol-functionalized acrylic acid (7:3), and a polycation composed of quaternized chitosan ion-paired with bis(trifluoromethane)sulfonamide (Tf_2N^-). The use of Tf_2N^- counterions allowed chitosan to dissolve in dimethylsulfoxide (DMSO). Without complex formation taking place, the polymers were combined in a single DMSO solution and
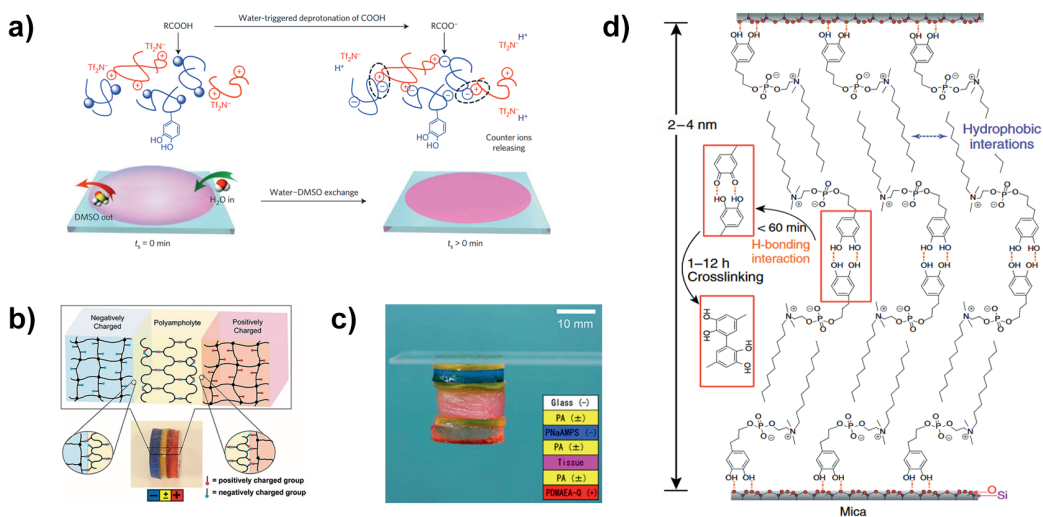
Figure 2.6 – a) A complex coacervate, based on catechol-functionalized poly(acrylic acid) and chitosan, was used for the formation of a wet adhesive. Solvent exchange of the initial solvent DMSO and bulk water resulted in deprotonation of acrylic acid followed by complex coacervation. Reprinted by permission from Macmillan Publishers Ltd: Nat. Mater. (Ref. 55), copyright 2016. **b)** Polyampholyte gels (yellow), with equal amounts of positive and negative charges, adhered to both anionic (blue, left) and cationic (red, right) hydrogels. The blue and red dots in the scheme represent the anionic and cationic charges, respectively. Counterions were omitted from the scheme for clarity. **c)** The polyampholyte gel also adhered to glass and pork tissue that are both moderately charged. Copyright by John Wiley & Sons, Inc. (2015). Reprinted with permission from Ref. 56. **d)** Adhesives can also be made from amphiphilic zwitterions. A double bilayer was formed between the mica surfaces through H-bonding and hydrophobic interactions. Further strengthening of the adhesive was obtained by covalent crosslinking through DOPA oxidation. Reproduced from Ref. 57 (Nat. Commun.).

subsequently applied onto a water-immersed glass slide. Miscibility of DMSO and water enabled solvent exchange, which resulted in deprotonation of acrylic acid by water, followed by complexation of acrylic acid and chitosan (Figure 2.6a). The material sedimented, spread over the glass surface, and initial setting occurred in 25 s. After a few more minutes, water blasting could be resisted and after immersing two glass slides in demineralized water for one hour, an adhesive energy of 2 J m^{-2} was measured with an SFA. Such strong adhesion was attributed to the catechol units in the polyanion because adhesion weakened considerably when the catechol units were omitted or blocked for surface interaction by addition of Fe^{3+}. The catechol content also affected the structure of the material, as increasing the catechol content increased porosity. The polyelectrolyte complex adhesive attached to a wide variety of surfaces, ranging from glass to plastics and from metals to wood, making it a multifunctional underwater glue.[55]

Also examples of synthetic coacervate-based adhesives where electrostatic interactions take place inter- and intramolecularly, i.e. polyampholytes, have been reported. Seo et al. synthesized catechol-functionalized mimics of mfp-3s with varying amounts

of nonpolar and ionic monomers to investigate the influence on catechol oxidation, adhesion and cohesion, by cyclic voltammetry and SFA, respectively.[43] Two polymers without or with a reduced number of nonpolar groups were analyzed. It was shown that nonpolar groups efficiently inhibited oxidation of catechol and provided cohesion to the adhesive material. However, very thin layers of polymer (1-6 nm) have been used for these SFA measurements. At such small length scales, the surface affects the conformation of the polymers throughout the whole film. Therefore, the observed cohesion does not reflect the cohesive properties of bulk material, but only that of the measured film. Furthermore, the pH dependence of adhesion was tested, showing a maximum at pH 4 (17.0 mJ m^{-2}) through optimal surface coverage because of the coacervate phase. However, both optimal adhesion and cohesion to mica was obtained by increasing the pH from 4 to 7 (Table 2.1), possibly because of optimal surface coverage combined with reduced repulsion between the polymers after pH increase.

Ionic gels

Roy et al. developed a polyampholyte gel, i.e. a covalently crosslinked copolymer, containing monomers of opposite charge (Figure 2.6b).[56] Covalent crosslinking was necessary to acquire sufficient strength. Despite the crosslinks, the gel was soft, viscoelastic and contained about 52% water. In addition to the polyampholyte hydrogel also several anionic, cationic and neutral gels were prepared that functioned as substrate for adhesion. By tensile and lap shear tests, the researchers showed that the polyampholyte gel adhered to both cationic and anionic gels. For anionic substrates, a maximum adhesive shear energy of 30 J m^{-2} and a tensile bond strength of 236 kPa were observed. On the contrary, adhesion to neutral hydrogels was significantly weaker with only 0.3 J m^{-2} shear energy and 42 kPa bond strength. As a result, the researchers concluded that adhesion of the polyampholyte hydrogel was based on ionic interactions, regardless of the nature of the surface charge, as both cationic and anionic charges are present in the gel. Pork tissue, which is slightly charged, was used as a model system for adhesion in medical applications (Figure 2.6c). The anionic hydrogels did not adhere to liver tissue at all, and cationic hydrogels only adhered shortly, while the polyampholyte outperformed all other gels with a critical energy of 3 J m^{-2} and a bond strength of 24 kPa. For this reason, ampholytic gels may be promising adhesives for applications in life sciences.

Zwitterions

The group of Ahn developed low molecular weight zwitterions for preparing complexes as an alternative to polyampholytes (Figure 2.6d).[57] The zwitterions were functionalized with two short aliphatic carbon tails of which one contained a catechol unit at the end. In agreement with the findings of Seo et al., a longer carbon tail, thus higher hydrophobicity, led to a decreased solubility and increased resistance to catechol oxidation.[43] Adhesion was determined after adsorbing the zwitterions in thin films onto the mica surface of the SFA. As deduced from the interfacial energies, all

films failed cohesively (Table 2.1). The thickness of the adhesive layer depended on the tail length (2-4 nm). Based on this observation, the authors suggest that the zwitterion coating consists of a double bilayer that is formed by attachment of the catechol groups to the surface through hydrogen bonding. A second layer of zwitterions then binds hydrophobically to the first layer. When this process takes place at two surfaces, the outer catechol groups on either bilayer can again form hydrogen bonds upon contact (Figure 2.6d). Adhesion by the zwitterions could be further improved via covalent crosslinking of the catechol groups through oxidation with sodium periodate. The combination of crosslinking and drying of the material resulted in optimal adhesion to silicon (175 mJ m^{-2}).

Ionic crosslinking of polyelectrolytes

Metal ion-enhanced complex coacervates

It is also possible to enhance or induce complexation by adding non-polymeric ions to polyelectrolytes. The effect of metal ions in complex coacervate adhesives was explored by Shao et al. who complexed an anionic catechol-functionalized random copolymer that contained phosphate groups, with a cationic amine-functionalized random copolymer.[58] Adding a 4:1 mixture of Mg^{2+} and Ca^{2+} to the complex coacervate of these polymers enhanced complexation and increased the mass of the concentrated phase. Wet adhesion to bones was tested after curing with sodium periodate (pH 7.4, 24 h, 100% humidity), and was improved with an increasing amount of metal cations. It was hypothesized that singly charged amine groups of the polymer were replaced by the doubly charged metal ions, supposedly leading to a conformational change in the network and stronger adhesion. Despite the addition of the metal ions and sodium periodate for covalent crosslinking of catechol, limited bond strengths of only 1/3 of the natural sandcastle worm glue were measured.

Hereafter, Shao and Stewart further investigated the influence of adding divalent cations to complex coacervates using a slightly different system. This material was prepared from a cationic aminated collagen hydroxylate polymer, and an anionic copolymer of monoacryloxyethyl phosphate and dopamine methacrylamide.[61] The resulting complex coacervates were toughened with either Ca^{2+} or Mg^{2+}, resulting in solidification of the complex with increasing metal concentration and pH. Optimal bond strengths were obtained by covalent curing of the catechol moieties through oxidation by sodium periodate. Magnesium-containing complexes adhered with 0.77 MPa to aluminum, which was 40% higher compared to calcium-enhanced complexes (Table 2.2).[61]

Subsequent work presented a calcium-enhanced adhesive for craniofacial reconstruction,[62] a process where loose bone parts of the face or skull are repositioned and fixated for improved bone healing. The adhesive was tested in rats and it maintained alignment of the fixated bones, improved bone regeneration, and it was biodegradable. Blood did not dilute the adhesive nor did it flow in between the adhesive and bone interface, which is one of the key advantages of using complex coacervate based systems.
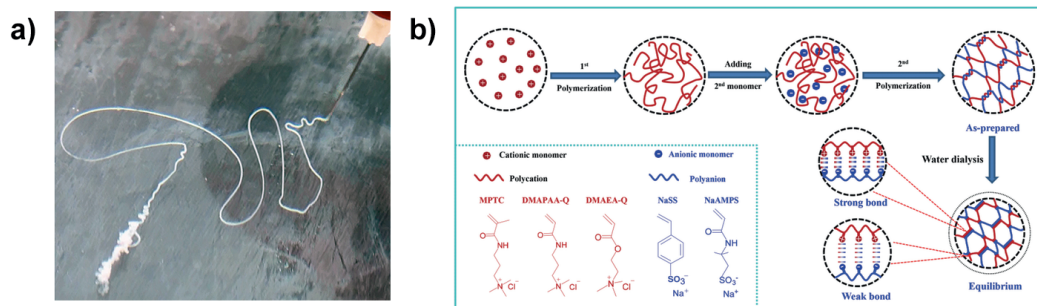
Figure 2.7 – a) Kaur et al. developed an adhesive via a combination of complex coacervation and a separate covalently crosslinked network. The water-insoluble adhesive displayed shear thinning behavior which enabled extrusion from a syringe. Reprinted with permission from Ref. 59. Copyright 2011 American Chemical Society. **b)** An alternative route for preparing double-network systems was applied by Luo et al. A cationic polymer was synthesized, followed by drying and grinding of the product. Subsequently, the ground polymer was dispersed in a solution of anionic monomer, followed by their polymerization. The double-network hydrogel was further strengthened by counterion removal. Copyright by John Wiley & Sons, Inc. (2015). Reprinted with permission from Ref. 60.

Therefore these metal enhanced complex coacervate glues are interesting systems for application in humid environments.

The same material, enhanced by addition of calcium and covalent crosslinking of the catechols, was further strengthened by addition of a separate network of covalently crosslinked poly(ethylene glycol) diacrylate. Crosslinking took about 24 h for reaching a conversion of approximately 40%, and doubled the lap shear strength to 973 kPa (Table 2.2). Moreover, inclusion of the second network induced shear thinning at high shear rates. As a result, the material could be easily dispersed from a syringe as shown in Figure 2.7a.[59] In addition, Mann et al. filled the adhesive with silica nanoparticles and investigated the potential use for sealing fetoscopic defects.[63] Fetoscopy is a procedure where the fetus is evaluated or treated during pregnancy by entering the uterus, which has to be sealed post treatment. The adhesive was tested by adhering a patch onto model tissue. The glue spread nicely over the tissue/patch interface, thereby sealing the defect; exposure to a water solution did not result in leakage. Human cells did not reveal any cytotoxicity after exposure, which is promising for future research of this and similar adhesives.[64]

Ion-crosslinked polyelectrolytes

A simplification of ion-crosslinked systems was proposed by Lapitsky and coworkers who prepared a gel from cationic polyallylamine (120-200 kDa) combined with multivalent anionic pyrophosphate or tripolyphosphate.[65, 66] Because of the high charge density on the polymer, high crosslinking densities enabled both anions to form stiff gels with storage moduli of about 400 kPa. Adhesion strengths comparable to natural wet-adhesives (0.35-0.45 MPa) were observed for attachment to both hydrophilic

and hydrophobic surfaces, using a universal testing machine. Interestingly, adhesion to the hydrophilic surface resulted in cohesive failure, while adhesion to the hydrophobic surface showed adhesive failure. This means that the interactions between the gel and hydrophilic surface were stronger than the bonds to the hydrophobic surface. Remarkable features of this adhesive were its ease of production and facile upscaling; the order of mixing did not make a difference and bulk quantities of the precursors were inexpensive. Additionally, the pH and ionic strength could be used to adjust the storage modulus from 60 to 400 kPa, and to adjust the tensile strength from 0.05 to 0.45 MPa.[65, 66]

Promising ionic materials for use in adhesives

Polyelectrolyte complexation

Several additional systems based on electrostatic interactions have been reported in literature, but have not yet been investigated for their adhesive performance. Since some of these systems may be interesting for use in adhesives, a selection will be provided below.

Zhang et al. used ring-opening polymerization to synthesize two oppositely charged copolypeptides from randomly copolymerized N-carboxyanhydride monomers.[67] Using this method, the researchers tried to mimic the proteins of the sandcastle worm (aiming for similar chemical functionality and molecular weight), while reducing nature's complexity. Six different amino acids were used: aromatic DOPA and tyrosine, nonpolar glycine, cationic lysine, polar serine and anionic phosphoserine. At high salt concentrations, i.e. 4.0-4.7 M, the oppositely charged polymers formed complex coacervates. At lower salt concentrations, however, complexation was inhibited due to a net negative charge on the material. Because of oxidation of DOPA, complex coacervates darkened with time. Using an acidic buffer solution, oxidation could be prevented and surface tensions were reduced, i.e. 35 mN m^{-1} for non-buffered and 15 mN m^{-1} for buffered coacervates. In rheology, exceptionally high shear thinning (4 orders of magnitude) was observed for non-buffered coacervates. In addition, the rheological data revealed long relaxation times showing long lifetimes of interchain connections and a relatively low storage modulus, representing a low crosslinking density. It would be interesting to study the adhesive performance of this material, because it exhibits features that are promising for underwater adhesion.[67]

For transcatether embolization, Jones et al. developed a polyelectrolyte complex from polycationic salmine sulfate and polyanionic phytic acid, enhanced with tantalum powder.[68] Transcatheter embolization is a method for blocking blood vessels by injecting a liquid embolic, to stop bleeding or selectively disrupt blood supply to certain (e.g. cancer) tissues. Liquid embolics have to be injectable, but have to be insoluble in blood and stiff enough to block the blood vessel. A high salt concentration (1.2 M) resulted in a fluid-like material that, upon injection in the blood vessel, formed a gel at physiological conditions (0.15 M salt) while it shrank by only 3%. Tantalum powder was added to increase the viscosity, that also resulted in shear thinning behavior that is

advantageous for injection. The tantalum-enhanced polyelectrolyte complex was injectable, fully blocked the vessel till the deepest capillaries, and kept its position for the first 90 minutes after injection. Furthermore, non-toxic materials were used and thus no toxic response was observed. However, the individual components have very short life-times in blood and therefore long term stability of the complex has to be investigated.

Double-networks

An innovative strategy to obtain ionic hydrogels was suggested by Luo et al. Instantaneous homogeneous materials were obtained by first polymerizing the cation, followed by drying and powdering. The ground polycation was subsequently immersed in a solution containing anionic monomers, followed by their polymerization (Figure 2.7b).[60, 69] The resulting polyion complexes, were elastic but soft ($\sim$0.1 MPa stress at 16 mm/mm strain in tensile testing) due to an excess of counterions that remained in the hydrogel after polymerization. Equilibration of the hydrogels in deionized water resulted in shrinkage, but doubled the strength and toughness. Despite the low amount of unbound ions, bonds could break and reform, as was shown by the gradual disappearance of stress after deformation. In addition to not being cytotoxic, the hydrogels were stable at a pH ranging from 0 to 12, at salt concentrations up to physiological conditions (0.15 M salt) and till temperatures as high as 90 °C.[60] In subsequent research, Luo et al. showed that small changes in the monomer structure had a large impact on the properties of the gel. They showed that the introduction of methyl groups on the polymer backbone (i.e. acrylates were exchanged for methacrylates, and acrylamides for methacrylamides) stiffened the chain and strengthened the ionic bonds, which resulted in tougher hydrogels. The choice for an acrylamide- or acrylate-based monomer changed the morphology of the hydrogels as well, resulting in varying stiffnesses, extensibilities and self-recovering properties. These examples demonstrate that the combination of polyelectrolyte complexation and optimization of the monomer structure can be an innovative approach for designing self-healing adhesive materials.

Besides sandcastle worms and mussels, plenty of other organisms are capable of strong underwater adhesion. This includes the larvae of the caddisfly, which were mimicked by Lane et al.[70] Caddisfly larvae live in water and use silk to form composite protective structures from objects out of their surroundings. This silk consists of a double-network of proteins that lack DOPA and are mainly nonpolar, highly phosphorylated and contain large amounts of Ca^{2+}. It is suggested that Ca^{2+} forms complexes with the silk proteins, however, the most interesting mechanical properties are likely caused by the double-network structure. Therefore Lane et al. chose to synthesize a metal-ion-enriched double-network gel from acrylamides, and methacrylates that bear carboxylate, hydroxyl and phosphate side chains. After hydrogel formation, divalent cations were introduced that enabled complexation with the phosphate and carboxylate groups. Tough hydrogels, with a maximum yield stress of 3.5 MPa (Zn^{2+}), were obtained by optimizing the phosphate content. For calcium-enhanced hydrogels,

System & conditions	Substrate	Wet/dry	Solvent conditions	Strength		Ref.
mfp-3s						
u	Mica	Dry	N/A	3.7	mJ m^{-2}	47
Quaternized chitosan/catechol functionalized poly(acrylic acid) (30 mol%)						
u	Glass	Wet	Water	2000	mJ m^{-2}	55
u, w/o catechol functionalization	Glass	Wet	Water	$\sim$0	mJ m^{-2}	55
Random copolymer of 3-(3,4-dihydroxyphenyl)-2-hydroxypropyl acrylate (30 mol%), 2-(diethylamino)ethylacrylate						
(6 mol%), acrylic acid (4 mol%), hydroxyethyl acrylate (51 mol%), methyl acrylate (9 mol%)						
u	Mica	Wet	Water (pH 7)	32.9	mJ m^{-2}	43
Zwitterions						
Z-Cat-C10, u	Mica	Wet	Deionized water	10.1	mJ m^{-2}	57
Z-Cat-C10, o, dried	Silicon	Dry	N/A	175	mJ m^{-2}	57
Z-Cat-C4, u	Mica	Wet	Deionized water	19.2	mJ m^{-2}	57
Z-Cat-C8, u	Mica	Wet	Deionized water	2.5	mJ m^{-2}	57
Z-Ben-C8, u (benzene i/o cat)	Mica	Wet	Deionized water	0	mJ m^{-2}	57
Z-Cat-Cat, u (cat i/o alkyl)	Mica	Wet	Deionized water	8.1	mJ m^{-2}	57

Table 2.1 – Overview of adhesion strengths of electrostatically-based adhesives measured by SFA. Complex coacervates are depicted as polycation/polyanion. Unoxidized DOPA (u), oxidized DOPA (o), coacervated (c) and catechol (Cat).

a high stiffness (10.3 MPa) was combined with self-healing properties (90% recovery of the initial length and modulus after being unloaded for 90 min). This behavior was attributed to the rupture and rebonding of the phosphate/Ca^{2+} salt bridges.[70] This material exhibits an interesting combination of a covalently crosslinked double-network and reversible electrostatic crosslinks, which is essential for the design of an adhesive.

System & conditions	Substrate	Wet/dry	Solvent conditions	Strength		Ref.
mfp-5						
u	Aluminum	Dry	N/A	1.1	MPa	51
u, c HA	Aluminum	Dry	N/A	1.7	MPa	51
mfp-131						
u	Aluminum	Dry	N/A	1.87	MPa	52
u, c HA	Aluminum	Dry	N/A	4	MPa	52
mfp-151						
u	Aluminum	Dry	N/A	1.98	MPa	52
u, c HA	Aluminum	Dry	N/A	3.17	MPa	52
u, c HA	Aluminum	Wet	Deionized water	0.24	MPa	52
o, c HA	Aluminum oxide	Wet	Water	0.88	MPa	6
o, c HA, w/o DOPA	Aluminum oxide	Wet	Water	0.11	MPa	6
Poly(acrylamide-*co*-aminopropyl methacrylamide)/2-(methacryloyloxy) ethyl phosphate dopamine methacrylamide						
o	Bone	Wet	Phosphate buffer, 170 mM (pH 7.4)	0.06	MPa	58
o, Ca^{2+}	Bone	Wet	Phosphate buffer, 170 mM (pH 7.4)	0.1	MPa	58
Aminated collagen hydroxylate/poly(monoacryloxyethyl phosphate-*co*-dopamine methacrylamide)						
u, Ca^{2+}	Aluminum	Wet	Water (pH 7.4, 37 °C)	0.27	MPa	61
u, Mg^{2+}	Aluminum	Wet	Water (pH 7.4, 37 °C)	0.65	MPa	61
o, Ca^{2+}	Aluminum	Wet	Water (pH 7.4, 37 °C)	0.55	MPa	61
o, Mg^{2+}	Aluminum	Wet	Water (pH 7.4, 37 °C)	0.77	MPa	61
poly(acrylamide-*co*-aminopropyl methacrylamide)/2-(methacryloyloxy) ethyl phosphate dopamine methacrylamide						
o, Ca^{2+}	Aluminum	Wet	Water (RT)	0.512	MPa	59
o, Ca^{2+}, DN 17.7 wt%	Aluminum	Wet	Water (RT)	0.973	MPa	59

Table 2.2 – Overview of adhesion strengths of electrostatically-based adhesives measured by lap shear tests. Complex coacervates are depicted as polycation/polyanion. Unoxidized DOPA (u), oxidized DOPA (o), coacervated (c) and hyaluronic acid (HA).

Conclusion

In this chapter several materials were discussed of which adhesion was tested in different ways. Despite these differences, we compare the adhesive strength of the materials to find trends for obtaining optimal adhesive properties (Table 2.1 and Table 2.2). At first, for strong adhesion, it is necessary to balance the cation and anion content in the adhesive materials. When either one of the two charges was present in the adhesive material, such as in uncomplexed proteins, very low adhesive strengths were found, while adhesion improved after complex coacervation with a polycounterion.[47, 51, 52] In addition, only one unit of (each) charge per molecule was insufficient to obtain strong bonding, while multiple charged groups per molecule showed stronger adhesion. This can be deduced from the strong adhesion of the complex coacervate of quaternized chitosan/catechol functionalized poly(acrylic acid), compared to the zwitterions, and the low molecular weight copolymer of Seo et al., independent of the fact that these materials include catechol groups.[43, 55, 57] However, it seems that the addition of multiple catechol groups enhanced the adhesive strength, because the absence of catechol groups strongly reduced the adhesive strength in three systems.[6, 55, 57] An even higher adhesive performance, especially in wet conditions, could be obtained by oxidizing the catechol groups, which can lead to covalent cross linking of the adhesive.[6, 52, 61] At last, inclusion of metal ions or a second covalent network into the adhesive material further enhanced the adhesive strength of complex coacervate based materials.[58, 59, 61]

Acknowledgements

Bibliography

[1] G. Walker. The histology, histochemistry and ultrastructure of the cement apparatus of three adult sessile barnacles, elminius modestus, balanus balanoides and balanus hameri. *Mar. Biol.*, 7:239–248, 1970.

[2] J. H. Waite, N. H. Andersen, S. Jewhurst, and C. Sun. Mussel adhesion: Finding the tricks worth mimicking. *J. Adhes.*, 81:297–317, 2005.

[3] R. J. Stewart, J. C. Weaver, D. E. Morse, and J. H. Waite. The tube cement of phragmatopoma californica: a solid foam. *J. Exp. Biol.*, 207:4727–4734, 2004.

[4] R. J. Stewart, T. C. Ransom, and V. Hlady. Natural underwater adhesives. *J. Polym. Sci. Part B Polym. Phys.*, 49:757–771, 2011.

[5] M. E. Yu, J. Y. Hwang, and T. J. Deming. Role of l-3,4-dihydroxyphenylalanine in mussel adhesive proteins. *J. Am. Chem. Soc.*, 121:5825–5826, 1999.

[6] H. J. Kim, B. H. Hwang, S. Lim, B.-H. Choi, S. H. Kang, and H. J. Cha. Mussel adhesion-employed water-immiscible fluid bioadhesive for urinary fistula sealing. *Biomaterials*, 72:104–111, 2015.

[7] H. Lee, B. P. Lee, and P. B. Messersmith. A reversible wet/dry adhesive inspired by mussels and geckos. *Nature*, 448:338–341, 2007.

[8] H. Lee, N. F. Scherer, and P. B. Messersmith. Single-molecule mechanics of mussel adhesion. *Proc. Natl. Acad. Sci. U. S. A.*, 103:12999–13003, 2006.

[9] E. Faure, C. Falentin-Daudré, C Jérôme, J. Lysakawa, D. Fournier, P. Woisel, and C. Detrembleur. Catechols as versatile platforms in polymer chemistry. *Prog. Polym. Sci.*, 38:236–270, 2013.

[10] S. Moulay. Dopa/catechol-tethered polymers: Bioadhesives and biomimetic adhesive materials. *Polym. Rev.*, 54:436–513, 2014.

[11] P. K. Forooshani and B. P. Lee. Recent approaches in designing bioadhesive materials inspired by mussel adhesive protein. *J. Polym. Sci. Part A Polym. Chem.*, 55:9–33, 2017.

[12] M. Krogsgaard, V. Nue, and H. Birkedal. Mussel-inspired materials: Self-healing through coordination chemistry. *Chem. Eur. J.*, 22:844–857, 2016.

[13] J. H. Waite. Mussel adhesion - essential footwork. *J. Exp. Biol.*, 220:517–530, 2017.

[14] R. J. Stewart, C. S. Wang, I. T. Song, and J. P. Jones. The role of coacervation and phase transitions in the sandcastle worm adhesive system. *Adv. Colloid Interface Sci.*, 239:88–96, 2017.

[15] R. J. Stewart, C. S. Wang, and H. Shao. Complex coacervates as a foundation for synthetic underwater adhesives. *Adv. Colloid Interface Sci.*, 167:85–93, 2011.

[16] B. J. Endrizzi and R. J. Stewart. Glueomics: An expression survey of the adhesive gland of the sandcastle worm. *J. Adhes.*, 85:546–559, 2009.

[17] M. J. Stevens, R. E. Steren, V. Hlady, and R. J. Stewart. Multiscale structure of the underwater adhesive of phragmatopoma californica: A nanostructured latex with a steep microporosity gradient. *Langmuir*, 23:5045–5049, 2007.

[18] H. Zhao, C. Sun, R. J. Stewart, and J. H. Waite. Cement proteins of the tube-building polychaete phragmatopoma californica. *J. Biol. Chem.*, 280:42938–42944, 2005.

[19] C. S. Wang and R. J. Stewart. Multipart copolyelectrolyte adhesive of the sandcastle worm, phragmatopoma californica (fewkes): Catechol oxidase catalyzed curing through peptidyl-dopa. *Biomacromolecules*, 14:1607–1617, 2013.

[20] S. L. Perry and C. E. Sing. Prism-based theory of complex coacervation: Excluded volume versus chain correlation. *Macromolecules*, 48:5040–5053, 2015.

[21] C. S. Wang and R. J. Stewart. Localization of the bioadhesive precursors of the sandcastle worm, phragmatopoma californica (fewkes). *J. Exp. Biol.*, 215:351–361, 2012.

[22] C. S. Wang, K. K. Svendsen, and R. J. Stewart. *Biological Adhesive Systems; From Nature to Technical and Medical Application*. Springer Vienna, 1 edition, 2010.

[23] E. Spruijt. *Strength, structure and stability of polyelectrolyte complex coacervates*. PhD thesis, Wageningen University, 2012.

[24] D. S. Hwang, H. Zeng, A. Srivastava, D. V. Krogstad, M. Tirrell, J. N. Israelachvili, and J. H. Waite. Viscosity and interfacial properties in a mussel-inspired adhesive coacervate. *Soft Matter*, 6:3232–

3236, 2010.

[25] S. Kim, J. Huang, Y. Lee, S. Dutta, H. Y. Yoo, Y. M. Jung, Y. S. Jho, H. Zeng, and D. S. Hwang. Complexation and coacervation of like-charged polyelectrolytes inspired by mussels. *Proc. Natl. Acad. Sci. U. S. A.*, 5:3191–3202, 2016.

[26] S. Kim, H. Y. Yoo, J. Huang, Y. Lee, S. Park, Y. Park, S. Jin, Y. M. Jung, H. Zeng, D. S. Hwang, and Y. Jho. Salt triggers the simple coacervation of an underwater adhesive when cations meet aromatic pi electrons in sewater. *ACS Nano*, 11:6764–6772, 2017.

[27] H. Zeng, D. S. Hwang, J. N. Israelachvili, and J. H. Waite. Strong reversible fe3+-mediated bridging between dopa-containing protein films in water. *Proc. Natl. Acad. Sci. U. S. A.*, 107:12850–12853, 2010.

[28] C. J. Sun, G. E. Fantner, J. Adams, P. K. Hansma, and J. H. Waite. The role of calcium and magneium in the concrete tubes of the sandcastle worm. *J. Exp. Biol.*, 210:1481–1488, 2007.

[29] J. Yang, M. A. Cohen Stuart, and M. Kamperman. Jack of all trades: versatile catechol crosslinking mechanisms. *Chem. Soc. Rev.*, 43:8271–8298, 2014.

[30] H. G. Silverman and F. F. Roberto. Understanding marine mussel adhesion. *Mar. Biotechnol.*, 9:661–681, 2007.

[31] T. Priemel, E. Degtyar, M. N. Dean, and M. J. Harrington. Rapid self-assembly of complex bio-molecular architectures during mussel byssus biofabrication. *Nat. Commun.*, 8:14539–14551, 2017.

[32] R. Mirshafian, W. Wei, J. N. Israelachvili, and J. H. Waite. α,β-dehydro-dopa: A hidden participant in mussel adhesion. *Biochemistry*, 55:743–750, 2016.

[33] L. Petrone, A. Kumar, C. N. Sutanto, N. J. Patil, S. Kannan, A. Palaniappan, S. Amini, B. Zappone, C. Verma, and A. Miserez. Mussel adhesion is dictated by time-regulated secretion and molecular conformation of mussel adhesive proteins. *Nat. Commun.*, 6:8737–8749, 2015.

[34] B. K. Ahn. Perspectives on mussel-inspired wet adhesives. *J. Am. Chem. Soc.*, 139:10166–10171, 2017.

[35] B. P. Lee, P. B. Messersmith, J. N. Israelachvili, and J. H. Waite. Mussel-inspired adhesives and coatings. *Annu. Rev. Mater. Res.*, 41:99–132, 2011.

[36] V. V. Papov, T. V. Diamond, K. Biemann, and J. H. Waite. Hydroxyarginine-containing polyphenolic proteins in the adhesive plaques of the marine mussel mytilus edulis. *J. Biol. Chem.*, 270:20183–20192, 1995.

[37] H. Zhao, N. B. Robertson, S. A. Jewhurst, and J. H. Waite. Probing the adhesive footprints of mytilus californianus byssus. *J. Biol. Chem.*, 281:11090–11096, 2006.

[38] J. H. Waite and X. Qin. Polyphosphoprotein from the adhesive pads of mytilus edulis. *Biochemistry*, 40:2887–2893, 2001.

[39] H. Zhao and J. H. Waite. Linking adhesive and structural proteins in the attachment of plaque of mytilus californianus. *J. Biol. Chem.*, 281:26150–26158, 2006.

[40] D. S. Hwang, H. Zeng, A. Masic, M. J. Harrington, J. N. Israelachvili, and J. H. Waite. Protein- and metal-dependent interactions of a prominent protein in mussel adhesive plaques. *J. Biol. Chem.*, 285:25850–25858, 2010.

[41] G. P. Maier, M. V. Rapp, J. H. Waite, J. N. Israelachvili, and A. Butler. Adaptive synergy between catechol and lysine promotes wet adhesion by surface salt displacement. *Science*, 349:628–632, 2015.

[42] W. Wei, L. Petrone, Y. Tan, H. Cai, J. N. Israelachvili, A. Miserez, and J. H. Waite. An underwater surface-drying peptide inspired by a mussel adhesive protein. *Adv. Funct. Mater.*, 26:3496–3507, 2016.

[43] S. Seo, S. Das, P. J. Zalicki, R. Mirshafian, C. D. Eisenbach, J. N. Israelachvili, J. H. Waite, and A. K. Ahn. Microphase behavior and enhanced wet-cohesion of synthetic copolyampholytes inspired by a mussel foot protein. *J. Am. Chem. Soc.*, 137:9214–9217, 2015.

[44] W. Wei, J. Yu, C. Broomell, J. N. Israelachvili, and J. H. Waite. Hydrophobic enhancement of dopa-mediated adhesion in a mussel foot protein. *J. Am. Chem. Soc.*, 135:377–383, 2013.

[45] J. Yu, W. Wei, E. Danner, R. K. Ashley, J. N. Israelachvili, and Waite J. H. Mussel protein adhesion depends on thiol mediated redox modulation. *Nat. Chem. Biol.*, 7:588–590, 2012.

[46] S. C. T. Nicklisch, J. E. Spahn, H. Zhou, C. M. Gruian, and J. H. Waite. Redox capacity of an extracellular matrix protein associated with adhesion in mytilus californianus. *Biochemistry*, 55:2022–2030, 2016.

[47] W. Wei, Y. Tan, N. R. Martinez Rodriguez, J. Yu, J. N. Israelachvili, and J. H. Waite. A mussel-derived one component adhesive coacervate. *Acta Biomater.*, 10:1663–1670, 2014.

[48] Q. Lu, D. S. Hwang, Y. Liu, and H. Zeng. Molecular interactions of mussel protective coating protein, mcfp-1, from mytilus californianus. *Biomaterials*, 33:1903–1911, 2012.

[49] L. Li and H. Zeng. Marine mussel adhesion and bio-inspired wet adhesives. *Biotribol.*, 5:44–51, 2016.

[50] M. A. Gebbie, W. Wei, A. M. Schrader, T. R. Cristiani, H. A. Dobbs, M. Idso, B. F. Chmelka, J. H. Waite, and J. N. Israelachvili. Tuning underwater adhesion with cation-π interactions. *Nat. Chem.*, 9:473–479, 2017.

[51] Y. S. Choi, D. G. Kang, S. Lim, Y. J. Yang, C. S. Kim, and H. J. Cha. Recombinant mussel adhesive protein fp-5 (map fp-5) as a bulk bioadhesive and surface coating material. *Biofouling*, 27:729–737, 2011.

[52] S. Lim, D. G. Choi, Y. S. Kang, Y. H. Song, and H. J. Cha. The adhesive properties of coacervated recombinant hybrid mussel adhesive proteins. *Biomaterials*, 31:3715–3722, 2010.

[53] H. J. Kim, B.-H. Choi, S. H. Jun, and H. J. Cha. Sandcastle worm-inspired blood-resistant bone graft binder using a sticky mussel protein for augmented in vivo bone regeneration. *Adv. Healthc. Mater.*, 113:E847–E853, 2016.

[54] D. S. Hwang, Y. Gim, H. J. Yoo, and H. J. Cha. Practical recombinant hybrid mussel bioadhesive fp-151. *Biomaterials*, 28:3560–3568, 2007.

[55] Q. Zhao, D. W. Lee, B. K. Ahn, S. Seo, Y. Kaufman, J. N. Israelachvili, and J. H. Waite. Underwater contact adhesion and microarchitecture in polyelectrolyte complexes actuated by solvent exchange. *Nat. Mater.*, 15:407–412, 2016.

[56] C. K. Roy, H. L. Guo, T. L. Sun, A. Bin Ihsan, T. Kurokawa, M. Takahata, T. Nonoyama, T. Nakajima, and J. P. Gong. Self-adjustable adhesion of polyampholyte hydrogels. *Adv. Mater.*, 27:7344–7348, 2015.

[57] B. K. Ahn, S. Das, R. Linstadt, Y. Kaufman, N. R. Martinez-Rodriguez, R. Mirshafian, E. Kesselman, Y. Talmon, B. H. Lipshutz, J. N. Israelachvili, and J. H. Waite. High-performance mussel-inspired adhesives of reduced complexity. *Nat. Commun.*, 6:8663–8670, 2015.

[58] H. Shao, K. N. Bachus, and R. J. Stewart. A water-borne adhesive modeled after the sandcastle glue of p. californica. *Macromol. Biosci.*, 9:464–471, 2009.

[59] S. Kaur, G. M. Weerasekare, and R. J. Stewart. Multiphase adhesive coacervates inspired by the sandcastle worm. *ACS Appl. Mater. Interfaces*, 3:941–944, 2011.

[60] F. Luo, T. L. Sun, T. Nakajima, T. Kurokawa, Y. Zhao, K. Sato, A. Bin Ihsan, X. Li, H. Guo, and J. P. Gong. Oppositely charged polyelectrolytes form tough, self-healing, and rebuildable hydrogels. *Adv. Mater.*, 27:2722–2727, 2015.

[61] H. Shao and R. J. Stewart. Biomimetic underwater adhesives with environmentally triggered setting mechanisms. *Adv. Mater.*, 22:729–733, 2010.

[62] B. D. Winslow, H. Shao, R. J. Stewart, and P. A. Tresco. Biocompatibility of adhesive complex coacervates modeled after the sandcastle glue of phragmatopoma californica for craniofacial reconstruction. *Biomaterials*, 31:9373–9381, 2010.

[63] L. K. Mann, R. Papanna, K. J. Moise, R. H. Byrd, E. J. Popek, S. Kaur, S. C. G. Tseng, and R. J. Stewart. Fetal membrane patch and biomimetic adhesive coacervates as a sealant for fetoscopic defects. *Acta Biomater.*, 8:2160–2165, 2012.

[64] R. Papanna, L. K. Mann, S. C. G. Tseng, R. J. Stewart, S. S. Kaur, M. M. Swindle, T. R. Kyriakides, N. Tatevian, and K. J. Moise Jr. Cryopreserved human amniotic membrane and a bioinspired underwater adhesive to seal and promote healing of iatrogenic fetal membrane defect sites. *Placenta*, 36:888–894, 2015.

[65] Y. Huang, P. G. Lawrence, and Y. Lapitsky. Self-assembly of stiff, adhesive and self-healing gels from common polyelectrolytes. *Langmuir*, 30:7771–7777, 2014.

[66] P. G. Lawrence and Y. Lapitsky. Ionically cross-linked poly(allylamine) as a stimulus-responsive underwater adhesive: Ionic strength and ph effects. *Langmuir*, 31:1564–1574, 2015.

[67] L. Zhang, V. Lipik, and A. Miserez. Complex coacervates of oppositely charged co-polypeptides inspired by the sandcastle worm glue. *J. Mater. Chem. B*, 4:1544–1556, 2016.

[68] J. P. Jones, M. Sima, R. G. O□Hara, and R. J. Stewart. Water-borne endovascular embolics inspired by the undersea adhesive of marine sandcastle worms. *Adv. Healthcare Mater.*, 5:795–801, 2016.

[69] F. Luo, T. L. Sun, T. Nakajima, T. Kurokawa, X. Li, H. Guo, Y. Huang, H. Zhang, and J. P. Gong. Tough polyion-complex hydrogels from soft to stiff controlled by monomer structure. *Polymer*, 116:487–497, 2017.

[70] D. D. Lane, S. Kaur, G. M. Weerasakare, and R. J. Stewart. toughened hydrogels inspired by aquatic caddisworm silk. *Soft Matter*, 11:6981–6990, 2015.

Synthesis of thermo-responsive polyelectrolytes by reversible addition-fragmentation chain transfer polymerization (RAFT)

3

The polymers that were discussed in this thesis, were synthesized through Reversible Addition-Fragmentation chain Transfer (RAFT) polymerization. By using RAFT, control over the polymerization reaction is obtained, resulting in the formation of polymers with well-defined molecular weights and narrow polydispersities (M_w/M_n).[1, 2, 3, 4] Also, RAFT permits reinitiation of the polymerization, enabling the synthesis of block copolymers with well-defined compositions. In this chapter, we will briefly introduce RAFT and describe the syntheses performed to obtain temperature-responsive polyelectrolytes.

Introduction

Mechanism

RAFT polymerization is a type of free radical polymerization (FRP). In FRP, polymers are synthesized through the formation of a radical by a conventional initiator, which initiates chain propagation. The chain grows quickly till termination occurs. Over time, new chains are initiated and shorter chains are produced, as the monomer concentration decreases, resulting in broad polydispersities. To obtain low polydispersities, propagation of the chains should occur simultaneously and termination should be prevented. This control can be achieved by creating a dormant state of the propagating radical.[1, 3] The dormant state can be obtained through reversible addition of the propagating chain to a chain transfer agent (CTA). This CTA, or RAFT agent, often contains a thiobenzoate or trithiocarbonate group that enables reversible chain transfer.

The mechanism of RAFT polymerization is shown in Scheme 3.1. Similar to FRP, the polymerization is initiated by the formation of a propagating chain through a conventional radical initiator, step I. The propagating chain attaches to the CTA, leading to the subsequent release of the leaving group R, step II. The radical-carrying R-group initiates a new polymer chain, step III, which can reversibly bind to the CTA, leading to the release of the previously attached dormant chain, step IV. Equilibrium between propagating and dormant chains provides control over the reaction, leading to a simultaneous growth of all polymer chains. Termination can occur as in all radical polymerizations, step V, by either combination or disproportionation, but is limited by using a relatively low amount of radicals.[3, 4]

Selection of the chain transfer agent

For obtaining good control over the polymerization, the CTA has to be chosen carefully to match the selected monomer. Two classes of monomers can be distinguished, more activated monomers (MAMS), and less activated monomers (LAMS).[3] MAMS are monomers where the vinyl group is attached to an aromatic, carbonyl or nitrile group, such as styrene, methacrylates or acrylamides, Scheme 3.2. LAMS on the other hand have an electron donating group attached to the vinyl group. These monomers are for example N-vinylpyrrolidone or vinyl acetate. Most RAFT agents provide good control over the polymerization of MAMS while they inhibit or retard the polymerization of LAMS, or the other way around. When making copolymers, it is therefore important to realize whether the desired polymer is synthesized from MAMS or LAMS.

To select a good CTA the R- and Z- group have to be considered, Scheme 3.1. As mentioned before, R is the radical leaving group of the CTA, see step II, while Z can
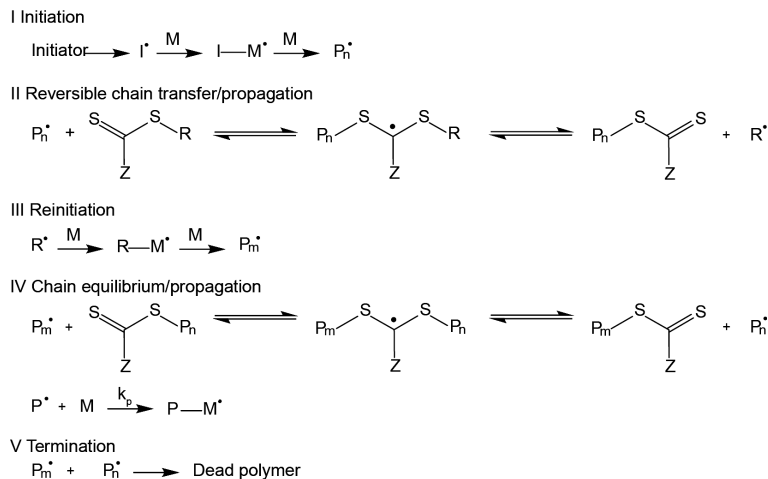
Scheme 3.1 – Reaction scheme of RAFT polymerization.

either activate or deactivate the sulphur double bond, and influences the stability of the intermediate radicals and dormant state. For fast initiation, rapid fragmentation, i.e., cleavage of the R-group, is required without causing any side reactions. Furthermore, the R-group should be able to reinitiate the polymerization, i.e. step III.[1, 3] From these conditions, a difference in reactivity is observed between methacrylates or methacrylamides, and acrylates or acrylamides. Methacrylates are more efficient in radical stabilization, and are therefore better leaving groups than acrylates.[3] As a result, R-groups for methacrylate polymerization should be a better leaving group, or radical stabilizer, as well.[4] If this condition is not met, a methacrylate chain is more likely to cleave from the intermediate radical, than the R-group, which prevents efficient reinitiation. Furthermore, in block copolymer synthesis, the block originating from the least reactive monomer should be synthesized first to allow efficient reinitiation and thus prevent the formation of homopolymers of the second monomer. At last, when synthesizing block copolymers, the Z-group of the RAFT agent should be suitable for both monomers.[2, 3]

Reaction conditions

When choosing the correct reaction conditions for a RAFT polymerization, three relations are important. At first, the ratio between the monomers and RAFT agent determines the degree of polymerisation which provides control over the molecular weight of the polymer. For this reason, the length of the polymers, and thus the block ratios in copolymers, can be controlled. Additionally, the ratio between the RAFT agent and initiator determines the number of chains initiated by the RAFT agent (R-group), or by the initiator. In addition, large amounts of initiator will lead to more termination, and therefore to higher polydispersities. Furthermore, terminated polymers
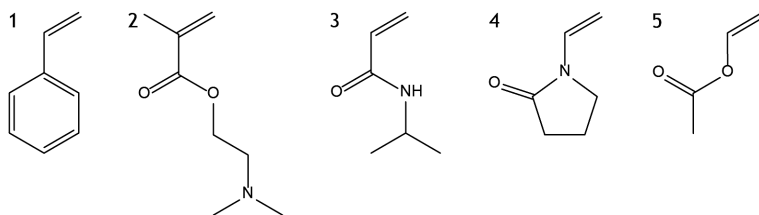
Scheme 3.2 – Examples of MAMS, **1** styrene, **2** 2-(dimethylamino)ethyl methacrylate, **3** *N*-isopropylacrylamide, and LAMS, **4** *N*-vinylpyrrolidone, **5** vinylacetate.

cannot be reinitiated which makes copolymerization impossible. At last, the polymerization rate is influenced by the initiator to monomer ratio, and by the concentration of all reactants, i.e. low concentrations increase the reaction time. When the aforementioned three ratios are taken together, the chain length of a well-controlled RAFT polymerization, can be predicted using Equation 5.1.

$$M_n \approx ([M]_0 - [M]_t)/([CTA]_0) * m_M + m_{CTA} \qquad (3.1)$$

Here, $[M]_0$ and $[CTA]_0$ are the monomer and RAFT agent concentration at the start of the reaction, respectively, $[M]_t$ is the monomer concentration at time t, and m_M and m_{CTA} are the molecular weights of the monomer and RAFT agent, respectively. Equation 5.1 is valid when sufficiently low initiator concentrations are used, allowing the neglection of chains formed by the initiator. In addition, to reduce the number of dead chains, monomer conversions are generally kept below 70%.[2, 3, 4]

The formation of unwanted side products through termination or disproportionation can be monitored by following the change in monomer concentration over time.[5] The rate of propagation, R_p, of a polymerization is expressed by Equation 3.2,

$$R_p = k_p * [M^\bullet] * [M]_t \qquad (3.2)$$

where k_p is the rate constant for propagation, Scheme 3.1, and [M•] is the concentration of chain radicals. From this formula, it can be determined that the change in monomer concentration with time, t, is given by:

$$log([M]_0)/[M]_t) = k_p * [M^\bullet] * t = k_{app} * t \qquad (3.3)$$

In case of a well-controlled polymerization, the chain radical concentration is constant, leading to a linear relation between $log(([M]_0/[M]_t))$ and t, and a slope that is equal to the apparent rate constant, k_{app}. In case of termination or a badly controlled polymerization, the chain radical concentration decreases as will be observed by a decreasing slope. Therefore, the degree of control on the polymerization can be assessed by following the monomer conversion during polymerization, as is done for the PNIPAM-*b*-PDMAEMA-*b*-PNIPAM polymerization.

Polymers synthesized for this thesis

In this thesis, trithiocarbonates were used as CTA for the synthesis of triblock co-polymers of *tert*-butylacrylate (*t*BA) flanked with *N*-isopropylacrylamide (NIPAM) blocks, both MAMS. The first CTA is the symmetric trithiocarbonate agent *S*,*S*'-bis(α,α'-dimethyl-α''-acetic acid) trithiocarbonate (BDAT) that has two R groups, Structure 1 in Scheme 3.3. The second CTA is a symmetric R-coupled trithiocarbonate, i.e. *C*,*C*'-[1,4-phenylenebis(methylene)] *C*,*C*'-dipropyl ester carbonotrithioic acid (CDP), Scheme 3.3, structure 2. Symmetric CTAs are convenient for the synthesis of symmetric ABA block copolymers in two synthesis steps. The reason for using two different CTAs are the block ratios of the desired polymers. When synthesizing triblock copolymers with asymmetric block lengths it is practically advantageous to synthesize the small block first. In this thesis, a polymer with only 20% PNIPAM was used, requiring the PNIPAM block to be synthesized first, and a polymer with 81% PNIPAM was prepared, which required *t*BA to be polymerized first. By using these two CTAs, the same block copolymer architecture could be obtained, even though the polymerization order was inverted for practicality. In addition, the order of the monomers could be easily converted as the reactivity of acrylates and acryl-amides are similar.[3] Also, CDP is an R-linked difunctional RAFT agent, which enables the synthesis of hydrolytically stable, symmetric triblock copolymers.[3] At last, CDP contains propyl Z-groups instead of the more commonly used dodecyl tails, which avoids the formation of aggregates in aqueous solutions. After successful polymerization, the PNIPAM-*b*-P*t*BA-*b*-PNIPAM copolymers will be converted into PNIPAM-*b*-PAA-*b*-PNIPAM by cleaving the *t*BA groups under acidic conditions, resulting in thermoresponsive polyanions.

Furthermore, it was attempted to synthesize narrow disperse temperature-responsive polycations, from PNIPAM and PDMAEMA. The polymerization of PNIPAM-*b*-PDMAEMA-*b*-PNIPAM involves the combination of a methacrylate and an acrylamide, requiring PDMAEMA to be synthesized before PNIPAM. For
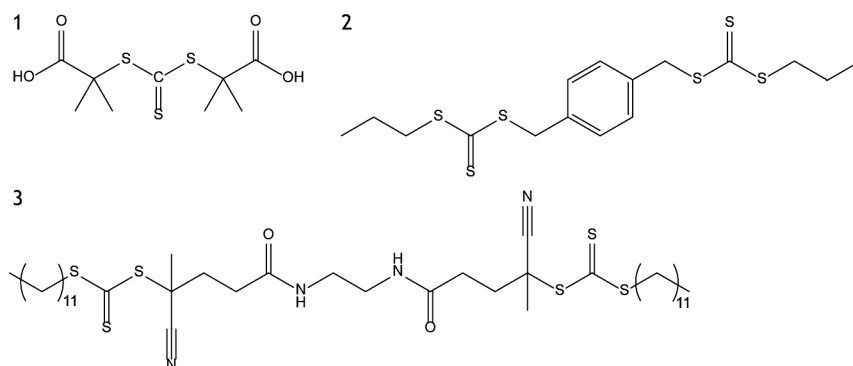
Scheme 3.3 – CTAs used for the synthesis of PNIPAM-*b*-PAA-*b*-PNIPAM, **1** BDAT and **2** CDP, and for the synthesis of PNIPAM-*b*-PDMAEMA-*b*-PNIPAM, **3** diCDTPA.

this reason, the convergent RAFT agent BDAT is unsuitable for this polymerization as it synthesizes from the outside to the inside of the triblock, which would result in PDMAEMA-*b*-PNIPAM-*b*-PDMAEMA leading to the undesired architecture. Furthermore, DMAEMA is a better leaving group than the dimethyl carboxylic acid R-group of BDAT, leading to poor control over the polymerization.[6] In addition, CDP is generally used for the polymerization of polystyrenes and acrylates/acrylamides, and unsuitable for the synthesis of a methacrylate.[7] As an alternative, a bisadduct of 4-cyano-4-[(dodecylsulfanylthiocarbonyl)sulfanyl]pentanoic acid (CDTPA) was prepared by using a Steglich esterification, structure 3 Scheme 3.3. For methacrylates, the cyano-containing R-group is known to provide better control over the polymerization.[8]

Experimental

Materials

Triethylamine (TEA) (≥99%), propanethiol (99%), carbon disulphide (≥99%), 4-cyano-4-[(dodecylsulfanylthiocarbonyl)sulfanyl]pentanoic acid (97%) (CDTPA), *N,N'*-dicyclohexylcarbodiimide (97%) (DCC), acetic acid (≥99.8%), saturated sodium bicarbonate solution, magnesium sulphate, 1,4-dioxane (99.8%), *N*-isopropyl-acrylamide (NIPAM) (97%), azobisisobutyronitrile (AIBN) (98%), *tert*-butylacrylte (*t*BA) (98%), aluminium oxide (neutral, Brockmann I) and hydrochloric acid (37%) were purchased from Sigma Aldrich and used as received. NIPAM (97%) was purchased from TCI, and 1,4-bis(chloromethyl)benzene (BCMB) (98%), 4-(dimethylamino)pyridine (99%) (DMAP), and hydrochloric acid (37%) were obtained from Acros organics. Dichloromethane (anhydrous, 99.7%) (DCM) was purchased from Alfa Aesar, and ethylenediamine and ninhydrin were purchased from Fluka. Methanol (HPLC grade), DCM (AR), diethyl ether (AR), 1,1,1,3,3,3-hexafluoro-2-propanol (HFIP) (AR), ethyl acetate (analytical reagent grade (AR)), acetone (AR), and *n*-hexane (HPLC grade) were purchased from Biosolve and used as received. Sodium hydroxide solution (TitriPUR, 0.1 M) was bought from Merck chemicals. The chain transfer agent (BDAT) was synthesized following a previously described procedure.[9, 10] AIBN and NIPAM were recrystallized twice from methanol and *n*-hexane, respectively, and kept refrigerated before use. Furthermore, *t*BA and DMAEMA were passed over a basic alumina column to remove inhibitor and used immediately.

Methods

Synthesis of poly(*N*-isopropylacrylamide) from BDAT

A round-bottom flask was charged with 31 mg (0.19 mmol) AIBN, 266 (94.2 mmol) mg BDAT, 8.5 g (75 mmol) NIPAM, and 43 mL dioxane (initiator:CTA:monomer (i:R:m) as 0.2:1:80, [m] 0.8 M). The reactants were dissolved and the mixture was sparged with nitrogen for 60 minutes. The polymerization took place at 70 °C for 85 minutes. Subsequently, the reaction was quenched by exposure to air and rapid cooling. ^{1}H-NMR of the reaction mixture indicated a monomer conversion of 89%. The resulting polymer was purified by precipitation from dioxane into di-ethyl ether twice. The final product was dried in a vacuum oven. ^{1}H-NMR (400 MHz, D_2O): δ 1.05 (s, 6H), 1.36 - 2.1 (m, 3H), 3.80 (s, 1H), 6.24 (s, 1H) ppm and M_n 8.3 kDa. GPC (HFIP): M_n 7.6 kDa and M_w/M_n 1.26.

Synthesis of PNIPAM-*b*-P*t*BA-*b*-PNIPAM from BDAT based PNIPAM

A round-bottom flask was loaded with 16 mg (0.10 mmol) AIBN, 4.1 g (0.54 mmol) PNIPAM macro-CTA, 24.4 g (190 mmol) *t*BA and 48 mL dioxane (i:R:m as 0.2:1:380, [m] 3.9 M). The reactants were dissolved and the mixture was purged with nitrogen for 60 minutes. The polymerization took place for 55 minutes at 70 °C, till a conversion of 62%. The reaction was quenched by exposure to air and rapid cooling. The polymer was purified by precipitation in a cold methanol/water mixture, 3/1 v/v, for three times. A dry product was obtained by redissolving in minimal DCM and subsequent drying under vacuum using a rotavap and vacuum oven, subsequently. ^{1}H-NMR (400 MHz, $CDCl_3$): δ 1.11 (s, 6H, $(CH_2)_2$ isopropyl), 1.4-1.5 (s, 9H, $(CH_3)_3$ *tert*-butyl), 1.6 – 2.2 (m, backbone), 3.99 (s, 1H, CH isopropyl) ppm, M_n 30.2 kDa, 20 mole% PNIPAM. ^{13}C-NMR (400 MHz, MeOD): δ 22.38 $((CH_3)_2$ isopropyl), 28.07 $((CH_3)_3$ *tert*-butyl), 36 – 40 (backbone), 41.9 (CH isopropyl), 42.38 (backbone), 174.12 ((C=O)N amide) ppm.

Deprotection of PNIPAM-*b*-P*t*BA-*b*-PNIPAM

The resulting *t*BA-copolymer was deprotected by dissolving 16.8 g of the polymer in 860 mL HFIP containing 0.12 M (1 equivalent) HCl and the mixture was left to stir for 3 hours.[11] The sample was dried by rotary evaporation and redissolved in water, and subsequently by neutralization using 0.1 M sodium hydroxide solution. The polymer solution was centrifuged to remove any insoluble byproducts and was further purified by dialysis against water to remove the remaining monomer. The final product was obtained after freeze drying. ^{1}H-NMR (400 MHz, MeOD): δ 1.16 (s, 6H, $(CH_3)_2$ isopropyl), 1.4 - 2.3 (m, backbone), 3.97 (s, 1H, CH isopropyl) ppm. ^{13}C-NMR (400 MHz, D_2O): δ 21.65 $((CH_3)_2$ isopropyl), 35 – 40 (backbone), 41.8 (CH isopropyl), 44.80 (backbone), 175.4 ((C=O)N amide), 183.4 ((C=O)OH carboxylic acid) ppm. GPC (sodium phosphate buffer in H_2O): M_n 26.8 kDa and M_w/M_n 1.59.

Synthesis of divalent RAFT agent CDP

The chain transfer agent *C,C'*-[1,4-phenylenebis(methylene)] *C,C'*-dipropyl ester carbonotrithioic acid (CDP) was synthesized using an adapted method previously described by Bivigou-Koumba et al.[12] 2.6 g (34 mmol) carbon disulphide and 2.5 g (33 mmol) propanethiol were added to 10 mL chloroform and purged with nitrogen for 30 minutes. Subsequently, 3.5 g (35 mmol) TEA was added dropwise to the solution, resulting in a dark orange/yellow solution that evolved heat. The solution was left to stir for 30 minutes and subsequently 2.8 g (16 mmol) BCMB was added under nitrogen flow, again resulting in a warm solution. The solution was stirred overnight and subsequently diluted with 10 mL of chloroform, transferred to a separation funnel and washed thrice with 50 mL water. The organic layer was dried over magnesium sulphate and concentrated under reduced pressure. The resulting product was purified by recrystallization from DCM twice, and yielded a dark yellow solid, 5.8 g (90 %). ^{1}H-NMR (400 MHz, CDCl$_3$, Figure A3.1): δ 1.03 (t, 6H, CH$_3$ propyl), 1.74 (s6, 4H, CH$_2$ propyl), 3.54 (t, 4H, CH$_2$ propyl), 4.60 (s, 4H, CH$_2$ methyl), 7.29 (s, 4H, benzyl) ppm. ^{13}C-NMR (400 MHz,): δ 13 (CH$_3$), 22(CH$_2$ propyl), 39 (CH$_2$ thiol), 40(CH$_2$-aryl), 130 (CH aryl), and 135 (C aryl) ppm.

Synthesis of P*t*BA from CDP

A round-bottom flask was loaded with 4.6 mg (0.028 mmol) AIBN, 230 mg (0.57 mmol) CDP, 15.5 g (121 mmol) *t*BA, and 44 mL dioxane (i:R:m as 0.05:1:210, [m] 2 M). The clear yellow solution was purged with nitrogen for 60 minutes. The polymerization took place for 5 h at 70 °C, till a conversion of 80% was reached. The reaction was quenched by exposure to air and rapid cooling. The polymer was purified by precipitation into a cold 3/1 (v/v) methanol/water mixture three times. The product was obtained as a yellow powder by drying in a vacuum oven and yielded 10 g (83%). ^{1}H-NMR (400 MHz, CDCl$_3$): δ 1.4 (s, 9H, (CH$_3$)$_3$ *tert*-butyl), 1.6 – 2.3 (m, backbone) ppm, M_n 21.5 kDa. GPC (HFIP): M_n 22.0 kDa, M_w/M_n 1.25.

Synthesis of PNIPAM-*b*-P*t*BA-*b*-PNIPAM from CDP containing P*t*BA

In a round-bottom flask 1.6 mg (0.0097 mmol) AIBN from a stock solution, 4.0 g (0.18 mmol) P*t*BA and 28.1 g (248 mmol) NIPAM were dissolved in 100 mL dioxane (i:R:m as 0.05:1:1250, [m] 2 M). The reactants were dissolved and the mixture was purged with nitrogen for 150 min. The polymerization was allowed to run for 6 h at 70 °C, till a conversion of 65% was reached. Subsequently, the reaction was quenched by exposure to air and rapid cooling. The resulting polymer was purified by precipitation into a 4/1 (v/v) *n*-hexane/diethyl ether mixture for five times. The final product was dried in a vacuum oven to yield 17 g white powder. ^{1}H-NMR (400 MHz, MeOD): δ 1.17 (s, 6H, (CH$_2$)2 isopropyl), 1.49 (s, 9H, (CH$_3$)$_3$ *tert*-butyl), 1.55 – 2.3 (m, backbone), 3.98 (s, 1H, CH isopropyl) ppm, M_n 92.0 kDa, 81 mole% PNIPAM. GPC (HFIP): M_n 61.6 kDa and M_w/M_n 1.61.

Deprotection of PNIPAM-*b*-P*t*BA-*b*-PNIPAM

The resulting block-copolymer was deprotected by dissolving 6 g in 140 mL HFIP, containing 0.1 M hydrochloric acid (1.8 equivalent) and the mixture was left to stir for 5 h at room temperature.[11] The sample was dried using rotary evaporation, redissolved in water and neutralized by using 1 M sodium hydroxide solution. The final product was obtained after freeze drying. ^{1}H-NMR (400 MHz, MeOD): δ 1.16 (s, 6H, $(CH_3)_2$ isopropyl), 1.55 - 2.3 (m, backbone), 3.97 (s, 1H, CH isopropyl).

Synthesis of diCDTPA

diCDTPA was synthesized by following an adapted literature procedure.[13] A 25 mL oven-dried two-neck round-bottom flask was filled with 0.199 g of CDP (0.493 mmol), which was then purged to remove oxygen. After CDP was dissolved in 2.4 mL anhydrous DCM, the flask was cooled to 0 °C by using an ice bath. Meanwhile, another flask was filled with 0.0176 g DMAP (0.144 mmol) and purged with nitrogen. Next, 0.11 mL ethylene diamine (0.0967 g, 1.61 mmol) and 7 mL anhydrous DCM were added. Then, 1.0 mL of the ethylene diamine (14 mg, 0.23 mmol) and DMAP (0.021 mmol) stock solution was added to the CDP solution. Immediately afterwards, the reaction was started by addition of 0.118 g (0.572 mmol) DCC. Initially the reaction was allowed to proceed at 0 °C for 4 h. Progress of the reaction was monitored by TLC, using ninhydrin and KMnO4 staining, and was allowed to proceed at room temperature till completion. The mixture was diluted with 20 mL DCM and filtered. The filtrate was further diluted with DCM until a volume of 50 mL and subsequently washed three times with 50 mL saturated sodium bicarbonate solution. The organic layer was dried over magnesium sulphate and concentrated under reduced pressure. The product was purified by silica column chromatography using a 4/1 (v/v) hexane/ethyl acetate mixture. After impurities had eluted, the eluent was slowly changed to pure ethyl acetate to collect the product. The solvent was removed under reduced pressure and the product, a yellow solid, was further dried under vacuum. ^{1}H-NMR (DMSO): δ 0.85 (t, 6H, CH_3), 1.24 (s, 32H, alkyl), 1.34 (t, 2H, CH_2), 1.64 (t, 2H, CH_2), 1.85 (s, 3H, CH_3), 2.32 (m, 4H, CH_2-CH_2), 3.10 (s, 2H, CH_2), 3.8 (t, 2H, CH_2), 8.01 (s, 1H, NH) ppm.

Synthesis of PDMAEMA from diCDTPA

A flask was filled with 3.1 mg (0.019 mmol) AIBN, 83.5 mg (0.10 mmol) diCDTPA, 8.5 mL (7.9 g, 50 mmol) DMAEMA, and 11.4 mL anhydrous dioxane (i:R:m as 0.2:1:500, [m] 2.5 M). The reactants were dissolved and the solution was purged for 90 minutes with nitrogen. The polymerization took place for 5 h at 70 °C, till a conversion of 50%. During the reaction, a syringe was used to sample the reaction mixture, and the monomer conversion was determined by NMR. The reaction was quenched by exposure to air and rapid cooling. The resulting polymer was purified by precipitation in *n*-hexane and dried in a vacuum oven. ^{1}H-NMR (CDCl₃): δ 0.91

and 1.05 (d, 3H, CH₃), 1.82 and 1.91 (d, 2H, CH₂), 2.28 (s, 6H, (CH₃)₂), 2.56 (s, 2H, CH₂), 4.06 (s, 2H, CH₂) ppm and M_n 40.1 kDa. GPC: 33.3 kDa, M_w/M_n 1.47.

Synthesis of PNIPAM-*b*-PDMAEMA-*b*-PNIPAM

A flask was loaded with 1.2 mg (0.0073 mmol) AIBN, 1.6 g (0.039 mmol) PDMAE-MA macro-CTA, 0.65 g (5.7 mmol) NIPAM (i:R:m as 0.24:1:250, [m] 1.6 M). The reactants were dissolved in 3.6 mL anhydrous dioxane and the solution was purged with nitrogen for 30 minutes. The polymerization took place for 5 h at 70 °C, till a conversion of 65%. During the reaction, a syringe was used to sample the reaction mixture, and the monomer conversion was determined by NMR. The reaction was quenched by exposure to air and rapid cooling. The solvent was removed under vacuum and the resulting polymer was redissolved in water to be purified by dialysis against water, followed by freeze drying. ¹H-NMR (CDCl₃): δ 0.90 and 1.04 (d, 3H, CH₃), 1.13 (s, 6H, CH₃ isopropyl), 1.3-2.0 (backbone), 2.27 (s, 6H, (CH₃)₂), 2.55 (s, 2H, CH₂), 4.05 (s, 2H, CH₂ and s, 1H, CH isopropyl), M_n 44.3 kDa, 31 mole% PNIPAM. GPC: 16.9 kDa, M_w/M_n 2.7.

Characterization

NMR was used to determine the purity of the products and the block copolymer composition. The measurements were carried out on a Bruker AMX-400 spectrometer (400 MHz) at room temperature. Gel permeation chromatography (GPC) of the polymers in HFIP was performed using an Omnisec Reveal system with an Omnisec Resolve detector, equipped with two PSS PFG columns. The samples were run in HFIP containing 0.02 M potassium trifluoroacetate at a flow rate of 0.7 mL/min. The system was calibrated using narrow PMMA standards. Aqueous GPC was performed on an Agilent 1260 Infinity II gel permeation chromatograph, equipped with a Waters Ultrahydrogel500 column, using a buffer of 0.01 M Na2HPO4/NaH2PO4 with 0.1 M NaNO3 as eluent. The system was calibrated using narrow PMAA standards. GPC of PNIPAM-*b*-PDAMEMA-*b*-PNIPAM and its precursor was run using an Agilent Technologies 1200 series gel permeation chromatograph that was equipped with a PLgel 5 μm Mixed-D column (M_w range 200–400,000 Da, Polymer Laboratories Ltd) and an Agilent 1200 differential refractometer. The column was calibrated using PS standards. Samples were run using tetrahydrofuran with 5% triethylamine as eluent at 35°C and a flow rate of 1 mL/min. Molecular weights (M_n number average molecular weight) (M_n) and M_w/M_n values were calculated with Omnisec software V4.6.

Results and Discussion

Synthesis of PNIPAM-*b*-PAA-*b*-PNIPAM

From BDAT
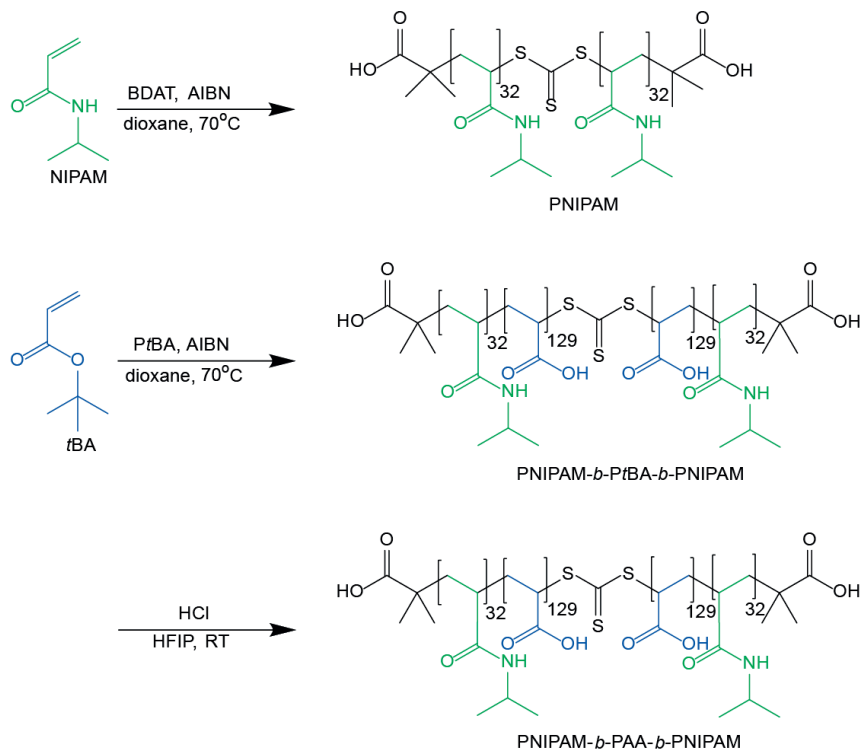
Scheme 3.4 – Reaction mechanism for the synthesis of PNIPAM-*b*-PAA-*b*-PNIPAM from RAFT–agent BDAT. At first the PNIPAM macro-CTA is synthesized, followed by the copolymerization with *t*BA to yield PNIPAM-*b*-P*t*BA-*b*-PNIPAM. Subsequently the *tert*-butyl groups are removed under acidic conditions to yield PNIPAM-*b*-PAA-*b*-PNIPAM.

The PNIPAM-*b*-PAA-*b*-PNIPAM copolymer with a small PNIPAM content was synthesized using the convergent RAFT agent BDAT, Figure Figure 3.1. At first, the PNIPAM macro-CTA was synthesized, followed by copolymerization with *t*BA, to obtain the ABA triblock copolymer, Scheme 3.4. Figure 3.1B shows the GPC traces of the macro-CTA in HFIP and of the deprotected block copolymer in aqueous solution. It can be seen that the peak corresponding to PNIPAM is narrow and shows minor tailing at higher retention volumes. This tail can be either caused by termination

of active chains, or by undesired interactions between the column and the PNIPAM polymer. PNIPAM is known to interact with various column materials, leading to artificially low molecular masses and broader molecular weight distributions. However, from previous experience we know that PSS PFG columns are suitable for the analysis of PNIPAM with molecular weights till 50 kDa. Since the obtained M_w/M_n of 1.26 is still low, the high monomer conversion is likely the cause of the small degree of termination and can be decreased by using lower initiator concentrations.[4] The GPC trace of the copolymer is slightly broader, i.e. a M_w/M_n of 1.59 was measured and the M_n deviates from the conversion obtained value. A small asymmetry is observed in the GPC peak, which can either be explained by the presence of terminated chains in the macro-CTA, or by interactions with the column. However, the polymers were measured at different machines and it is hard to judge which of the two hypotheses is right. From the GPC data, PNIPAM has a M_n of 7.6 kDa (DP 64). From the integrals in NMR, Figure 3.1C, the degree of polymerization of the tBA is calculated to be 258, leading to a M_n 40.7 kDa for PNIPAM-b-PtBA-b-PNIPAM. As a result, the copolymer consists of 20 mole% PNIPAM, Table 3.1.
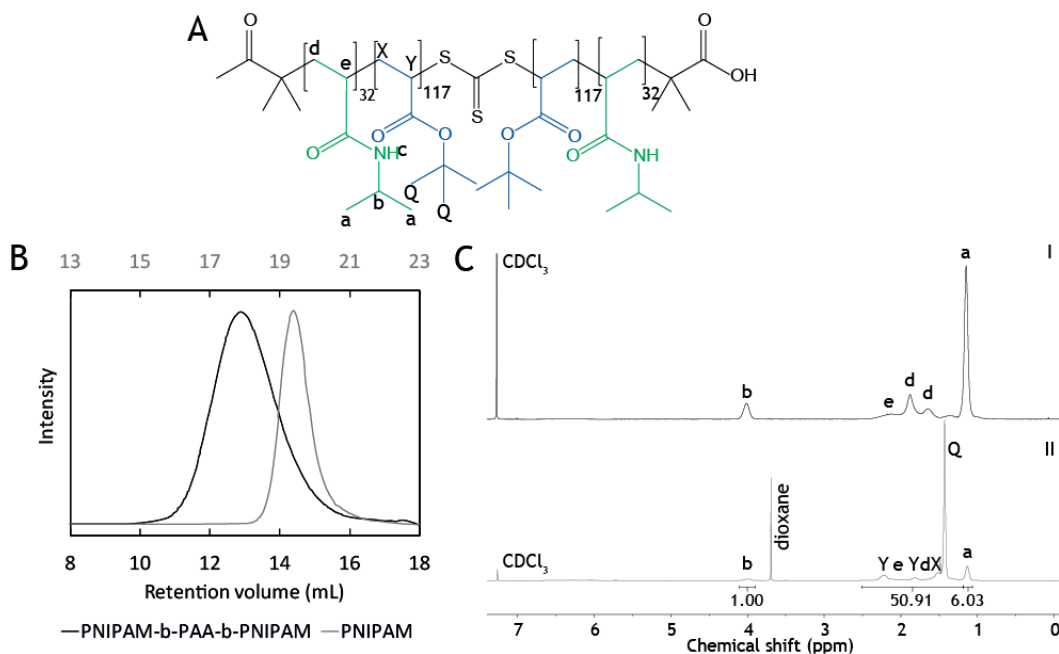

Figure 3.1 – **A** Chemical structure of the PNIPAM-b-PtBA-b-PNIPAM polymer synthesized from BDAT. **B** GPC traces of the PNIPAM macro-CTA, and PNIPAM-b-PAA-b-PNIPAM, synthesized using BDAT. The macro-CTA was measured using HFIP (grey), and the block copolymer was measured using aqueous GPC (black). The intensities are normalized to the maximum detector response. Note that the spectra cannot be compared as a result of using different GPC setups. **C** ^{1}H-NMR in CDCl$_3$ of the PNIPAM macro-CTA (I) and the block copolymer PNIPAM-b-PtBA-b-PNIPAM (II). The groups are assigned as in A.

Polymer	m : R : i	[m]$_0$	Time	Conv.	$M_{n,calc}$	$M_{n,GPC}$	M_w/M_n	PNIPAM content
	-	M	h	%	kDa	kDa	-	mole%
N-B	80 : 1 : 0.2	0.8	1.5	89	8.3	7.6	1.26	-
NTN-B	380 : 1 : 0.2	3.9	1	62	37.8	n.a.	n.a.	20
NAN-B	380 : 1 : 0.2	3.9	1	62	24.6	26.8	1.59	20
T-C	210 : 1 : 0.05	2.0	5	80	21.9	17.6	1.25	-
NTN-C	1250 : 1 : 0.05	2.0	6	65	110	61.6	1.61	82

Table 3.1 – Synthesis conditions for the PNIPAM-*b*-P*t*BA-*b*-PNIPAM polymers. The PNIPAM macro CTA from BDAT is abbreviated as N-B, the P*t*BA macro CTA from CDP is noted as T-C, and NTN represents the PNIPAM-*b*-P*t*BA-*b*-PNIPAM block copolymers containing BDAT (B) and CDP (C). For the copolymer synthesized from BDAT, GPC data are available for PNIPAM-*b*-PAA-*b*-PNIPAM, therefore the polymer is also noted after deprotection as NAN-B. The $M_{n,calc}$ is calculated from the monomer conversion as determined by NMR and, for the block copolymers, summed with the $M_{n,GPC}$ from the macro-CTA. The PNIPAM content is calculated using the integral ratio by NMR, and the $M_{n,GPC}$ of the macro-CTA.

From CDP

The PNIPAM-*b*-PAA-*b*-PNIPAM copolymer with a large PNIPAM content was synthesized using the divergent RAFT agent CDP, Scheme 3.5. At first, the P*t*BA macro-CTA was synthesized, followed by a copolymerization with NIPAM to obtain the BAB triblock copolymer. The GPC traces of the macro-CTA and the block copolymer are shown in Figure 3.2A and B, and are measured in HFIP. It can be seen that the peak of the P*t*BA is narrow and highly symmetric, also a low M_w/M_n of 1.25, and similar M_n values are found when NMR and GPC results are compared. These observations indicate that CDP provided good control over the P*t*BA synthesis and that termination was limited. The signal of the PNIPAM-*b*-P*t*BA-*b*-PNIPAM copolymer shifted to lower retention volumes and broadened. As a result, a M_w/M_n of 1.61 is obtained, and large deviations are found between M_n values obtained with GPC and conversion. Moreover, the peak has a shoulder at higher retention volumes, indicating the presence of smaller molecules. As the shoulder does not overlap with the P*t*BA macro-CTA, it can be concluded that all P*t*BA chains are extended. The smaller polymers can therefore be terminated block copolymers, or PNIPAM homopolymers. Interactions between PNIPAM and the column are unlikely, as those usually show up in the data by long tails instead of shoulders.

Using this RAFT agent, Bivigou-Koumba et al. previously synthesized PNIPAM, yielding a M_w/M_n of 1.25, which is equal to the M_w/M_n obtained for the P*t*BA macro-CTA used here.[12] However, for their chain extension, using styrene, lower M_w/M_n values of 1.33 were obtained. In the copolymerization of P*t*BA with NIPAM, different measures were taken to ensure a low M_w/M_n, i.e. the ratio between RAFT agent and initiator was halved compared to Bivigou-Koumba et al., and low conversions were achieved, typically <70%. Moreover, it was shown by Bivigou-Koumba et al. that
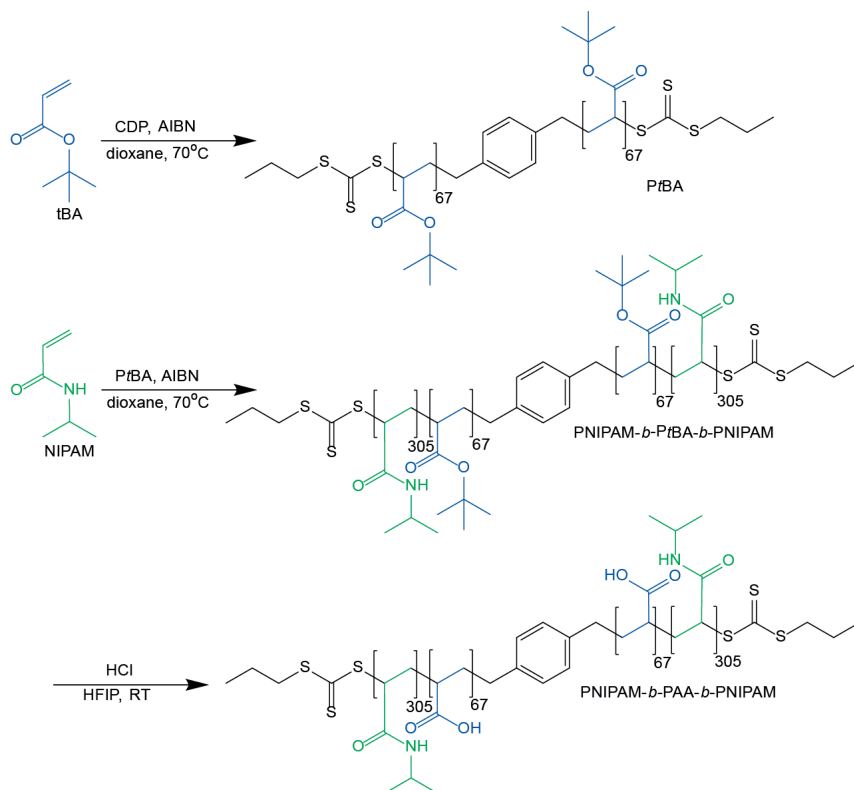
Scheme 3.5 – Reaction mechanism for the synthesis of PNIPAM-*b*-PAA-*b*-PNIPAM from RAFT-agent CDP. At first the P*t*BA macro-CTA is synthesized, followed by the copolymerization with NIPAM to yield PNIPAM-*b*-P*t*BA-*b*-PNIPAM. Subsequently the *tert*-butyl groups are removed under acidic conditions to yield PNIPAM-*b*-PAA-*b*-PNIPAM.

the RAFT agent CDP is able to control NIPAM polymerizations till 50 kDa. For these reasons, the slightly higher M_w/M_n can only be explained by the high degree of polymerization for NIPAM which may also cause the shoulder at high retention volumes. In addition small factors such as the quality of the NIPAM, solvent, or degassing may contribute.[4] From GPC, an M_n of 17.6 kDa (DP 134) was measured for P*t*BA. From the integrals in the NMR, Figure 3.2C, a NIPAM degree of polymerization of 610 is calculated, leading to a M_n of 86.8 kDa for the PNIPAM-*b*-P*t*BA-*b*-PNIPAM. As a result, the polymer has 82 mole% NIPAM over *t*BA.

Deprotection of PNIPAM-*b*-P*t*BA-*b*-PNIPAM

After successful synthesis of PNIPAM-*b*-P*t*BA-*b*-PNIPAM, the block copolymers were converted into PNIPAM-*b*-PAA-*b*-PNIPAM by cleaving the *tert*-butyl groups in HFIP under acidic conditions at room temperature. The more commonly used
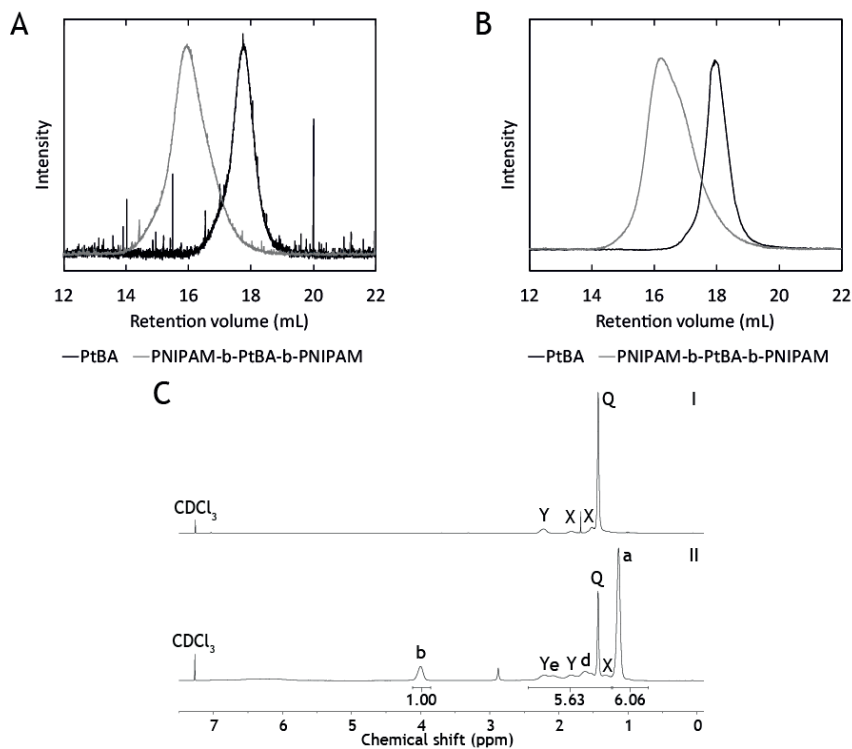
Figure 3.2 – HFIP GPC traces from **A** the light scattering and **B** the RI signal. The intensities of the GPC curves are normalized to the maximum detector response. **C** ^{1}H-NMR in CDCl$_3$ of the PtBA macro-CTA (I), and PNIPAM-b-PtBA-b-PNIPAM (II), the peaks are assigned as in Figure 3.1
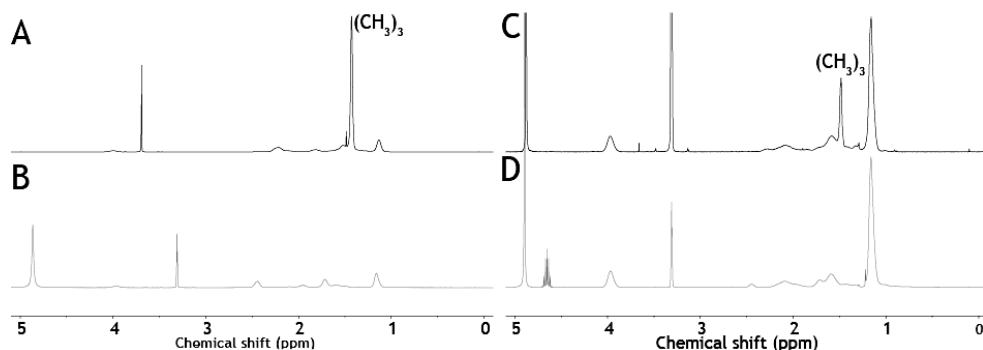
Figure 3.3 – ^{1}H-NMR of block copolymers synthesized with **A**, **B** BDAT and **C**, **D** CDP. The PNIPAM-*b*-P*t*BA-*b*-PNIPAM are shown in A and C, while the deprotected polymers, PNIPAM-*b*-PAA-*b*-PNIPAM, are shown in B and D. The signal in the upper spectrum of figure A is slightly shifted as this sample was prepared from CDCl$_3$, while all other spectra are measured in MeOD.

and slower TFA/DCM method frequently results in incomplete deprotection, i.e. yields polymers that still contain small amounts of *t*BA, as was discovered by Filippov et al.[11] These small amounts of *t*BA were found to significantly affect the viscosity of PNIPAM-*b*-PAA-*b*-PNIPAM in water. As our triblock copolymers are prepared for application in aqueous solution, the *t*BA groups should be completely removed. NMR, Figure 3.3, demonstrated full cleavage of the *t*BA groups for the polymers used in this thesis, as can be observed by the disappearance of the *tert*-butyl peaks.

Synthesis of PNIPAM-*b*-PDMAEMA-*b*-PNIPAM

From diCDTPA

The RAFT agent diCTPA was synthesized through a Steglich esterification, using the carboxylic acid groups of CDTPA and ethylene diamine as linker. To avoid the formation of mono-functionalized ethylene diamine, CDTPA was added in excess. As a result, unreacted CDTPA will be present in the crude reaction mixture and has to be fully separated to enable the synthesis of monodisperse block copolymers. By NMR in DMSO-d6, the purity of diCDTPA can be assessed by checking the carboxylic acid signals, e.g. at 12.5 ppm in a ^{1}H-NMR or at 173 or 157 ppm in a ^{13}C-NMR. DMSO-d6 was used to ensure the observation of a signal for the carboxylic acid peaks, even at low amounts. In the product, typical signals of carboxylic acid groups are absent, Figure 3.4A. Furthermore, the integration of the peaks at low chemical shifts, Figure 3.4B, are all within a 10% deviation from the theoretical value, indicating that no reactants or side products remained and a pure product was obtained. The purification of diCDTPA turned out to be challenging. To obtain a good separation of CDTPA and diCDTPA, long columns should be used and the solvent should be slowly changed from the 4/1 hexane/ethylacetate mixture to pure ethylacetate.
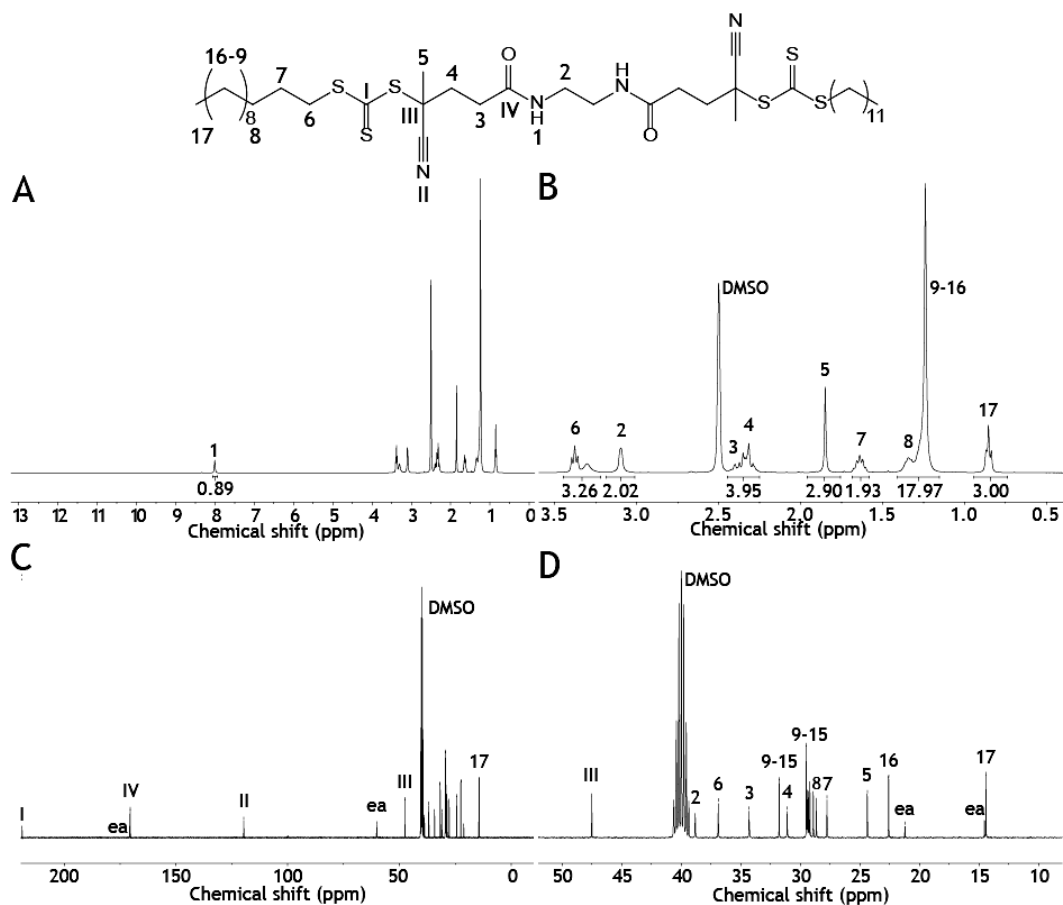
Figure 3.4 – NMR spectra (DMSO-d6) of diCDTPA after esterification and purification. Both, **A** the full and **B** a more detailed ^{1}H-spectrum of the low ppm values are shown. Also, **C**, **D** the ^{13}C-spectra are depicted, in which traces of ethylacetate are depicted as ea. The peaks are assigned based on a HSQC NMR, Figure A3.2.
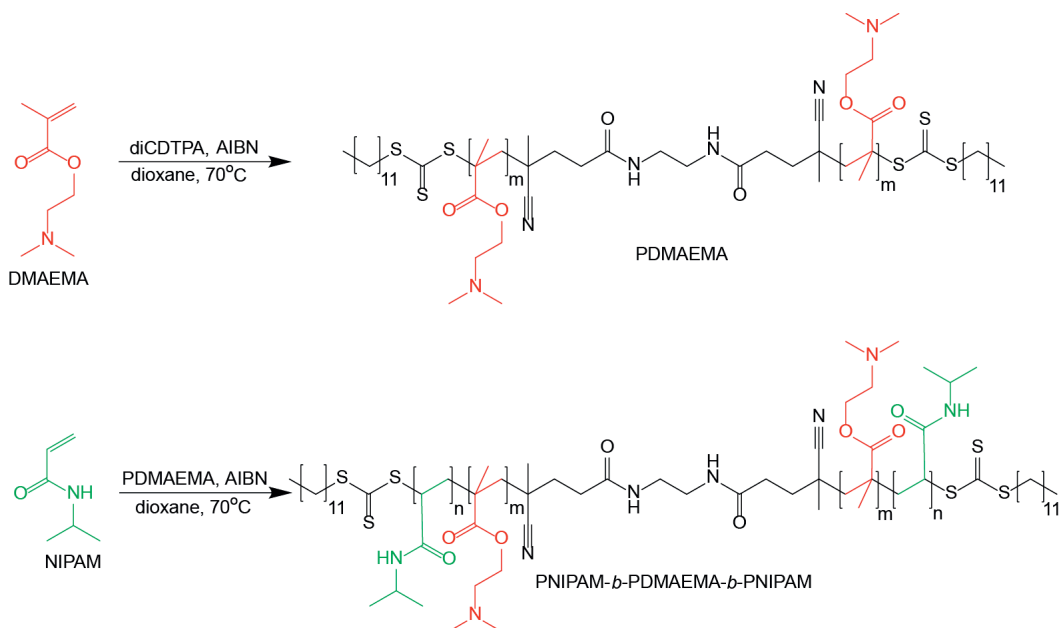
Synthesis of PDMAEMA from diCDTPA

Kinetics of the polymerization of DMAEMA using diCDTPA as a CTA was studied by sampling the reaction mixture, Table 3.2 and Figure 3.5 . By sampling regularly, the conversion of monomers could be followed by ^{1}H-NMR. A linear relation between the time and $\log(M_0/M_t)$ shows that unwanted side reactions, such as termination, are sufficiently suppressed during the reaction, as is observed for all three reactions, Figure 3.5.[1, 4] However, reaction 2 shows unexpected behaviour. In polymerization 2, the initiator concentration is doubled compared to polymerization 1. Higher initiator concentrations should result in a faster polymerization and a shorter inhibition time, however, the inhibition period was elongated. Polymerization 3 was performed to confirm that the conversion could be increased by using a longer reaction time, which was indeed the case. Furthermore, a 23% difference is found between the highest and lowest k_{app} versus time. The observed variation in the data can have two causes. First, the reaction was sampled using a syringe. By doing so, oxygen may be introduced into the reaction vessel causing termination of propagating chains, and a subsequent decreasing reaction rate. To avoid termination, a large reaction mixture can be split into smaller batches, purged and reacted at different times. When deoxynation is ensured for each batch, less variation in the reaction rate might be observed. However, the influence of sampling seems minimal here, as the conversions keep increasing linearly. Second, and more likely, are the low amounts, 1.3 - 3.8 mg, of AIBN that have been used to initiate these polymerizations. Although the balance should be sufficiently accurate, weighing such small amounts may easily introduce relatively large errors. Alternatively, AIBN can be added via a stock solution, of which a considerable volume is required, to obtain smaller deviations in the polymerization kinetics.

Figure 3.5 shows the GPC trace and NMR spectrum of polymerization 1. The acquired M_w/M_n is 1.47, which is slightly high for a controlled radical polymerization, and higher than reported before for the same monomer/CTA combination.[4, 8, 14, 15, 16] However, using a similar protocol with uncoupled CDTPA, M_w/M_n values between 1.40 and 1.48 were found for PDMAEMA. These values are also relatively

Polymer	i : R : m	$[m]_0$	Time	Conv.	k_{app}	$M_{n,NMR}$	$M_{n,GPC}$	M_w/M_n
	-	M	h	%	h^{-1}	kDa	kDa	-
1	0.2 : 1 : 510	2.5	5	50	0.059	40.1	33.3	1.47
2	0.4 : 1 : 550	2.5	6	60	0.077	52.7	n.a.	n.a.
3	0.2 : 1 : 470	2.3	23	91	0.068	68.1	n.a.	n.a.

Table 3.2 – Overview of used reaction conditions for the polymerization of DMAEMA in the presence of diCDTPA. To determine k_{app}, the slope of $\log(M_0/M_t)$ versus time was determined by taking a linear trend line. As some reactions show inhibition, the first data point of reactions 2 and 3 was not taken into account. For reaction 1, the trend line was forced to cross the y-axis at 0, as inhibition seems absent.

Scheme 3.6 – Reaction mechanism for the synthesis of PNIPAM-*b*-PDMAEMA-*b*-PNIPAM from RAFT-agent diCDTPA. At first the PDMAEMA macro-CTA is synthesized, followed by the copolymerization with NIPAM to yield PNIPAM-*b*-PDMAEMA-*b*-PNIPAM.

high for a controlled radical polymerization, but are similar to the value obtained using the difunctional RAFT agent diCDTPA. Therefore, the coupling of the RAFT agents does not influence the control over the polymerization. Improvements on the M_w/M_n can be obtained by lowering the initiator concentration from R : i as 1 : 0.2 to at least 1 : 0.1. From the GPC results, a M_n of 33.3 kDa (DP 210) was found which is different from the M_n of 40.1 kDa that was determined from the conversion. This difference indicates that the reaction conditions should be further improved to obtain a well-controlled radical polymerization.

Synthesis of PNIPAM-*b*-PDMAEMA-*b*-PNIPAM

The monomer conversion over time of the copolymerization of PDMAEMA with NIPAM is presented in Figure 3.7A, and follows a linear trend. However, $\log(M_0/M_t)$ seems to be higher for polymerization 5 than for polymerization 4, while a similar k_{app} is found. A possible origin of this shift is the difficulty of determining the monomer conversion from NMR. The conversion is calculated using trioxane as an internal standard, which is equally distributed over the reaction solvent, noN-volatile, and unable to react, resulting in a constant integral in the NMR measurements during the polymerization. Most often, the ratio between the integrals of the trioxane and vinyl signals is used to determine the monomer conversion. However, the amide sig-
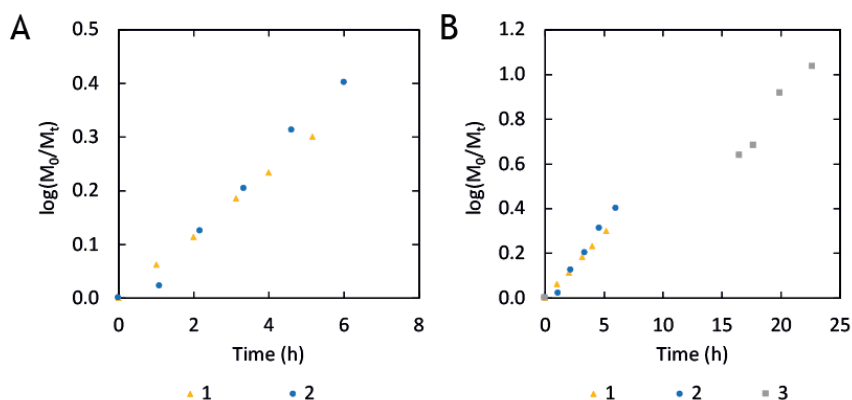
Figure 3.5 – Reaction kinetics of DMAEMA polymerization using diCDTPA. The reaction conditions are mentioned in Table 3.2
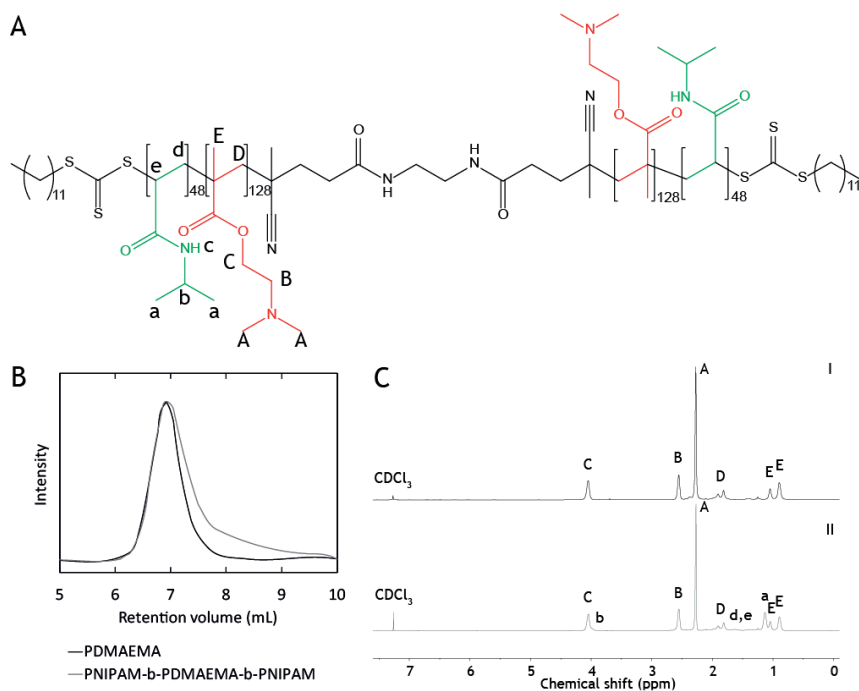

Figure 3.6 – **A** Chemical structure of the PNIPAM-*b*-PDMAEMA-*b*-PNIPAM polymer synthesized from diCDTPA. **B** GPC traces of the PDMAEMA macro-CTA, and PNIPAM-*b*-PDMAEMA-*b*-PNIPAM copolymer (polymerization 4). The GPC measurements were performed in THF using 5% TEA to minimize interactions of PNIPAM with the column. The intensities are normalized to the maximum detector response. **C** ^{1}H-NMR in CDCl$_3$ of the macro-CTA (I) and the block copolymer PNIPAM-*b*-PDMAEMA-*b*-PNIPAM (II). Peaks are assigned as in A.

Polymer	Macro-CTA	i : R : m	[m]$_0$	Time	Conv.	k_{app}	$M_{n,NMR}$	$M_{n,GPC}$	M_w/M_n
		-	M	h	%	h^{-1}	kDa	kDa	-
4	1	0.2 : 1 : 150	1.6	5	65	0.087	44.3	16.9	2.7
5	3	0.2 : 1 : 250	1.5	5	64	0.112	86.2	n.a.	n.a.

Table 3.3 – Overview of used reaction conditions for the copolymerization of PDMAEMA with NIPAM.

nal of PNIPAM, peak c, appears during polymerization and overlaps with the vinyl signal. As a result, the integrals of the vinyl peaks increase, despite the consumption of monomers. Also, in polymerization 4, a relatively low trioxane concentration has been used, making the integration of the signal very sensitive to treatment of the data, e.g. to baseline determination. As an alternative method, the ratio between the trioxane and PNIPAM integrals can be used to determine the conversion. However, the PNIPAM signals overlap with the PDMAEMA signals which complicates the analysis, see Figure 3.7B. Overall, the most reliable monomer conversion is obtained by using the ratio between the integrals of PDMAEMA peak B and the vinyl peak at 6.0 ppm. This vinyl peak is the least affected by the amide signal of the PNIPAM, Figure A3.3. By using this integral ratio, a linear relation between $\log(M_0/M_t)$ and time is found for the copolymerization, suggesting the absence of undesired side reactions and termination. Figure 3.6B shows the GPC trace and NMR of the purified PNIPAM-*b*-PDMAEMA-*b*-PNIPAM copolymer. GPC shows a shoulder at the high elution volumes indicating poor control over the polymerization. Furthermore, it is worth noticing that the peak of the copolymer seems to have the same elution volume as the peak of the macro-CTA, implying that elongation did not take place and that PNIPAM homopolymer was formed. Moreover, PNIPAM is commonly known to cause interactions with the column, leading to artificially high elution volumes and broader molecular weight distributions.[17] To properly evaluate this experiment, column interactions should be prevented, e.g., by using a different column and solvent, such as DMF with LiBr. However, based on syntheses reported before, CDTPA should be able to control the polymerization of NIPAM resulting in low molecular weight distributions.[18, 17, 8, 19] For future experiments, improvement of the M_w/M_n may be obtained by lowering the monomer concentration to e.g. 1.8 M, or by lowering the RAFT to initiator ratio, R : i, to 1 : 0.1. From NMR, the degree of polymerization of NIPAM is 96 for polymerization 4, resulting in a M_n of 109.2 kDa and PNIPAM content of 31 mole%.

Alternatives for synthesizing temperature-responsive polycations

Besides adjusting the monomer and initiator concentrations, other parameters can be adjusted to obtain narrow disperse temperature-responsive polycations by RAFT. At first, different monomer chemistries can be chosen, such as the weak cationic monomer dimethylaminoethylacrylamide,[19] or dimethylaminopropylacrylamide, which was briefly explored but has proven to be difficult.[20] The reactivity of these
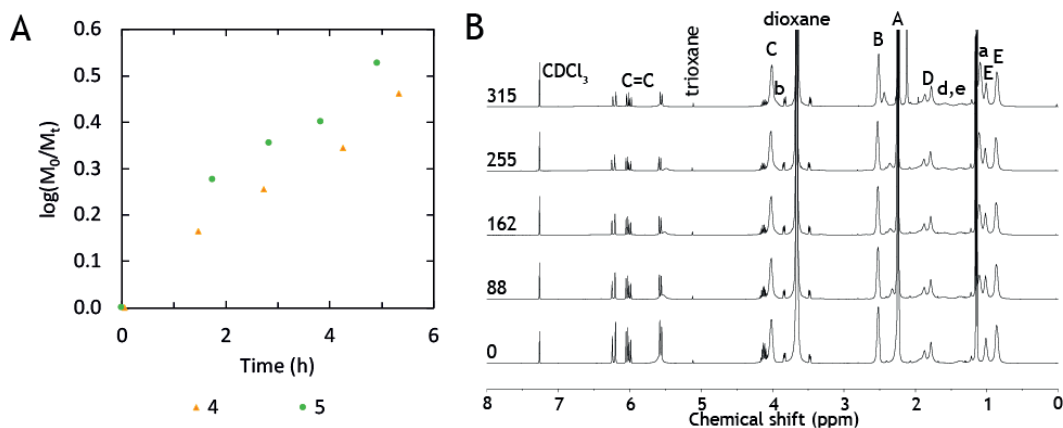
Figure 3.7 – A Polymerization kinetics of NIPAM copolymerization using a PDMAEMA macro-CTA synthesized from diCDTPA. The reaction conditions are provided in Table 3.3. **B** Overview of ^{1}H-NMR measurements in CDCl$_3$ to follow the kinetics of synthesis 4. C=C denotes the peaks from the vinyl group of the NIPAM monomers. The numbers on the left indicate the reaction time in minutes.

cationic monomers is comparable to the reactivity of NIPAM and therefore the synthesis order is no longer important. Therefore, the selection, and thus the availability, of RAFT agents is greatly simplified. Secondly, a different RAFT agent may be chosen, despite the fact that CDTPA was shown to allow control over the polymerization of both DMAEMA and NIPAM.[8, 14, 15, 16, 17, 19] Narrow disperse PDMAEMA-*b*-PNIPAM was synthesized from the RAFT agent 4-cyanopentanoic acid dithiobenzoate (CTAB) by Smith et al.[21] Therefore, using a bis-adduct of CTAB could also be a possible route towards symmetric PNIPAM-*b*-PDMAEMA-*b*-PNIPAM triblock copolymers. However, dithiobenzoates are prone to hydrolysis, which might require the controlled removal of the CTA after copolymerization. At last, one may consider changing the reaction solvent, although dioxane has been frequently used for the synthesis of PDMAEMA and PNIPAM,[8, 14, 15, 16, 17, 19, 21] also ethyl acetate,[18] toluene,[22] DMF,[23] and a mixture of DMF, THF and water[24] were reported.

Conclusion

Temperature-responsive polyelectrolytes were synthesized by using different RAFT agents. The divalent and convergent RAFT agent BDAT enabled controlled synthesis of PNIPAM-*b*-P*t*BA-*b*-PNIPAM with small PNIPAM outer blocks. A similar block copolymer with large PNIPAM outer blocks was synthesized from the divergent RAFT agent CDP. Both copolymers were quantitatively deprotected by

cleaving the *tert*-butyl groups of P*t*BA in HFIP under acidic conditions, and yielded the temperature-responsive polyanion PNIPAM-*b*-PAA-*b*-PNIPAM. Synthesis of the temperature-responsive polycation PNIPAM-*b*-PDMAEMA-*b*-PNIPAM from diCDTPA turned out to be more complicated. The synthesis and purification of the RAFT agent diCDTPA has been successful. Also, the preparation of the macro-CTA PDMAEMA seemed controlled. However, it is inconclusive whether extension of PDMAEMA with NIPAM has succeeded, as becomes clear from the low molecular weight shoulder in the GPC curve. To obtain monodisperse block copolymers with diCDTPA, experiments with lower monomer and initiator concentrations should be investigated. Alternatively, different cationic monomers, RAFT agents, or solvents may be chosen to obtain narrow disperse temperature-responsive polycations.

Appendix

Experimental

Synthesis of P*t*BA using CDP
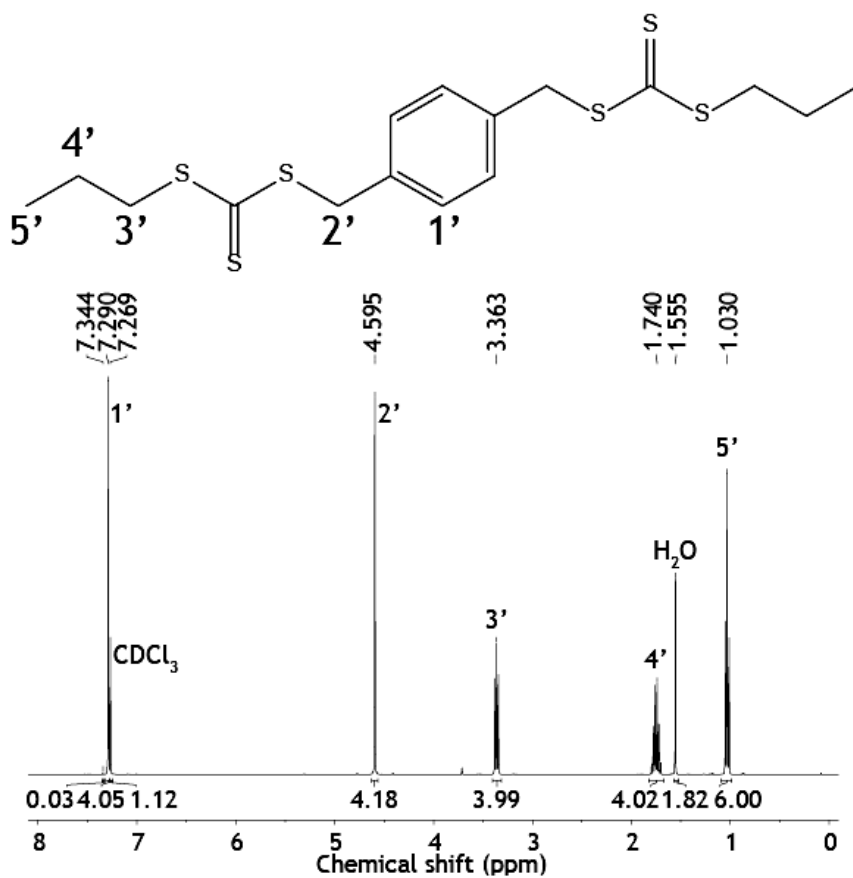
Figure A3.1 – ^{1}H-NMR spectrum in CDCl$_3$ of purified CDP.

Results and discussion

Synthesis of diCDTPA
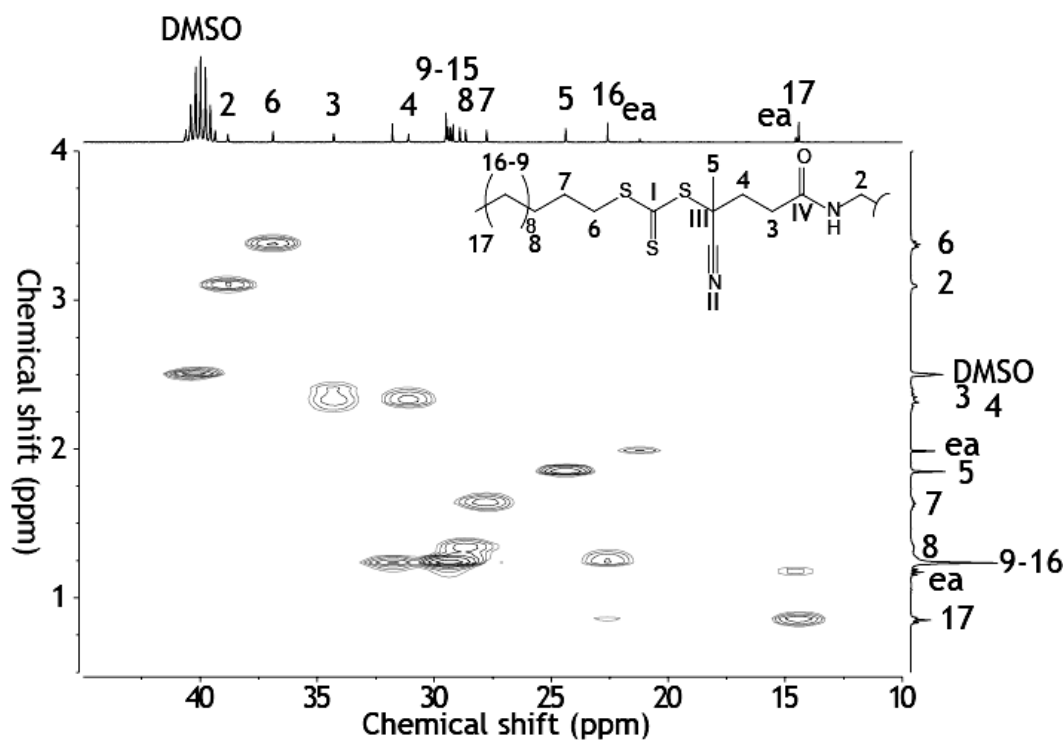
Figure A3.2 – HSQC NMR that was used to assign the peaks of diCDTPA in the ^{13}C-NMR. The spectrum was measured in DMSO-d6. Small traces of ethyl acetate are assigned as ea.
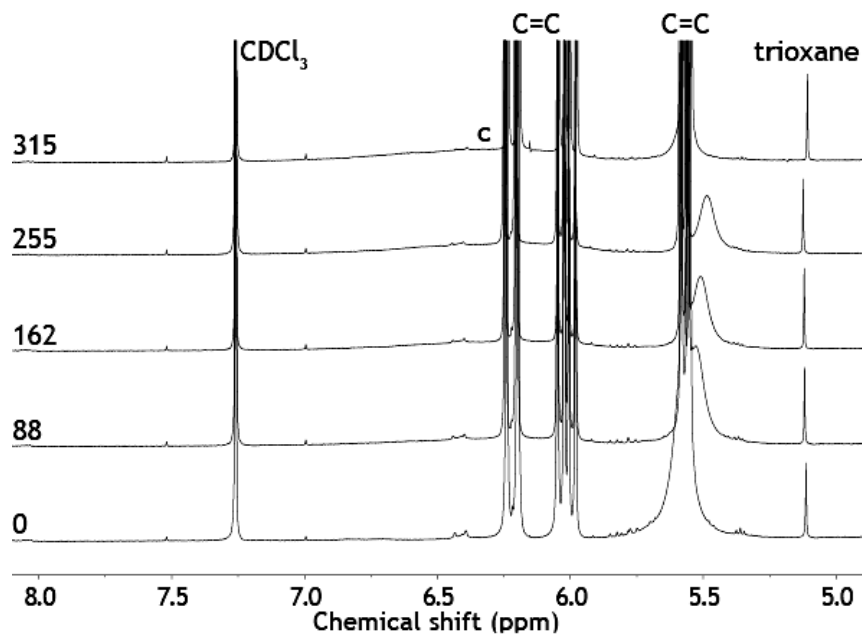
Synthesis of PNIPAM-*b*-PDMAEMA-*b*-PNIPAM

Figure A3.3 – ^{1}H-NMR spectra recorded at different time intervals during the copolymerization of NIPAM from PDMAEMA. The reaction time is indicated in minutes on the left side of the spectra. A broad peak around 6.2 ppm develops and increases with the reaction time. The vinyl group of the NIPAM monomers is indicated with C=C.

Bibliography

[1] J. Chiefari, Y. K. Chong, F. Ercole, J. Krstina, J. Jeffery, T. P. T. Le, R. T. A. Mayadunne, G. F. Meijs, C. L. Moad, G. Moad, E. Rizzardo, and S. H. Thang. Living free-radical polymerization by reversible addition-fragmentation chain transfer: The raft process. *Macromolecules*, 31(16):5559–5562, 1998.

[2] A. Gregory and M. H. Stenzel. Complex polymer architectures via raft polymerization: From fundamental process to extending the scope using click chemistry and nature's building blocks. *Progress in Polymer Science*, 37(1):38–105, 2012.

[3] D. J. Keddie. A guide to the synthesis of block copolymers using reversible-addition fragmentation chain transfer (raft) polymerization. *Chemical Society Reviews*, 43(2):496–505, 2014.

[4] S. Perrier and P. Takolpuckdee. Macromolecular design via reversible addition-fragmentation chain transfer (raft)/xanthates (madix) polymerization. *Journal of Polymer Science Part a-Polymer Chemistry*, 43(22):5347–5393, 2005.

[5] K. Matyjaszewski, T. E. Patten, and J. H. Xia. Controlled/"living" radical polymerization. kinetics of the homogeneous atom transfer radical polymerization of styrene. *Journal of the American Chemical Society*, 119(4):674–680, 1997.

[6] P. E. Millard, L. Barner, J. Reinhardt, M. R. Buchmeiser, C. Barner-Kowollik, and A. H. E. Muller. Synthesis of water-soluble homo- and block-copolymers by raft polymerization under gamma-irradiation in aqueous media. *Polymer*, 51(19):4319–4328, 2010.

[7] G. Moad, E. Rizzardo, and S. H. Thang. Living radical polymerization by the raft process - a third update. *Australian Journal of Chemistry*, 65(8):985–1076, 2012.

[8] Q. L. Li, X. He, Y. L. Cui, P. F. Shi, S. T. Li, and W. Q. Zhang. Doubly thermo-responsive nanoparticles constructed with two diblock copolymers prepared through the two macro-raft agents co-mediated dispersion raft polymerization. *Polymer Chemistry*, 6(1):70–78, 2015.

[9] M. Cetintas, J. de Grooth, A. H. Hofman, H. M. van der Kooij, K. Loos, W. M. de Vos, and M. Kamperman. Free-standing thermo-responsive nanoporous membranes from high molecular weight ps-pnipam block copolymers synthesized via raft polymerization. *Polymer Chemistry*, 8(14):2235–2243, 2017.

[10] J. T. Lai, D. Filla, and R. Shea. Functional polymers from novel carboxyl-terminated trithiocarbonates as highly efficient raft agents. *Macromolecules*, 35(18):6754–6756, 2002.

[11] A. D. Filippov, I. A. van Hees, R. Fokkink, I. K. Voets, and M. Kamperman. Rapid and quantitative de-tert-butylation for poly(acrylic acid) block copolymers and influence on relaxation of thermoassociated transient networks. *Macromolecules*, 51(20):8316–8323, 2018.

[12] A. M. Bivigou-Koumba, J. Kristen, A. Laschewsky, P. Muller-Buschbaum, and C. M. Papadakis. Synthesis of symmetrical triblock copolymers of styrene and n-isopropylacrylamide using bifunctional bis(trithiocarbonate)s as raft agents. *Macromolecular Chemistry and Physics*, 210(7):565–578, 2009.

[13] M. H. Allen, S. T. Hemp, M. S. Zhang, M. Q. Zhang, A. E. Smith, R. B. Moore, and T. E. Long. Synthesis and characterization of 4-vinylimidazole aba triblock copolymers utilizing a difunctional raft chain transfer agent. *Polymer Chemistry*, 4(7):2333–2341, 2013.

[14] T. Sentoukas and S. Pispas. Poly(dimethylaminoethyl methacrylate)-b-poly(hydroxypropyl methacrylate) copolymers: Synthesis and ph/thermo-responsive behavior in aqueous solutions. *Journal of Polymer Science Part a-Polymer Chemistry*, 56(17):1962–1977, 2018.

[15] A. R. Shirin-Abadi, A. Darabi, P. G. Jessop, and M. F. Cunningham. Tuning the aggregation and redispersion behavior of co2-switchable latexes by a combination of dmaema and pdmaema-b-pmma as stabilizing moieties. *Polymer*, 106:303–312, 2016.

[16] A. Skandalis and S. Pispas. Pdmaema-b-plma-b-poegma triblock terpolymers via raft polymerization and their self-assembly in aqueous solutions. *Polymer Chemistry*, 8(31):4538–4547, 2017.

[17] Q. L. Li, C. Q. Gao, S. T. Li, F. Huo, and W. Q. Zhang. Doubly thermo-responsive abc triblock copolymer nanoparticles prepared through dispersion raft polymerization. *Polymer Chemistry*, 5(8):2961–2972, 2014.

[18] C. H. Hornung, C. Guerrero-Sanchez, M. Brasholz, S. Saubern, J. Chiefari, G. Moad, E. Rizzardo, and S. H. Thang. Controlled raft polymerization in a continuous flow microreactor. *Organic Process*

Research & Development, 15(3):593–601, 2011.

[19] M. A. Nash, P. Yager, A. S. Hoffman, and P. S. Stayton. Mixed stimuli-responsive magnetic and gold nanoparticle system for rapid purification, enrichment, and detection of biomarkers. *Bioconjugate Chemistry*, 21(12):2197–2204, 2010.

[20] M. Khimani, S. Yusa, A. Nagae, R. Enomoto, V. K. Aswal, E. Kesselman, D. Danino, and P. Bahadur. Self-assembly of multi-responsive poly(n-isopropylacrylamide)-b-poly(n,n-dimethylaminopropylacrylamide) in aqueous media. *European Polymer Journal*, 69:96–109, 2015.

[21] A. E. Smith, X. W. Xu, T. U. Abell, S. E. Kirkland, R. M. Hensarling, and C. L. McCormick. Tuning nanostructure morphology and gold nanoparticle "locking" of multi-responsive amphiphilic diblock copolymers. *Macromolecules*, 42(8):2958–2964, 2009.

[22] J. E. Laaser, E. Lohmann, Y. M. Jiang, T. M. Reineke, and T. P. Lodge. Architecture-dependent stabilization of polyelectrolyte complexes between polyanions and cationic triblock terpolymer micelles. *Macromolecules*, 49(17):6644–6654, 2016.

[23] A. K. S. Chandel, D. Kannan, B. Nutan, S. Singh, and S. K. Jewrajka. Dually crosslinked injectable hydrogels of poly(ethylene glycol) and poly[(2-dimethylamino)ethyl methacrylate]-b-poly(n-isopropyl acrylamide) as a wound healing promoter. *Journal of Materials Chemistry B*, 5(25):4955–4965, 2017.

[24] D. Sprouse, Y. M. Jiang, J. E. Laaser, T. P. Lodge, and T. M. Reineke. Tuning cationic block copolymer micelle size by ph and ionic strength. *Biomacromolecules*, 17(9):2849–2859, 2016.

Self-assembly of oppositely charged polyelectrolyte block copolymers containing short thermoresponsive blocks

4

The assembly of oppositely charged block copolymers, containing small thermoresponsive moieties, was investigated as a function of salt and temperature. Aqueous solutions of poly-(N-isopropylacrylamide)-b-poly(dimethylaminoethyl methacrylate) (NIPAM$_{44}$-b-DMAEMA$_{216}$) and PNIPAM-b-poly(acrylic acid)-b-PNIPAM (NIPAM$_{35}$-b-AA$_{200}$-b-NIPAM$_{35}$) were mixed at equal charge stoichiometry, and analysed by light scattering (LS), NMR spectroscopy and small angle X-ray scattering (SAXS). At room temperature, two different micelle morphologies were found at different salt concentrations. At NaCl concentrations below 0.75 M, complex coacervate core micelles (C3M) with a PNIPAM corona were formed as a result of interpolyelectrolyte complexation. At NaCl concentrations exceeding 0.75 M, the C3M micelles inverted into PNIPAM cored micelles (PCM), containing a water soluble polyelectrolyte corona. This behavior is ascribed to the salt dependence of both the lower critical solution temperature (LCST) of PNIPAM, and the complex coacervation. Above 0.75 M NaCl, the PNIPAM blocks are insoluble in water at room temperature, while complexation between the polyelectrolytes is prevented because of charge screening by the salt. Upon increasing the temperature, both types of micelles display a cloud point temperature (T$_{cp}$), despite the small thermoresponsive blocks, and aggregate into hydrogels. These hydrogels exist of a complexed polyelectrolyte matrix with microphase separated PNIPAM domains. Controlling the morphology and aggregation of temperature sensitive polyelectrolytes can be an important tool for drug delivery systems, or the application and hardening of underwater glues.

I. A. van Hees, P. J. M. Swinkels, R. G. Fokkink, A. H. Velders, I. K. Voets, J. van der Gucht and M. Kamperman

Introduction

Complex coacervation is a liquid-liquid phase separation that occurs when two oppositely charged polyelectrolyte solutions are mixed, resulting in two coexisting phases: 1) the complex coacervate, a water-insoluble polyelectrolyte phase, and 2) the dilute solvent phase.[1] Complex coacervates display unique characteristics, such as a low interfacial tension and a high water content, while being water-insoluble.[2, 3] This combination of properties makes complex coacervates interesting for many applications, such as underwater adhesives or encapsulants.[4, 5, 6, 7, 8]

The properties of complex coacervates depend on several parameters, including the chemical nature of the polyelectrolytes, the salt concentration, and in case of weak polyelectrolytes, the pH. These parameters influence not only the water content, but also the interaction strength and mobility of the polyelectrolytes in the complex.[3, 9] Complex coacervate core micelles (C3M) (also known as poly-ion complex (PIC) micelles, block ionomer complex (BIC) micelles, or interpolyelectrolyte complex (IPEC) micelles) can be formed when water-soluble blocks are connected to the polyelectrolytes. These water-soluble blocks will form a stabilizing corona around the water-insoluble complex coacervate core of the C3M.[9, 10, 11]

A special class of C3Ms are stimuli responsive micelles, which are promising systems for sensors or controlled delivery systems, and many reports describe C3Ms that are responsive to ionic strength, pH or temperature.[9, 12, 13, 14, 15, 16, 17, 18, 19, 20] Most of these C3Ms are designed to be stable in solution, which is important for applications such as drug delivery. Therefore, large stabilizing blocks with a minimum block length of 30 mole% are typically used to form the corona.[13, 14, 15, 16, 17, 18] However, for applications such as adhesives, the formation of a dense solid phase is needed and smaller temperature responsive blocks may be preferred to obtain a different morphology.

In this article, we study the assembly of oppositely charged block copolymers with short temperature-sensitive blocks. The system is composed of two block-copolymers, poly-(N-isopropylacrylamide)-b-poly(dimethylaminoethyl methacrylate) (PNIPAM-b-PDMAEMA) and PNIPAM-b-poly(acrylic acid)-b-PNIPAM (PNIPAM-b-PAA-b-PNIPAM) (Figure 4.1). Both PDMAEMA and PAA are weak polyelectrolytes that are positively and negatively charged at neutral pH, respectively, therewith enabling complex coacervation.[1, 3] Thermo-responsiveness is introduced into the system by means of PNIPAM, which is a well-explored polymer displaying a lower critical solution temperature (LCST).[21] Below the LCST, PNIPAM is water-soluble while above the LCST the polymer chain collapses and PNIPAM becomes water-insoluble.[22] The LCST of PNIPAM in aqueous solution is about 32 °C, but varies with molecular weight, salt concentration, and block length ratio when
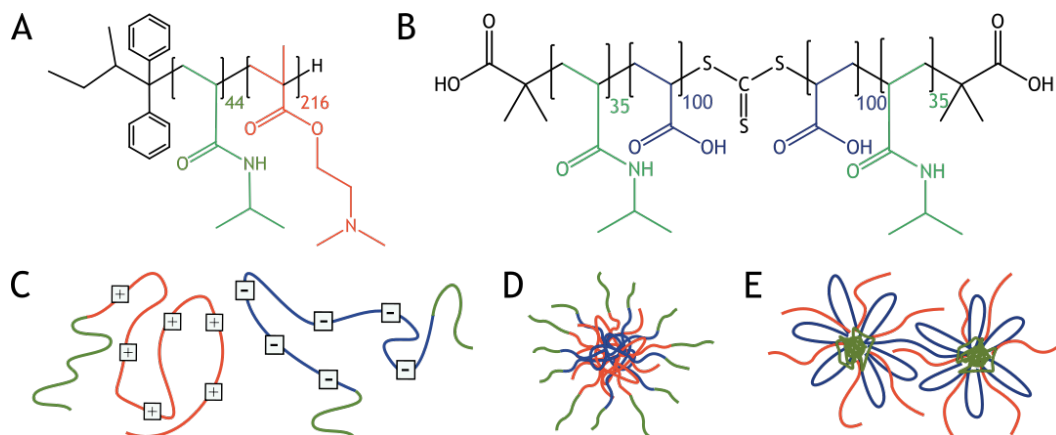
Figure 4.1 – Chemical structures of **A** cationic PNIPAM-*b*-PDMAEMA which was synthesized by anionic polymerization, and **B** PNIPAM-*b*-PAA-*b*-PNIPAM which was synthesized by reversible addition fragmentation chain transfer (RAFT) polymerization. Schematic representations of **C** PNIPAM-*b*-PDMAEMA and PNIPAM-*b*-PAA-*b*-PNIPAM, **D** a C3M, and **E** PCMs. The red block represents PDMAEMA, the blue block PAA and the green blocks PNIPAM.

copolymerized.[22, 23, 24, 25]

We study both the influence of salt concentration and temperature on the morphology of the block copolymer mixtures. Analysis is performed using light scattering (LS), nuclear magnetic resonance spectroscopy (NMR), and small angle X-ray scattering (SAXS). We show that at low salt concentrations, C3Ms with a PNIPAM corona are formed, Figure 4.1. However, sufficiently elevated salt concentrations turn the C3Ms inside out, leading to PNIPAM-cored micelles (PCMs) with a water-soluble polyelectrolyte corona. Upon temperature increase, both C3Ms and PCMs aggregate and form hydrogels, displaying a salt dependent cloud point temperature (T_{cp}).

Experimental

Materials

1,4-Dioxane (99.8%), NIPAM (97%), azobisisobutyronitrile (AIBN) (98%), *tert*-butyl acrylate (98%, 10-20 ppm monomethyl ether hydroquinone inhibitor), aluminium oxide (neutral, Brockmann I) and hydrochloric acid (37%, RG) were purchased from Sigma Aldrich and used as received, unless mentioned otherwise. Sodium chloride (>99.5%) was bought from Acros organics. Methanol (HPLC grade), dichloromethane (DCM) (AR), diethyl ether (AR), 1,1,1,3,3,3-hexafluoro-2-propanol (HFIP) (AR) and *n*-hexane (HPLC grade) were purchased from Biosolve and used as received, unless mentioned otherwise. Sodium hydroxide solution (TitriPUR, 0.1 M)

was bought from Merck chemicals. PNIPAM-*b*-PDMAEMA was purchased from Polymer Source, M_n 38.2 kDa and PDI 1.05, Figure A4.1. The chain transfer agent *S,S*'-bis(α,α'-dimethyl-α"-acetic acid) trithiocarbonate (BDAT) was synthesized using a previously described method.[26, 27]

Triblock synthesis and characterization

Synthesis of poly-(*N*-isopropylacrylamide)

NIPAM was recrystallized twice from *n*-hexane. AIBN was recrystallized from methanol prior to use. A round bottom flask was filled with 30.9 mg AIBN, 266 mg BDAT, 8.5 g NIPAM, and 43 mL dioxane (m:R:i as 80:1:0.2, [m] 0.8 M). The reactants were dissolved and the mixture was purged with nitrogen for 60 minutes. The polymerization took place at 70 °C for 85 minutes. Subsequently, the reaction was quenched by exposure to air and rapid cooling. The resulting polymer was purified by precipitation in diethyl ether. The final product was dried under vacuum. ^{1}H-NMR (400 MHz, D$_2$O, Figure A4.2): δ 1.05 (s, 6H), 1.36 - 2.1 (m, 3H), 3.80 (s, 1H), 6.24 (s, 1H). GPC: M_n 7.6 kDa and PDI 1.26.

Synthesis of poly(NIPAM-*b*–acrylic acid-*b*-NIPAM)

Tert-butyl acrylate was run over an alumina column to remove inhibitor. AIBN was recrystallized from methanol. A round bottom flask was loaded with 16.4 mg AIBN, 4.1 g poly-NIPAM macro-CTA, 24.4 g *tert*-butyl acrylate and 48 mL dioxane (m:R:i as 380:1:0.2, [m] 3.9 M). The reactants were dissolved and the mixture was purged with nitrogen for 60 minutes. The polymerization took place for 55 minutes at 70 °C. The reaction was quenched by exposure to air and rapid cooling. The polymer was purified by precipitation in a cold methanol/water mixture, 3/1 v/v. A dry product was obtained by redissolving in minimal DCM and subsequent drying under vacuum. ^{1}H-NMR (400 MHz, CDCl$_3$): δ 1.11 (s, 6H, (CH$_2$)$_2$ isopropyl), 1.4-1.5 (s, 9H, (CH$_3$)$_3$ tert-butyl), 1.6 – 2.2 (m, backbone), 3.99 (s, 1H, CH isopropyl). ^{13}C-NMR (400 MHz, MeOD): δ 22.38 ((CH$_3$)$_2$ isopropyl), 28.07 ((CH$_3$)$_3$ tert-butyl), 36 – 40 (backbone), 41.9 (CH isopropyl), 42.38 (backbone), 174.12 ((C=O)N acrylamide).

The resulting *tert*-butyl acrylate copolymer was deprotected by dissolving in HFIP containing 0.12 M hydrochloric acid and the mixture was left to stir for 3 hours.Filippov2018 The sample was dried under vacuum and redissolved in water, followed by neutralization using 0.1 M sodium hydroxide solution. The polymer solution was centrifuged to remove any insoluble by-products of the deprotection and was further purified by dialysis. The final product was obtained after freeze drying. ^{1}H-NMR (400 MHz, MeOD, Figure A4.3): δ 1.16 (s, 6H, (CH$_3$)$_2$ isopropyl), 1.4 - 2.3 (m, backbone), 3.97 (s, 1H, CH isopropyl). ^{13}C-NMR (400 MHz, D$_2$O, Figure A4.4): δ 21.65 ((CH$_3$)$_2$ isopropyl), 35 – 40 (backbone), 41.8 (CH isopropyl), 44.80 (backbone), 175.4 ((C=O)N acrylamide), 183.4 ((C=O)OH carboxylic acid). GPC: M_n 26.8 kDa and PDI 1.59.

Polymer characterization

NMR was used to determine the purity of all the products and the conversion of the monomers in polymerization. ^{1}H and ^{13}C NMR-spectroscopy measurements were carried out on a Bruker AMX-400 spectrometer (400 MHz) at room temperature. Gel permeation chromatography (GPC) of the PNIPAM macroRAFT agent was performed using an Omnisec Reveal system with an Omnisec Resolve detector, equipped with two PSS PFG columns. The samples were run in 1,1,1,3,3,3-hexafluor-2-isopropanol containing 0.02 M potassium trifluoroacetate. GPC of the triblock was obtained with an Agilent 1260 Infinity II HPLC gel permeation chromatograph, equipped with a Waters Ultrahydrogel500 column. The samples were run using an aqueous buffer of 0.01 M Na_2HPO_4/NaH_2PO_4 with 0.1 M $NaNO_3$ as eluent.

Methods

Sample preparation

The polymers were dissolved in water as stock solutions with a concentration of max. 300 g/L and the pH was adjusted to 6.5±0.2. Samples were prepared by making a NaCl solution with the desired salt concentration. Then, first the polyanion was added to the salt solution, followed by the polycation, such that the total final chargeable monomer concentration was 0.1 M. The order of mixing is important as it determines the degree of coacervation. Also, the polymers were added at equal charge, meaning that the amount of positively charged monomers equals the amount of negatively charged monomers, as was verified by zetapotential measurements that should result in about 0 mV (Figure A4.7). The solution was shaken and left refrigerated to equilibrate before use.

Zetapotential measurements

Charge stoichiometry was verified using zetapotential measurements. All measurements were performed using a Malvern Zetasizer Nano ZS (Malvern Instruments, U.K.) at 25 °C after a temperature equilibration time of 30 s. The number of runs was selected automatically by the Zetasizer software (version 7.02, Malvern Instruments, U.K.). A 4 mW He−Ne ion laser at 633 nm was used and the signal was detected at a fixed angle of 173°. Each measurement was repeated six times. Samples were prepared at 0.5 M NaCl and 0.1 M charged monomers, followed by a dilution of three times using demineralised water.

Light scattering

LS experiments were performed on an ALV CGS-3 compact goniometer system equipped with a JDSU 1145P laser, operated at a wavelength of 633nm, and a ALV/LSE-5004 external correlator. The measurements were carried out at a measuring angle of 90°. The data was analysed with a second order cumulant fit using

ALV-7004 Correlator software and checked for monodispersity using CONTIN. The temperature was controlled with a Julabo Refrigerated – Heating Circulator. The temperature increased in steps of 2 °C, using a time interval of 10 minutes. This time is sufficient to equilibrate the micelles, as waiting steps of 1 hour gave similar results. Furthermore, samples containing a charged monomer concentration of 0.1 M were used and demonstrated radii similar to samples containing 0.01 M charged monomers. Therefore, we assumed that interparticle interactions do not influence the results at the used concentration.

LS has been used to determine the cloud point temperature T_{cp}. In this article, the T_{cp} of the assemblies is defined as the temperature where the scattering intensity has doubled compared to its value at 17 °C for 0.75 M NaCl, and 25 °C for all other samples. The data used for this determination is shown in Figure A4.8.

NMR

1D ^{1}H and 2D ^{1}H^{1}H-NOESY NMR experiments were performed on a Bruker AVANCE 600 NMR spectrometer equipped with a TCI cryoprobe. Standard Bruker pulse sequences were used with typical mixing times for the NOESY experiments of 100 ms. 90' degree pulses were calibrated for each sample to account for the high salt concentrations.

Small angle X-ray scattering

SAXS measurements were performed on a SAXSLAB GANESHA 300 XL SAXS machine equipped with a GeniX 3D Cu Ultra Low Divergence micro focus sealed tube source producing X-rays with a wavelength of λ = 1.54 Å at a flux of 15.8x106 ph s^{-1} and a Pilatus 300 K silicon pixel detector with 487x619 pixels of 172 μm^2 in size placed at a sample-to-detector distance of 441 mm and/or 1041 mm to access a q-range of 0.004 ≤ q ≤ 0.710 Å^{-1}, and a q-range of 0.003 ≤ q ≤ 0.296 Å^{-1} with q = 4π/λ(sinθ), where 2θ represents the observation angle. Silver behenate was used for calibration of the beam centre and the q-range. Samples were contained in 2 mm quartz capillaries (Hilgenberg GmbH, Germany) and temperature controlled using a Julabo heating circulator. The two-dimensional SAXS patterns were azimuthally averaged to obtain one dimensional SAXS profiles.

Results and discussion

NaCl concentrations up to 0.75 M

Light scattering

In this section, samples containing up to 0.75 M NaCl will be discussed, while samples with more salt will be discussed below. The described block copolymers were mixed at different NaCl concentrations, at constant pH, and equal charge. The charge fraction,

$$f^+ = \frac{n^+}{n^+ + n^-} \tag{4.1}$$

was set at 0.5 (Figure A4.7) by adding equal amounts of DMAEMA and AA monomers, which should approximately result in a net zero charge at pH 6.5. To verify this, zetapotential measurements were performed, and the ratio between the monomers was adjusted when needed. The samples were investigated using light scattering while increasing the temperature (Figure A4.8). At room temperature a single phase is observed, while at elevated temperatures an aggregated system is found. To show the transition between these systems, a summary of the LS data is given in Figure 4.2. In the single phase system at salt concentrations below 0.75 M, objects with well-defined and monodisperse hydrodynamic radii are observed at room temperature (Figure A4.9). CONTIN analysis revealed a monomodal decorrelation curve, suggesting assembly of the polymers into well-defined objects, such as C3Ms.
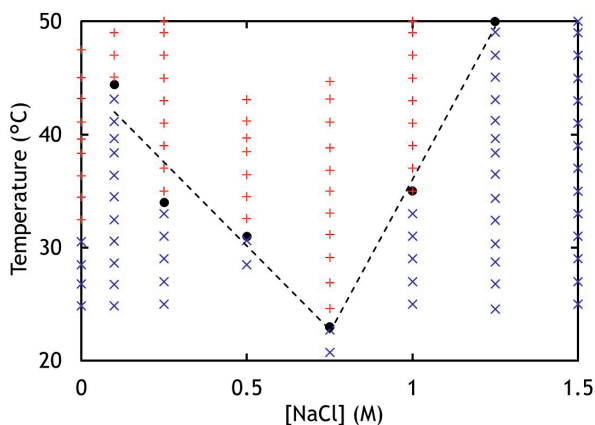
Figure 4.2 – Light scattering was used to determine the T_{cp} of samples containing PNIPAM-*b*-PDMAEMA and PNIPAM-*b*-PAA-*b*-PNIPAM with varying concentrations of NaCl. The results were used to create a phase diagram; the blue crosses represent a one phase system, and the red plusses represent an aggregated system. The dotteld lines represent the phase bouldary that was deduced from the observed T_{cp}s (black dots).

Assembly of the polymers into C3Ms can be explained by the interactions between the polyelectrolytes and the solubility of PNIPAM in these conditions. Mixed homopolymers of PDMAEMA and PAA, of block lengths comparable to the electrolyte blocks used in this research, form complexes below the critical salt concentration (c_s) of ≈1.1 M NaCl.[3] This means that below 0.75 M NaCl, complex coacervation between the PDMAEMA and PAA blocks can occur. PNIPAM, on the other hand, is soluble at room temperature and at salt concentrations of 0.75 M NaCl and below. Regarding the well-defined objects observed in LS, the PNIPAM blocks are able to solubilize the complexed polyelectrolytes, resulting in C3Ms with a PNIPAM corona.

From LS, an estimated size for the C3Ms can be obtained. For 0.5 M NaCl, a R_h of 31 nm was observed. This value is similar to values that were reported before.[9, 13] By using LS, Voets et al. observed C3Ms with an apparent R_h of 31.3±0.9 nm that were composed of poly(N-methyl-2-vinyl pyridinium iodide)-b- poly(ethylene oxide), $PM2VP_{38}$-b-PEO_{211}, and PAA_{55}-b-$PNIPAM_{88}$. Park et al. observed micelles upon mixing poly(2-isopropyl-2-oxazoline)-b-poly(lysine), $PiPrOx_{45}$-b-$P(Lys)_{85}$, and $PiPrOx$-b-poly(aspartic acid), $PiPrOx_{45}$-b-$P(Asp)_{76}$, with an apparent R_h of 22.6 nm by LS.

Upon sufficient temperature increase, aggregation of the micelles from solution was observed as is indicated by a sudden increase in radius, scattering intensity, and/or polydispersity in the LS data (Figure A4.8 and Figure A4.10).[17] In Figure 4.2, the determined T_{cp} (black dots) are shown for all measured salt concentrations. It was observed that below 0.75 M NaCl, the T_{cp} decreases with increasing salt. This trend can be attributed to the salt dependent solubility of PNIPAM. PNIPAM solubility decreases when salt concentrations increase, which is expressed by a decreasing LCST and thus collapsing of the polymer chain at lower temperatures (Figure A4.21).[23, 28] Not only for PNIPAM containing micelles, but also for micelles containing different temperature-responsive blocks, similar behaviour was observed.[13] After sufficient cooling of the samples, aggregates disappeared again and radii similar to the sizes observed before heating were measured, demonstrating the reversibility of the system.

The T_{cp} observed at 0 M NaCl deviates from the tendency of increasing T_{cp} with decreasing salt concentration. Without added salt, oppositely charged polyelectrolytes strongly interact immediately upon mixing, through electrostatic bonds with long relaxation times. This most likely results in a heterogeneous and kinetically trapped system. The system may not have enough mobility to arrange in stable micelles, which in turn, will result in a lower T_{cp}.

NMR

NMR is used to verify the presence of C3Ms at 0.5 M salt. In the ^{1}H spectra of the mixtures, Figure 4.3, the peaks of the backbone between 1.0 and 2.2 ppm are broadened compared to the unmixed PDMAEMA and PAA (Figure A4.11 and Figure A4.12). Also, the peak of PDMAEMA (peak A) at 2.9 ppm is broadened. Peak broadening occurs when the mobility, and thus solubility, of the molecules is decreased, e.g. in the case of complexation. In contrast, the PNIPAM peak at 3.8 ppm remained sharp,

which shows an unchanged mobility of the PNIPAM blocks.

NOESY-NMR is a 2D-NMR technique that establishes correlations between chemical moieties that are in close proximity through space, i.e. within 1 nm distance from each other. Therefore, this NMR technique can also be used to verify the proposed micelle morphologies.[14] Figure A4.15 depicts the NOESY spectrum at 0.5 M NaCl. A cross-peak between the PDMAEMA and PAA (2.1;2.9) can be observed in the spectrum at room temperature.

Furthermore, cross peaks can be observed between peaks belonging to the same polymer block, e.g. for PNIPAM peak b at 3.9 ppm. In NOESY spectra taken from un-mixed polymer solutions, cross-peaks can only be observed between PNIPAM peaks, or only between polyelectrolyte peaks (Figure A4.19 and Figure A4.20). Altogether, the data show that PAA and PDMAEMA are close in space when the polymers are mixed. Therefore, both 1D and 2D NMR techniques indicate the presence of C3Ms, with a water insoluble complex coacervate core and a hydrated PNIPAM corona at low salt and temperature.

Additionally, NMR experiments were performed at elevated temperatures to investigate whether aggregation of the micelles leads to differences in morphology between the samples at different salt concentrations. At 67 °C, the peak splitting and peak intensities of the PDMAEMA (peaks A and B), and of the PNIPAM (peaks a and b) decreased even further, Figure 4.3. This reflects the decreased solubility of the micelles at elevated temperatures. In NOESY, cross-peaks that were present between DMAEMA and PAA at room temperature disappeared after increasing the temperature (Figure A4.16). Both observations can be explained by the reduced solubility of the polymers resulting from the aggregation, which reduces visibility in NMR. After cooling the samples back to room temperature, similar ^{1}H spectra could be obtained as before heating, showing the reversibility of the system (Figure A4.13).

Small angle X-ray scattering

SAXS measurements were performed to investigate the size and shape of the micelles at room temperature, and the morphological features of the hydrogels at elevated temperatures. The scattering intensity of the 0.5 M NaCl sample at room temperature was low, which resulted in noisy data after 8h of data collection, see Figure 4.4A. As a result, we limit ourselves to an estimation of the slope from $q \approx 0.03$ till 0.2 Å^{-1} as -2. For spheres, or micelles with a sufficient density difference between the core and corona, a slope of -4 is expected. Therefore, we suggest that the micelle has a an indistinct boundary between core and corona, which is the result of the high water content of the complex coacervate core.

The SAXS spectra at elevated temperature exhibit more morphological features compared to the spectra at room temperature. At 67 °C, a peak has appeared at 0.032 Å^{-1}, corresponding to a characteristic distance of $\approx$ 20 nm. It is plausible that the observed distance corresponds to the typical distance between PNIPAM and complex coacervate domains. However, the lack of higher order peaks suggests that there is no specific long range arrangement of the domains.
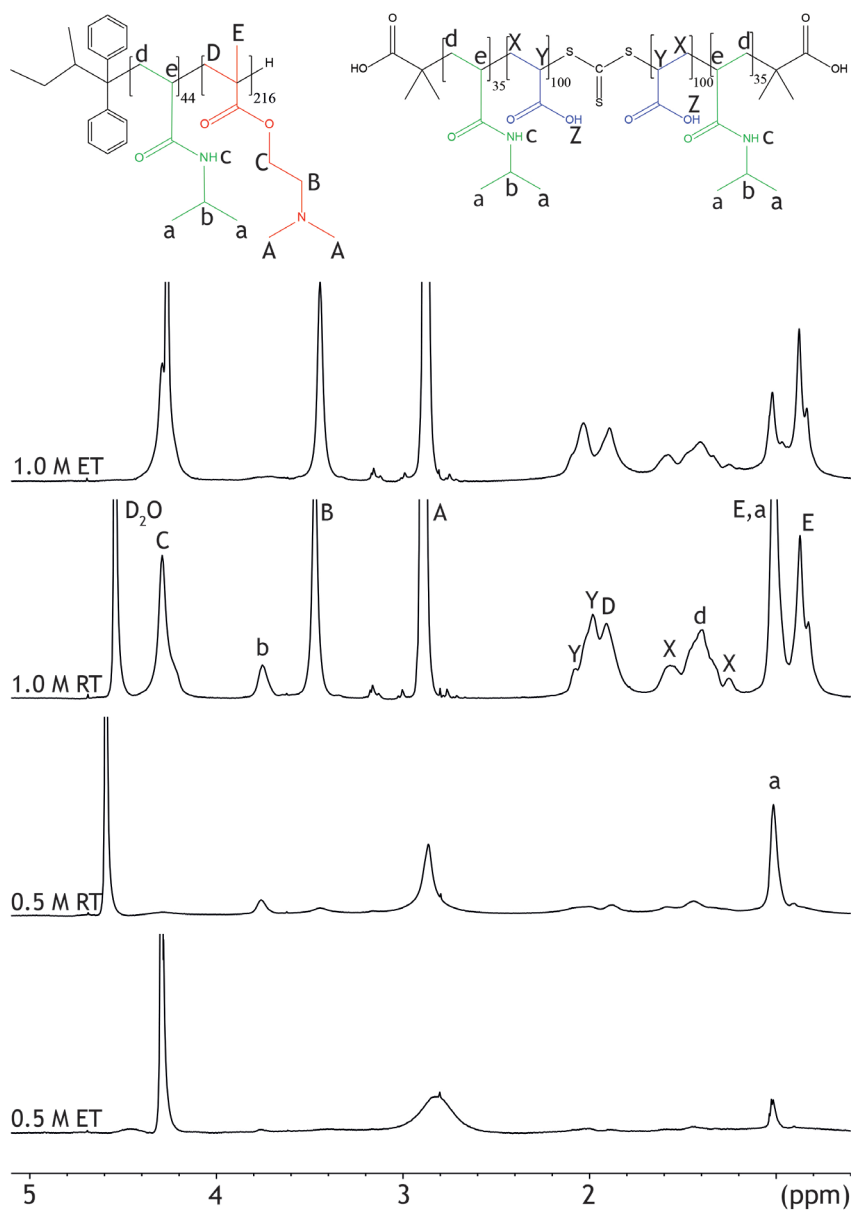
Figure 4.3 – ¹H-NMR spectra of mixtures of PNIPAM-*b*-PDMAEMA and PNIPAM-*b*-PAA-*b*-PNIPAM in 0.5 and 1.0 M NaCl, at 27 °C (RT), and 67 °C (ET).

Sample stability

In this research, all samples were prepared at charge neutrality, as was checked by zeta-potential measurements. Equal charge ratios appeared to be a requirement for obtaining macroscopic aggregation, and for the sudden steep increase in radius, scattering intensity and polydispersity that were observed in LS. Samples prepared off charge stoichiometry displayed T_{cp} like behaviour, but showed a more gradual increase in radius and scattering intensity. This behaviour can be explained by the presence of like-charged micelles with excess charge in the corona, leading to repulsion between the micelles and at sufficient net charge prevention of macroscopic aggregation.[11, 29] Furthermore, PNIPAM that was copolymerized with hydrophilic moieties also shows a more gradual aggregation.[30] Dautzenberg et al., who investigated complexation between thermo-sensitive polyelectrolytes with large PNIPAM blocks, did not observe steep increases in radius, scattering intensity, and polydispersity. The samples in that article might be prepared off the theoretical net zero charge point, and therefore were likely charged. However, no zetapotential data was provided in the article to verify this hypothesis.[16]

To obtain monodisperse micelle solutions, equilibration of the samples is a key factor. Immediately after preparation of the 0.5 M NaCl samples, little pieces with a gel like structure appeared in the 0.5 M NaCl solutions and dissolved over time. Dissolution of these solid pieces could be speeded up by refrigerating, which is also reported by Park et al.[13] Furthermore, for elevated polymer concentrations at room temperature, micelle solutions at low salt were not fully stable and after one day sediments of complex coacervate coexisted with a dilute phase which contained micelles. This observation can be explained by the short PNIPAM chains that are likely not able to completely stabilize the micelles in solutions with higher polymer concentrations, resulting in aggregation and sedimentation. Similar behaviour was observed by De Santis et al. who investigated C3Ms with different sizes of water-soluble blocks.[17] Micelles composed of block copolymers with the smallest stabilizing blocks formed aggregates, while the other micelles did not. However, Bayati et al. also observed aggregation of PNIPAM-containing micelles but underlined that PNIPAM can not only aggregate above the LCST, but also below the LCST due to weak hydrophobic interactions, leading to aggregation as well.[14] Furthermore, they observed that increasing polymer concentrations resulted in increased aggregation, similar to our findings.

NaCl concentrations from 0.75 M and above

Light scattering

Preparing samples at NaCl concentrations of 0.75 M, and above, at room temperature, resulted in objects with high polydispersities, as observed from the PDI from LS (Figure A4.9), and displayed multimodal decorrelations in the CONTIN analysis. The formation of objects in these conditions is unexpected as the formation of coacervates, and thus C3Ms, is prevented when the salt concentration exceeds a critical salt con-

centration ($c_{s,cr}$), which is at about 1.0 M NaCl for this system. Above 0.75 M NaCl, PNIPAM is insoluble at room temperature which leads to the formation of micelles consisting of an insoluble PNIPAM core, stabilized by the polyelectrolytes (PCMs) (Figure A4.21).

With LS, polydisperse structures are observed. As a control, angle dependent LS was performed on samples containing 1.25 M NaCl, and 0.01 M charged groups. These measurements resulted in a linear relation between the decay rate Γ and q^2, that only slightly deviated at high q. The linear decay indicates the presence of spherical particles at elevated salt concentrations, instead of, for example, cylindrical objects. The triblock PNIPAM-b-PAA-b-PNIPAM can form bridges between the different micelles, as is schematically shown in Figure 4.1E. The presence of interconnected micelles at higher polymer concentrations could be an explanation for the polydisperse structures observed with LS.

For PCMs, aggregation is observed with increasing T_{cp} for higher salt concentrations, Figure 4.2, while at lower salt concentrations a decrease in T_{cp} was observed. Aggregation of PCMs is caused by the reoccurrence of complexation of the polyelectrolytes, which can be explained by two phenomena. Firstly, complex coacervation is most likely entropically driven, thus temperature dependent.[31] Secondly, by increasing the temperature, the $c_{s,cr}$ also increases. When $c_{s,cr}$ exceeds the salt concentration of the sample, complex coacervates can be formed. For higher salt concentrations, higher temperatures are needed to exceed the $c_{s,cr}$. This behaviour was observed before for PAA/PDMAEMA homopolymers and in addition for other homopolymer couples, such as poly(trimethyl amino ethyl methacrylate) (PTMAEMA) and poly(sulphopropyl methacrylate) (PSPMA).[31] Influence of the LCST of PDMAEMA on the aggregation at high salt is considered unlikely, as charges on the polyelectrolyte prevent LCST behaviour. At this pH the PDMAEMA is charged, and the charges cannot be screened by PAA due to the high salt concentration. Increasing T_{cp} with increasing NaCl concentrations are therefore likely the result of increased polyelectrolyte solubility, and a complex coacervation-driven aggregation of the PCMs.

With LS, different tendencies in the radii can be observed with increasing temperature, between the samples at low and high salt, Figure A4.8. Below 1.0 M NaCl, the radius steeply increases with increasing temperature, while at high salt first a decrease in radius is observed, followed by an increase. This tendency might be explained by a collapse of either core or corona preceding aggregation.[29] As a result, the scattering intensity would increase while the micellar radius decreases, as is observed at 1.0 M NaCl.

Equal to samples containing less than 0.75 M NaCl, sedimentation was observed for the samples prepared above 0.75 M NaCl. However, the sedimentation only occurred after a couple of days. The polyelectrolyte blocks of the PCMs are much larger than the, in these conditions, insoluble PNIPAM blocks and therefore more efficiently stabilize the micelles without aggregating. Therefore, also higher polymer concentrations could be obtained without visible aggregation within a day.
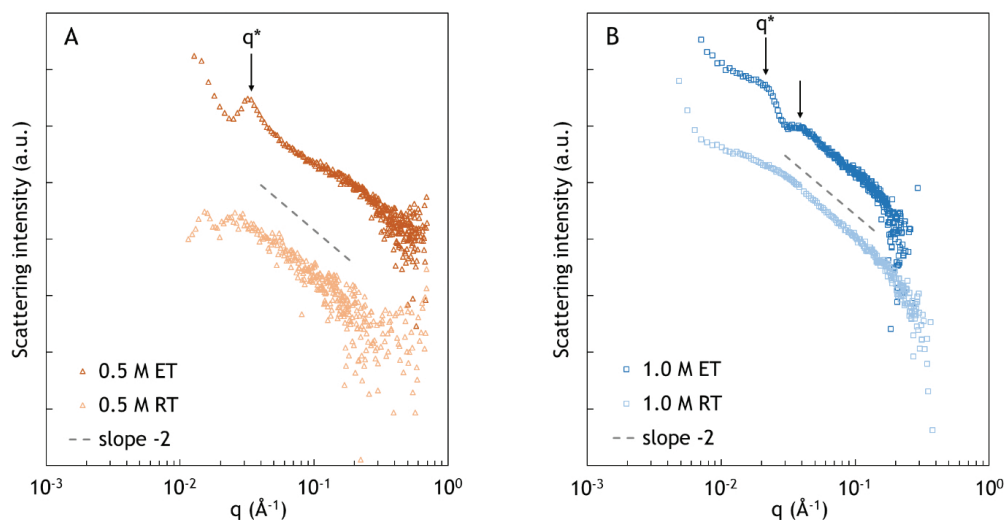
Figure 4.4 – SAXS spectra of PNIPAM-*b*-PDMAEMA and PNIPAM-*b*-PAA-*b*-PNIPAM in **A** 0.5 M and **B** 1.0 M NaCl at 27 °C (RT), and 67 °C (ET). As a guide to the eye, a dashed line is displayed to indicate a slope of -2. The presented data was corrected for solvent contributions and plotted on a log-log scale. Scattering intensities of the ET data were adjusted for clear display.

NMR

For 1.0 M NaCl, similar peak patterns are observed when comparing the 1D spectra of unmixed and mixed polymers. Also, when comparing the polymer mixtures at 0.5 and 1.0 M NaCl, the peak intensity is higher and the peak splitting is more defined at increased salt, Figure 4.3. This indicates a higher mobility, and thus a higher solubility of the polymers at high salt. Furthermore, in the NOESY spectra, no cross-peaks between PDMAEMA and PAA can be observed at room temperature for representative resonances at 2.1 and 2.9 ppm, Figure A4.17. This can be caused by an inability of the system to detect nuclear Overhauser cross-peaks, for example due to low solubility of the polymers, or due to a large distance between the polymers. From the proton spectra, it is known that the polymers have a high mobility, therefore it is most likely that correlations are not present on the timescale of the measurement, because of a larger separation of the polyelectrolyte blocks. Together, this supports the hypothesis of the presence of PCMs with a dehydrated PNIPAM core and a hydrated polyelectrolyte corona at high salt concentrations.

At 67 °C, the intensity of the peaks has slightly decreased and the proton peak of the PNIPAM has even disappeared, Figure 4.3. This indicates a reduced solubility at temperatures above the LCST. Also at this salt concentration, the temperature transition is a reversible process, Figure A4.14. Furthermore, cross-peaks between PDMAEMA and PAA, 2.1;2.9 ppm, appear in the NOESY spectra when the temperature is increased, Figure A4.18. The appearance of the cross-peaks indicates reoccur-

ring complex coacervation at elevated temperature.[32]

Small angle X-ray scattering

At 1.0 M NaCl, the scattering intensity is higher as compared to 0.5 M NaCl, because of the denser core and thus, a higher density difference between the core and the solvent, which resulted in higher scattering intensities and clearer data. At room temperature, a scaling of -2 can be observed. As spherical particles are expected from the multi-angle LS results, we expect a similar morphology as for the 0.5 M NaCl samples, i.e. a weak distinction between the core and corona, causing a lower slope. At low q values, an upturn in the scattering intensity is observed, which is ascribed to the presence of larger sized objects.[18, 32] These objects may form upon bridge formation between micelles.

At elevated temperature, two broad peaks can be observed at approximately 0.021 and 0.037 Å^{-1}, as is indicated with the black arrows in Figure 4.4B. Similar to 0.5 M NaCl, the peaks likely originate from a typical distance between PNIPAM and complex coacervate domains. The broad higher order peak at $q \approx 0.037$ Å^{-1}, indicates ordering over longer distances. However, the shape and order of the domains cannot be determined from the spectrum. From q^*, the characteristic distance between the domains is calculated as ≈ 30 nm.[33, 34, 35, 36] Compared to the sample at 0.5 M NaCl, the characteristic distance is larger, which could be because of the difference in salt concentration, and thus the difference in water content, as was also observed in the peak splitting in NOESY-NMR. The sample with high salt has weaker interpolyelectrolyte interactions, leading to a looser structure and lower polymer concentration, and thus larger distances between the PNIPAM domains, as was also found by Krogstad et al.[3, 33]

Conclusions

By mixing oppositely charged polyelectrolytes functionalized with PNIPAM, different micelle morphologies could be obtained at room temperature. At low salt, C3Ms were observed with a PNIPAM corona and a polyelectrolyte core. At sufficiently high salt concentration, the micelles turned inside out, into PCMs with a water-soluble polyelectrolyte corona, and a PNIPAM core. Both micelles displayed a salt dependent T_{cp}, leading to aggregation and sedimentation in aqueous solution. The resulting concentrated phase contains domains of PNIPAM and complex coacervate with a salt dependent separation distance. The ability to adjust the morphology and solubility of the micelles can be an important tool to apply complex coacervates as drug delivery vehicles, or as underwater or medical adhesives.

Appendix
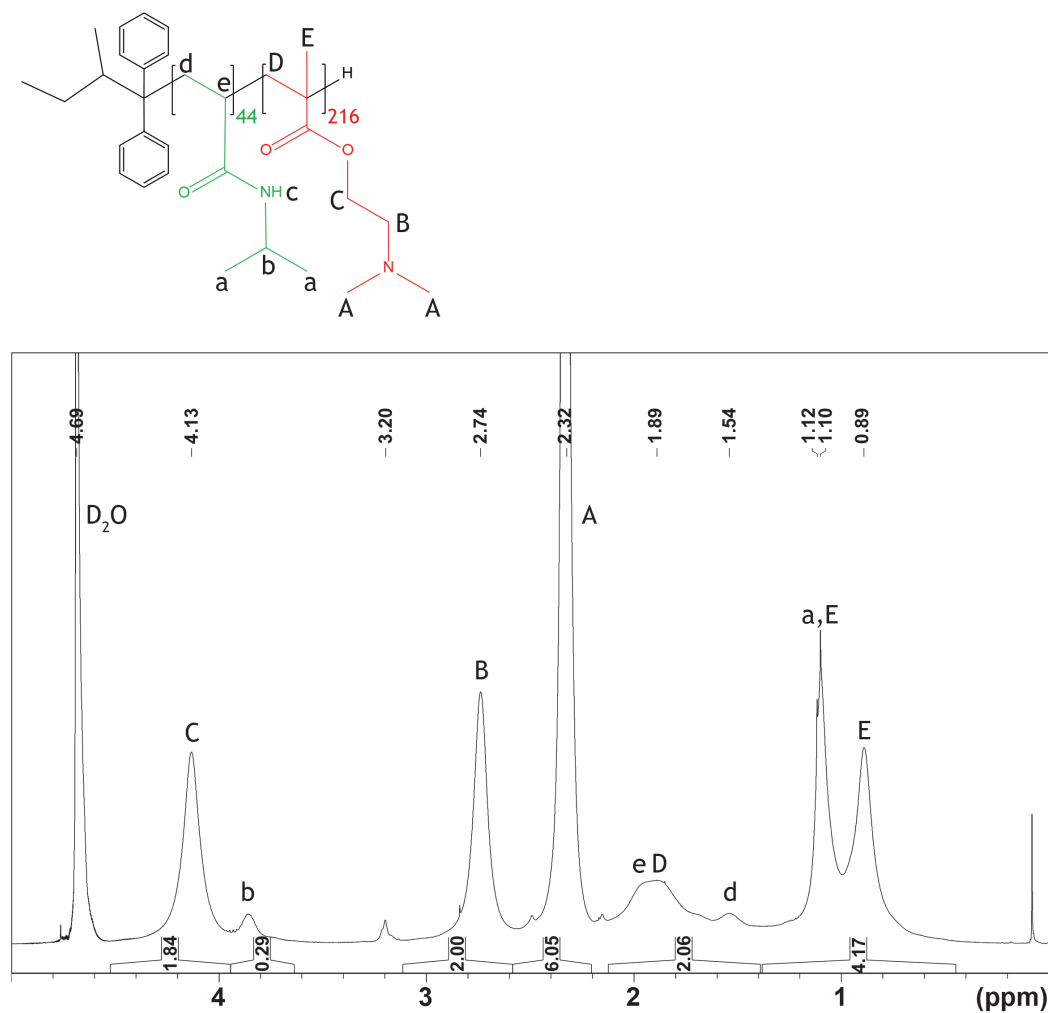
1D NMR spectra of purified polymers

Figure A4.1 – ^{1}H-NMR spectrum of PNIPAM-*b*-PDMAEMA, purchased from Polymer Source Ltd, in D$_2$O. As provided by the supplier; M_n 38.2 kDa, PDI 1.05.
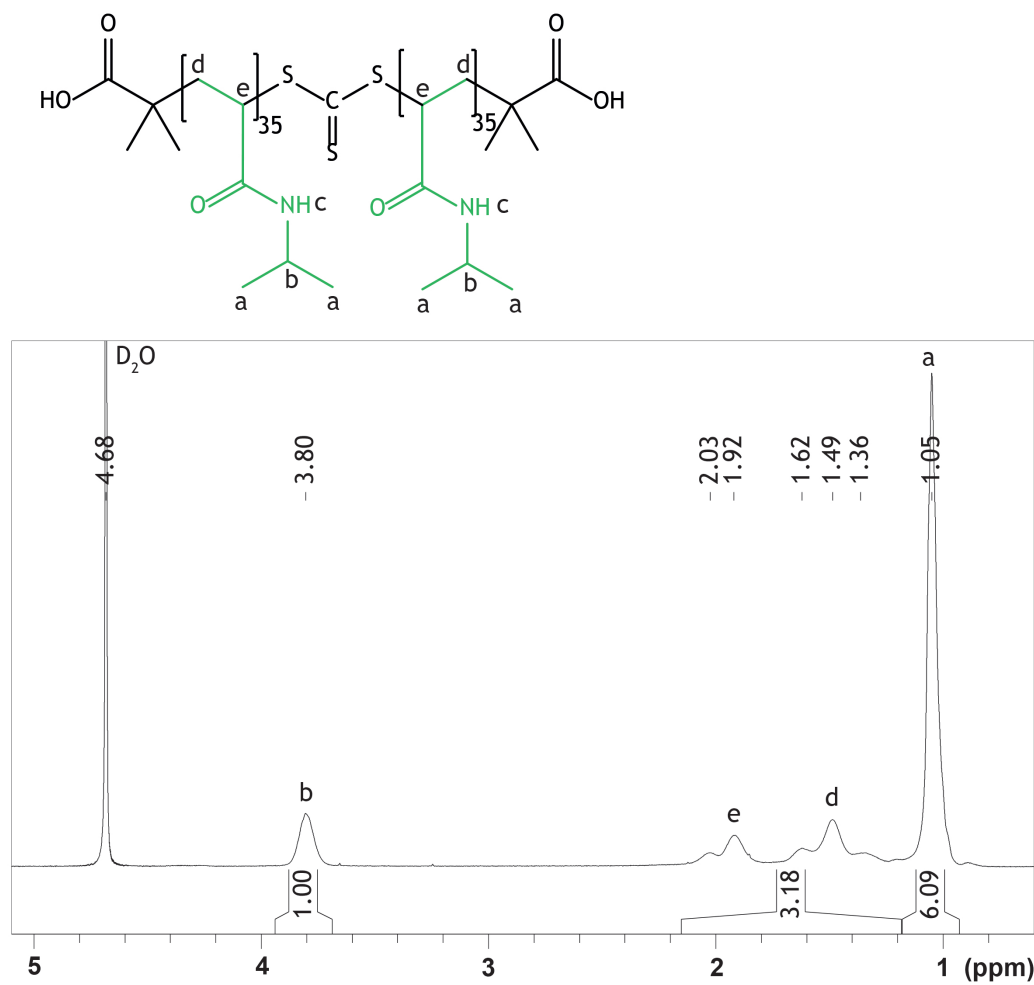
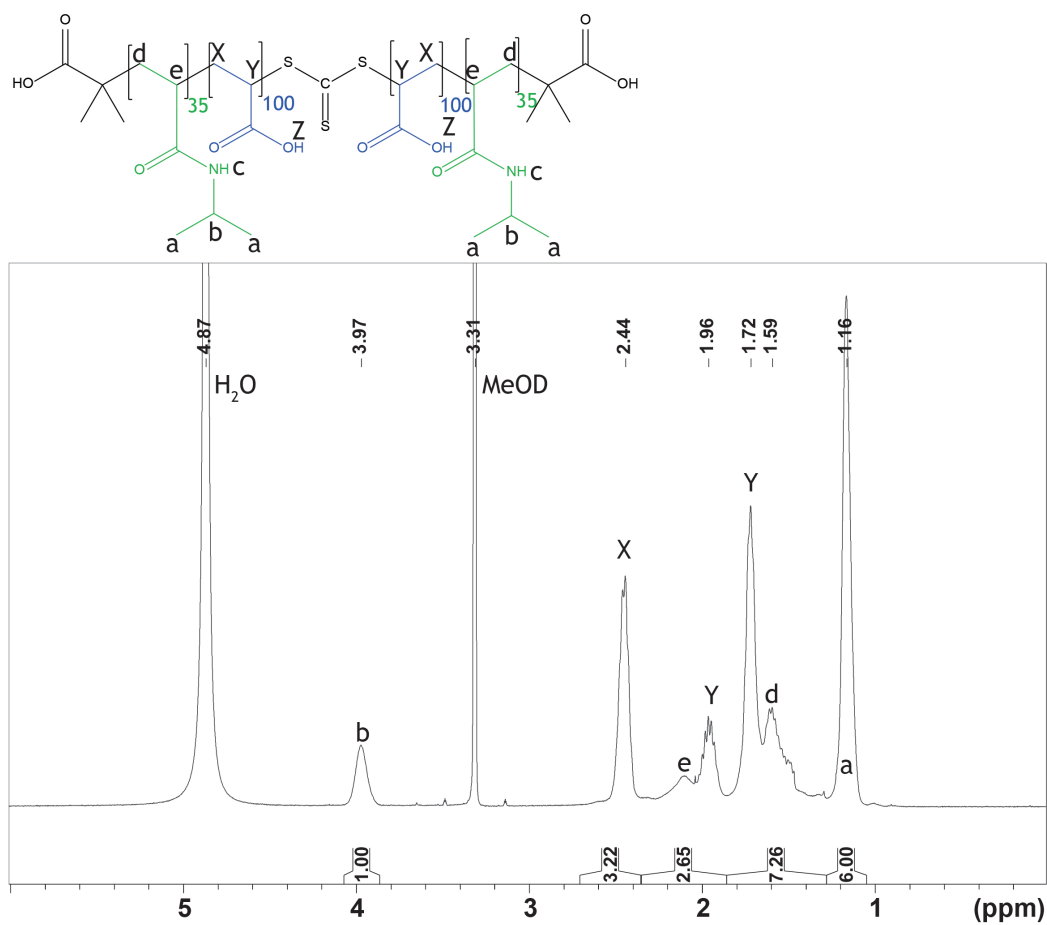**Figure A4.2** – ^{1}H-NMR spectrum of the PNIPAM precursor used to synthesize PNIPAM-*b*-PAA-*b*-PNIPAM, measured in D$_2$O.

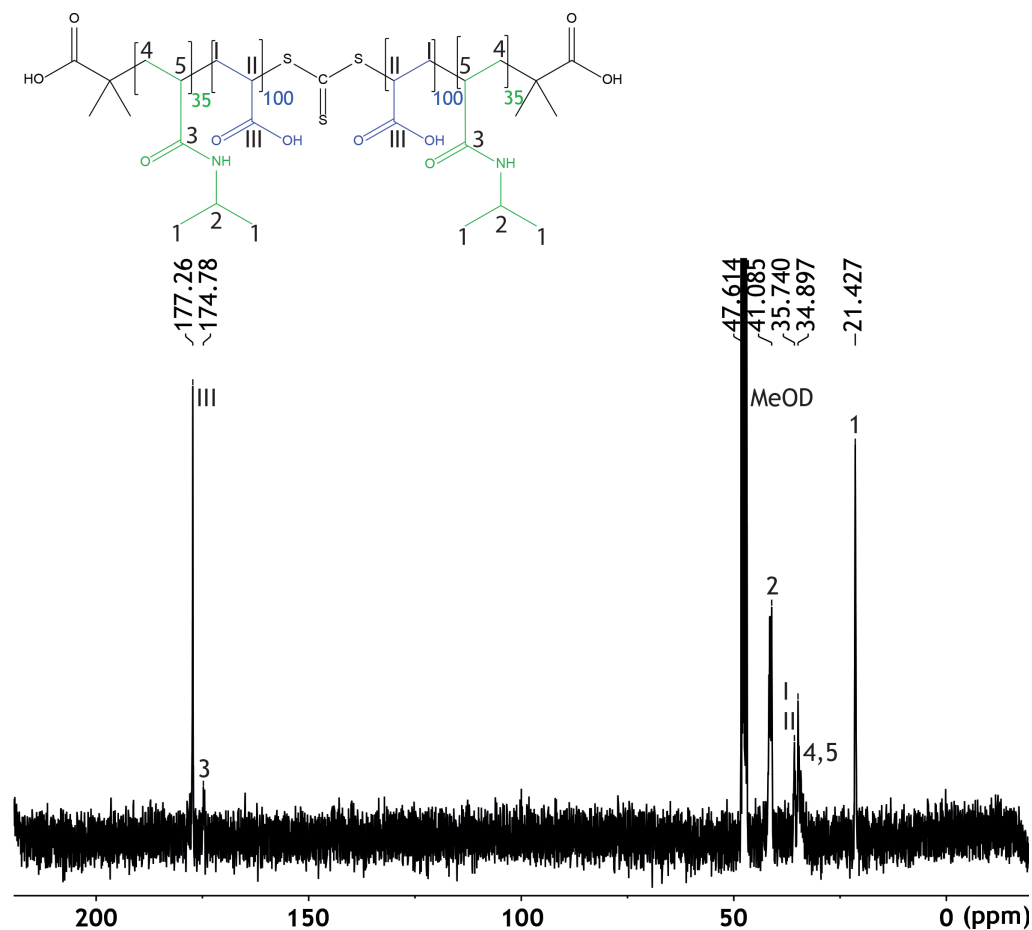**Figure A4.3** – ^{1}H-NMR spectrum of PNIPAM-*b*-PAA-*b*-PNIPAM after deprotection in HFIP, measured in MeOD.

Figure A4.4 – ^{13}C-NMR spectrum of NIPAM-*b*-AA-*b*-NIPAM after deprotection in HFIP, measured in MeOD. A clear carboxylic acid peak can be observed at 177 ppm, while *tert*-butyl is absent as it normally appears around 28 ppm

COSY NMR spectra of purified polymers in D₂O
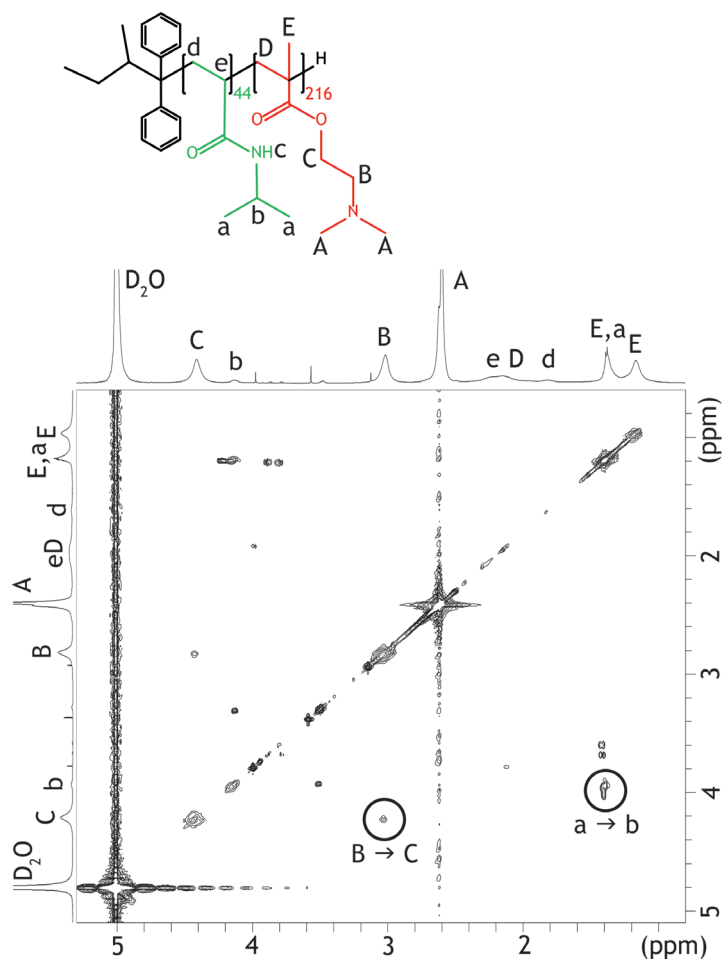
Figure A4.5 – COSY spectrum of PNIPAM-*b*-PDMAEMA in D₂O. Two clear cross–peaks are observed, the first shows the ethyl group in the DMAEMA side chain, while the second shows the propyl group of the PNIPAM. Other cross–peaks are assigned to small impurities in the sample. As the backbone peaks have a relatively low intensity, cross–peaks cannot be observed.
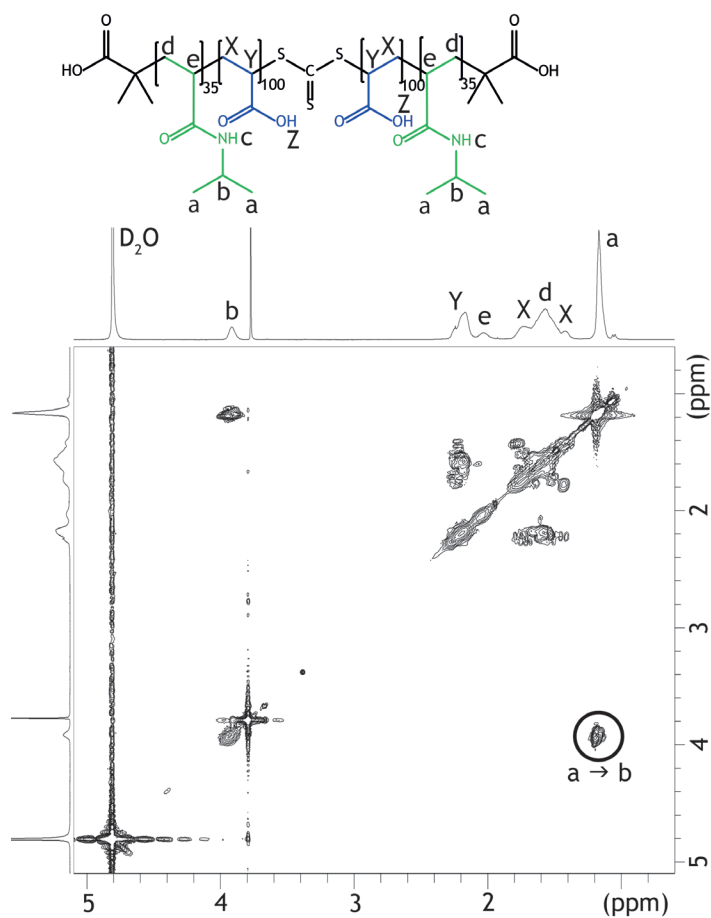
Figure A4.6 – COSY spectrum of PNIPAM-*b*-PAA-*b*-PNIPAM in D$_2$O. Only one clear cross-peak is observed, that shows the propyl group of the PNIPAM. As the backbone peaks of the PNIPAM have a relatively low intensity, cross-peaks cannot be observed.

Zeta potential measurements
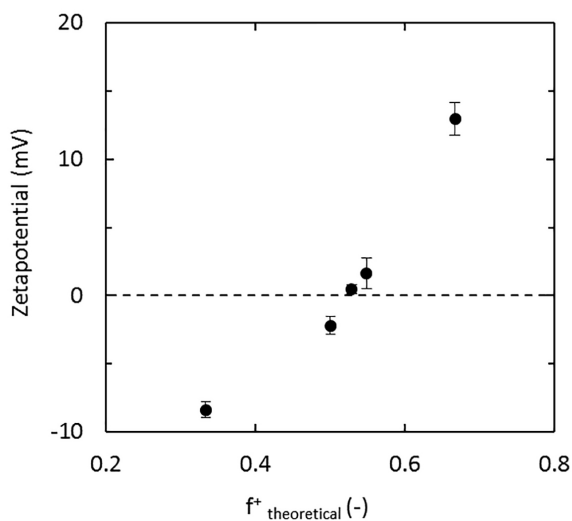
Figure A4.7 – Representative determination of equal charge by zeta potential determination, based on the charge fraction f^+. Using $f^+ = \frac{n^+}{n^+ + n^-}$, with n^+ being the number of cationic monomers and n^- the number of anionic monomers present in solution. For every new combination of stock solutions, the fraction of equal charge has to be determined.

Light scattering
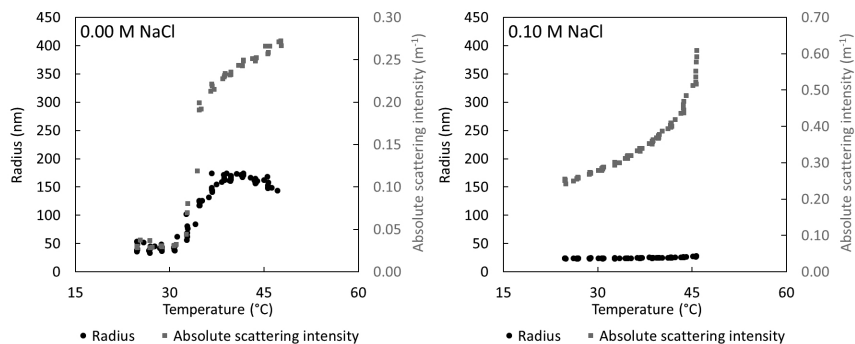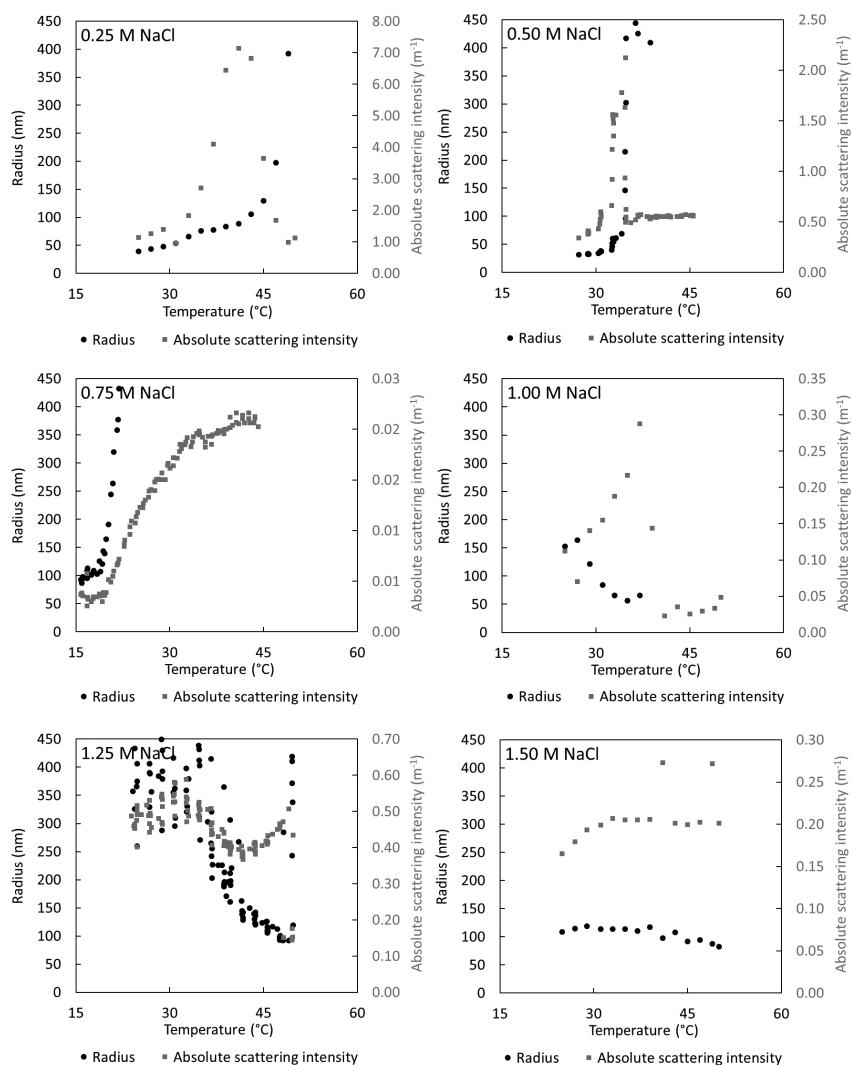
Figure A4.8 – Overview of dynamic light scattering results of charge balanced polymer solutions, containing varying concentrations of NaCl, measured while the temperature was increased with 2 °C per 10 minutes. The data points shown are averages of 5 measurements for the 0.00, 0.10, 0.50, 0.75 and 1.25 M NaCl samples. Samples of 0.25, 1.00 and 1.50 M NaCl were measured on the Malvern Zetasizer Nano ZS and are averages of three consecutive measurements existing of multiple data points.
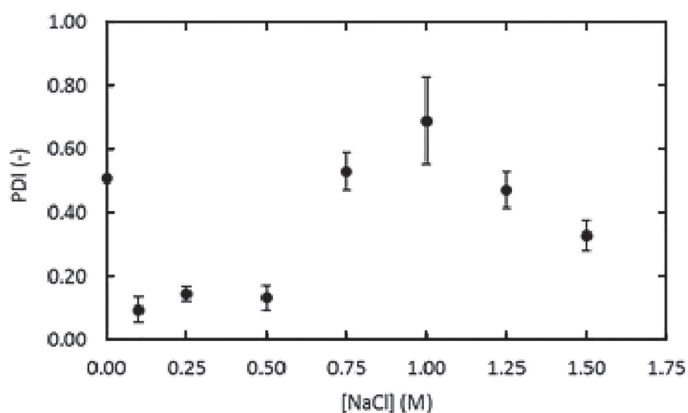
Figure A4.9 – Overview of the PDI values below LCST as measured by DLS and calculated using ALV-7004 Correlator software or using Zetasizer software (version 7.02, Malvern Instruments, U.K.) using the second cumulant. For the samples containing 0.10, 0.25 and 0.50 M NaCl, narrow PDI values, comparable to values found in literature., were observed.[13, 16] From this, it can be concluded that the radii for these can be used as realistic values for the objects present in solution below LCST. Also, for these samples at low salt monomodal decorrelation curves have been observed using CONTIN. However, the variation in radii of the other samples is too high to determine the objects sizes from these values. Therefore, only qualitative comparisons are made. Additionally, multimodal decorrelation curves have been observed for CONTIN analysis, meaning that objects with multiple sizes are present in solution and therefore the value for the radius from the ALV software cannot be used. Error bars show the standard deviation from the calculated average PDI of all measurements below LCST.

Figure A4.10 – Picture of PNIPAM-*b*-PDMAEMA and PNIPAM-*b*-PAA-*b*-PNIPAM at 1 wt% in 0.5 M NaCl at 50 °C. As a result of the elevated temperature, a white concentrated phase coexists with a dilute solvent phase. The solid phase sticks to the bottom of the tube when the tube is inverted.
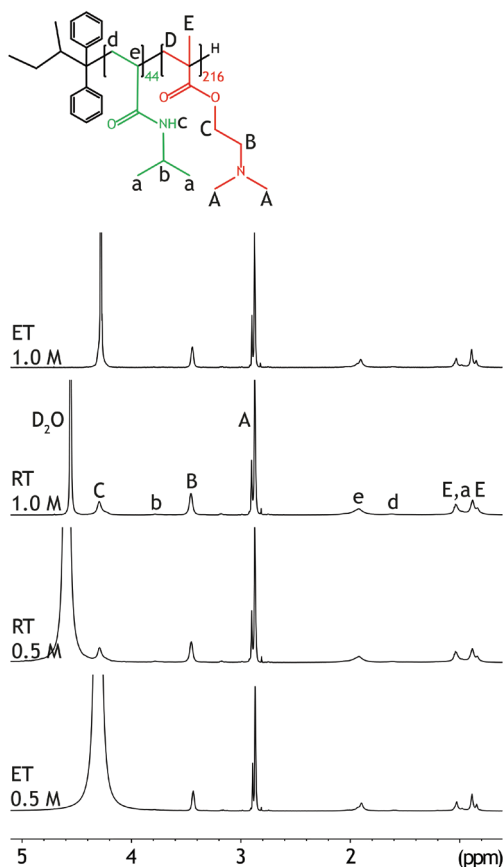
¹H-NMR spectra in deuterated salt solutions

Figure A4.11 – ¹H NMR in 0.5 M and 1.0 M NaCl at room temperature (RT) and 67 °C (ET) of NIPAM-*b*-DMAEMA. The peak intensities are normalized by the intensity of DMAEMA, peak A. Due to storage of the samples water was attracted by the samples. This effect was more severe for the 0.5 M NaCl sample than for the 1.0 M NaCl sample, causing a broader solvent peak at low salt. Increasing temperature causes minor differences in the NIPAM peaks. When comparing to the polymer mixtures, peak broadening can be observed at 2.9 ppm for the DMAEMA side group, and between 2.1 and 1.7 ppm for the backbone area in the spectrum of the mixture, Figure 4.3.
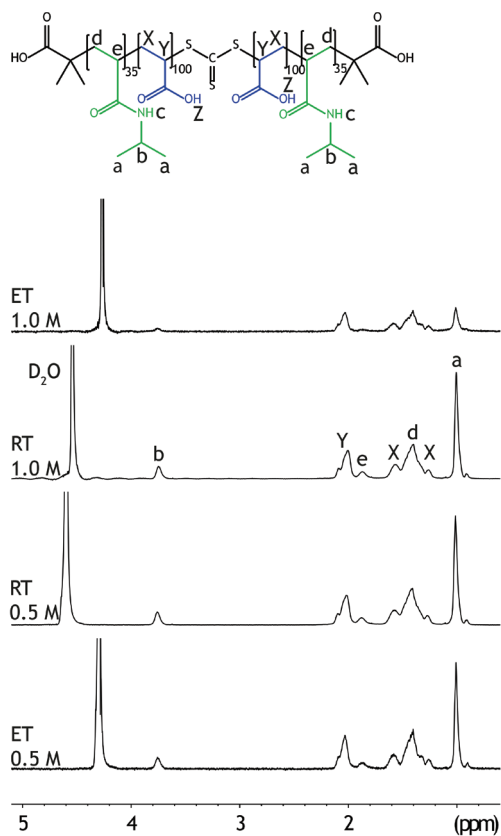
Figure A4.12 – ^{1}H NMR in 0.5 M and 1.0 M NaCl at room temperature (RT) and 67 °C (ET) of NIPAM-*b*-AA-*b*-NIPAM. The peak intensities are normalized by the area of the solvent peak. Increasing temperature results in decreasing peak intensities for peaks at 1.0 M NaCl. When comparing to the polymer mixtures, peak broadening can be observed between 2.1 and 1.2 ppm for the backbone area in the spectrum of the mixture, Figure 4.3.
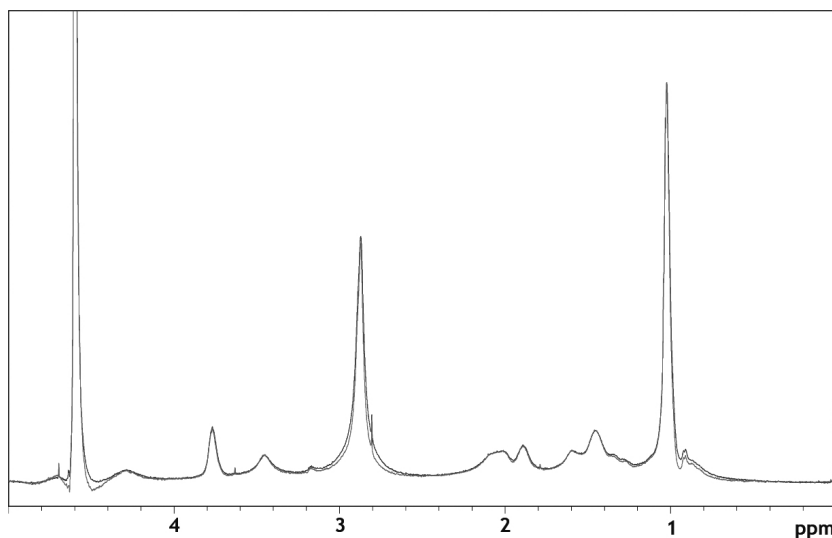
Figure A4.13 – ^{1}H-NMR of the mixture of PNIPAM-*b*-PDMAEMA and PNIPAM-*b*-PAA-*b*-PNIPAM in 0.5 M NaCl at room temperature, before (dark grey) and after (light grey) heating. Both spectra largely overlap, showing the full reversibility of the system.
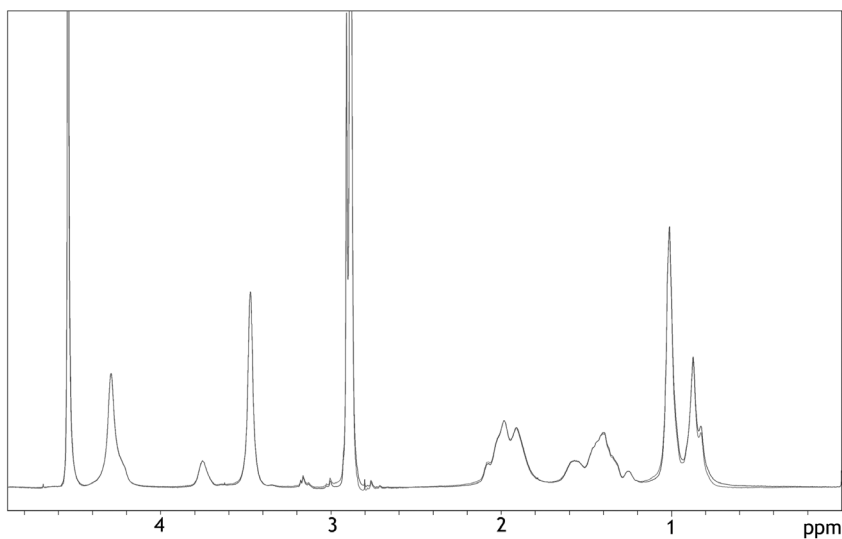

Figure A4.14 – ^{1}H-NMR of the mixture of PNIPAM-*b*-PDMAEMA and PNIPAM-*b*-PAA-*b*-PNIPAM in 1.0 M NaCl at room temperature, before (dark grey) and after (light grey) heating. Both spectra largely overlap, showing the full reversibility of the system.

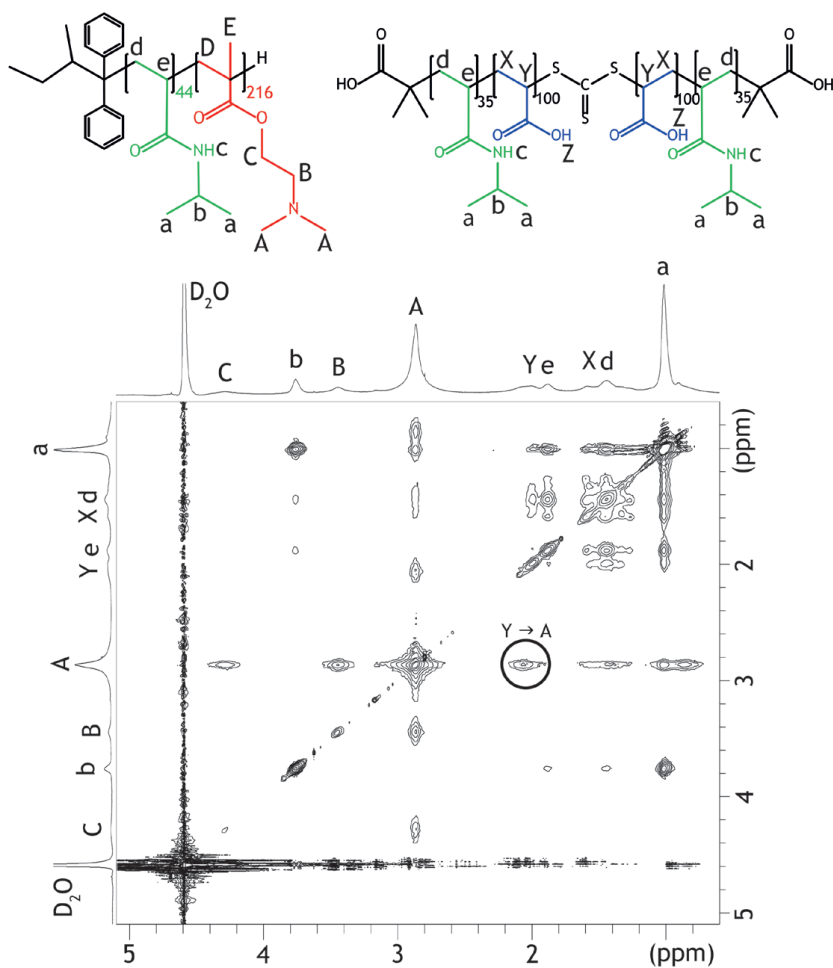# NOESY NMR spectra in deuterated salt solutions

Figure A4.15 – NOESY NMR of the mixture of PNIPAM-*b*-PDMAEMA and PNIPAM-*b*-PAA-*b*-PNIPAM in 0.5 M NaCl at room temperature. A cross-peak between the blocks is present between PAA and PDMAEMA (black circle).
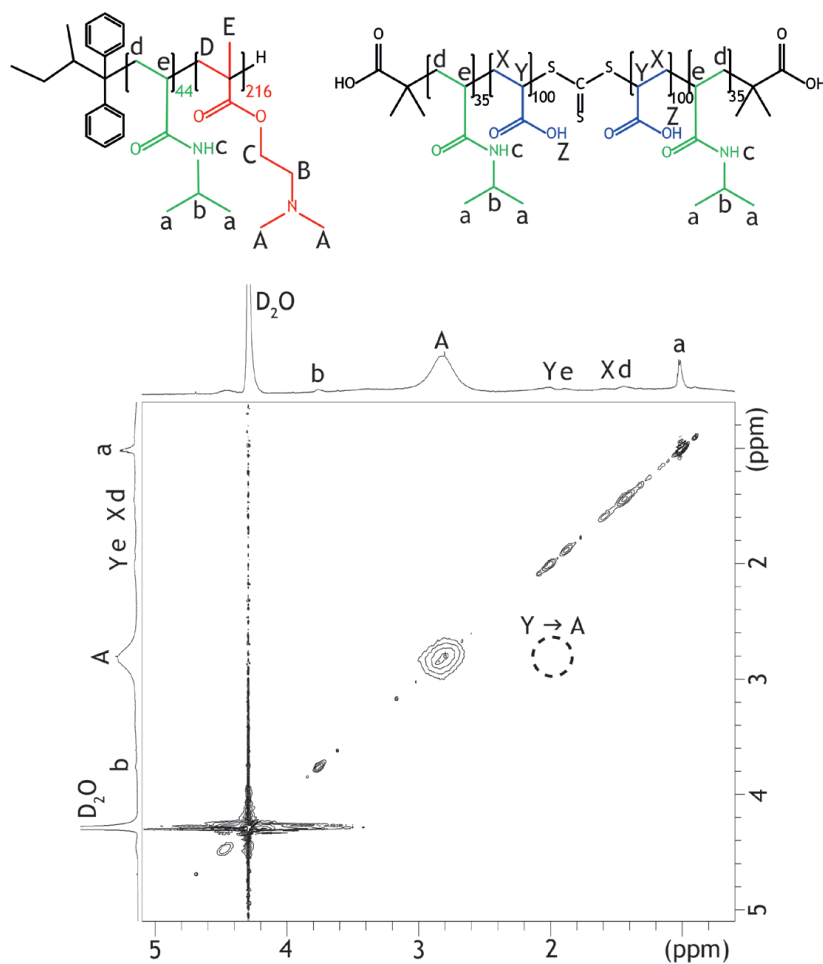
Figure A4.16 – NOESY NMR of the mixture of PNIPAM-*b*-PDMAEMA and PNIPAM-*b*-PAA-*b*-PNIPAM in 0.5 M NaCl at 67 °C. Cross-peaks between the blocks are absent.
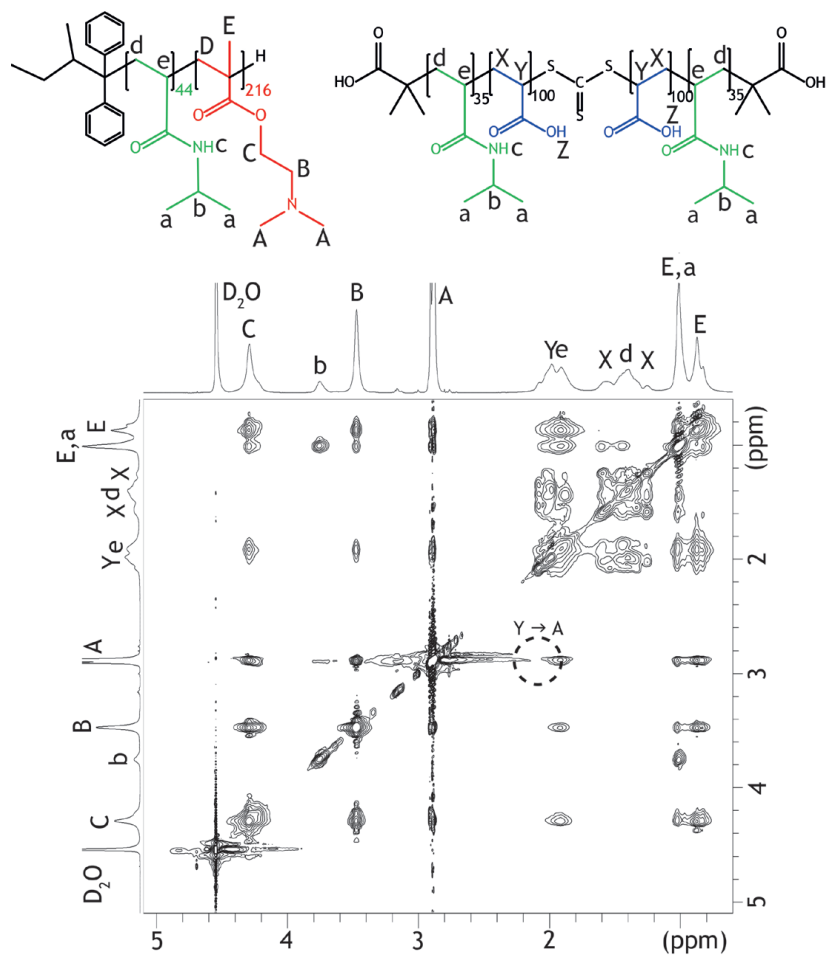
Figure A4.17 – NOESY NMR of the mixture of PNIPAM-*b*-PDMAEMA and PNIPAM-*b*-PAA-*b*-PNIPAM in 1.0 M NaCl at RT. Cross-peaks between the blocks are absent.
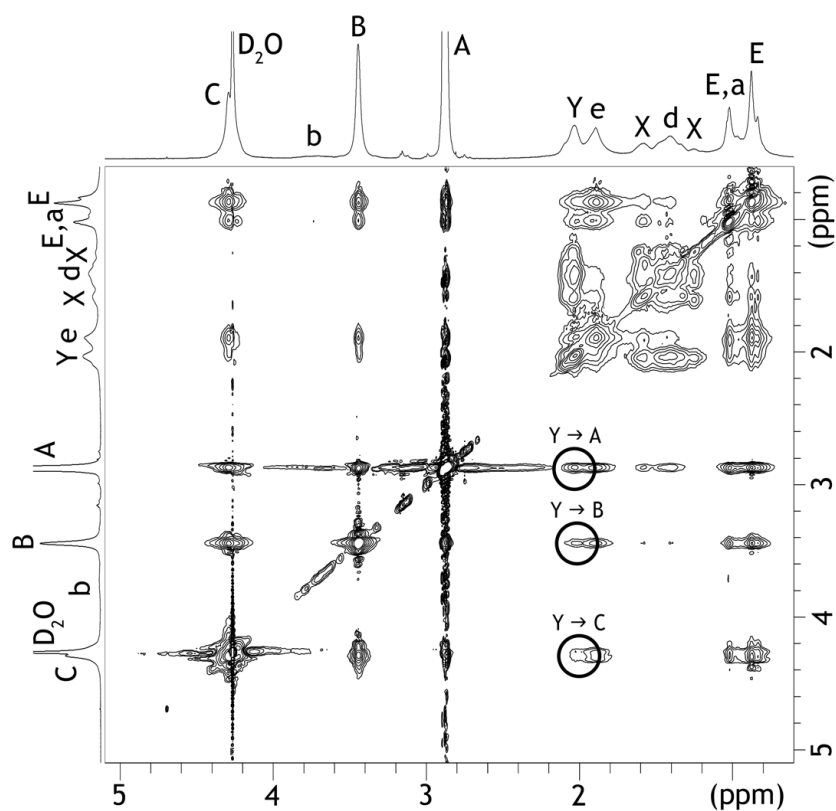
Figure A4.18 – NOESY NMR of the mixture of PNIPAM-*b*-PDMAEMA and PNIPAM-*b*-PAA-*b*-PNIPAM in 1.0 M NaCl at 67 °C. Cross-peaks between the polyelectrolytes blocks are present. Peaks are assigned as in Figure A4.17
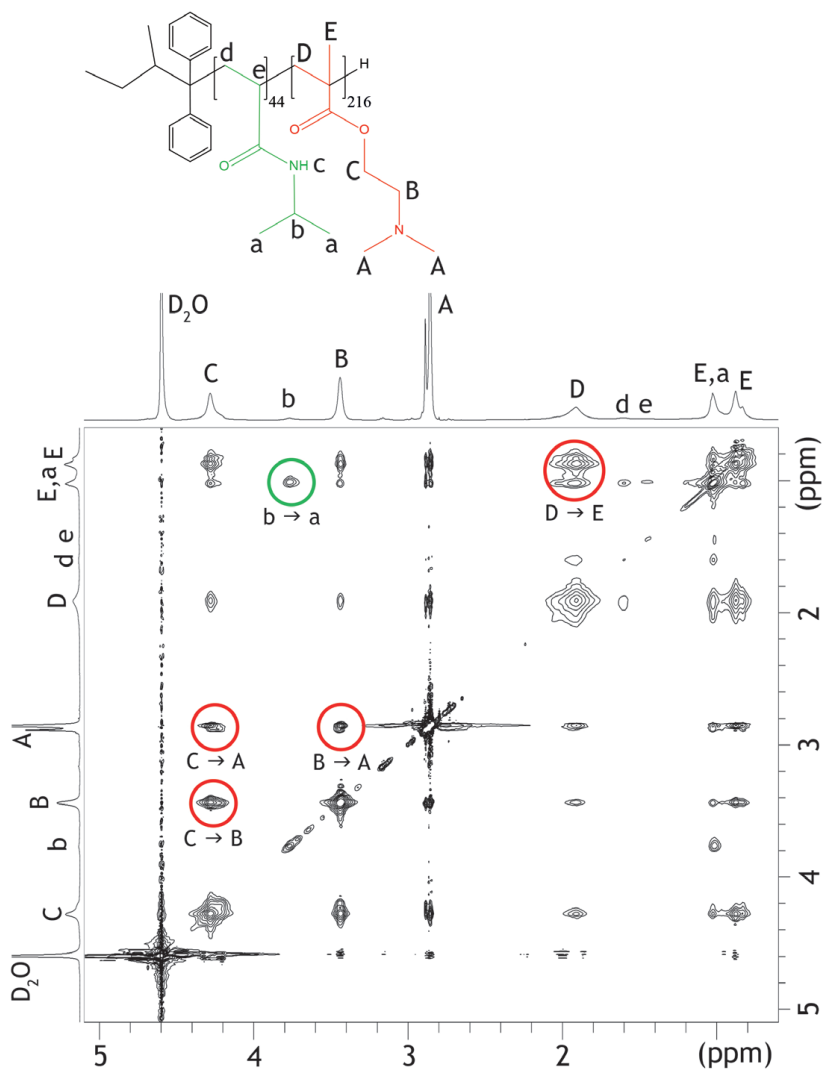
Figure A4.19 – NOESY NMR of PNIPAM-*b*-PDMAEMA in 0.5 M NaCl at room temperature. Cross-peaks can be observed between the DMAEMA peaks (red circles) e.g. at 1.9;0.9, 1.9;2.9, 1.9;3.4 and 1.9;4.3 ppm, or between the NIPAM peaks (green circle) at 1.0;3.8 ppm.
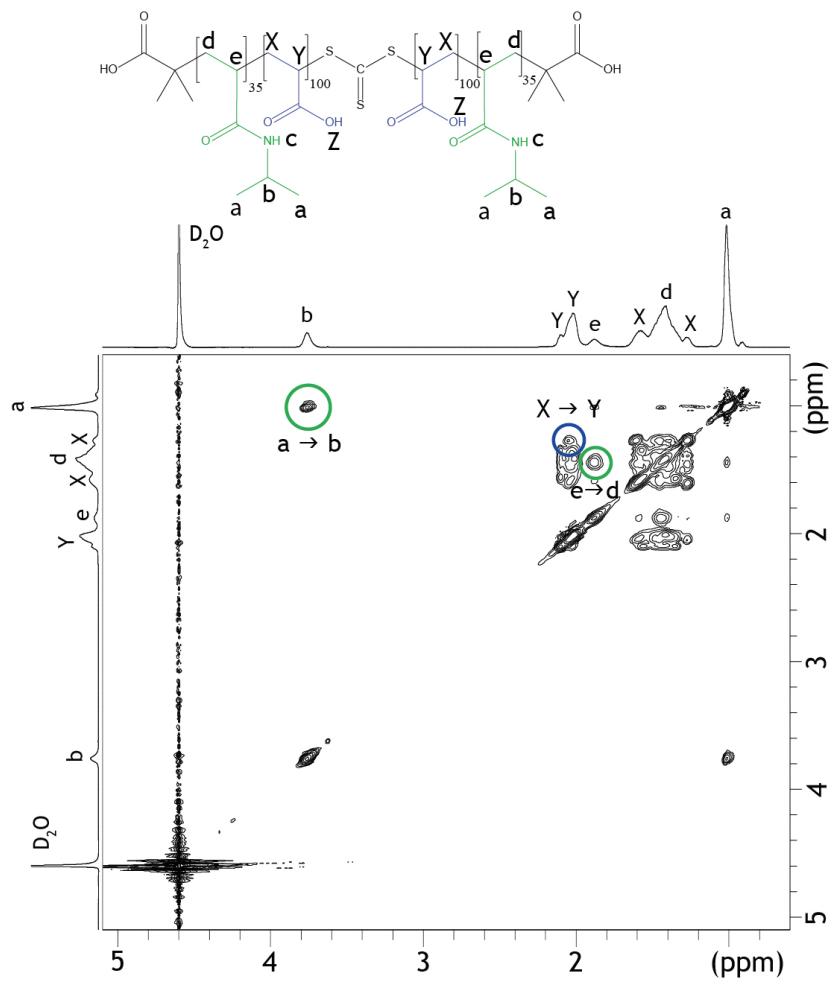
Figure A4.20 – NOESY NMR of PNIPAM-*b*-PAA-*b*-PNIPAM in 0.5 M NaCl at room temperature. Two cross-peaks between the PNIPAM compounds (green circles) are present in the spectrum at 1.0;3.8 and 1.9;3.8 ppm. A cross-peak between PAA and PNIPAM (black circle) can be found at 1.4;3.8 ppm.

PNIPAM solubility

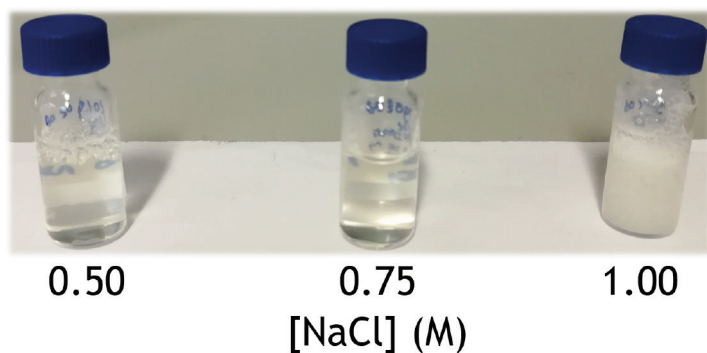**Figure A4.21** – Solubility of 1 wt% PNIPAM, which was used as precursor to synthesize PNIPAM-*b*-PAA-*b*-PNIPAM, in NaCl solutions with changing concentrations. At 0.50 and 0.75 M NaCl clear solutions are observed, while at 1.00 M NaCl turbidity is seen. This indicates that the PNIPAM is soluble at 0.50 and 0.75 M NaCl, but insoluble at 1.00 M NaCl. At the moment the picture was taken, the temperature in the room was 19 °C.

Bibliography

[1] E. Spruijt, M. A. C. Stuart, and J. van der Gucht. Linear viscoelasticity of polyelectrolyte complex coacervates. *Macromolecules*, 46(4):1633–1641, 2013.

[2] J. van der Gucht, E. Spruijt, M. Lemmers, and M. A. C. Stuart. Polyelectrolyte complexes: Bulk phases and colloidal systems. *Journal of Colloid and Interface Science*, 361(2):407–422, 2011.

[3] E. Spruijt, A. H. Westphal, J. W. Borst, M. A. C. Stuart, and J. van der Gucht. Binodal compositions of polyeleetrolyte complexes. *Macromolecules*, 43(15):6476–6484, 2010.

[4] R. J. Stewart, C. S. Wang, and H. Shao. Complex coacervates as a foundation for synthetic underwater adhesives. *Advances in Colloid and Interface Science*, 167(1-2):85–93, 2011.

[5] S. Kaur, G. M. Weerasekare, and R. J. Stewart. Multiphase adhesive coacervates inspired by the sand-castle worm. *Acs Applied Materials & Interfaces*, 3(4):941–944, 2011.

[6] A. S. Hoffman. Hydrogels for biomedical applications. *Advanced Drug Delivery Reviews*, 64:18–23, 2012.

[7] D. Priftis and M. Tirrell. Phase behaviour and complex coacervation of aqueous polypeptide solutions. *Soft Matter*, 8(36):9396–9405, 2012.

[8] A. H. Hofman, I. A. van Hees, J. Yang, and M. Kamperman. Bioinspired underwater adhesives by using the supramolecular toolbox. *Advanced Materials*, 30(19), 2018.

[9] I. K. Voets, P. M. Moll, A. Aqil, C. Jerome, C. Detrembleur, P. de Waard, A. de Keizer, and M. A. C. Stuart. Temperature responsive complex coacervate core micelles with a peo and pnipaam corona. *Journal of Physical Chemistry B*, 112(35):10833–10840, 2008.

[10] A. Harada and K. Kataoka. Formation of polyion complex micelles in an aqueous milieu from a pair of oppositely-charged block-copolymers with poly(ethylene glycol) segments. *Macromolecules*, 28(15):5294–5299, 1995.

[11] D. V. Pergushov, A. H. E. Muller, and F. H. Schacher. Micellar interpolyelectrolyte complexes. *Chemical Society Reviews*, 41(21):6888–6901, 2012.

[12] N. Rapoport. Physical stimuli-responsive polymeric micelles for anti-cancer drug delivery. *Progress in Polymer Science*, 32(8-9):962–990, 2007.

[13] J. S. Park, Y. Akiyama, Y. Yamasaki, and K. Kataoka. Preparation and characterization of polyion complex micelles with a novel thermosensitive poly(2-isopropyl-2-oxazoline) shell via the complexation of oppositely charged block ionomers. *Langmuir*, 23(1):138–146, 2007.

[14] S. Bayati, K. E. Bergquist, K. Z. Zhu, B. Nystrom, J. S. Pedersen, L. Galantini, and K. Schillen. Mixed micelles of oppositely charged poly(n-isopropylacrylamide) diblock copolymers. *Journal of Polymer Science Part B-Polymer Physics*, 55(19):1457–1469, 2017.

[15] G. Masci, S. De Santis, and C. Cametti. Dielectric properties of micellar aggregates due to the self-assembly of thermoresponsive diblock copolymers. *Journal of Physical Chemistry B*, 115(10):2196–2204, 2011.

[16] H. Dautzenberg, Y. B. Gao, and M. Hahn. Formation, structure, and temperature behavior of polyelectrolyte complexes between ionically modified thermosensitive polymers. *Langmuir*, 16(23):9070–9081, 2000.

[17] S. De Santis, R. D. Ladogana, M. Diociaiuti, and G. Masci. Pegylated and thermosensitive polyion complex micelles by self-assembly of two oppositely and permanently charged diblock copolymers. *Macromolecules*, 43(4):1992–2001, 2010.

[18] C. Dahling, G. Lotze, H. Mori, D. V. Pergushov, and F. A. Plamper. Thermoresponsive segments retard the formation of equilibrium micellar interpolyelectrolyte complexes by detouring to various intermediate structures. *Journal of Physical Chemistry B*, 121(27):6739–6748, 2017.

[19] J. Li, W. D. He, N. He, S. C. Han, X. L. Sun, L. Y. Li, and B. Y. Zhang. Synthesis of peg-pnipam-plys hetero-arm star polymer and its variation of thermo-responsibility after the formation of polyelectrolyte complex micelles with paa. *Journal of Polymer Science Part a-Polymer Chemistry*, 47(5):1450–1462, 2009.

[20] M. Kamimura, J. O. Kim, A. V. Kabanov, T. K. Bronich, and Y. Nagasaki. Block ionomer complexes of peg-block-poly(4-vinylbenzylphosphonate) and cationic surfactants as highly stable, ph responsive

drug delivery system. *Journal of Controlled Release*, 160(3):486–494, 2012.

[21] M. A. Ward and T. K. Georgiou. Thermoresponsive polymers for biomedical applications. *Polymers*, 3(3):1215–1242, 2011.

[22] K. J. Krzyminski, M. Jasionowski, and A. Gutowska. Reversible sol-gel transitions in aqueous solutions of n-isopropylacrylamide ionic copolymers. *Polymer International*, 57(4):592–604, 2008.

[23] T. Patel, G. Ghosh, S. Yusa, and P. Bahadur. Solution behavior of poly(n-isopropylacrylamide) in water: Effect of additives. *Journal of Dispersion Science and Technology*, 32(8):1111–1118, 2011.

[24] J. Adelsberger, A. Kulkarni, A. Jain, W. N. Wang, A. M. Bivigou-Koumba, P. Busch, V. Pipich, O. Holderer, T. Hellweg, A. Laschewsky, P. Muller-Buschbaum, and C. M. Papadakis. Thermoresponsive ps-b-pnipam-b-ps micelles: Aggregation behavior, segmental dynamics, and thermal response. *Macromolecules*, 43(5):2490–2501, 2010.

[25] H. Feil, Y. H. Bae, J. Feijen, and S. W. Kim. Effect of comonomer hydrophilicity and ionization on the lower critical solution temperature of n-isopropylacrylamide copolymers. *Macromolecules*, 26(10):2496–2500, 1993.

[26] M. Cetintas, J. de Grooth, A. H. Hofman, H. M. van der Kooij, K. Loos, W. M. de Vos, and M. Kamperman. Free-standing thermo-responsive nanoporous membranes from high molecular weight ps-pnipam block copolymers synthesized via raft polymerization. *Polymer Chemistry*, 8(14):2235–2243, 2017.

[27] J. T. Lai, D. Filla, and R. Shea. Functional polymers from novel carboxyl-terminated trithiocarbonates as highly efficient raft agents. *Macromolecules*, 35(18):6754–6756, 2002.

[28] Y. J. Zhang, S. Furyk, D. E. Bergbreiter, and P. S. Cremer. Specific ion effects on the water solubility of macromolecules: Pnipam and the hofmeister series. *Journal of the American Chemical Society*, 127(41):14505–14510, 2005.

[29] C. M. Li, N. J. Buurma, I. Haq, C. Turner, S. P. Armes, V. Castelletto, I. W. Hamley, and A. L. Lewis. Synthesis and characterization of biocompatible, thermoresponsive abc and aba triblock copolymer gelators. *Langmuir*, 21(24):11026–11033, 2005.

[30] H. G. Schild. Poly (n-isopropylacrylamide) - experiment, theory and application. *Progress in Polymer Science*, 17(2):163–249, 1992.

[31] E. Spruijt. *Strength, structure and stability of polyelectrolyte complex coacervates*. Wageningen University, Wageningen, 2012.

[32] H. Wu, J. M. Ting, O. Werba, S. Q. Meng, and M. V. Tirrell. Non-equilibrium phenomena and kinetic pathways in self-assembled polyelectrolyte complexes. *Journal of Chemical Physics*, 149(16), 2018.

[33] D. V. Krogstad, N. A. Lynd, S. H. Choi, J. M. Spruell, C. J. Hawker, E. J. Kramer, and M. V. Tirrell. Effects of polymer and salt concentration on the structure and properties of triblock copolymer coacervate hydrogels. *Macromolecules*, 46(4):1512–1518, 2013.

[34] A. V. Ruzette, S. Tence-Girault, L. Leibler, F. Chauvin, D. Bertin, O. Guerret, and P. Gerard. Molecular disorder and mesoscopic order in polydisperse acrylic block copolymers prepared by controlled radical polymerization. *Macromolecules*, 39(17):5804–5814, 2006.

[35] J. K. Kim, H. H. Lee, S. Sakurai, S. Aida, J. Masamoto, S. Nomura, Y. Kitagawa, and Y. Suda. Lattice disordering and domain dissolution transitions in polystyrene-block-poly(ethylene-co-but-1-ene)-block-polystyrene triblock copolymer having a highly asymmetric composition. *Macromolecules*, 32(20):6707–6717, 1999.

[36] F. M. Abuzaina, A. J. Patel, S. Mochrie, S. Narayanan, A. Sandy, B. A. Garetz, and N. P. Balsara. Structure and phase behavior of block copolymer melts near the sphere-cylinder boundary. *Macromolecules*, 38(16):7090–7097, 2005.

Temperature responsive polyelectrolyte complexes for bio-inspired underwater adhesion

5

Adhesive proteins of marine organisms are mimicked using temperature respons-ive polyelectrolyte complexes (TERPOCs) with a high poly(N-isopropylacrylamide) (PNIPAM) content. Upon mixing aqueous solutions of PNIPAM-b-poly(acylic acid)-b-PNIPAM and poly(dimethylaminoethyl methacrylate) (PDMAEMA), com-plexation between the oppositely charged polyelectrolytes occurs. At low temperatures, complex coacervate core micelles (C3M) are formed, and upon temperature increase the solution turns into a strong solid. The gelation temperature, T_{gel}, and the strength of the TERPOC can be adjusted by altering the salt and polymer concentration. The strongest gel with the lowest T_{gel} is obtained at a high salt and polymer concentration (0.6 M NaCl and 10 wt%). Yet, the best adhesion performance is obtained for a slightly lower salt concentration. Overall, TERPOCs show promising properties for application as injectable underwater adhesives for example in marine environments.

Introduction

Adhesion is weakened by the presence of water, making it challenging to obtain good adhesive performance underwater.[1] Nevertheless, in nature, several marine organisms are found to survive the harsh ocean conditions by adhering themselves onto rocks or by building protective shells using adhesive proteins. A close look at the amino acid composition of the adhesive proteins used by these organisms reveals a high degree of hydrophobic, cationic and anionic amino acids.[2]

Hydrophobic moieties can be beneficial for underwater adhesion in several ways. First, water has to be repelled from the surface to enable proper binding between the surface and the adhesive, and therefore increased hydrophobicity may facilitate contact formation.[2] Second, in several natural systems, complexation occurs between oppositely charged proteins, resulting in phase separation and the formation of a complex coacervate. [3] This phase separation is promoted by hydrophobic groups through decreasing the solubility of the proteins in aqueous solution.[2, 4, 5] Third, the presence of hydrophobic domains within a complex coacervate reduces the mobility of the system and leads to more solid-like behaviour.[6] However, for a water-based adhesive, large amounts of hydrophobic moieties result in processing difficulties, i.e. the viscosity increase will make it difficult to inject the material.[7] For this reason, we investigate the use of a temperature responsive polymer, poly(N-isopropyl acrylamide) (PNIPAM), to mimic the hydrophobic amino acids of the natural adhesive proteins without sacrificing the injectability.

PNIPAM is a well-studied temperature responsive polymer with a lower critical solution temperature (LCST).[8] Hence, PNIPAM is soluble in aqueous solutions at room temperature, but becomes insoluble when the LCST of approximately 32 °C is exceeded.[9] This change is induced by the formation of hydrogen bonds within the PNIPAM chains, leading to a chain collapse and the formation of a solid material.[10] Using PNIPAM in underwater adhesives allows easy processing at low temperatures and solidification at high temperatures.[11]

To provide the material with viscoelastic properties, oppositely charged polyelectrolytes are inserted into the PNIPAM based adhesive, which results in complexation. Complex coacervates are fluid-like, water rich, and water insoluble materials that exhibit good surface wetting.[5, 12] The fluidity enables easy application of an adhesive, e.g. by injection, and good surface wetting permits an optimal contact between the surface and the adhesive.[2, 12] Moreover, by adjusting the salt concentration, the viscoelastic properties of the complex can be adjusted, which is a useful tool in the development of underwater adhesives. Because of these characteristics, complex coacervates are interesting materials to be combined with PNIPAM for obtaining underwater adhesion.
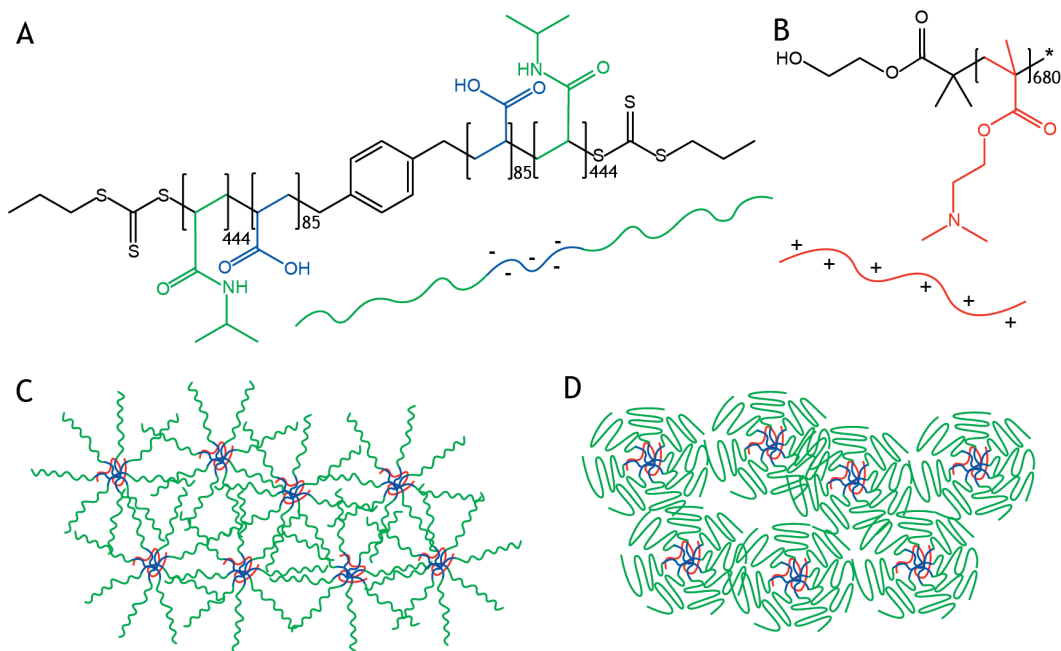
Figure 5.1 – Chemical structure and schematic representation of **A** PNIPAM-*b*-PAA-*b*-PNIPAM and **B** PDMAEMA. The morphology of the polymers is shown **C** below T_{gel} where C3Ms are found, and **D** above T_{gel} where an unordered morphology is found. The green blocks represent PNIPAM, the blue blocks PAA, and the red blocks PDMAEMA.

Recently, Dompé et al. reported a bioinspired underwater adhesive based on PNIPAM-grafted oppositely charged polyelectrolytes containing 30 wt% PNIPAM.[11] These systems showed promising values for the work of adhesion, W_{adh}. Here, we use a combination of oppositely charged polyelectrolytes and PNIPAM also, but with different polymer architectures and compositions. First, instead of poorly defined graft copolymers, we use a mixture of a linear block copolymer and a homopolymer. This allows us to study the morphological features by small angle X-ray scattering and relate this to the mechanical properties, as measured by rheology. Moreover, it is interesting to study the effect of homopolymer addition on the mechanical properties, as these chains do not contribute to the PNIPAM network. Second, the materials of Dompé et al. were still relatively soft and the natural underwater adhesives contain more than 30% hydrophobic amino acids. Therefore, we investigate temperature responsive polyelectrolyte complexes (TERPOCs) with a higher PNIPAM content of 70 wt%.[2]

The TERPOCs are composed of a cationic homopolymer, and an anionic triblock copolymer that contains large PNIPAM outer blocks. Upon mixing aqueous solutions of the polymers, the charged compounds complex, forming a charge neutral assembly. Consequently, the TERPOC may be compared with hydrogels made of

triblock copolymers with a hydrophilic middle block and large temperature responsive outer blocks.[13, 14, 15] However, the use of polyelectrolytes provides additional parameters to adjust the rheological properties of the gel. An increasing salt concentration will weaken the polyelectrolyte complex and therefore salts can alter the characteristics of TERPOCs.[16] Moreover, weak polyelectrolytes have a pH dependent degree of ionization. At low degrees of ionization, the polymers are more hydrophobic because of the uncharged moieties, which leads to more solid coacervates.[6, 12] Finally, the degree of charge compensation can be used to weaken or strengthen TERPOCs, as excess charge is displayed on the surface of the micelle core. [12] Charge repulsion between the micelles may lead to more extendable gels.

In this work, TERPOCs are prepared by mixing PNIPAM-*b*-poly(acrylic acid)-*b*-PNIPAM (NIPAM$_{444}$-*b*-AA$_{170}$-*b*-NIPAM$_{444}$) and poly(dimethylaminoethyl methacrylate) (DMAEMA$_{680}$), Figure 5.1. At low temperatures, the polyelectrolytes complex and stable complex coacervate core micelles (C3M) are obtained, Figure 5.1C, resulting in a low viscosity polymer solution.[17] The insoluble polyelectrolyte core is stabilized by the long PNIPAM chains in the corona. Upon increasing the temperature, PNIPAM becomes insoluble resulting in gelation, and a TERPOC is formed, Figure 5.1D. By changing the NaCl and polymer concentration, changes in the gelation temperature (T_{gel}), morphology, and adhesive strength are obtained, as is observed by SAXS, rheology, and probe tack testing, respectively. Moreover, it is shown that charge neutralization is required for obtaining strong gels.

Experimental

Materials

Sodium chloride (>99.5%), was bought from Acros organics. Sodium hydroxide solution (TitriPUR, 0.1 M) and hydrochloric acid (TitriPUR, 1M) were bought from Merck chemicals. DMAEMA$_{680}$ (M_n 107 kDa, PDI 1.26) was purchased from Polymer Source, Figure A5.1. The synthesis of the polyanions, NIPAM$_{444}$-*b*-AA$_{170}$-*b*-NIPAM$_{444}$ (M_n 61.6 kDa and PDI 1.61 (PNIPAM-*b*-P*t*BA-*b*-PNIPAM)) and PAA (M_n 44.5 kDa, PDI 1.61), is described in 3.

Methods

Sample preparation

The polymers were dissolved in water as stock solutions with a concentration of max. 12.5 wt% and the pH was adjusted to 6.5±0.2. Samples were prepared by mixing the polycation with the NaCl solution, followed by the addition of the polyanion. The solution was vortexed and left refrigerated to equilibrate. Then, the pH was checked and adjusted to 6.5±0.2 using 1 M NaOH or HCl. Finally, water was added to obtain

the desired concentration, and the samples were kept refrigerated until further use. The order of mixing the polyelectrolytes is important as it determines the degree of co-acervation. Also, the polymers were added at equal charge, meaning that the amount of positively charged monomers equals the amount of negatively charged monomers to maximize complexation. Charge stoichiometry was verified by zetapotential measurements that should give values of about 0 mV.

SAXS

Small-angle X-ray scattering (SAXS) measurements were carried out at the Dutch-Belgian Beamline (DUBBLE) station BM26B of the European Synchrotron Radiation Facility (ESRF) in Grenoble, France.[18, 19] The sample-to-detector distance (Dectris Pilatus 1M) was ca. 2.5 m. The scattering vector q is defined as $q = 4\,\pi/\lambda \sin(\theta)$ with 2θ being the scattering angle and λ the wavelength of the X-rays (1.03 Å). Silver behenate was used to calibrate the q-range, which reached from $6.05*10^{-2}$ to 3.66 nm^{-1}. Two dimensional images were radially averaged around the centre of the primary beam to obtain the isotropic SAXS profiles. The data was corrected for absorption, and background scattering of the salt solutions. The samples were placed in a 2 mm quartz capillary and heated from 10 to 50 °C taking steps of 2-5 °C, with the temperature kept constant after each step for five or ten minutes. For details see Table A5.1. The acquisition time was 30 seconds per frame. Every second-last frame of each temperature step was taken for analysis.

Rheology

Rheological measurements were performed on an Anton Paar MCR 301 rheometer equipped with a 25 mm cone plate geometry. The temperature was controlled using a Peltier element. After making contact with the cone, the sample was immersed with tetradecane oil to avoid evaporation of water from the sample. First, the samples were equilibrated for 1 h at 10 °C, then the temperature was increased from 10 to 50 °C with 0.13 °C/min, followed by another equilibration for 2 h at 50 °C. During these steps the sample was measured using an oscillatory shear with 1% strain, and an angular frequency of 1 rad/s. After temperature increase, either shear start up experiments were performed using a rotation with a fixed shear rate of 0.1 s^{-1}, or frequency sweeps were measured using an oscillation with 1% strain, and angular frequencies of 0.1 to 100 rad/s.

Probe tack testing

Adhesion tests were performed by using the probe tack method using an Instron 5333 materials testing system equipped with a 10 N load cell. A parallel contact and detachment between glass and the TERPOCs was made. In detail: A stainless steel probe, with a glass slide attached, was fixed onto the load cell. The polymer solution was pipetted onto a glass slide which subsequently was fastened to the bottom of the chamber

using plastic screws. Contact between the clean glass slide and the polymer solution was made at 20 °C until a thickness of 0.5 mm was reached. Then, a 37 °C aqueous NaCl solution, with the same salt concentration as the polymer solution, was poured into the chamber and kept at this temperature. Thereafter, the probe was kept at a fixed distance from the glass surface for 1 minute, followed by detachment at a fixed strain rate of 0.2 s^{-1}. Raw data of force and displacement were converted into stress and strain values to obtain the work of adhesion. The strain ε was obtained by normalizing the displacement by the initial thickness of the sample (t_0). The normalized stress σ was obtained by dividing the force with the contact area. The work of adhesion W_{adh} was calculated as 5.1

$$W_{adh} = t_0 \int_0^{\varepsilon_{max}} \sigma \, d\varepsilon \qquad (5.1)$$

Two or three replicates were conducted for every experiment to ensure data reproducibility, the work of adhesion is calculated using two measurements.

Results and Discussion

SAXS

SAXS experiments are performed to determine the morphology of the polymers both in solution and in the TERPOC for various salt and polymer concentrations. First, the scattering curves of all samples at 10 °C will be discussed. Subsequently, the changes induced by increasing the temperature from 10 to 50 °C are explained, and, finally, the scattering curves at 50 °C are compared.

At 10 °C, PNIPAM is soluble, while the polyelectrolytes can form complex coacervates. In previous work we have shown that under these conditions C3Ms with a polyelectrolyte core and PNIPAM corona are formed.[17] Therefore, scattering peaks in the SAXS profiles are most likely caused by the complex coacervate cores. At low salt concentrations, two or three peaks can be observed, while at high salt concentration only a broad peak is detected, Figure 5.2A.[20] The two peaks at low q values are attributed to be structure peaks, and are used to determine the morphology. For 0.3 M NaCl, the two structure peaks are located at 0.157 nm^{-1} and ≈0.25 nm^{-1}, and the ratio between these q values is approximately √2.7. Generally, spheres in a face centred cubic (fcc) lattice display a second order peak at √4/3 q^* and a more intense third order peak at √8/3.[21] Therefore, it can be expected that the peak at 0.25 nm^{-1} is a third order peak of an fcc ordering with a spacing of ≈40 nm, while the second order peak is invisible. When increasing the salt concentration, the structure peaks shift to higher q, indicating smaller domain spacing. This can be explained by the PNIPAM chains that shrink with increasing salt concentration, thereby decreasing the distance between the complex coacervate domains.[22, 23] Also, increased salt concentrations cause swelling of complex coacervates resulting in less contrast between the coacervate
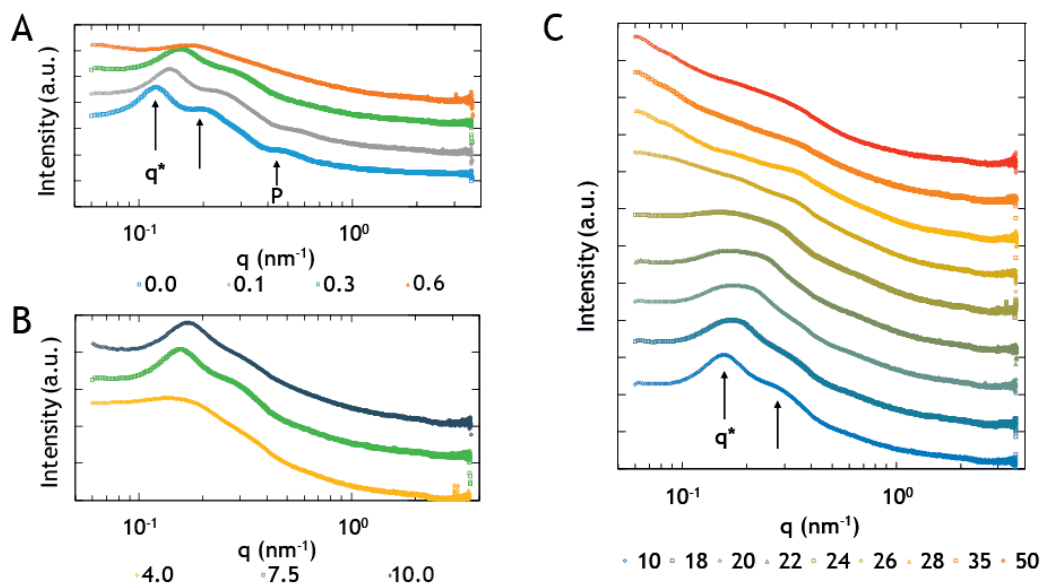
Figure 5.2 – **A** Scattering profiles with varying NaCl concentration (M) and 7.5 wt% polymer at 10 °C. The structure peaks are indicated with the arrows, and the form factor peak is indicated with P. **B** Scattering profiles with varying polymer concentration (wt%) and 0.3 M NaCl at 10 °C. **C** Scattering profiles of 0.3 M NaCl and 7.5 wt% polymer with increasing temperature (°C) (from bottom to top), for clarity temperatures at which no changes occurred have been left out. The curves are shifted over the y-axis for a better visibility.

and PNIPAM phases occurs. Therefore the peaks broaden, as is observed at 0.6 M NaCl. Furthermore, by changing the polymer concentration, the structure peaks shift, Figure 5.2B. For higher polymer concentrations, q^* moves to higher q values, as is seen for 7.5 and 10 wt% polymer. As reported before, the interdomain spacing depends on the polymer concentration, and decreases with increasing concentration.[24] For 4 wt% polymer, however, only a broad peak can be observed which is caused by loss of order which occurs at low polymer concentrations.[21]

The form factor peak can be used to determine the coacervate domain size.[24] At 0.0 and 0.1 M NaCl, a form factor peak (P) is visible at high q. For 0.0 M NaCl, Figure 5.2A, the peak is located at ≈0.44 nm^{-1}, and a core radius of 14 nm is calculated, while for 0.1 M NaCl q≈0.52 nm^{-1} and 12 nm is found. This slight difference in size may originate from the lower relaxation time of the electrostatic interactions with increasing salt, leading to a better equilibration of the coacervate domains and thus a lower size. When the salt concentration increases, the intensity of the form factor peak lowers because of less contrast between the two phases. This can be explained by swelling of the complex coacervate cores, and shrinking of the PNIPAM chains at higher salt concentrations. The form factor peaks are absent in the samples where the polymer concentration is varied, Figure 5.2B, probably because the salt concentration is too high to provide a good contrast.
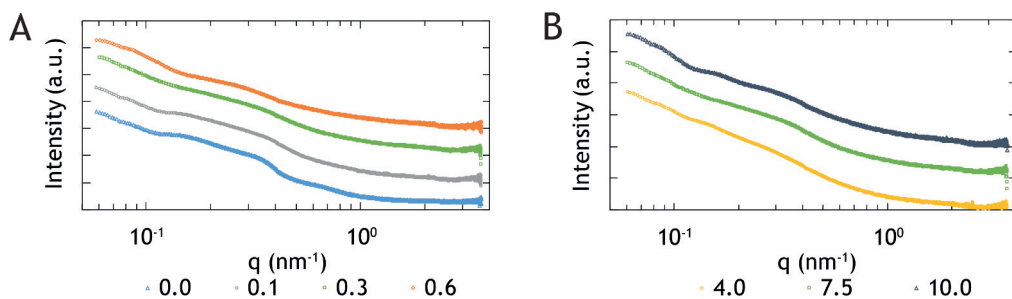
Figure 5.3 – A Scattering profiles with changing NaCl concentration (M) at 7.5 wt% polymer at 50 °C. **B** Scattering profiles with changing polymer concentration (wt%) at 0.3 M NaCl and 50 °C.

Upon increasing the temperature, several changes can be observed, Figure 5.2C. First, the structure peak shifts to higher q values, indicating a decrease of the interdomain distance, which is a result of the shrinking PNIPAM corona.[22, 23] Second, the structure peaks broaden which is clearly seen when comparing the scattering curves of 10 and 24 °C. Peak broadening indicates loss of contrast between core and corona, or loss of long range order due to a changing morphology.[25] At long range order, many narrow higher order peaks can be found, while a reduced order leads to loss of higher order peaks and peak broadening. Finally, the slope of the scattering curves at low q values increases from 26 °C onwards, which indicates the formation of aggregates in the samples, illustrating the gelation of the material.[26] Also, the LCST of PNIPAM decreases with increasing salt and polymer concentration, Figure A5.4 and Figure A5.3.[13, 27]

At 50 °C, a broad shoulder can be observed for the samples with 7.5 wt% polymer, Figure 5.3A. With increasing concentrations of NaCl, it can be seen that the width of the shoulder decreases, and the onset of the shoulder shifts to higher q values. This shift can be explained by salt induced deswelling of the PNIPAM, leading to lower interdomain spacing.[22, 23] At 0.3 M NaCl and 10 wt% polymer, Figure 5.3B, no broad shoulder, but two small peaks are observed, and, at low q values, small additional peaks are found as well. From these peaks, no distinct pattern can be discovered, and the material is probably in a disordered state.

The TERPOCs made from PNIPAM grafted polyelectrolytes with high polydispersities show no features in the SAXS data, indicating a disordered structure, at all temperatures.[11] This behaviour is in contrast to the results obtained from TERPOCs made with narrowly dispersed linear polymers, where features are clearly visible. Narrow dispersed polymers are more likely to show ordering at small length scales, than polymers with highly dispersed sizes, which results in the observed differences.

Rheology

Rheology is used to determine the mechanical properties of the polyelectrolyte complexes, and illustrates the gelation of the micelle solution. Here, it is discussed how T_{gel}, G', G'', tan δ, and the non-linear rheology are effected by different NaCl, polymer, and PNIPAM concentrations, as well as different degrees of charge neutralization.

Salt dependence

Temperature sweep The temperature dependent behaviour at three different salt concentrations at a fixed polymer concentration of 7.5 wt% are presented. Lower polymer concentrations were not used because they were found to phase separate into a concentrated polymer and dilute water phase. Moreover, higher polymer concentrations were shown to shrink and fracture spontaneously upon temperature increase. Both of these responses complicate rheological examination. At a polymer concentration of 7.5 wt% no macroscopic phase separation is observed and limited shrinking. Figure 5.4A shows the gelation of the micelle solution while increasing the temperature. At low temperatures, G'' exceeds G' indicating fluid-like materials. Moreover, at these temperatures, the material is so weak that G' and G'' are close to the detection limit of the rheometer. When the temperature increases, the moduli increase and a cross-over between G' and G'' is observed at T_{gel}. This cross-over indicates the gelation of the polymer solution which is induced by the LCST of PNIPAM. Following the cross-over, a further increase of G' and G'' is observed, and finally plateau moduli are found at 50 °C. From this pattern, it becomes evident that the temperature response is an abrupt transition from fluid to solid. Furthermore, in Figure 5.4, it is seen that the temperature induced changes in the moduli, occur at lower temperatures for higher salt concentrations. Affirmingly, it is known that the LCST of PNIPAM decreases linearly with increasing NaCl concentrations, which decreases T_{gel}.[10, 17, 27] Besides, samples with less than 0.3 M NaCl have an unstable increase of the moduli, because water is expelled upon gelation and causes wall-slip, Figure A5.6.

The storage modulus at 50 °C, first increases slightly with increasing salt concentration, and exhibits a maximum around 0.3 M NaCl, Figure 5.4B. Increasing

[NaCl]	tan δ	
(M)	min	max
0.3	0.19	0.34
0.6	0.12	0.15
0.75	0.08	0.11

Table 5.1 – Tan δ as determined from the ratio between the loss and storage modulus. All samples contained 7.5 wt% polymer and were measured at 50 °C.
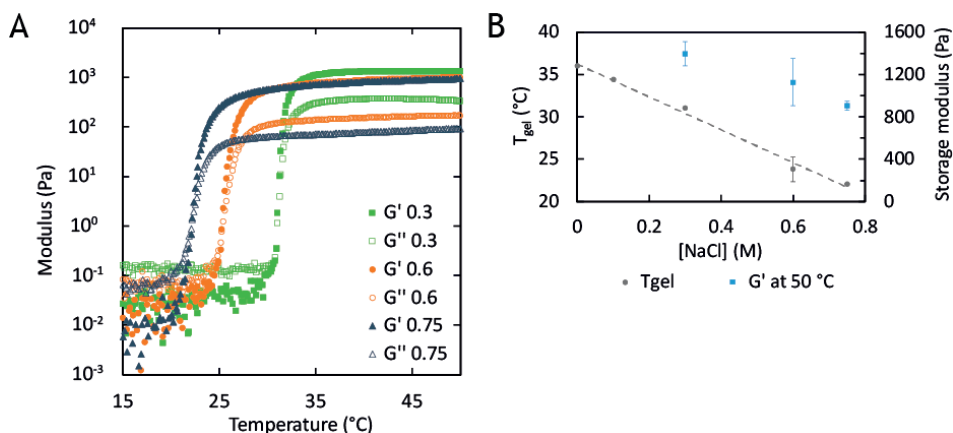
Figure 5.4 – A Storage and loss moduli at 1 rad/s as a function of temperature, for varying NaCl concentrations (M) at 7.5 wt% polymer. **B** G' as obtained at 50 °C before equilibration, and T_{gel} as determined from the crossover temperature, are shown as function of NaCl concentration. The error bars show the standard deviations. Except for 0.0 and 0.1 M NaCl, all samples have been measured multiple times.

salt concentrations decreases the strength of the electrostatic interactions, which leads to a lower relaxation time of the electrostatic interactions.[5, 12] As a result, the contribution of the polyelectrolyte complexation to G' decreases with increasing salt. At the same time, increasing salt concentrations lower the solvent quality of PNIPAM, leading to higher relaxation times of the hydrophobic interactions. As a result, more elastic materials are obtained with increasing salt concentration, which is also shown by the decreasing tangent of the phase angle, tan δ = G''/G', Table 5.1.[28] The TERPOCs can be compared to gels of NIPAM$_{455}$-b-DMA$_{210}$-b-NIPAM$_{455}$ or NIPAM$_{320}$-b-HEMA$_{80}$-b-NIPAM$_{320}$ which contain hydrophilic centre blocks instead of a polyelectrolyte block which is complexed. Higher G' are observed for TERPOCs at 50 °C, while lower polymer concentrations are used, compared to the uncomplexed gels.[13, 15] Consequently, polyelectrolyte complexes improve the strength of temperature responsive polymer gels by creating additional electrostatic cross-links.

Shear start-up At 50 °C, shear start-up experiments are performed to determine the fracture behaviour of the gel. The stress first increases and then drops sharply, indicating fracture of the gel, Figure 5.5A. The strain and stress at the peak are highest for 0.6 M NaCl, Figure 5.5B. This optimum can be explained by the dependence of electrostatic interactions on the salt concentration. Upon rupture, the electrostatic bonds between the polyelectrolyte can be reformed. The relaxation time of the electrostatic bonds decreases with increasing salt, leading to a higher deformability. Therefore, at 0.3 M NaCl, the ruptured bonds cannot be restored timely and the stress-strain peak is observed at lower strain. However, upon exceeding a certain salt concentration, the relaxation time becomes this short that the bonds contribute very little to the strength of the material, as observed for 0.75 M NaCl. Therefore, it is important for optimal
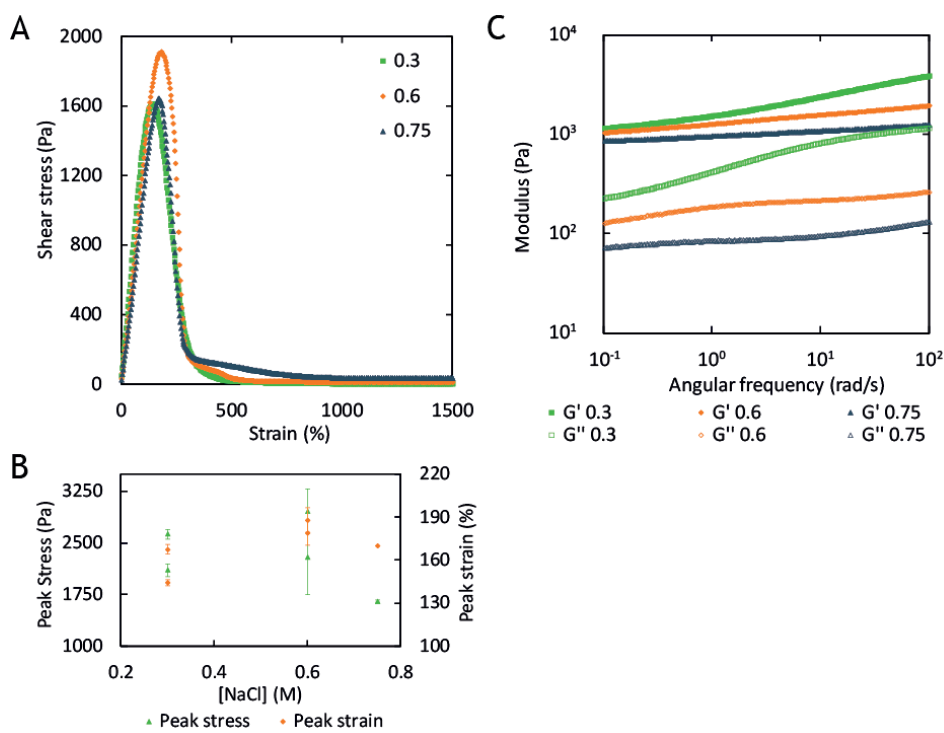
Figure 5.5 – A Shear stress as function of strain, **B** overview of average peak stress and strain, and **C** storage and loss modulus as function of angular frequency, for varying NaCl concentrations (M) at 7.5 wt% polymer and 50 °C. The error bars depicted in B show the standard deviations. For 0.3 M NaCl three samples were measured, whereas for 0.6 and 0.75 M NaCl two samples were measured. For concrete values, see Table A5.1.

stretchability to balance the salt concentration.

Frequency sweep Figure 5.5C shows the frequency dependence of the storage and loss modulus, and different behaviours are observed. The sample with 0.3 M NaCl is viscoelastic because increasing moduli and a changing tan δ are observed, with increasing frequency. At 0.6 M NaCl, a critical gel seems to be found, which is an intermediate state between liquid and solid. Critical gels are characterized by a power law relation with scaling n between the moduli and frequency, and by a constant tan δ which is determined as $\tan(n\pi/2)$.[14] The sample at 0.6 M NaCl is highly physically cross-linked, as indicated by the low n≈0.09. Finally, the sample at 0.75 M NaCl, looks like an elastic solid, which is characterized by a constant modulus with changing frequency.[24] At 0.75 M, the NaCl concentration has severely reduced the contribution of the complex coacervates. Consequently, the frequency independent behaviour is mainly caused by the PNIPAM interactions, while the frequency dependence is mainly caused by the electrostatic interactions.

Effects of charge compensation

PDMAEMA is (partially) omitted to investigate the effect of incomplete charge neutralization of the PAA. The samples are prepared as if 7.5 wt% was the final polymer concentration and at 0.3 M NaCl. When PDMAEMA is fully omitted, the material hardly strengthens, Figure 5.6A, and the final material is so weak that the torque, ≈2 nNm to ≈7 nNm, does not exceed the limits of detection. Therefore, either complexation with a polycation or a higher polymer concentration is required to obtain strong gels with PNIPAM-*b*-PAA-*b*-PNIPAM at pH 6.5.

Stable gelation occurred when only half of the anionic charges was compensated by PDMAEMA, Figure 5.6B. Nevertheless, the moduli at 50 °C are an order of magnitude lower compared to charge neutral samples. Accordingly, more charge compensation than 50% is needed to reach an optimum amount of crosslinks. Furthermore, the stress strain curves look slightly different and it seems that the peak strain is higher when only half of the charges are neutralized, Figure 5.6C. This can be explained by a higher chance to reform ruptured bonds, as anionic charges are always available. Moreover, the frequency dependent behaviour is comparable, Figure 5.6D, while tan δ is lowered for the charged TERPOC. A lower tan δ value can be caused by a higher relative PNIPAM content which results in a slightly more solid material. Overall, charge compensation is required to obtain strong gels and can be used to adjust the properties of TERPOCs.

Polymer concentration dependence

The effects of the polymer concentration on the properties of the TERPOCs was investigated at 0.3 M NaCl, Figure 5.7A. In accordance with literature, a decreasing T_{gel} with increasing polymer concentration is observed. This effect can be ascribed to a higher probability of polymers to entangle when the concentration increases, which causes a lower LCST and thus a lower T_{gel}. [13, 26, 29, 30, 31] Furthermore, the plateau modulus shows an optimum for 7.5 wt% polymer. The increase in modulus from 4 to 7.5 wt% can easily be explained by an increasing number of (PNIPAM) nodes because of the higher polymer concentration, causing a higher storage modulus. Also, the dissipation of energy can become more likely when the polymers get closer, causing a higher loss modulus. However, a surprisingly small difference is observed between 7.5 and 10 wt% polymer. The more or less equal moduli indicate that the number of nodes has not increased with the polymer concentration. A possible explanation can be that the higher PNIPAM concentration causes a quicker gelation. Therefore, equilibration of the sample is hindered and node formation may be prevented.

In the shear start-up experiments, Figure 5.7B, the peak strain and stress increase strongly with increasing concentration. Accordingly, while preparing adhesives, one should strive for the highest polymer concentration. Furthermore, the frequency dependence of the moduli, Figure 5.7C, is similar for all polymer concentrations, because of the constant salt concentration. In addition, tan δ becomes less frequency dependent upon increasing the polymer concentration, Figure A5.7B , which shows
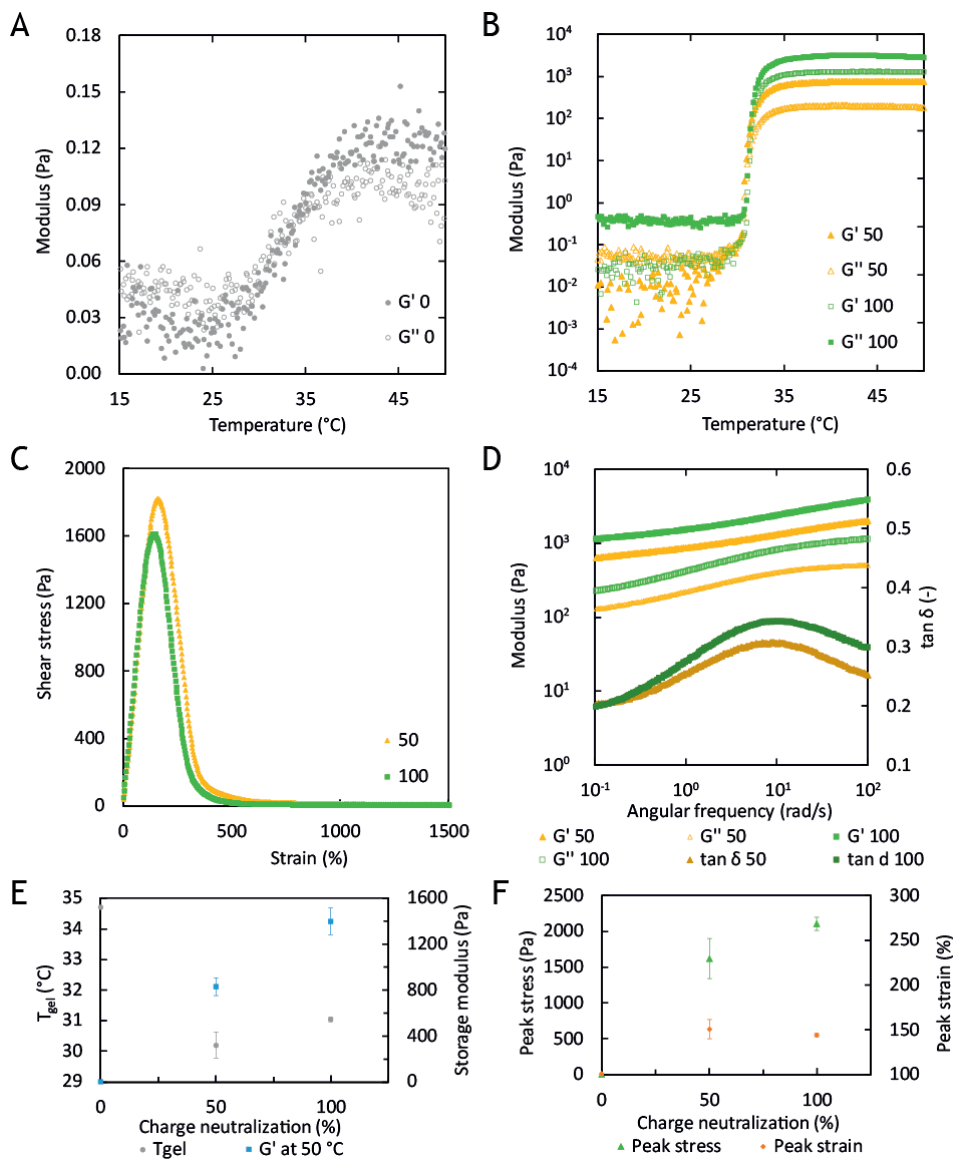
Figure 5.6 – A Storage and loss moduli are shown as a function of temperature for 0.3 M NaCl and without any PDMAEMA, (c_{pol} 6 wt%). The torque increased from $\approx$2 nNm till $\approx$7 nNm, which is in any case in the limits of detection. **B** Storage and loss moduli are shown as a function of temperature for 0.3 M NaCl and PDMAEMA to compensate half (50) (c_{pol} 6.75 wt%) or all (100) (c_{pol} 7.5 wt%) of the anionic charges. **C** The shear stress as function of rotational strain and **D** the frequency dependent behaviour of the moduli and tan , for the same samples. The results of the **E** temperature sweep and **F** stress strain curves have been averaged for two measurements and are depicted with the standard deviations. For the sample without PDMAEMA only one sample was measured.
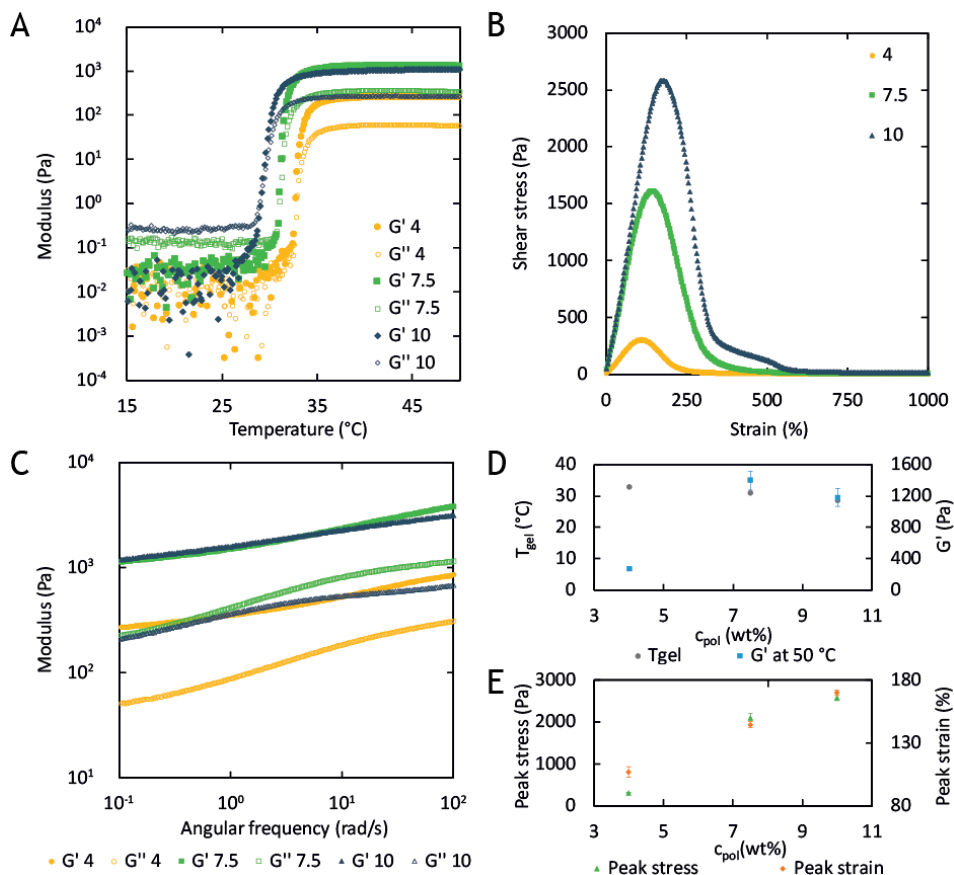
Figure 5.7 – A Storage and loss modulus as function of temperature for 0.3 M NaCl and varying polymer concentrations (wt%). **B** Shear stress as function of strain, and **C** storage and loss modulus as function of angular frequency, at 50 °C, are shown for the same samples. **D** Average T_{gel} and storage modulus, as obtained at 50 °C before equilibration, as function of polymer concentration, c_{pol}. **E** Overview of average peak stress and strain, at varying polymer concentrations. The error bars show the standard deviation. For 7.5 wt% three samples were measured, whereas for 4 and 10 wt% polymer two samples were measured.
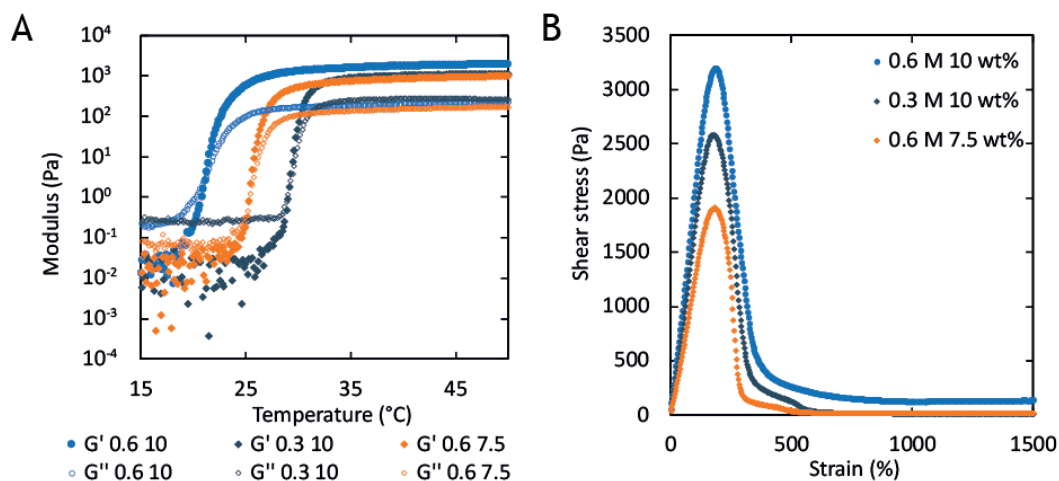
Figure 5.8 – A Storage and loss moduli as function of temperature, for different NaCl (M) and polymer (wt%) concentrations. **B** Shear stress as function of strain at 50 °C for the same samples.

that the fluidity is reduced.

Optimal conditions

Both, the sample with 0.6 M NaCl and 7.5 wt%, and the sample with 0.3 M NaCl and 10 wt% have shown an optimum performance in the stress strain curves. To determine whether an even better material can be obtained, a sample with 0.6 M NaCl and 10 wt% polymer is investigated. For this sample, T_{gel} decreases even further and G' increases, while G'' shows only minor differences, Figure 5.8A. The decreasing T_{gel}, can be explained by a lower LCST and a higher probability of bridging through the increased polymer concentration. Moreover, a higher salt concentration reduces T_{gel} as well. Furthermore, an increased polymer concentration may lead to a higher number of nodes, causing a higher G'. In addition, the stress strain curve, Figure 5.8B, shows a higher peak stress, while the strain for this sample is not further increased. Therefore, we can conclude that increasing both the salt and polymer concentration creates a stronger material. Also, the sample at 0.6 M NaCl and 7.5 wt% looks like a critical gel as the moduli increase with frequency, while tan δ remains constant, Figure A5.8. This confirms that the salt concentration alters the frequency response, while the polymer concentration does not.

Compared to the rheological properties found for 30% PNIPAM graft copolymers by Dompé et al., this system shows a lower cross-over temperature, and the moduli are an order of magnitude higher.[11] Both of these observations can be explained by the higher PNIPAM content of ≈70 wt%. Higher PNIPAM concentrations enhance the formation of hydrophobic interactions, which lowers the LCST and increases the cross-linking in the solid PNIPAM phase. The values found for tan δ, and

the dependence of the moduli on the angular frequency are similar, which suggests comparable elasticity of the materials. However, the peak stress in block copolymer materials has increased tremendously, while the peak strain has decreased. This shows that the material with 70 wt% PNIPAM can withstand higher loads, but is less extensible as it breaks at lower deformations.

Probe tack testing

Probe tack experiments are performed to determine the adhesive strength of the TERPOCs. The samples are applied onto a glass slide and contact was made, followed by a sudden increase in temperature till 37 °C, by pouring a heated salt solution into the chamber. The salt concentration of the solution is equal to the salt concentration of the sample, to only investigate the temperature responsive curing. Moreover, a temperature of 37 °C was chosen to mimic body temperature and asses the TERPOCs for applications in wound closure.

Two clear trends can be observed in the data, Figure 5.9A. First, higher polymer concentrations lead to a higher work of adhesion. This can be explained by an increased amount of adhesive and cohesive bonds that have to be broken, before rupture of the adhesive occurs. Secondly, higher salt concentrations lead to a decreased W_{adh}. This can be caused by the decreased relaxation time of the electrostatic interactions. Consequently, the electrostatic bonds break more quickly, which reduces the W_{adh}. Besides, salt addition leads to a lower T_{gel} which may hinder the formation of adhesive interactions between the polymers and the glass surface.[11] By contrast, Dompé et al. found an increasing W_{adh} for higher salt concentrations. In the article, it is suggested that salt is needed to obtain mobile polymers to form PNIPAM domains, which are required for good adhesive performance.[11] In this work, the mobility of the PNIPAM was improved by selecting a large block length. Consequently, PNIPAM domains are more easily formed and salts are not required to enable sufficient flexibility of the polymers.

The data obtained from the probe tack tests can be compared to the stress-strain curves obtained from rheology. With the probe tack test, a higher peak strain is observed for 0.3 M NaCl than for 0.6 M NaCl at 10 wt%, while the opposite is found with rheology, Figure 5.9D and Figure 5.8B. This variation may be caused by the different temperature treatment and the lower T_{gel} of the sample with 0.6 M NaCl. In rheology, the sample is cooled for 1 h at 10 °C before the temperature increases slowly, which allows sufficient time to equilibrate. With the probe tack test, however, the sample is applied onto the surface at room temperature and heated suddenly, which may result in a different polymer morphology and stress-strain behaviour. Moreover, the T_{gel} of 0.6 M NaCl is about 21 °C and therefore gelation can occur before making contact. Consequently, the sample has a different morphology upon application which could lead to a lower peak strain. In addition, with probe tack, similar peak strains are obtained for samples with comparable T_{gel}. This suggests that tuning of the T_{gel}, is needed to obtain an optimal W_{adh}.

Two techniques are commonly used to determine the adhesive strength, i.e. probe

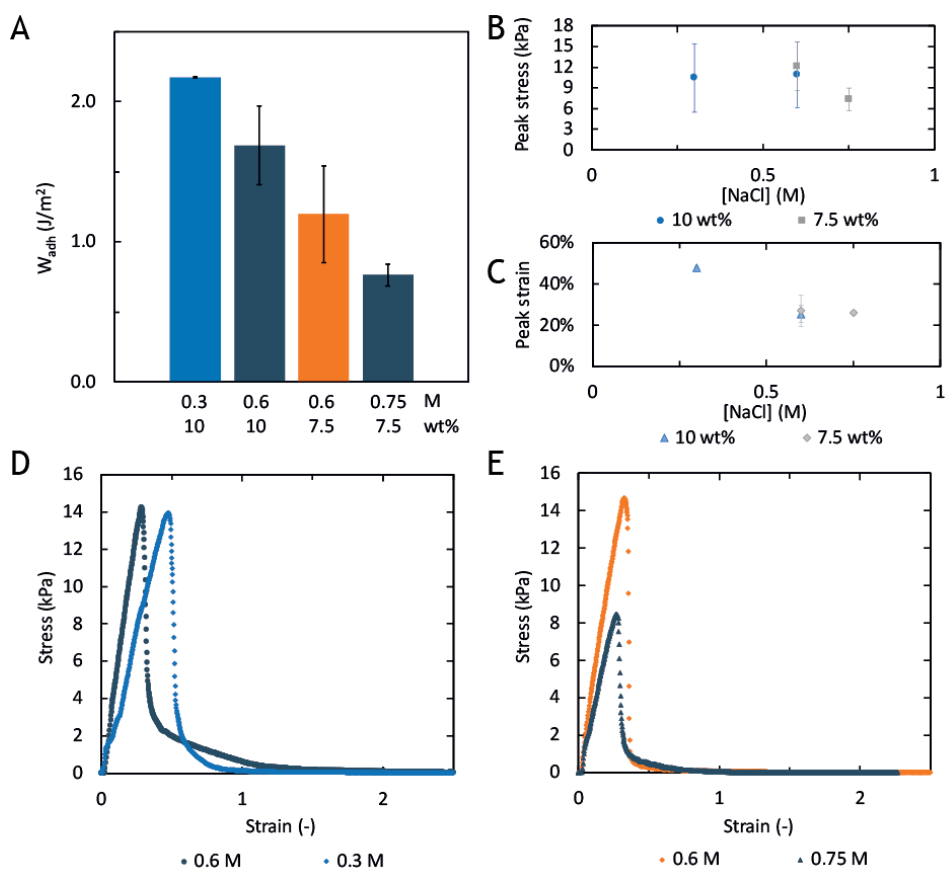**Figure 5.9 – A** Work of adhesion for four different samples containing 71 wt% PNIPAM and varying NaCl (M) and polymer concentrations (wt%) at 37 °C. Average peak **B** stress and **C** strain values with their standard deviations as calculated from two representative measurements. Typical stress strain curves for varying NaCl concentrations and **D** 10 wt% or **E** 7.5 wt% polymer.
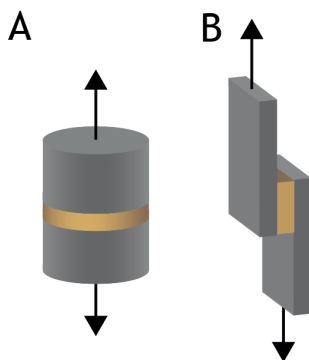
Figure 5.10 – Schematic overview of **A** probe tack and **B** lap shear testing, where the grey parts show the surfaces and the yellow parts are the adhesive joint. The arrows indicate the direction in which the surfaces are pulled during the measurement.

tack testing and lap shear experiments, Figure 5.10. During these measurements, the adhesives are treated differently, resulting in different contributions of the adhesive and cohesive properties of the glue and therefore incomparable quantities.[32] In literature, commonly used medical adhesives are tested with lap shear experiments, while we used probe tack tests, making a comparison difficult.[33] Moreover, the adhesive strength is influenced by various experimental conditions, such as the sample thickness, strain rate, surface type, and the amount of water. Consequently, additional measurements are needed to compare the adhesive strength of our TERPOCs with conventional biomedical glues.

An optimal work of adhesion (W_{adh}) of 2.7 kJ/m² was obtained for PNIPAM rich TERPOCs submerged in salty solutions. This adhesion is way stronger than the negligible W_{adh} reported for commonly used pressure sensitive adhesives (PSA), where just one drop of seawater was applied.[34] Furthermore, for other biomimetic underwater adhesives, values between 0.003 and 75 J/m² are found.[11, 34] Most of these materials contain catechols, or need a chemical reaction to solidify, while TERPOCs set easily and safely by changing the temperature. Therefore, TERPOCs seem to be a suitable and simple compound for developing underwater adhesives. However, Dompé et al. observed a maximum W_{adh} of 3.8 J/m² with the same probe tack experiment for the grafted polyelectrolytes with 30% PNIPAM. The weaker adhesion of the TERPOCs can be explained by the increased brittleness due to the higher PNIPAM content. Therefore, it is interesting to investigate TERPOCs with a PNIPAM content between 30 and 70 wt% to find an optimum. In addition, the TERPOCs behave differently with their morphology or block lengths. Therefore, also these parameters can be adjusted to enhance the adhesive strength. Over all, we believe that TERPOCs are promising materials for the development of underwater adhesives.

Conclusion

Temperature responsive polyelectrolytes were used to prepare PNIPAM rich TERPOCs for underwater adhesion. Upon heating, the C3M solution gels, resulting in strong, but somewhat brittle TERPOCs because of the high PNIPAM content. Moreover, the polyelectrolytes enhance gelation, improve the strength of the gel, and prevent shrinking upon solidification. In addition, charge neutralization by PDMAEMA is required to obtain strong gels. However, a net charge seems to result in a slightly better extensibility. Furthermore, the properties of the TERPOCs could be altered by varying the salt and polymer concentration. The strongest gel is obtained for the highest polymer and salt concentration, through additional molecular interactions with increased relaxation times. However, the strongest adhesion is found for a slightly lower salt concentration. Less salt increases T_{gel} which improves contact formation upon application, through a better deformability of the TERPOC. The obtained W_{adh} looks promising and PNIPAM rich TERPOCs seem a suitable and simple system for the development of underwater adhesives.

Acknowledgements

Appendix

Experimental
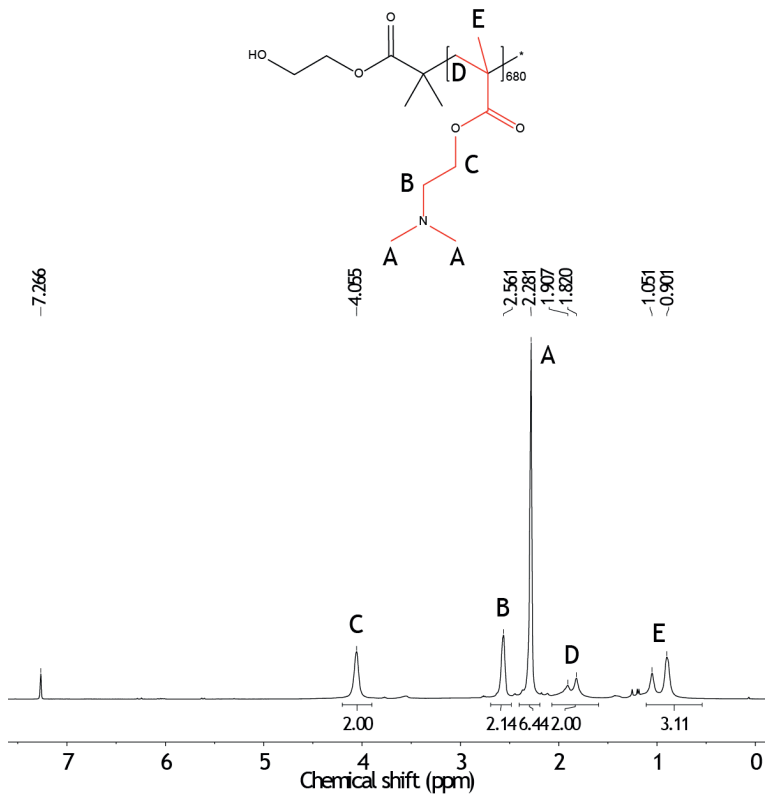
Figure A5.1 – ^{1}H-NMR spectrum of PDMAEMA in CDCl$_3$ as purchased from Polymer Source.

Temperature	10	15	18	20	22	24	26	28	30	32	35	40	45	50
Time	5	5	10	10	10	10	10	10	10	10	5	5	5	5

Table A5.1 – Heating scheme of SAXS measurements, with temperature (°C) and time (min).
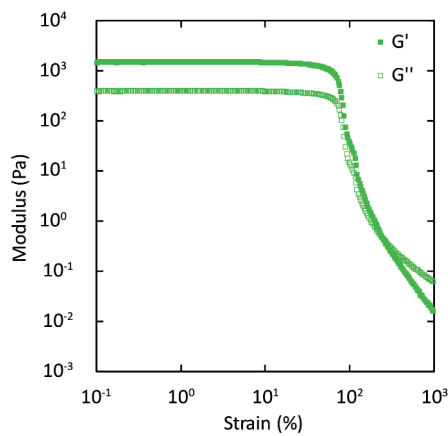
Figure A5.2 – Oscillatory strain sweep measured for 0.3 M NaCl and 7.5 wt%, at 1 rad/s, and 50 °C, to prove that the oscillatory measurements took place in the linear regime.

Results and discussion

SAXS
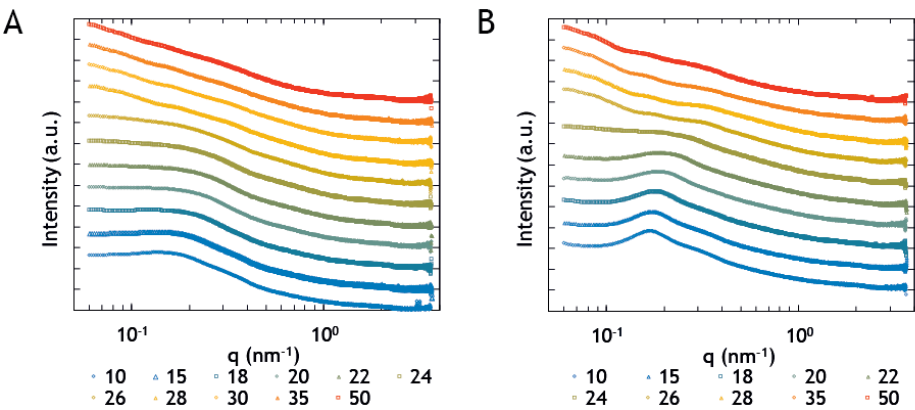
Figure A5.3 – Scattering profiles with increasing temperature, from bottom to top, are shown for 0.3 M NaCl with 4 wt% (**A**), or 10 wt% (**B**) polymer are shown. For clarity, curves at which no changes occur compared to the previous curve are not shown.
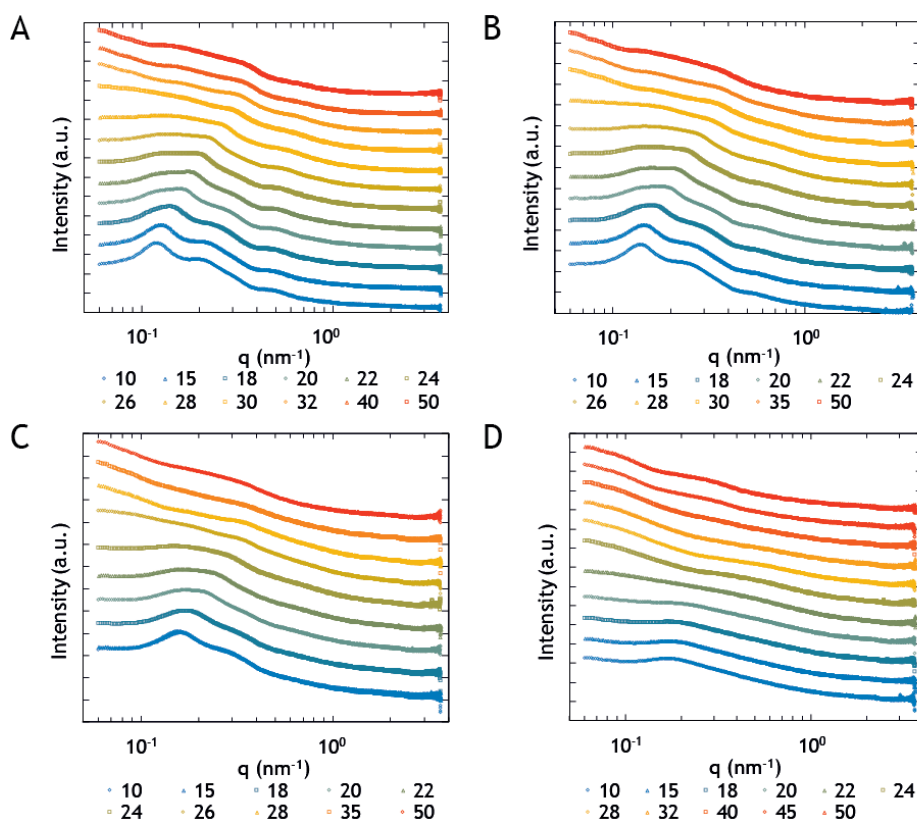
Figure A5.4 – Scattering profiles with increasing temperature, from bottom to top, are shown for 7.5 wt% and 0.0 M NaCl (**A**), 0.1 M NaCl (**B**), 0.3 M NaCl (**C**), and 0.6 M NaCl (**D**). For clarity, curves at which no changes occur compared to the previous curve are not shown.

Rheology

Temperature loop Figure A5.5 shows a temperature loop obtained using the same heating rate as for the temperature sweeps, i.e. 0.13 °C/min. It is clearly visible that the heating and cooling curves show hysteresis, as has been observed before.[35, 36] First, the cross-over temperature has decreased in the cooling step, which can be explained by the time needed to macroscopically observe the formation and breakdown of the hydrophobic interactions between the PNIPAM chains.[37] Second, a slight increase in the moduli above T_{gel} can be observed when cooling. Finally, the eventual moduli at 10 °C seem slightly higher compared to the starting moduli. PNIPAM chains do not only interact above LCST, but some researchers also report some interactions below LCST.[37] After the higher temperature has induced hydrophobic interactions between the PNIPAM chains, not all of those interactions will be disrupted immediately upon cooling. This behaviour is illustrated by the observation of lower T_{gel} upon reheating the sample, without cooling at a sufficiently low temperature and for a sufficiently long time. However, it should be noted that the obtained torque at 10 °C is very low, and therefore one has to be careful with drawing conclusions from the obtained moduli below T_{gel}.

Figure A5.5 – Moduli as function of temperature are shown for a temperature loop for a sample with 0.3 M NaCl and 7.5 wt% polymer. The temperature increases with 0.13 °C/min from 10 till 50 °C. Upon reaching 50 °C, the temperature decreases to 10 °C using the same heating rate.
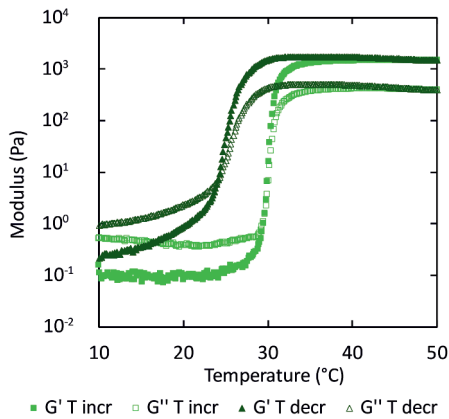
Unstable increase of moduli In this research, also samples with 0 and 0.1 M NaCl were measured. For these samples an increasing modulus is observed, but at a few degrees above T_{gel}, the moduli drop, Figure A5.2A. Similar behaviour is observed for two samples that consist of 10 wt% PNIPAM, Figure A5.2B. This drop of moduli can be attributed to brittleness or the exclusion of water as a result of collapsing PNIPAM chains above the LCST, which can cause shrinkage and droplet formation on the polymer surface. In samples without polyelectrolyte, the water cannot stay within the polymer material and has to be expelled, leading to shrinkage, fracturing and the formation of water drops on the surface of the solid. For samples with polyelectrolytes, the polyelectrolyte complexes might be able to absorb the water, and more water can be absorbed at higher salt concentrations, which may prevent fracturing of the
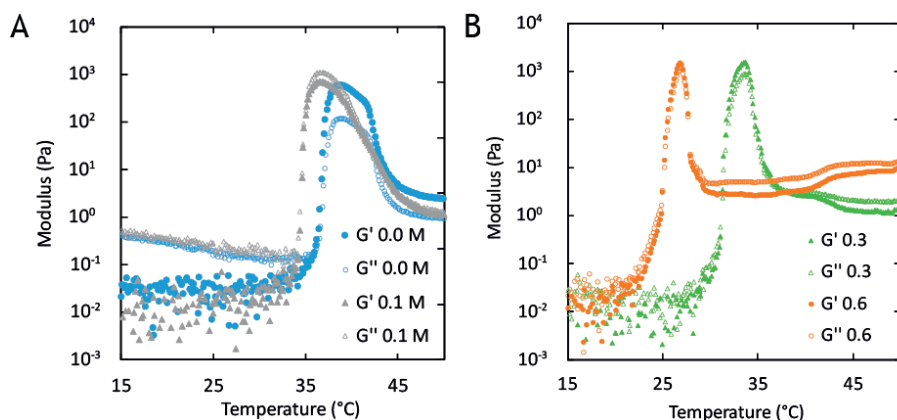
Figure A5.6 – Storage and loss moduli as a function of temperature for **A** 7.5 wt% polymer, and **B** 10 wt% PNIPAM, at varying NaCl concentrations (M). PNIPAM was synthesized using the RAFT agent *S*-propyl-*S'*-(isobutyric acid) trithiocarbonate, and has a M_n of 39.8 kDa (GPC) and PDI of 1.65.

sample.[5] Alternatively, the addition of complex coacervates provides the gel with a degree of flexibility that might enable the formation of water pockets. Increasing salt concentrations lead to more flexible polyelectrolyte domains, which may facilitate pocket formation. Finally, Kirkland et al. have shown that sufficient bridging of the polymers is needed to obtain stable moduli.[13] Bridging is promoted by a decreasing solvent quality for the PNIPAM chains, which is obtained by increasing the salt concentration. To conclude, from our observations, it becomes clear that more than 0.1 M additional NaCl is needed to obtain stable moduli for the TERPOCs.

Frequency sweep

Figure A5.7 – Tan δ as function of the angular frequency at 50 °C for **A** 7.5 wt% polymer, and varying NaCl concentrations, and **B** 0.3 M NaCl and varying polymer concentrations.

Optimal conditions

Figure A5.8 – A Storage and loss moduli and **B** tan δ as function of angular frequency at 50 °C for various polymer and NaCl concentrations.

PNIPAM concentration dependence The contribution of the PNIPAM content to the final properties is an interesting parameter to investigate, as is shown by the comparison between the 70 wt% PNIPAM containing block copolymer system, and 30% PNIPAM containing graft copolymers of Dompé et al.[11] Adjustment of the system can be achieved by either synthesizing a new block copolymer with a different composition, or by mixing in homopolymer PAA, which is less time consuming. However, one needs to pay careful attention to the homogenization of the material. Upon mixing, the homopolymers of PDMAEMA and PAA can form insoluble complex coacervates. Sufficient time in the fridge is required to undo this complexation, and obtain homogeneous samples.

With decreasing PNIPAM content, the cross-over temperature and final tan δ increase, while the moduli decrease, Figure A5.9A. A higher cross-over temperature is caused by the lower PNIPAM content, which is a generally observed phenomenon caused by a lower probability of PNIPAM forming hydrophobic interactions. Also, at low PNIPAM contents, a dual increase in the moduli can be observed. This two-step temperature response has been observed before in case of increasing salt concentrations, or for smaller polymers.[27, 30] Here, we argue that the salt concentration relative to the PNIPAM content is increased, which can cause the dual response. The decreased moduli indicate a lower degree of cross-linking and energy dissipation in the system, which is most likely caused by a disruption of the PNIPAM matrix by a higher polyelectrolyte content. Also, fewer polyelectrolytes are connected to PNIPAM, which can lead to less connections between the polyelectrolyte and PNIPAM phases. This effect is also observed in the decrease of the elasticity as is

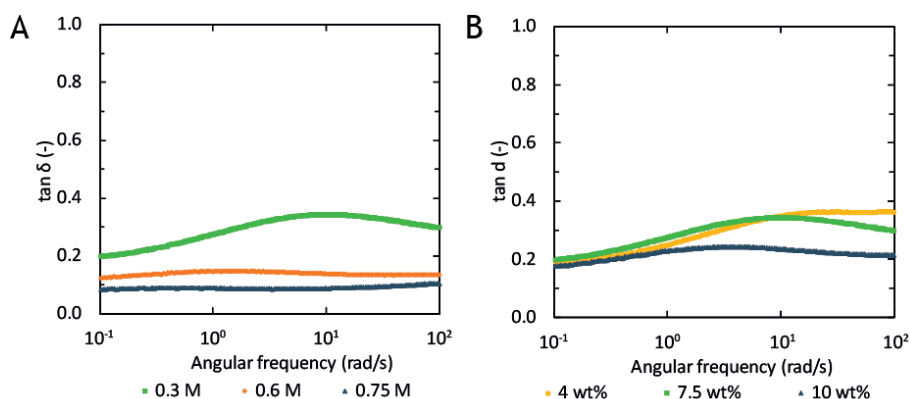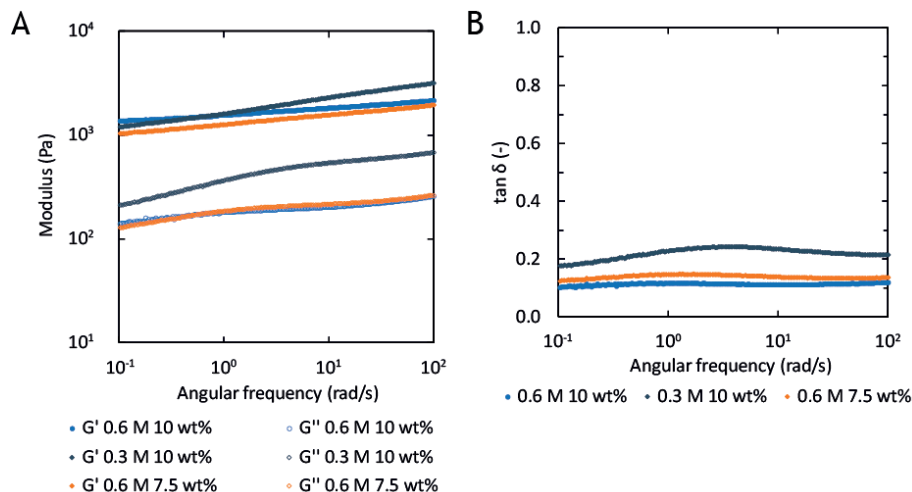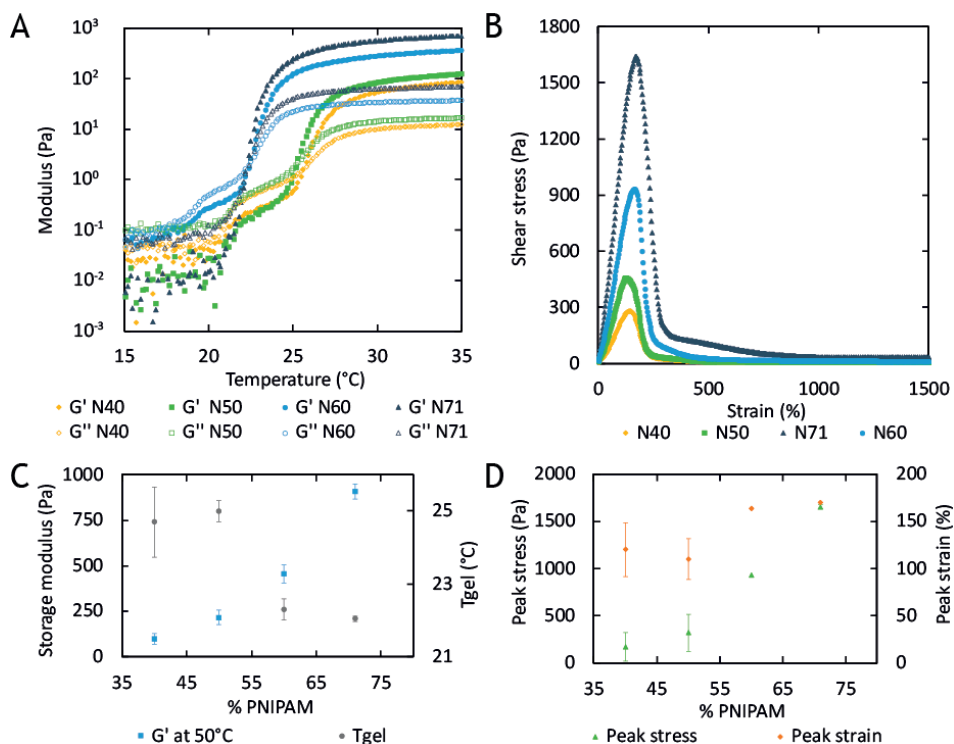**Figure A5.9 – A** Storage and loss modulus as function of temperature for 0.75 M NaCl, 7.5 wt% polymer, and varying PNIPAM content (wt%). **B** Shear stress as function of strain for the same samples at 50 °C. **C** Average storage modulus, when 50 °C has reached before equilibration, and T_{gel} as a function of PNIPAM content. **D** Average peak stress and peak strain as a function of PNIPAM content. All stress strain curves are measured twice, except for N60 which has been measured once. The error bars show the standard deviation.

observed from tan δ, and a lower strain at break, Figure A5.9B. As the relaxation time of the electrostatic bonds is shorter than the relaxation time of the hydrophobic interactions of the PNIPAM, the material might become more stretchable. However, this is not the case, probably due to fewer interactions between the coacervate and PNIPAM domains. In addition, the peak strain also decreases, to values even below those observed by Dompé et al., although their materials contained about 9 wt% polymer, which is more than the 7.5 wt% used here.[11] As can be seen in Figure A5.9C and D, the standard deviations of the T_{gel}, peak stress, and peak strain increase with decreasing PNIPAM contents. This is most likely caused by the increased amount of mixed in homopolymer PAA. Therefore, it seems that mixing in homopolymer to decrease the PNIPAM content functions well till a certain amount of homopolymer PAA is added. However, further investigation of this method to lower the PNIPAM content has to be done by synthesizing the block polymers with lower PNIPAM contents, and make a proper comparison.

[NaCl]	c_{pol}	Peak stress		Peak strain	
M	wt%	Pa		%	
		average	±	average	±
0.3	4	309	12	107	4
0.3	7.5	2105	92	144	2
0.3	10	2630	70	169	2
0.6	7.5	2290	537	188	8
0.6	10	2960	325	179	8
0.75	7.5	1655	21	170	0

Table A5.2 – Overview of average peak stress and strain values, with their standard deviations. For all conditions two samples have been measured, while for 0.3 M NaCl and 7.5 wt% three samples were checked.

Control experiments
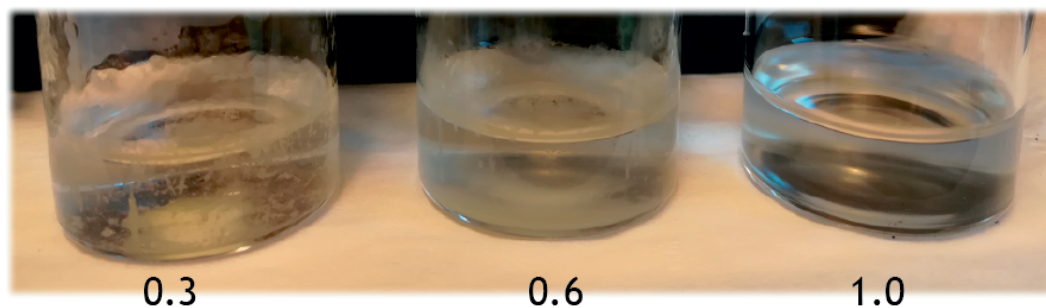
Figure A5.10 – Complex coacervates of DMAEMA$_{680}$ and AA$_{155}$ in NaCl solutions with various concentrations (M). At 0.3 M NaCl, the polymers precipitated into one big lump, while at 0.6 M NaCl a fluid, turbid phase is formed. At 1.0 M NaCl, a clear phase of polymers is found at the bottom of the vial. This shows that 1.0 M NaCl is close to the $c_{s,cr}$ of this polymer pair. AA$_{155}$ is obtained from deprotecting the macro-RAFT PtBA according to the same method as for AA$_{600}$.

Bibliography

[1] J. H. Waite. Natures underwater adhesive specialist. *Chemtech*, 17(11):692–697, 1987.

[2] A. H. Hofman, I. A. van Hees, J. Yang, and M. Kamperman. Bioinspired underwater adhesives by using the supramolecular toolbox. *Advanced Materials*, 30(19), 2018.

[3] E. Spruijt, M. A. C. Stuart, and J. van der Gucht. Linear viscoelasticity of polyelectrolyte complex coacervates. *Macromolecules*, 46(4):1633–1641, 2013.

[4] T. Akagi, K. Watanabe, H. Kim, and M. Akashi. Stabilization of polyion complex nanoparticles composed of poly(amino acid) using hydrophobic interactions. *Langmuir*, 26(4):2406–2413, 2010.

[5] E. Spruijt, A. H. Westphal, J. W. Borst, M. A. C. Stuart, and J. van der Gucht. Binodal compositions of polyeleetrolyte complexes. *Macromolecules*, 43(15):6476–6484, 2010.

[6] M. Tekaat, D. Butergerds, M. Schonhoff, A. Fery, and C. Cramer. Scaling properties of the shear modulus of polyelectrolyte complex coacervates: a time-ph superposition principle. *Physical Chemistry Chemical Physics*, 17(35):22552–22556, 2015.

[7] Y. Lee, C. J. Xu, M. Sebastin, A. Lee, N. Holwell, C. V. Xu, D. M. Nieves, L. Y. Mu, R. S. Langer, C. P. Lin, and J. M. Karp. Bioinspired nanoparticulate medical glues for minimally invasive tissue repair. *Advanced Healthcare Materials*, 4(16):2587–2596, 2015.

[8] M. A. Ward and T. K. Georgiou. Thermoresponsive polymers for biomedical applications. *Polymers*, 3(3):1215–1242, 2011.

[9] H. G. Schild. Poly (n-isopropylacrylamide) - experiment, theory and application. *Progress in Polymer Science*, 17(2):163–249, 1992.

[10] T. Patel, G. Ghosh, S. Yusa, and P. Bahadur. Solution behavior of poly(n-isopropylacrylamide) in water: Effect of additives. *Journal of Dispersion Science and Technology*, 32(8):1111–1118, 2011.

[11] M. Dompé, F. J. Cedano-Serrano, O. Heckert, N. van den Heuvel, J. Van der Gucht, Y. Tran, D. Hourdet, C. Creton, and M. Kamperman. Thermoresponsive complex coacervate-based underwater adhesive. *Advanced Materials*, page 1808179, 2019.

[12] J. van der Gucht, E. Spruijt, M. Lemmers, and M. A. C. Stuart. Polyelectrolyte complexes: Bulk phases and colloidal systems. *Journal of Colloid and Interface Science*, 361(2):407–422, 2011.

[13] S. E. Kirkland, R. M. Hensarling, S. D. McConaughy, Y. Guo, W. L. Jarrett, and C. L. McCormick. Thermoreversible hydrogels from raft-synthesized bab triblock copolymers: Steps toward biomimetic matrices for tissue regeneration. *Biomacromolecules*, 9(2):481–486, 2008.

[14] T. Vermonden, N. A. M. Besseling, M. J. van Steenbergen, and W. E. Hennink. Rheological studies of thermosensitive triblock copolymer hydrogels. *Langmuir*, 22(24):10180–10184, 2006.

[15] X. L. Zhao, W. G. Liu, D. Y. Chen, X. Z. Lin, and W. W. Lu. Effect of block order of aba- and bab-type nipaam/hema triblock copolymers on thermoresponsive behavior of solutions. *Macromolecular Chemistry and Physics*, 208(16):1773–1781, 2007.

[16] E. Spruijt, J. Sprakel, M. Lemmers, M. A. C. Stuart, and J. van der Gucht. Relaxation dynamics at different time scales in electrostatic complexes: Time-salt superposition. *Physical Review Letters*, 105(20), 2010.

[17] I. A. Van Hees, P.J.M. Swinkels, R.G. Fokkink, A.H. Velders, I. K. Voets, J. Van der Gucht, and M. Kamperman. Self-assembly of oppositely charged polyelectrolyte block copolymers containing short thermoresponsive blocks. *Polymer Chemistry*, 2019.

[18] M. Borsboom, W. Bras, I. Cerjak, D. Detollenaere, D. G. van Loon, P. Goedtkindt, M. Konijnenburg, P. Lassing, Y. K. Levine, B. Munneke, M. Oversluizen, R. van Tol, and E. Vlieg. The dutch-belgian beamline at the esrf. *Journal of Synchrotron Radiation*, 5:518–520, 1998.

[19] W. Bras, I. P. Dolbnya, D. Detollenaere, R. van Tol, M. Malfois, G. N. Greaves, A. J. Ryan, and E. Heeley. Recent experiments on a combined small-angle/wide-angle x-ray scattering beam line at the esrf. *Journal of Applied Crystallography*, 36:791–794, 2003.

[20] M. Schwab and B. Stuhn. Thermotropic transition from a state of liquid order to a macrolattice in asymmetric diblock copolymers. *Physical Review Letters*, 76(6):924–927, 1996.

[21] G. A. Mcconnell, A. P. Gast, J. S. Huang, and S. D. Smith. Disorder-order transitions in soft-sphere polymer micelles. *Physical Review Letters*, 71(13):2102–2105, 1993.

[22] T. Lopez-Leon and A. Fernandez-Nieves. Macroscopically probing the entropic influence of ions: Deswelling neutral microgels with salt. *Physical Review E*, 75(1), 2007.

[23] B. Sierra-Martin, Y. Laporte, A. B. South, L. A. Lyon, and A. Fernandez-Nieves. Bulk modulus of poly(n-isopropylacrylamide) microgels through the swelling transition. *Physical Review E*, 84(1), 2011.

[24] J. H. Laurer, J. F. Mulling, S. A. Khan, R. J. Spontak, J. S. Lin, and R. Bukovnik. Thermoplastic elastomer gels. ii. effects of composition and temperature on morphology and gel rheology. *Journal of Polymer Science Part B-Polymer Physics*, 36(14):2513–2523, 1998.

[25] K. Mortensen. Structural properties of self-assembled polymeric micelles. *Current Opinion in Colloid & Interface Science*, 3(1):12–19, 1998.

[26] N. Beheshti, K. Z. Zhu, A. L. Kjoniksen, K. D. Knudsen, and B. Nystrom. Characterization of temperature-induced association in aqueous solutions of charged abcba-type pentablock tercopolymers. *Soft Matter*, 7(3):1168–1175, 2011.

[27] Y. J. Zhang, S. Furyk, D. E. Bergbreiter, and P. S. Cremer. Specific ion effects on the water solubility of macromolecules: Pnipam and the hofmeister series. *Journal of the American Chemical Society*, 127(41):14505–14510, 2005.

[28] K. J. Krzyminski, M. Jasionowski, and A. Gutowska. Reversible sol-gel transitions in aqueous solutions of n-isopropylacrylamide ionic copolymers. *Polymer International*, 57(4):592–604, 2008.

[29] C. Chassenieux, T. Nicolai, and L. Benyahia. Rheology of associative polymer solutions. *Current Opinion in Colloid & Interface Science*, 16(1):18–26, 2011.

[30] L. Despax, J. Fitremann, M. Destarac, and S. Harrisson. Low concentration thermoresponsive hydrogels from readily accessible triblock copolymers. *Polymer Chemistry*, 7(20):3375–3377, 2016.

[31] S. Kirkland-York, K. Gallow, J. Ray, Y. L. Loo, and C. McCormick. Temperature-induced ordering and gelation of star micelles based on aba triblocks synthesized via aqueous raft polymerization. *Soft Matter*, 5(11):2179–2182, 2009.

[32] W. C. Wake. Theories of adhesion and uses of adhesives - review. *Polymer*, 19(3):291–308, 1978.

[33] H. J. Kim, B. H. Hwang, S. Lim, B. H. Choi, S. H. Kang, and H. J. Cha. Mussel adhesion-employed water-immiscible fluid bioadhesive for urinary fistula sealing. *Biomaterials*, 72:104–111, 2015.

[34] S. K. Clancy, A. Sodano, D. J. Cunningham, S. S. Huang, P. J. Zalicki, S. Shin, and B. K. Ahn. Marine bioinspired underwater contact adhesion. *Biomacromolecules*, 17(5):1869–1874, 2016.

[35] D. G. Lessard, M. Ousalem, X. X. Zhu, A. Eisenberg, and P. J. Carreau. Study of the phase transition of poly(n,n-diethylacrylamide) in water by rheology and dynamic light scattering. *Journal of Polymer Science Part B-Polymer Physics*, 41(14):1627–1637, 2003.

[36] C. Tsitsilianis, G. Serras, C. H. Ko, F. Jung, C. M. Papadakis, M. Rikkou-Kalourkoti, C. S. Patricicios, R. Schweins, and C. Chassenieux. Thermoresponsive hydrogels based on telechelic polyelectrolytes: From dynamic to "frozen" networks. *Macromolecules*, 51(6):2169–2179, 2018.

[37] S. Bayati, K. E. Bergquist, K. Z. Zhu, B. Nystrom, J. S. Pedersen, L. Galantini, and K. Schillen. Mixed micelles of oppositely charged poly(n-isopropylacrylamide) diblock copolymers. *Journal of Polymer Science Part B-Polymer Physics*, 55(19):1457–1469, 2017.

Tuning the properties of temperature responsive polyelectrolyte complexes, comparing NaCl and guanidinium thiocyanate

6

Salts influence the solubility of polymers and proteins depending on the concentration or ion type, and can therefore be used to tune the properties of temperature-responsive polyelectrolyte complexes. In this chapter, we compare the influence of NaCl and guanidinium thiocyanate (GndSCN) on poly(N-isopropylacrylamide) (PNIPAM) functionalized poly(acrylic acid)/poly(N,N-dimethyl aminoethyl methacrylate) (PAA/PDMAEMA) complexes by SAXS and rheology. It was found that the critical salt concentration, $c_{s,cr}$, below which polyelectrolyte complexation occurs, is lower for GndSCN than for NaCl. This indicates a higher solubility of the polymers in the GndSCN solution and hence increased dynamics of the complexes. The complexes are fluid at room temperature, but gel upon temperature increase, as a result of the lower critical solution temperature (LCST) of PNIPAM. The data show that increasing amounts of NaCl and GndSCN lower the gelation temperature, T_{gel}. Above T_{gel}, the PNIPAM chains form domains that are micro-phase separated from the polyelectrolyte complexes. The increased dynamics of the GndSCN samples facilitates the achievement of conformations closer to thermodynamic equilibrium. Whereas for the NaCl samples no clear morphologies could be identified. For the GndSCN samples, lamellar morphologies are found for salt concentrations below $c_{s,cr}$, while rods are found above $c_{s,cr}$. In rheology, the increased dynamics for GndSCN samples also result in lower moduli and peak strains at 50°C as compared to the samples with NaCl. Overall, it was shown that changing the salt influences both the temperature response, and the polyelectrolyte complexation resulting in remarkably different morphologies and mechanical properties. Controlling these properties can be an important tool for applications such as drug delivery systems, or underwater adhesives.

Introduction

Salts are known to influence the solubility of polymers and proteins, e.g. the salting in and out effect that is used for protein purification. The effect of salts on macromolecule solubility depends on the ion type and is related to the hydration of the ions. More hydrated ions tend to decrease the solubility, while less hydrated ions cause an increased solubility. In this chapter, the effect of GndSCN and NaCl on temperature responsive polyelectrolyte complexes is compared. Gnd^+ is a more hydrated ion than Na^+ and will therefore decrease the polymer solubility, while SCN^- is less hydrated than Cl^- and will improve the solubility.[1, 2] Furthermore, it is known that anions have a larger effect on the solubility than cations.[3] Therefore, it can be expected that the polymer solubility is higher upon GndSCN addition than upon NaCl addition. In the following paragraphs, we will discuss the expected effects of the salts on the complexation of the polyelectrolytes, and on the temperature response of poly(N-isopropylacrylamide) (PNIPAM).

Complex coacervation is a liquid-liquid phase separation that originates from electrostatic interactions between oppositely charged polyelectrolytes. The resulting coacervate is a dense, fluidic, polymer rich phase that coexists with a dilute water phase.[1] Complex coacervates have unique characteristics, such as a low interfacial tension, and immiscibility with water, while having a high water content up to 90%.[4, 5, 6] These properties make coacervates ideal materials for applications such as encapsulants, membranes, and underwater adhesives.[4, 7, 8, 9, 10, 11, 12] The addition of ions to complex coacervates reduces the entropy gain of complexing polyelectrolytes, and sufficient salt turns the complexation from an exothermic into an endothermic process.[6] As a result, increasing amounts of salt lead to decreasing coacervate densities, and upon exceeding the $c_{s,cr}$, complexation is prevented altogether. Spruijt et al. have shown that $c_{s,cr}$ decreases upon adding less hydrated anions, while more hydrated cations cause $c_{s,cr}$ to increase.[3] These findings are in agreement with the expectation that less hydrated ions improve the solubility. Therefore, it can be expected that $c_{s,cr}$ is lower for GndSCN than for NaCl.

Temperature responsivity is introduced to the coacervate by copolymerizing PNIPAM with the polyelectrolyte. PNIPAM is a well-studied polymer that displays a lower critical solution temperature (LCST).[13] This means that PNIPAM is water soluble below the LCST, and turns into a precipitated solid at temperatures above the LCST. The transition from soluble to insoluble is induced by a collapse of the PNIPAM side chains, resulting in exclusion of water.[14] This mechanism can be used for tuning the properties of the coacervate, or to solidify underwater adhesives.[4] Upon salt addition, the LCST of PNIPAM is either increased or reduced, depending on the type of ions that are added to the solution.[15, 16] Zhang et al. have shown that the LCST decreases by adding sodium salts, and that the effect of salt addition is
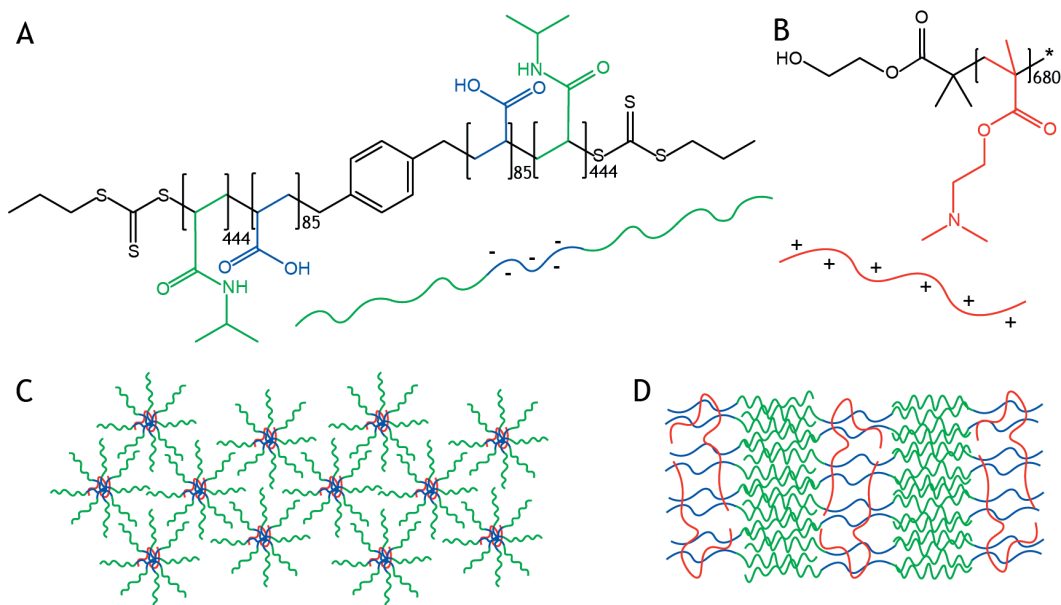
Figure 6.1 – Chemical structure and schematic representation of **A** PNIPAM-*b*-PAA-*b*-PNIPAM and **B** PDMAEMA. The morphology of the polymers is shown **C** below T_{gel} where C3Ms are found, and **D** above T_{gel} where mostly lamellae are observed. The green blocks represent PNIPAM, the blue blocks PAA, and the red blocks PDMAEMA.

reduced with decreasing hydration of the anion.[16] Therefore, it can be expected that the LCST of PNIPAM is decreased to a lesser extent upon the addition of GndSCN than upon the addition of NaCl.

The temperature responsive polyelectrolyte complexes are prepared by mixing PNIPAM-*b*-PAA-*b*-PNIPAM and PDMAEMA, Figure 6.1. PAA and PDMAEMA are weak polyelectrolytes that are, respectively, negatively and positively charged around neutral pH which results in coacervation upon mixing. The properties of the temperature responsive polyelectrolyte complexes are investigated for different temperatures, and GndSCN and polymer concentrations, by rheology, and small angle X-ray scattering (SAXS). The resulting data is discussed and compared to the data obtained with NaCl containing samples, which was presented in the previous chapter.

Experimental

Materials

Guanidinium thiocyanate (≥99%), was purchased from Sigma Aldrich, and sodium chloride (>99.5%) was bought from Acros Organics. Sodium hydroxide (TitriPUR, 1 M) and hydrochloric acid (TitriPUR, 1 M) were bought from Merck chemicals. PDMAEMA was purchased from Polymer Source, M_n 107 kDa, PDI 1.26, Figure A6.1. NIPAM$_{370}$-b-AA$_{170}$-b-NIPAM$_{370}$ was synthesized as described in Chapter 3, M_n 61.6 kDa and PDI 1.61 (PNIPAM-b-PtBA-b-PNIPAM).

Methods

Sample preparation

The polymers were dissolved in water as stock solutions with a concentration of max. 12.5 wt% and the pH was adjusted to 6.5±0.2. Also, aqueous 5.5 M stock solutions were made for both NaCl and GndSCN. Samples were prepared by mixing the polycation with the salt solution, followed by the addition of the polyanion. The solution was mixed and left refrigerated to equilibrate. Then the pH was checked, and adjusted to 6.5 ± 0.2 using 1 M NaOH or HCl. Finally, water was added to obtain the desired concentration, and the samples were kept refrigerated until further use.

The order of mixing the polyelectrolytes is important as it determines the degree of coacervation. Also, the polymers were added at equal charge, meaning that the amount of positively charged monomers equals the amount of negatively charged monomers to maximize complexation. Charge stoichiometry was verified by zetapotential measurements that should give values of about 0 mV.

SAXS

Small-angle X-ray scattering (SAXS) measurements were carried out at the Dutch-Belgian Beamline (DUBBLE) station BM26B of the European Synchrotron Radiation Facility (ESRF) in Grenoble, France.[17, 18] The sample-to-detector distance (Dectris Pilatus 1M) was ca. 2.5 m. The scattering vector q is defined as $q = 4\,\pi/\lambda\,\sin(\theta)$ with 2θ being the scattering angle and λ the wavelength of the X-rays (1.03 Å). Silver behenate was used to calibrate the q-range, which reached from $6.05*10^{-2}$ to 3.66 nm^{-1}. Two dimensional images were radially averaged around the centre of the primary beam to obtain the isotropic SAXS profiles. The data was corrected for absorption, and background scattering of the salt solutions. The samples were placed in a 2 mm quartz capillary and heated from 10 to 50 °C taking steps of 2-5 °C, with the temperature kept constant after each step for five or ten minutes. For details see Table A6.1. The acquisition time was 30 seconds per frame. Every second-last frame of each temperature step was taken for analysis.

Rheology

Rheological measurements were performed on an Anton Paar MCR 301 rheometer equipped with a 25 mm cone plate geometry. The temperature was controlled using a Peltier element. After making contact with the cone, the sample was immersed with tetradecane oil to avoid evaporation of water from the sample. At first, the samples were equilibrated for 1 h at 10 °C, then the temperature was increased from 10 to 50 °C with 0.13 °C/min, followed by another equilibration for 2 h at 50 °C. During these steps the sample was measured using an oscillatory shear with 1% strain, and an angular frequency of 1 rad/s. The T_{gel} is determined from the temperature at which the storage and loss modulus cross. After temperature increase, either shear start up experiments were performed using a rotation with a fixed shear rate of 0.1 s^{-1}, or frequency sweeps were measured using an oscillation with 1% strain, and angular frequencies of 0.1 till 100 rad/s.

Results and Discussion

SAXS

SAXS experiments are performed to determine the structure of the polymer solution while increasing the temperature from 10 till 50 °C. At first the scattering curves of all samples at 10 °C will be discussed. Subsequently, the changes induced by the temperature increase are explained for a representative example, and, finally, the scattering curves at 50 °C are compared.

At 10 °C, three peaks can be observed in the scattering profiles of samples with low GndSCN concentrations. For 0.3 M GndSCN and 7.5 wt% polymer, Figure 6.2A, the first two peaks are structure peaks and can be observed at 0.15 and 0.22 nm^{-1}. Based on the solubility, the peaks are most likely caused by the complex coacervate cores of the micelles that form below T_{gel}, Figure 6.1C. The ratio between the q values of the structure peaks is ≈ 1.5 or √2.3. Generally, closely packed spheres display a second order peak at √2 q^*, and cylinders at √3 q^*. Therefore, it is hard to tell what kind of ordering is present in the solution, based on the peak ratio of √2.3. When the salt concentration increases, the structure peaks shift to higher q values, indicating a lower interdomain spacing with increasing salt. This effect can be caused by the shrinking of the PNIPAM corona.[2, 19, 20] When $c_{s,cr}$ is approached at 0.6 M GndSCN, the structure peak shifts back to lower q, and the second order peak disappears. This disappearance indicates loss of order, or loss of contrast between the polyelectrolyte core and PNIPAM corona, which is induced by swelling of the complex coacervate core. At 1.0 M GndSCN, $c_{s,cr}$ is exceeded and only a broad bump from 0.17 till 1.16 nm^{-1} can be observed. At this salt concentration, the micelles have fallen apart into free polymers, which is indicated by a slope of -1.8 preceding the bump. This slope is found for dissolved polymers in between a fully swollen and a theta state.[21]
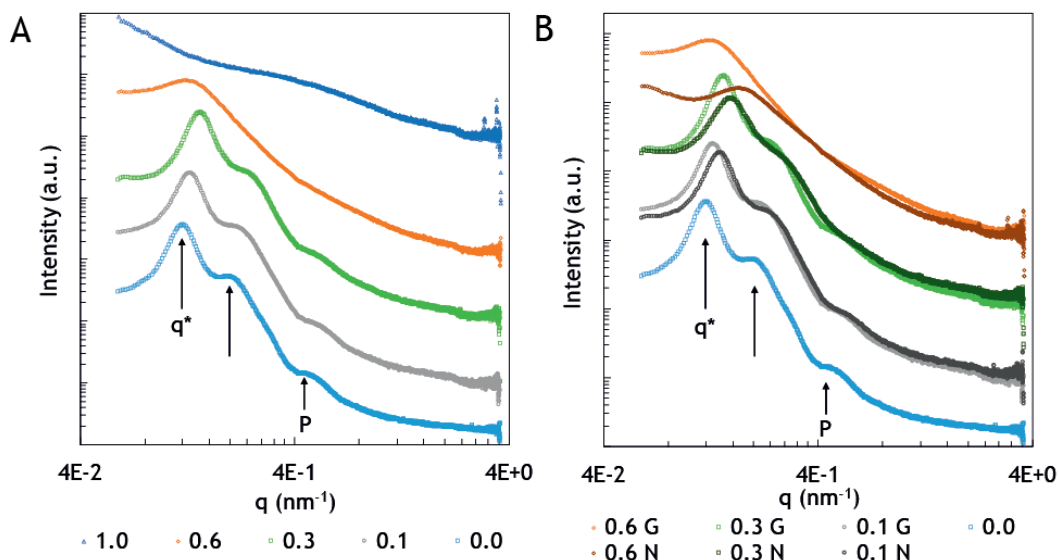
Figure 6.2 – Scattering profiles at 10 °C, for 7.5 wt% polymer, and **A** varying GndSCN concentrations (M). **B** For comparison, the same GndSCN (G) profiles combined with the scattering profiles of NaCl (N) (dark shades) that were discussed in the previous chapter. The arrows indicate the structure and form (P) factor peaks. The profiles are shifted for clarity.

Compared to samples with NaCl, Figure 6.2B, similar structure peaks are observed in samples with GndSCN. However, for GndSCN, the peak intensities are higher and the peaks are sharper, indicating a higher contrast between the core and corona, and/or less variation in the core distances. This difference may be explained by the lower $c_{s,cr}$ and higher T_{gel} for GndSCN, which facilitates equilibration, leading to better defined structures. Furthermore, it is expected that the PNIPAM corona deswells less upon adding GndSCN than upon adding NaCl. This is shown by the smaller shift of the structure peaks to higher q values when GndSCN is added. Also, at 0.6 M GndSCN, the structure peak shifts back to lower q, while for 0.6 M NaCl a shift to higher q is observed. This effect is caused by the lower $c_{s,cr}$ for GndSCN containing samples, inducing more swelling of the micelle cores.

To analyse the peak shift of the form factor with changing salt concentration, Iq^2 is plotted against q for the samples below 1.0 M GndSCN, Figure 6.3. From 0.0 to 0.1 M GndSCN, the form factor peak shifts to higher q, indicating that the core shrinks upon salt addition. Without added salt, the electrostatic interactions between the polyelectrolytes have long relaxation times, leading to slow equilibration and thus an entrapped coacervate core. Adding a small amount of salt lowers the relaxation time and enables equilibration, resulting in a smaller coacervate core. In addition, the aggregation number of the micelles can decrease upon salt addition, as a result of a reduced interfacial tension.[6, 22, 23] Then, at 0.3 M GndSCN, the form factor shifts
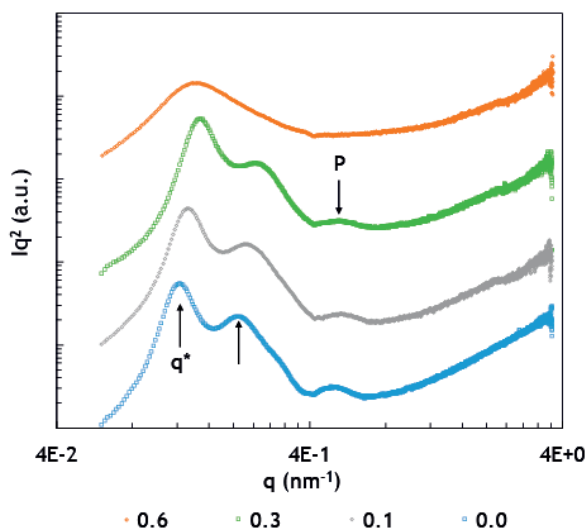
Figure 6.3 – Scattering profiles of 7.5 wt% polymer and varying GndSCN concentrations (M) at 10 °C, plotted as the scattering intensity, I, multiplied by q^2, against q. The structure peaks are indicated by the arrows pointing up, while the form factor peak is indicated by the arrow pointing down. The profiles are shifted for clarity.

slightly back to lower q, indicating a larger core of ≈14 nm. This is the result of weaker electrostatic interactions due to higher salt concentrations, leading to a less denser core and thus a larger coacervate volume.[2] Also, the peak seems to broaden and lose intensity, which is induced by less contrast between the core and corona of the micelles because of the swelling of the core, and deswelling of the corona. Finally, the contrast between the core and corona is higher for GndSCN containing samples than for NaCl containing samples, enabling a better visibility of the form factor peak till higher salt concentrations, Figure 6.2B.

Varying the polymer concentration leads to shifts in the structure factor peaks, and smaller interdomain distances are found for higher polymer concentrations, Figure 6.4A.[24] Also, for both 4 and 10 wt% polymer, the secondary structure peak is less clear than for 7.5 wt%. The $c_{s,cr}$ depends on the polymer concentration, as it depends on the number of electrostatic interactions on the polymers that have to be shielded to prevent complexation.[10] Therefore, 0.3 M GndSCN is a relatively higher salt concentration for 4 wt% polymer than for 7.5 wt%. As a result, the core of the micelle at 4 wt% can be more swollen resulting in less contrast with the corona, leading to broader structure peaks. For 10 wt%, this relation between $c_{s,cr}$ and c_P does not explain why only one peak is observed. However, at high polymer concentrations, a higher number of micelles is formed which are more closely packed. As a result, the coronae may mix, which decreases the contrast between the cores and coronae, resulting in broadened structure peaks. Furthermore, the form factor peak is only visible at 7.5
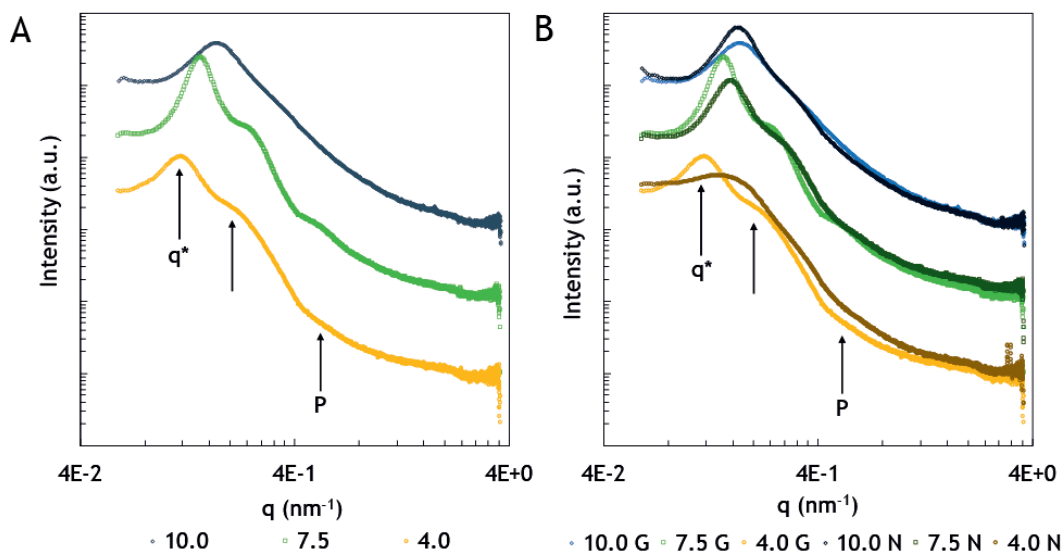
Figure 6.4 – Scattering profiles at 10 °C, for varying polymer concentrations (wt%) and **A** 0.3 M GndSCN. **B** For comparison, the same GndSCN (G) profiles combined with the scattering profiles of NaCl (N) (dark shades) that were discussed in the previous chapter. The arrows indicate the structure and form (P) factor peaks. The profiles are shifted for clarity.

wt% polymer.

The same differences between GndSCN and NaCl can be observed while changing the polymer concentration, as while changing the salt concentration. Firstly, clearer scattering patterns with better defined peaks are observed for GndSCN containing samples, Figure 6.4B. And, secondly, the maxima of the structure factors have shifted to lower q for GndSCN as a result of the lower corona deswelling upon GndSCN addition. Also, for both salts, scattering patterns become less pronounced when the polymer concentration deviates from 7.5 wt%.

Upon temperature increase of samples with 0.1 - 0.6 M GndSCN, the structure peaks first shift to higher q values, Figure 6.5A and Figure A6.2. This is caused by the deswelling of the PNIPAM corona, leading to lower interdomain distances.[19, 20] As a result of the deswelling, the volume ratio between the coacervate and PNIPAM phase changes, leading to a different ordering in the sample. This effect results in broadening of the structure peaks, disappearance of the second order structure peak, and fading of the form factor peak.[25] Then, at low q values, the slope of the scattering curve increases, showing the formation of larger clusters and illustrating the gelation of the solution.[26] So far, the behaviour of the GndSCN and NaCl containing samples is similar, Figure 6.5. However, for samples with GndSCN, two new structure peaks are formed at intermediate q, which are absent for samples with NaCl. For 0.3 M Gnd-SCN and 7.5 wt%, these structure peaks appear from 28 °C onwards. The peaks shift
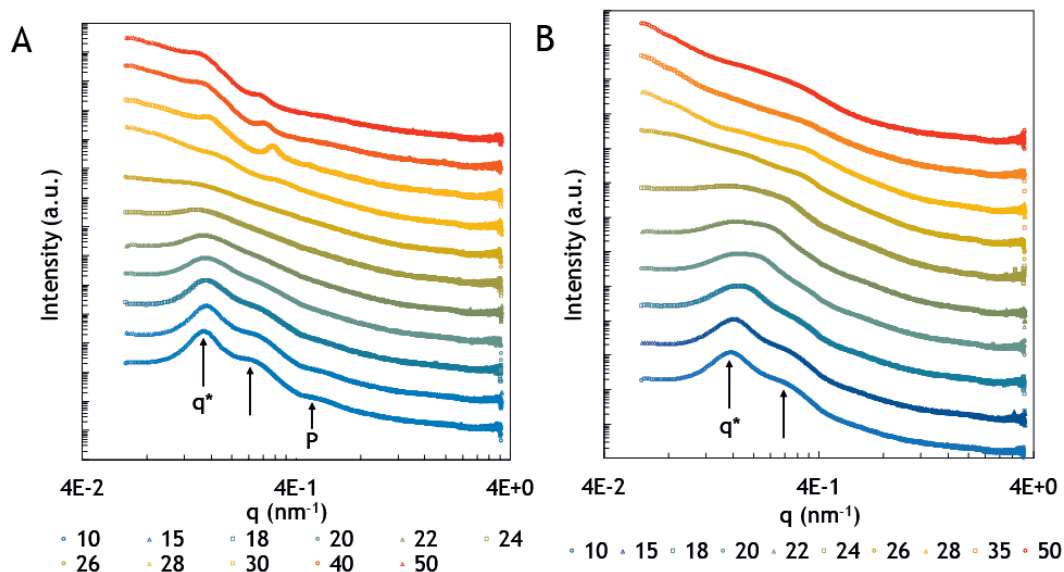
Figure 6.5 – Scattering profiles with increasing temperature (from bottom to top, °C) of 7.5 wt% polymer and **A** 0.3 M GndSCN or **B** 0.3 M NaCl. For clarity, temperatures at which no changes occurred have been left out of the figure. The arrows indicate the structure and form factor (P) peaks. The profiles are shifted over the vertical axis for clarity.

to lower q values when the solution is further heated and are approximately $\sqrt{4}$ apart, which suggest the presence of lamellae, Figure 6.1D.[27] Also, when looking carefully, Figure A6.3, a third peak seems to be present at 0.53 nm^{-1}, which can be the fourth order structure peak, as a ratio of $\sqrt{16}$ with q^* is found. In this case, the third order peak of $\sqrt{9}$ is invisible, as has been observed before.[21, 27] Similar structure peaks are found for the other GndSCN concentrations below $c_{s,cr}$ and at 7.5 wt% polymer, Figure A6.2. Furthermore, the change with temperature in the SAXS spectrum occurs at lower temperatures for higher GndSCN concentrations, indicating a decreasing PNIPAM LCST upon salt addition. Also, higher polymer concentrations show changes in the spectrum at lower temperatures, Figure A6.4. Compared to NaCl, the temperature transition for GndSCN containing samples is higher, as can be expected from the lower degree of hydration of the SCN$^-$ ions.

At 50 °C, the scattering patterns for 0.0 and 1.0 M GndSCN containing samples deviate from those with 0.1 – 0.6 M GndSCN, Figure 6.6A. At 0.0 M GndSCN, a shoulder is visible and no separate peaks can be distinguished. This is probably due to the absence of additional salt, which hinders the equilibration of the system, leading to a disordered structure. At 1.0 M GndSCN, the pattern looks considerably different. At first, the slope at low q is $\approx$ -1, while -2 is observed at lower GndSCN concentrations. A slope of -1 is typically found in the Guinier regime for rods in solution.[28, 29] In case of rods, the first and second minimum of the Fourier regime are a factor 1.8 apart,
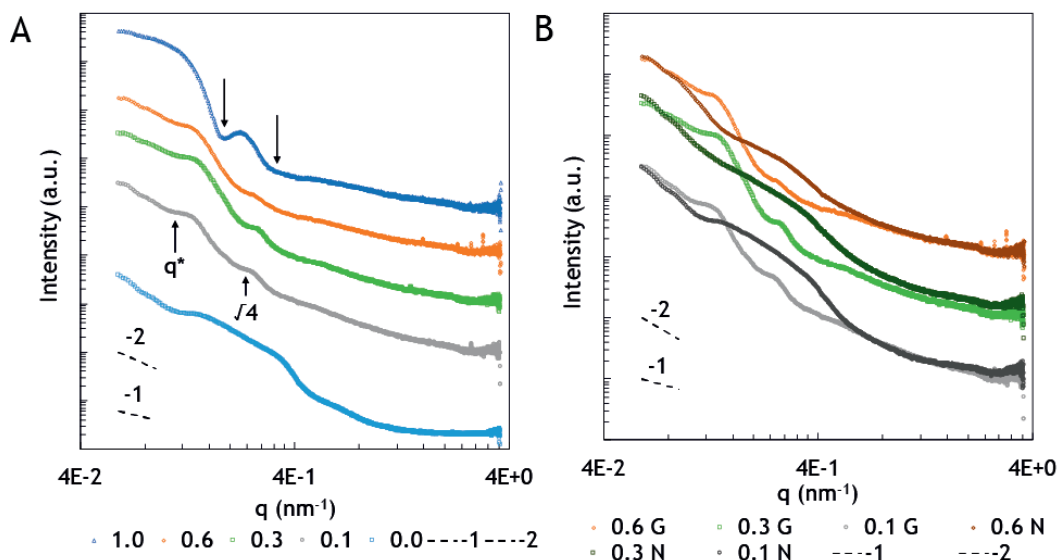
Figure 6.6 – Scattering profiles at 50 °C, for 7.5 wt% polymer, and **A** varying GndSCN concentrations (M). The arrows pointing up indicate the structure and form (P) factor peaks, while the arrows pointing down indicate the minima. **B** For comparison, the GndSCN (G) profiles combined with the scattering profiles of NaCl (N) (dark shades) that were discussed in the previous chapter. The profiles are shifted for clarity.

which is almost the case, as we find 0.18 and 0.31 nm^{-1} for the two minima.[30] From the onset of the Fourier regime at $9.6 *10^{-2}$ nm^{-1}, we can estimate the radius of the rod using $q^*R=1$, which gives approximately 10.5 nm.[31] The length of the rod cannot be estimated as the onset of the Guinier regime at $q^*L=\pi$ is beyond the range of the measurement.[31] As a result of the high GndSCN concentration, complexation of the polyelectrolytes is prevented, possibly leading to the formation of rod shaped, in-soluble PNIPAM domains, stabilized by polyelectrolytes. For the samples containing 0.1 - 0.6 M GndSCN, lamellae are observed as was described above. The domain spacing, d, of the lamellae can be estimated by $d=2\pi/q_{max}$, where q_{max} represents the peak maximum.[32] Accordingly, domain sizes of ≈46 - 48 nm were found.

Compared to NaCl, relatively well-defined features are observed for GndSCN, while for NaCl containing samples only broad bumps are observed. This is explained by the lower $c_{s,cr}$ for GndSCN which causes more swollen and thus more dynamic complex coacervate domains. Also, T_{gel} seems higher for GndSCN containing samples. Therefore, equilibration can be easier obtained for GndSCN, and the volume ratio between the PNIPAM and polyelectrolyte phases can be different compared to NaCl. As a result, lamellae are observed. Interestingly, the high and low q ends of the scattering patterns overlap, showing that the structures of the gels are comparable on those length scales.

For the different polymer concentrations at 50 °C, peak formation is most clear
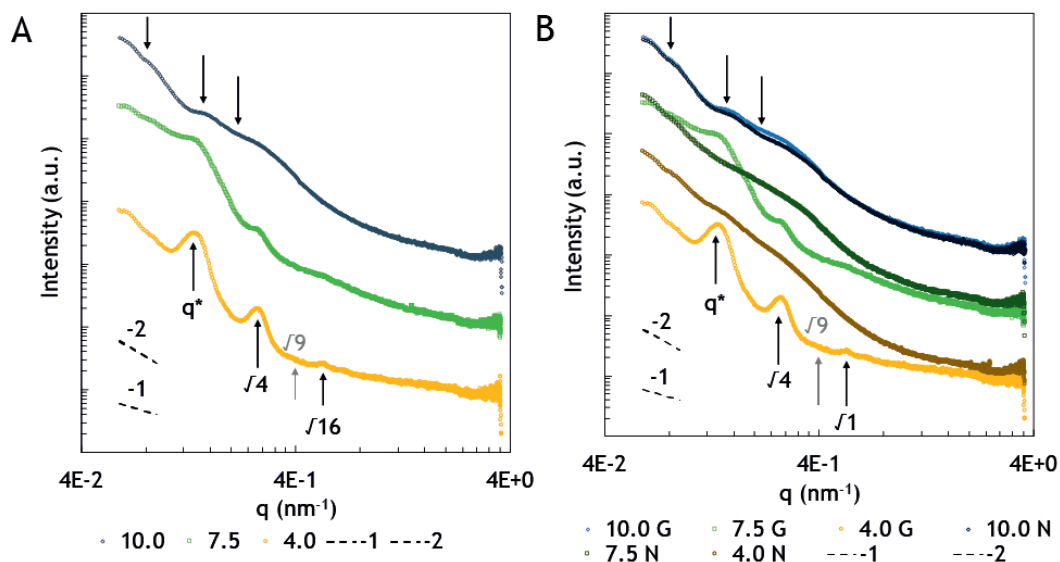
Figure 6.7 – Scattering profiles at 50 °C with changing polymer concentration (wt%) and **A** 0.3 M GndSCN. For comparison, **B** the GndSCN profiles are combined with the NaCl profiles. The black arrows indicate observed peaks, while the grey arrow shows a missing structure peak.

at 4 wt% and three peaks are observed, Figure 6.7A. The first two peaks are located at 0.14 and 0.27 nm^{-1}, which is roughly a factor $\sqrt{4}$ apart, and the third peak is found at 0.55 nm^{-1}, i.e. $\sqrt{16}$ q^*. Therefore, lamellae are found for both 4 and 7.5 wt% polymer, and both spectra lack a third order peak (grey arrow).[21, 27] For 10 wt% polymer, the peaks at intermediate q almost fused into one shoulder, and a small peak at low q has appeared. From this comparison, it becomes clear that equilibration is easier for lower polymer concentrations. Most likely this is caused by the lower absolute amount of PNIPAM in the sample at 4 wt%. PNIPAM collapses at temperatures above the LCST, leading to excretion of water. At lower polymer concentrations, the excreted amount of water is lower the amount of salt relative to the amount of polyelectrolyte is the highest for the low polymer concentration. As a result, the coacervate has a higher water content in the coacervate. At higher polymer concentrations, the amount of water that has to be excluded is higher and can be too much for the coacervate, which can frustrate the equilibration. Also, higher polymer concentrations, can complicate the equilibration into a new structure, therefore ordering may decrease with increasing polymer concentration.

Comparing to NaCl, it is again shown that GndSCN containing samples result in clearer scattering patterns than NaCl containing samples, especially for the low polymer concentrations. For 10 wt% polymer, however, the scattering patterns of both salts largely overlap, indicating that ordering is hindered for both types of salt.

Considering the block copolymer phase diagram, lamellae are formed when the

volume fraction of the two phases are similar, while cylinders are observed when the volume fractions deviate from eveness.[27, 33] In this research, samples with 70 wt% PNIPAM and 30 wt% polyelectrolyte are used. In case the water content of both systems would be similar, cylinders could be expected. However, upon exceeding the LCST, PNIPAM collapses and excretes water, leading to more equal volume fractions and thus the observation of lamellae.

Rheology

Rheology is used to determine the behaviour of the material upon applying strain. First, temperature sweeps are performed, Figure 6.8, in which the temperature is slowly increased from 10 till 50 °C, while monitoring the moduli. At low temperature, the samples are fluids, as is concluded from the loss modulus that is higher than the storage modulus. At T_{gel}, the loss and storage modulus cross and the material behaves as a solid, as can be seen from the storage modulus that exceeds the loss modulus. When the samples are compared, it can be observed that T_{gel} decreases with increasing GndSCN or polymer concentration, Table 6.1. The effect of the polymer concentration is explained by an increased probability of bridging for higher polymer concentrations, causing a lower T_{gel}, as is described in literature many times.[26, 34, 35, 36, 37] Also, higher polymer concentrations cause a higher number of PNIPAM connections, leading to higher moduli for higher polymer concentrations, as is observed as well.[34]

The effect of the GndSCN concentration on T_{gel} can be explained by the salt dependence of the LCST. As described in the introduction, it is expected that the LCST of PNIPAM drops with increasing GndSCN concentrations, which is confirmed by the lowering of T_{gel} with increasing GndSCN concentrations. Furthermore, it can be observed that higher GndSCN concentrations lead to lower moduli at 50 °C. This effect can be explained by the influence of salts on complex coacervation. With increasing ionic strength, charge screening of the polyelectrolytes increases, leading to shorter relaxation times of the electrostatic interactions, and thus lower moduli.[2] This behaviour is particularly clear for the sample at 1.0 M GndSCN where $c_{s,cr}$ is exceeded and final moduli of less than 1 Pa are reached, Figure A6.5A.

Comparing to NaCl, higher T_{gel} and a lower modulus at 50 °C is observed for Gnd-SCN containing samples, which can be explained by the solvent quality. A GndSCN solution has a better solvent quality for the polymer than a NaCl solution with the same salt concentration. As a result, lower relaxation times are observed for connections between the polymers, which leads to lower moduli.[37]

Obtaining rheology results on the GndSCN containing samples has proven to be challenging. For samples with low salt and polymer concentrations, an increase in moduli with increasing temperature was observed, followed by a dramatic drop in the moduli, Figure A6.5B. Similar behaviour is observed for samples with low amounts of NaCl Figure A5.6A), samples with just PNIPAM polymers (Figure A6.5C), and for samples of PNIPAM-*b*-PDMA-*b*-PNIPAM that were investigated by Kirkland et al.[37] In their article, it is described that a particular polymer concentration is
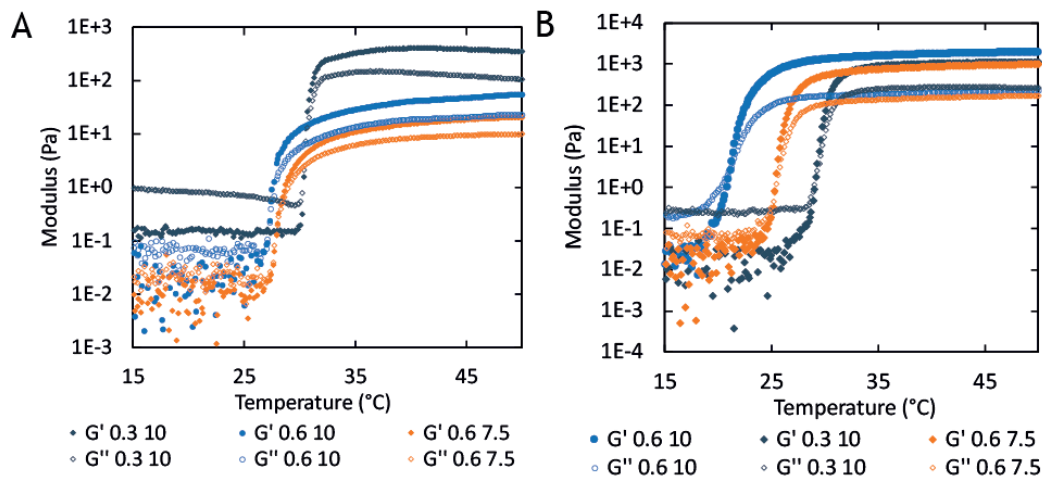
Figure 6.8 – Storage and loss moduli as function of temperature for different polymer and salt concentrations, i.e. **A** GndSCN (M), or **B** NaCl (M).

needed to obtain stable gelation, and that the critical polymer concentration decreases by adding minimal amounts of NaCl and phosphate buffer. As an explanation for the dropping moduli, they argue that at low polymer concentrations an insufficient degree of bridging occurs, leading to an easy breakdown of the sample. In agreement with their observations, dropping moduli were observed for 0.3 M GndSCN and 7.5 wt% polymer, while stable moduli were observed at 10 wt% polymer, Figure A6.5B and Figure 6.8. Furthermore, a decreasing solvent quality for the outer block results in increased bridging.[37] Therefore, samples with NaCl show stable moduli at lower salt concentrations than samples prepared with GndSCN, as a NaCl solution is a worse solvent for PNIPAM than a GndSCN solution. Furthermore, increasing salt concentration leads to a decreasing solvent quality for PNIPAM, resulting in stable moduli upon temperature increase when more salt is added. In addition, $c_{s,cr}$ is lower for GndSCN than for NaCl, which weakens the complex coacervate phase in the gel. Furthermore, the reproducibility of the moduli is challenging as is shown in Table 6.1. A possible explanation for these difficulties are the weak materials, causing higher relative deviations.

Shear start-up experiments are performed to determine the ability to dissipate energy, and to monitor the extensibility of the samples before failure. It became clear that the highest peak stress is observed for 0.3 M GndSCN and 10 wt% polymer, while the observed peak strains are in close proximity, Figure 6.9A and Table 6.2. Also, for the samples with 0.6 M GndSCN, a shoulder can be observed, suggesting that the failure occurs in two steps. Likely, first the PNIPAM chains are disconnected, while the electrostatic interactions of the complex coacervate only break at higher strains. This can be expected as the electrostatic interactions are more easily reformed than the hydro-

C_{GndSCN}	C_{pol}	T_{gel}	G'_{50}	G'_{eq}
M	wt%	°C	Pa	Pa
0.3	10	30.5 ± 0.0	575.0 ± 219.7	442.7 ± 268.8
0.6	10	26.4 ± 1.3	45.2 ± 14.2	45.6 ± 13.4
0.6	7.5	27.9 ± 0.2	43.2 ± 23.1	43.2 ± 23.5
0.3	7.5	32	-	-
1.0	7.5	33.6*	0.7	0.6

Table 6.1 – Showing the obtained T_{gel}, storage modulus of the heating ramp at 50 °C (G'_{50}), and storage modulus after 2 h of equilibration at 50 °C (G'_{eq}). For 0.3 M GndSCN and 7.5 wt% polymer, no stable moduli could be obtained upon increasing the temperature. *For 1.0 M GndSCN the cross-over of the moduli only occurs after the moduli have increased for a couple of degrees already, Figure A6.5A, while in all other cases the cross-over coincides with the increase in moduli. Samples with dropping or low moduli have been measured only once, therefore no standard deviation can be shown.
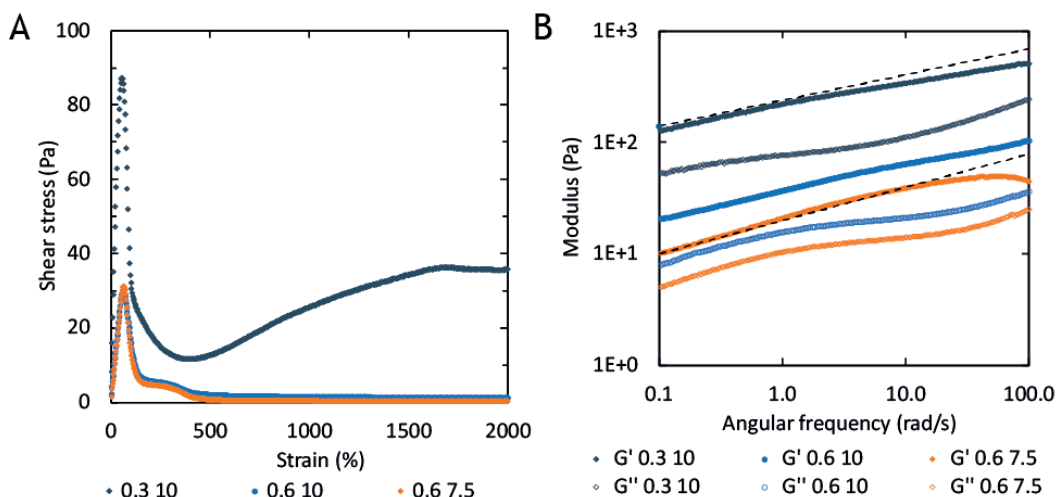

Figure 6.9 – **A** Shear stress as function of strain at 50 °C for varying GndSCN (M) and polymer (wt%) concentrations. **B** Frequency sweep for the same samples, also at 50 °C.

Table 6.2 – Overview obtained peak strains and stresses for varying GndSCN and polymer concentrations at 50 °C.

c_{GndSCN}	c_p	γ_{peak}	σ_{peak}
M	wt%	%	Pa
0.3	10	55.9	87.3
0.6	10	64.5	31.3
0.6	7.5	61.6	29.6

phobic interactions of PNIPAM, because of lower relaxation times.[3, 38] Compared to NaCl containing samples, the observed peak stress and peak strain are a lot lower. This can be explained by the improved solvent quality of the GndSCN solution for the polymers leading to decreasing relaxation times of polymer interactions.

Frequency sweeps are used to determine the viscoelastic response of the material. Elastic solids show frequency independent moduli, while critical gels show an increasing modulus, but constant tanδ=G"/G'. [24, 39] In Figure 6.9B, it can be seen that the moduli increase with increasing frequency, and also tan δ varies during the measurement, Figure A6.5D. For this reason, it can be concluded that the gels are viscoelastic solids. The most solid sample contains 0.3 M GndSCN and 10 wt% polymer, as is observed from the lowest tan δ value. This can be explained by the low GndSCN concentration, and therefore strong interactions between the polyelectrolytes. Also, this sample has a high polymer concentration, causing a higher extent of bridging and thus a higher solidity. Compared to the same samples with NaCl, higher tan δ values are observed, which can be caused by the improved solvent quality for the polymers, which enhances dissipation.[19, 20]

Conclusion

The addition of GndSCN to temperature responsive polyelectrolytes results in materials with remarkably different properties, compared to NaCl containing samples. This is caused by a better solvent quality of the PNIPAM, resulting in a higher T_{gel}, and a lower $c_{s,cr}$ for the complexation of PAA and PDMAEMA. Above T_{gel}, lamellae were found at GndSCN concentrations below $c_{s,cr}$, while above $c_{s,cr}$, rods were observed. In rheology, it was shown that the gels are a lot weaker compared to samples with NaCl. However, the strongest gel was obtained by using high polymer and low GndSCN concentrations. The ability to adjust the properties of temperature responsive polyelectrolyte complexes can be an important tool for applications such as injectable adhesives. Here, it was shown that the type of ion added to the polymer solution can make a big difference to the material properties.

Acknowledgements

Appendix

Experimental
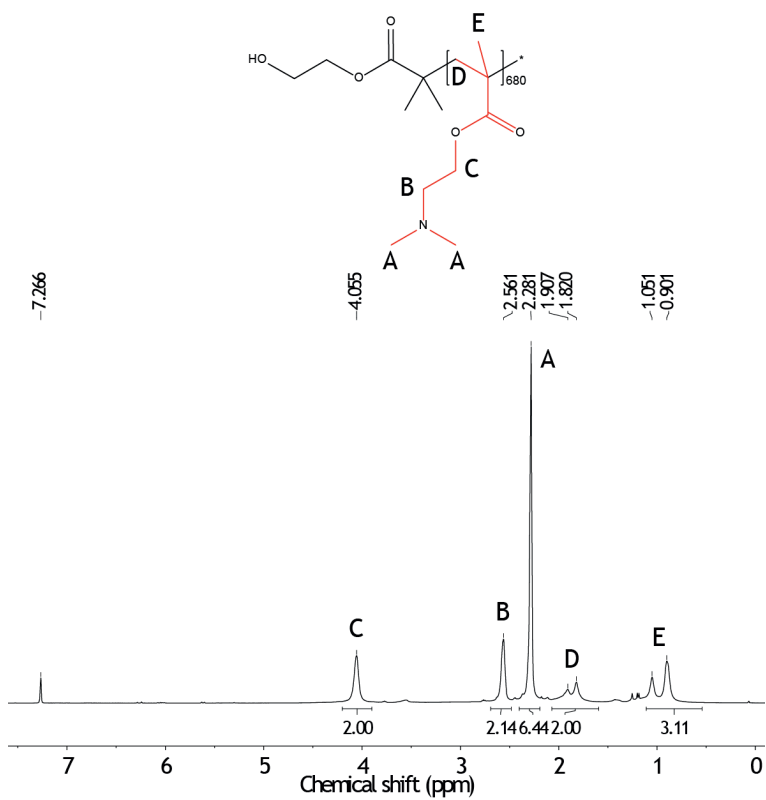
Figure A6.1 – ^{1}H-NMR spectrum of PDMAEMA in CDCl$_3$ as purchased from Polymer Source.

Temperature	10	15	18	20	22	24	26	28	30	32	35	40	45	50
Time	5	5	10	10	10	10	10	10	10	10	5	5	5	5

Table A6.1 – Heating scheme of SAXS measurements, with temperature (°C) and time (min).

Results and Discussion

SAXS
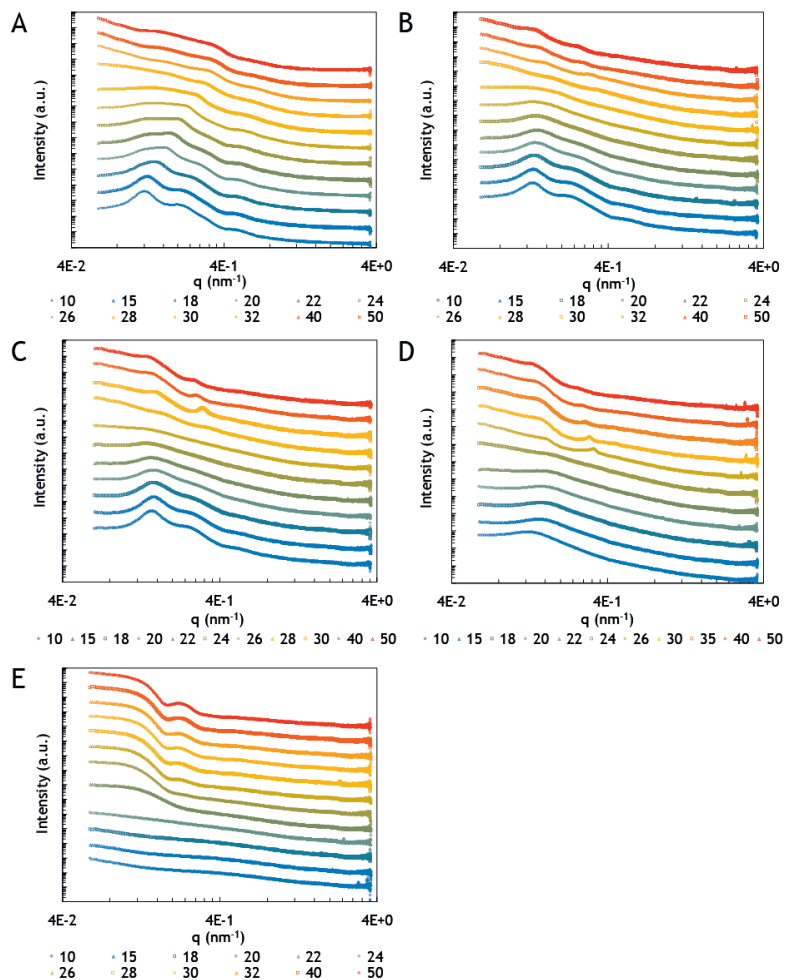
Figure A6.2 – Scattering profiles with increasing temperature (°C), from bottom to top, are shown for 7.5 wt% polymer and 0.0 M (**A**), 0.1 M (**B**), 0.3 M (**C**), 0.6 M (**D**) and 1.0 M (**E**) GndSCN. For clarity, curves at which no changes occur compared to the previous curve are not shown.
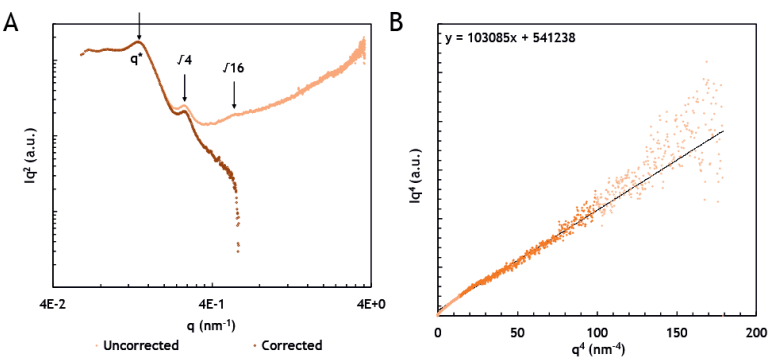
Figure A6.3 – A Scattering profiles of 7.5 wt% polymer and 0.3 M GndSCN at 50 °C, plotted as the scattering intensity I times q^2 against q. The arrows indicate the structure peaks. Both the uncorrected (orange) and corrected (brown) $((I-I_b)*q^2)$ spectra are shown.[32] It can be seen that correction is not needed, as the peak of q^* does not shift. Therefore the uncorrected q^* value can be used to determine the domain spacing d of the lamellae. **B** Plot of Iq^4 against q^4 that is used to determine the correction factor I_b from the intercept of the trend line. The trend line was made by using the closed circles.
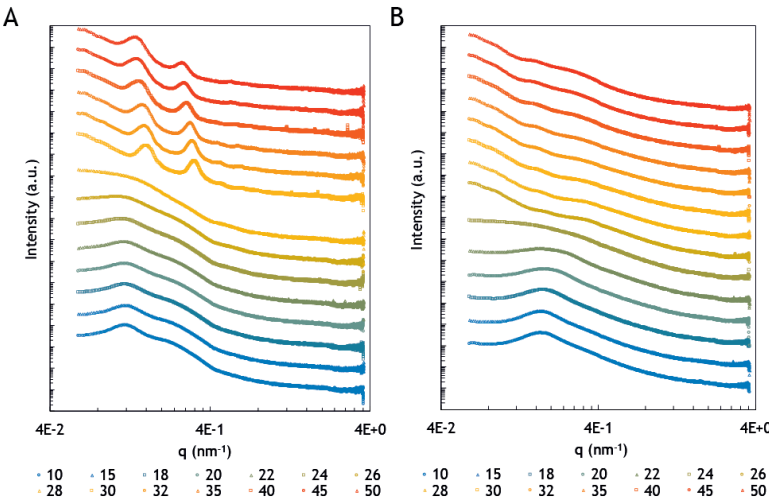
Figure A6.4 – Scattering profiles with increasing temperature (°C), from bottom to top, are shown for 0.3 M GndSCN with 4 wt% (**A**), and 10 wt% (**B**) polymer.

Rheology
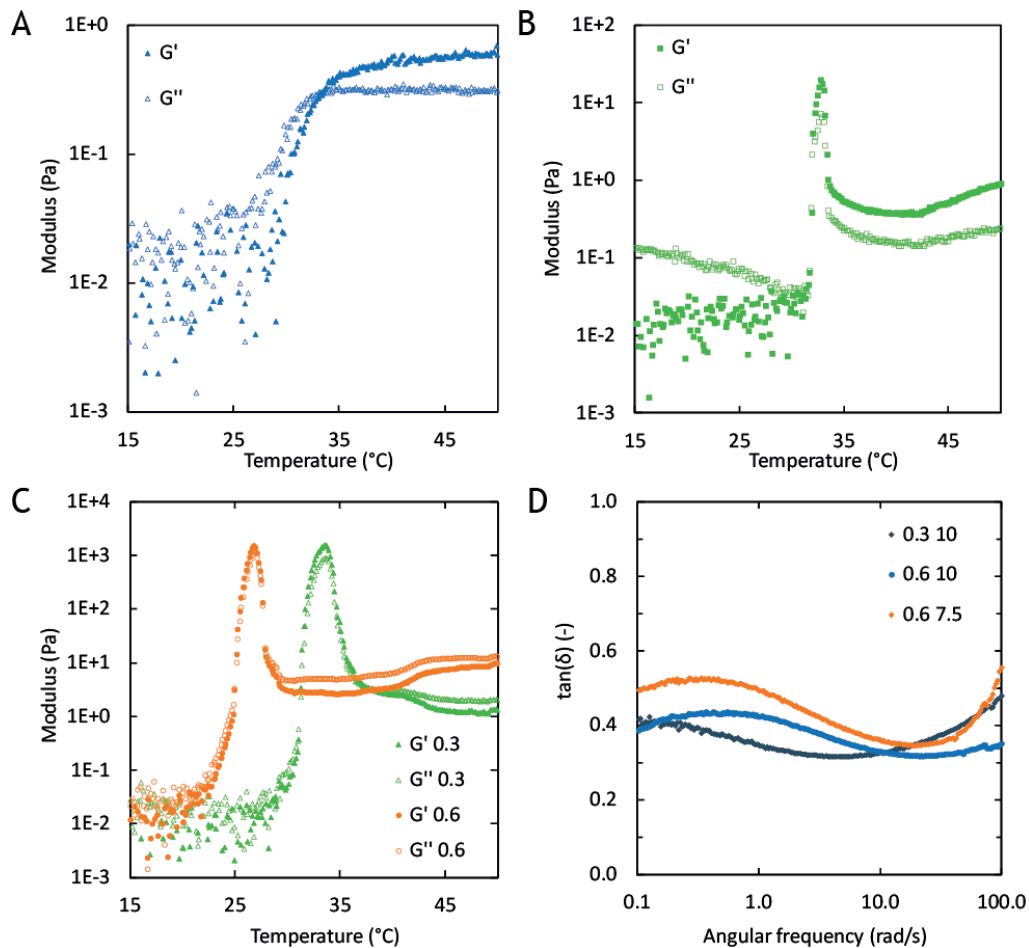
Figure A6.5 – Storage and loss moduli as function of temperature for 7.5 wt% TERPOC and **A** 1.0 M and **B** 0.3 M GITC. **C** The same experiment was performed for 0.3 and 0.6 M NaCl, and 10 wt% PNIPAM, M_n 39.8 kDa (GPC) and PDI of 1.65. **D** Tan δ values as calculated from the obtained G' and G'' in the frequency sweep of the TERPOC at 50 °C.

Control experiments
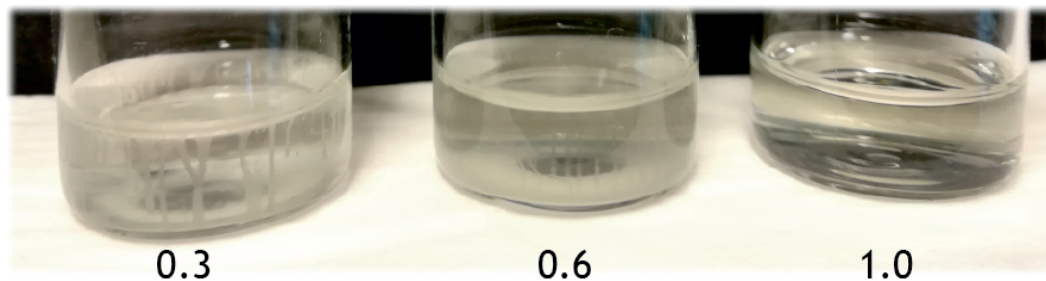
Figure A6.6 – Complexes of DMAEMA$_{680}$ and AA$_{155}$ in a GITC solution with various concentrations (M). At 0.3 and 0.6 M GITC, white precipitates can be observed, while at 1.0 M GITC a clear solution is present. This shows that the $c_{s,cr}$ is exceeded at 1.0 M. An interesting observation is that DMAEMA$_{680}$ turns the GITC solution turbid, even when PAA is not added yet. AA$_{155}$ was obtained from dissolving the PtBA macro-RAFT agent in DCM with 0.8 M TFA. After 4 days the DCM was evaporated and the polymer was redissolved in water, followed by neutralization using 1.0 M NaOH. A dry product was obtained by freeze-drying.
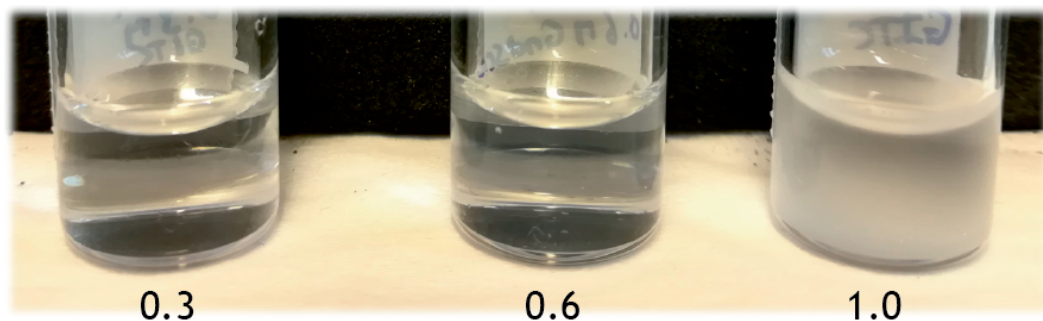
Figure A6.7 – Solution of 7.5 wt% PNIPAM in GndSCN with different concentrations (M) at 23 °C. M_n 39.8 kDa (GPC) and PDI of 1.65. It can be seen that the PNIPAM dissolves at 0.3 and 0.6 M GndSCN, while the LCST is exceeded for 1.0 M GndSCN.

Bibliography

[1] E. Spruijt, M. A. C. Stuart, and J. van der Gucht. Linear viscoelasticity of polyelectrolyte complex coacervates. *Macromolecules*, 46(4):1633–1641, 2013.

[2] E. Spruijt, A. H. Westphal, J. W. Borst, M. A. C. Stuart, and J. van der Gucht. Binodal compositions of polyeleetrolyte complexes. *Macromolecules*, 43(15):6476–6484, 2010.

[3] E. Spruijt. *Strength, structure and stability of polyelectrolyte complex coacervates*. Wageningen University, Wageningen, 2012.

[4] M. Dompé, F. J. Cedano-Serrano, O. Heckert, N. van den Heuvel, J. Van der Gucht, Y. Tran, D. Hourdet, C. Creton, and M. Kamperman. Thermoresponsive complex coacervate-based underwater adhesive. *Advanced Materials*, page 1808179, 2019.

[5] E. Spruijt, J. Sprakel, M. Lemmers, M. A. C. Stuart, and J. van der Gucht. Relaxation dynamics at different time scales in electrostatic complexes: Time-salt superposition. *Physical Review Letters*, 105(20), 2010.

[6] J. van der Gucht, E. Spruijt, M. Lemmers, and M. A. C. Stuart. Polyelectrolyte complexes: Bulk phases and colloidal systems. *Journal of Colloid and Interface Science*, 361(2):407–422, 2011.

[7] A. S. Hoffman. Hydrogels for biomedical applications. *Advanced Drug Delivery Reviews*, 64:18–23, 2012.

[8] A. H. Hofman, I. A. van Hees, J. Yang, and M. Kamperman. Bioinspired underwater adhesives by using the supramolecular toolbox. *Advanced Materials*, 30(19), 2018.

[9] S. Kaur, G. M. Weerasekare, and R. J. Stewart. Multiphase adhesive coacervates inspired by the sandcastle worm. *Acs Applied Materials & Interfaces*, 3(4):941–944, 2011.

[10] D. Priftis and M. Tirrell. Phase behaviour and complex coacervation of aqueous polypeptide solutions. *Soft Matter*, 8(36):9396–9405, 2012.

[11] R. J. Stewart, C. S. Wang, and H. Shao. Complex coacervates as a foundation for synthetic underwater adhesives. *Advances in Colloid and Interface Science*, 167(1-2):85–93, 2011.

[12] I. A. Van Hees, P.J.M. Swinkels, R.G. Fokkink, A.H. Velders, I. K. Voets, J. Van der Gucht, and M. Kamperman. Self-assembly of oppositely charged polyelectrolyte block copolymers containing short thermoresponsive blocks. *Polymer Chemistry*, 2019.

[13] M. A. Ward and T. K. Georgiou. Thermoresponsive polymers for biomedical applications. *Polymers*, 3(3):1215–1242, 2011.

[14] K. J. Krzyminski, M. Jasionowski, and A. Gutowska. Reversible sol-gel transitions in aqueous solutions of n-isopropylacrylamide ionic copolymers. *Polymer International*, 57(4):592–604, 2008.

[15] M. C. M. Costa, S. M. C. Silva, and F. E. Antunes. Adjusting the low critical solution temperature of poly(n-isopropyl acrylamide) solutions by salts, ionic surfactants and solvents: A rheological study. *Journal of Molecular Liquids*, 210:113–118, 2015.

[16] Y. J. Zhang, S. Furyk, D. E. Bergbreiter, and P. S. Cremer. Specific ion effects on the water solubility of macromolecules: Pnipam and the hofmeister series. *Journal of the American Chemical Society*, 127(41):14505–14510, 2005.

[17] M. Borsboom, W. Bras, I. Cerjak, D. Detollenaere, D. G. van Loon, P. Goedtkindt, M. Konijnenburg, P. Lassing, Y. K. Levine, B. Munneke, M. Oversluizen, R. van Tol, and E. Vlieg. The dutch-belgian beamline at the esrf. *Journal of Synchrotron Radiation*, 5:518–520, 1998.

[18] W. Bras, I. P. Dolbnya, D. Detollenaere, R. van Tol, M. Malfois, G. N. Greaves, A. J. Ryan, and E. Heeley. Recent experiments on a combined small-angle/wide-angle x-ray scattering beam line at the esrf. *Journal of Applied Crystallography*, 36:791–794, 2003.

[19] T. Lopez-Leon and A. Fernandez-Nieves. Macroscopically probing the entropic influence of ions: Deswelling neutral microgels with salt. *Physical Review E*, 75(1), 2007.

[20] B. Sierra-Martin, Y. Laporte, A. B. South, L. A. Lyon, and A. Fernandez-Nieves. Bulk modulus of poly(n-isopropylacrylamide) microgels through the swelling transition. *Physical Review E*, 84(1), 2011.

[21] J. P. A. Fairclough, I. W. Hamley, and N. J. Terrill. X-ray scattering in polymers and micelles. *Radiation Physics and Chemistry*, 56(1-2):159–173, 1999.

[22] M. Lemmers, I. K. Voets, M. A. C. Stuart, and J. van der Gucht. Transient network topology of interconnected polyelectrolyte complex micelles. *Soft Matter*, 7(4):1378–1389, 2011.

[23] J. Y. Wang, A. de Keizer, R. Fokkink, Y. Yan, M. A. C. Stuart, and J. van der Gucht. Complex coacervate core micelles from iron-based coordination polymers. *Journal of Physical Chemistry B*, 114(25):8313–8319, 2010.

[24] J. H. Laurer, J. F. Mulling, S. A. Khan, R. J. Spontak, J. S. Lin, and R. Bukovnik. Thermoplastic elastomer gels. ii. effects of composition and temperature on morphology and gel rheology. *Journal of Polymer Science Part B-Polymer Physics*, 36(14):2513–2523, 1998.

[25] K. Mortensen. Structural properties of self-assembled polymeric micelles. *Current Opinion in Colloid & Interface Science*, 3(1):12–19, 1998.

[26] N. Beheshti, K. Z. Zhu, A. L. Kjoniksen, K. D. Knudsen, and B. Nystrom. Characterization of temperature-induced association in aqueous solutions of charged abcba-type pentablock tercopolymers. *Soft Matter*, 7(3):1168–1175, 2011.

[27] A. L. Schmitt and M. K. Mahanthappa. Polydispersity-driven shift in the lamellar mesophase composition window of peo-pb-peo triblock copolymers. *Soft Matter*, 8(7):2294–2303, 2012.

[28] J. S. Pedersen. Form factors of block copolymer micelles with spherical, ellipsoidal and cylindrical cores. *Journal of Applied Crystallography*, 33(1):637–640, 2000.

[29] P. Schurtenberger, G. Jerke, C. Cavaco, and J. S. Pedersen. Cross-section structure of cylindrical and polymer-like micelles from small-angle scattering data .2. experimental results. *Langmuir*, 12(10):2433–2440, 1996.

[30] Th. Zemb and P. Lindner. *Neutron, X-rays and light scattering methods applied to soft condensed matter*. North Holland, 1 edition, 2002.

[31] A. Guinier and G. Fournet. *Small-Angle Scattering of X-rays.* John Wiley and Sons, New York, 1955.

[32] A. J. Ryan, W. Bras, G. R. Mant, and G. E. Derbyshire. A direct method to determine the degree of crystallinity and lamellar thickness of polymers - application to polyethylene. *Polymer*, 35(21):4537–4544, 1994.

[33] F. S. Bates. Polymer-polymer phase-behavior. *Science*, 251(4996):898–905, 1991.

[34] C. Chassenieux, T. Nicolai, and L. Benyahia. Rheology of associative polymer solutions. *Current Opinion in Colloid & Interface Science*, 16(1):18–26, 2011.

[35] L. Despax, J. Fitremann, M. Destarac, and S. Harrisson. Low concentration thermoresponsive hydrogels from readily accessible triblock copolymers. *Polymer Chemistry*, 7(20):3375–3377, 2016.

[36] S. Kirkland-York, K. Gallow, J. Ray, Y. L. Loo, and C. McCormick. Temperature-induced ordering and gelation of star micelles based on aba triblocks synthesized via aqueous raft polymerization. *Soft Matter*, 5(11):2179–2182, 2009.

[37] S. E. Kirkland, R. M. Hensarling, S. D. McConaughy, Y. Guo, W. L. Jarrett, and C. L. McCormick. Thermoreversible hydrogels from raft-synthesized bab triblock copolymers: Steps toward biomimetic matrices for tissue regeneration. *Biomacromolecules*, 9(2):481–486, 2008.

[38] A. D. Filippov, I. A. van Hees, R. Fokkink, I. K. Voets, and M. Kamperman. Rapid and quantitative de-tert-butylation for poly(acrylic acid) block copolymers and influence on relaxation of thermoassociated transient networks. *Macromolecules*, 51(20):8316–8323, 2018.

[39] T. Vermonden, N. A. M. Besseling, M. J. van Steenbergen, and W. E. Hennink. Rheological studies of thermosensitive triblock copolymer hydrogels. *Langmuir*, 22(24):10180–10184, 2006.

GENERAL DISCUSSION

7

Introduction

In this thesis, we describe the development of temperature responsive polyelectrolytes for mimicking the adhesive proteins of sandcastle worms. These proteins contain large amounts of oppositely charged and hydrophobic amino acids. Moreover, it is believed that complex coacervation, a liquid-liquid phase separation induced by mixing oppositely charged polymers, is a key element in the delivery of the natural adhesives.[1] For this reason, we mimic the adhesive proteins of sandcastle worms by mixing oppositely charged polymers that are functionalized with temperature responsive blocks. At elevated temperatures, the temperature-responsive blocks are insoluble in aqueous solution and therefore they mimic the hydrophobic amino acids. In this discussion, we reflect on the selected polymer chemistry and morphology, and the applicability of temperature responsive polyelectrolytes for underwater adhesives and possible other applications.

Polymers

In this research, temperature responsive polyelectrolytes have been synthesized. Based on previous research, the polycation poly(N,N-dimethylaminoethyl methacrylate) (PDMAEMA) and polyanion poly(acrylic acid) (PAA) have been chosen to be co-polymerized with poly(N-isopropylacrylamide) (PNIPAM).[2] PNIPAM is soluble in water at room temperature, but the polymers collapse upon exceeding the lower critical solution temperature (LCST), resulting in phase separation.[3] Above the LCST, PNIPAM mimics the hydrophobic amino acids of the natural proteins. In this section, we discuss the choice for the synthetic polymers, their specific chemistries and morphology.

In this thesis we aim for biomedical adhesives for wet conditions from synthetic polymers. Biomedical materials should be non-toxic and preferably biocompatible.

For this reason, it might be straightforward to use bio-polymers such as proteins and polysaccharides. However, isolating adhesive proteins from organisms such as mussels and sandcastle worms is costly due to low yields.[1] Alternatively, yeasts or bacteria, such as *E. Coli.*, are used to produce recombinant proteins. Unfortunately, these organisms are not able to apply post translational modifications that occur in the natural organisms, leading to crucial differences between the proteins. For example, mussels convert the amino acid tyrosine into the adhesion promotor L-3,4-dihydroxyphenylalanine (DOPA), while yeasts and bacteria cannot do this. As a result, treatment with an enzyme is required to obtain DOPA in proteins produced by bacteria.[1] An easier approach for mimicking natural underwater adhesives is to reduce the complexity and to use synthetic polymers. The polymers selected for this research are reported to have no toxicity and/or to be biocompatible.[4, 5, 6] Nevertheless, extensive studies for toxicity and biocompatibility are required before biomedical application. Moreover, for future research, one might investigate biodegradable polymers such as cationic poly(L-lysine), and anionic poly(glutamic acid) or hyaluronic acid.[7, 8, 9, 10, 11]

Polyelectrolyte selection

In complex coacervation, the chemistry of the polyelectrolytes determines the interaction strength between the polymers, and therefore the critical salt concentration, $c_{s,cr}$, above which complex coacervation no longer occurs. Spruijt et al. have shown that increasing hydrophobicity of the polymers increases the $c_{s,cr}$, because the ions are more depleted from the coacervate.[2, 12] Therefore, higher bulk concentrations are needed to disrupt the polyelectrolyte complex. In Chapter 6, it was shown that changing $c_{s,cr}$ influenced the morphology and properties of the temperature responsive polyelectrolyte complex (TERPOC) considerably. Namely, a higher $c_{s,cr}$ leads to higher moduli, and increased peak stresses upon shear deformation. Besides, a higher $c_{s,cr}$ leads to a slightly lower water content in complex coacervates. Preliminarily, Dompé et al. have shown that lower water contents lead to stronger adhesion, as long as the adhesive is deformable during application.[13] For these reasons, using a polyelectrolyte pair with a high $c_{s,cr}$, such as PAA and polyallylamine (PAH), may lead to a stronger adhesive.[2, 14]

PDMAEMA and PAA are weak polyelectrolytes, meaning that the degree of ionization of the polymers is pH dependent. For PDMAEMA and PAA, an optimum is found at neutral pH where both polyelectrolytes have a large degree of ionization, and efficient complexation is obtained.[2] Moreover, in biomedical applications, the pH of the environment is more or less constant and approximately neutral. Therefore no disadvantages are expected for biomedical applications once the mixing ratio for charge neutrality is determined. Excess charge should be avoided as it causes a net charge of the complex coacervate, micelle formation, and excretion of surplus polymer into the dilute phase, which can be disadvantageous.[2, 15] For applications at non-neutral or unstable pH, the use of weak polyelectrolytes may cause difficulties. When the pH is either acidic or basic, one of the two polyelectrolytes will have a low degree of ionization, while the oppositely charged polymer will have a high degree of ionization.

Accordingly, the ratio between the polycation and polyanion has to be adjusted to allow charge neutralization and assure complexation of all polymers. Moreover, different behaviour of the complex coacervate can be expected at non-neutral pH values, as uncharged monomers may form hydrophobic domains, resulting in a more solid like behaviour of the complex coacervate.[16] In addition, to the best of our knowledge, the stability of complex coacervates from weak polyelectrolytes upon pH fluctuations is not known and needs further investigation. Alternatively, to prevent pH dependent ionization of the polyelectrolytes, strong polyelectrolytes can be used, as those have a pH independent degree of ionization.[2] However, due to solubility issues, the synthesis of strong polyelectrolytes may be more challenging.

PNIPAM for hydrophobic interactions

Chapter 2 has shown that the proteins of sandcastle worms contain considerable amounts of hydrophobic amino acids, many of those are located next to DOPA to prevent oxidation.[1] However, hydrophobicity in the material may also contribute to underwater adhesion in several other ways. First, hydrophobic groups aid complex coacervation of the polyelectrolytes by decreasing their solubility in aqueous solution.[1, 17, 18] Secondly, water has to be repelled from the surface to enable proper binding between the surface and the adhesive, and therefore increased hydrophobicity may facilitate contact formation.[1] Thirdly, the presence of hydrophobic domains within the polyelectrolyte leads to more solid like behaviour, through long relaxation times in aqueous solution.[16] Finally, more hydrophobic materials will have a lower water content which can lead to an improved adhesion, as preliminarily found by Dompé et al.[13] However, the ratio between hydrophobic and hydrophilic compounds in the adhesive should be balanced carefully, as the resulting adhesive should be sufficiently fluid to obtain contact with the submerged surface.

Using hydrophobic groups complicates the equilibration of polyelectrolyte complexes in aqueous solution, and thus the reproducible analysis of the resulting adhesive. Therefore, the temperature responsive PNIPAM has been chosen to enhance the water-insolubility of the polyelectrolyte complexes. Below the LCST, PNIPAM is soluble in water and the polyelectrolytes can complex and equilibrate with little constraint leading to reproducible properties. Also, the polyelectrolyte complex is fluid and has good wetting properties, which favours adhesion, see Chapter 5.[1, 19] As expected, the addition of PNIPAM causes solidification upon temperature increase. However, nor in the grafted polyelectrolyte complexes, nor in the block copolymer complexes, a decrease in water content is observed.[19] A decrease in water content may be desired to obtain a better adhesion, as described above.[13] To obtain a lower water content, one could choose to insert hydrophobic monomers into the polymers. When carefully balanced, this should maintain the LCST behaviour of the PNIPAM blocks, while decreasing the water content. In addition, when the hydrophobic monomer is an aromatic moiety, one could take advantage of additional chemical interactions, such as cation-π interactions, as will be discussed below.[1] Alternatively, to reduce the amount of water in the adhesive, one might choose to extrude the

TERPOC, or to replace the PNIPAM for a hydrophobic polymer and use solvent exchange to solidify the complex, as done by Zhao et al.[20] Moreover, TERPOCs also solidify upon reducing the salt concentration after application. A lower salt concentration leads to longer relaxation times for the electrostatic interactions and therewith solidification of the TERPOC. A dual setting mechanism by temperature and salt reduction may also strengthen the adhesion.

Polymer morphology

So far, linear block copolymers and grafted copolymers have been used to make TERPOCs, but different polymer morphologies may be useful to explore also. As an example, star like polymers may be able to introduce more cross-links within the material. A higher degree of cross-linking will lead to higher storage moduli and thus a tougher, more cohesive, adhesive. In addition, one could choose to synthesize triblock copolymers with charged outer blocks and a PNIPAM inner block. Polymers with charged outer blocks were shown to form networks, which will increase the viscosity of the polymer solution and may even induce phase separation below LCST.[15] However, this morphology may lead to lower moduli above the LCST. Zhao et al. compared ABA block copolymers of PNIPAM and poly(2-hydroxyethyl methacrylate), with PNIPAM either on the inside or outside of the polymer. For PNIPAM outer blocks, slightly higher moduli were found than for polymers with a PNIPAM inner block.[21]

To enable reproducible and clear characterization of the resulting complexes, we aimed for polymers with narrow polydispersities, which is a costly synthesis.[2] For commercialization, the polymers should be produced at low cost and more polydisperse samples may be cheaper to produce. Furthermore, Heddleson et al. have shown that a broad molecular weight distribution favours tack and adhesion in pressure sensitive adhesives.[22] Therefore, higher polydispersities may result in stronger adhesion of TERPOCs as well.

Material properties

In the following sections, we elaborate on the use of TERPOCs for their application as (biomedical) adhesive, and for possible other purposes. Some suggestions are given to further improve the suitability of TERPOCs for these applications.

Applicability as adhesive

In the general introduction, it was described that biomedical adhesives should adhere well in wet conditions and be harmless to patients.[23, 24, 25, 26, 27, 28] Moreover, weak cohesion is observed for many currently available biomedical adhesives.[23] In

this thesis, we have shown that submerged TERPOCs adhere reasonably well and that increasing the PNIPAM content leads to stronger cohesion. Furthermore, TERPOCs are injectable and solidify quickly and safely. Therefore, TERPOCs are promising compounds to produce underwater adhesives. However, for biomedical applications, further investigations are required to assess the biocompatibility.

For biomedical applications, easy handling is required and determined by the viscosity of the material during application and by the solidification process. Low viscosities may result in adhesive flowing from the surface during application, while high viscosities can lead to reduced contact formation, or in the case of injections, blocking of the syringe.[29] It was shown that TERPOCs are fluid like at low temperatures and that varying salt and polymer concentrations, as well as salt type, lead to different gelation temperatures, T_{gel}, and viscosities at room temperature. Furthermore, the abrupt transition from fluid to solid allows quick curing and injectability of the samples at temperatures just below T_{gel}. As samples with low T_{gel} are slightly more viscous at room temperature and quick setting is needed, it is advised to select a T_{gel} slightly above room temperature.

Temperature induced solidification is easy and safe, as it does not require chemical reactions or the use of UV light. However, to secure the solid properties, the temperature has to remain above T_{gel}, as the temperature response of the TERPOC is reversible. All investigated TERPOCs are gelled at 37 °C and therefore solid joints are secured in biomedical applications. In other applications, the applicability of TERPOCs is limited as the environmental temperature may drop. Nonetheless, reversible bonding can also be a useful tool, for example in recyclable products.

A comparison was drawn between the adhesive strength of the linear PNIPAM-rich TERPOCs described in this thesis, and the grafted polyelectrolyte-rich TERPOCs of Dompé et al.[19] From the probe tack experiments, Chapter 5, it was shown that PNIPAM-rich TERPOCs show both adhesive and cohesive failure when bound to glass, while the polyelectrolyte-rich TERPOCs show cohesive failure only.[19] This implies that the addition of hydrophobic interactions has improved the cohesion. Accordingly, it is interesting to investigate TERPOCs with different PNIPAM and polyelectrolyte ratios also.

In addition to electrostatic and hydrophobic interactions, also covalent bonds, metal coordination, π-π and cation-π interactions can be found in the natural adhesive proteins, Chapter 2.[1] These interactions may be used to further improve the adhesive performance of TERPOCs, for example by the addition of aromatic moieties in the polymer. Especially catechols, such as DOPA, were shown to enhance underwater adhesion by a variety of chemical interactions.[30] In addition, catechols can be used for covalent curing, which was shown to further improve the adhesive performance in other adhesives. Also, covalent curing will ensure the solidification of TERPOCs below the gelation temperature which can be required for non-medical applications.[1]

Different applications of temperature responsive polyelectrolytes

Temperature responsive polyelectrolytes may not only be suitable as adhesive, but may also be applied as drug carrier, wound dressing, ionic conductor, or membrane. At first, the block copolymers can form complex coacervate core micelles at room temperature, Chapter 4. This type of micelles was shown to carry and release drugs.[7, 31, 32, 33, 34] Moreover, as gels are obtained at elevated temperature, TERPOCs may be useful as wound dressing or tissue replacement.[35, 36] Wound dressings should adhere onto the damaged tissue, and may carry and release drugs that enhance wound healing.[37, 38] Incorporating drugs into TERPOCs is possible as complex coacervates are known to be good drug carriers with a high loading capacity.[7, 39] Furthermore, adhesive ionic gels are used to prepare ionic conductors, for example for wearable devices. However, improvements on the extendibility and transparency of TERPOCs would be needed for such applications.[40, 41] Finally, membranes can be prepared from polyelectrolytes and possibly also from TERPOCs. Membranes are important for the purification of drinking water which becomes more scarce.[42, 43] The inclusion of a thermo-responsive moiety may be useful for temperature dependent size selectivity or easy rinsing.[44] Overall, temperature responsive polyelectrolytes can be useful compounds for various applications.

Conclusion

In this discussion, we elaborated on the parameters that can be used to adjust the properties of TERPOCs and suggestions for future research were given. To summarize, the TERPOCs can be improved further by decreasing the water content, while maintaining fluidity upon application. This can be achieved by for example extrusion or by introducing more hydrophobic chemistries. Moreover, introducing monomers that provide additional chemical interactions, such as catechols, may improve the adhesive properties. Finally, the characteristics of TERPOCs can be tuned by the polymer chemistry and composition, as well as the polymer and salt concentrations. Over all, we believe that TERPOCs are a good foundation for the development of underwater adhesives.

Bibliography

[1] A. H. Hofman, I. A. van Hees, J. Yang, and M. Kamperman. Bioinspired underwater adhesives by using the supramolecular toolbox. *Advanced Materials*, 30(19), 2018.

[2] E. Spruijt. *Strength, structure and stability of polyelectrolyte complex coacervates*. Wageningen University, Wageningen, 2012.

[3] H. G. Schild. Poly (n-isopropylacrylamide) - experiment, theory and application. *Progress in Polymer Science*, 17(2):163–249, 1992.

[4] G. P. Andrews, T. P. Laverty, and D. S. Jones. Mucoadhesive polymeric platforms for controlled drug delivery. *European Journal of Pharmaceutics and Biopharmaceutics*, 71(3):505–518, 2009.

[5] P. C. Naha, K. Bhattacharya, T. Tenuta, K. A. Dawson, I. Lynch, A. Gracia, F. M. Lyng, and H. J. Byrne. Intracellular localisation, geno- and cytotoxic response of polyn-isopropylacrylamide (pnipam) nanoparticles to human keratinocyte (hacat) and colon cells (sw 480). *Toxicology Letters*, 198(2):134–143, 2010.

[6] J. Robbens, C. Vanparys, I. Nobels, R. Blust, K. Van Hoecke, C. Janssen, K. De Schamphelaere, K. Roland, G. Blanchard, F. Silvestre, V. Gillardin, P. Kestemont, R. Anthonissen, O. Toussaint, S. Vankoningsloo, C. Saout, E. Alfaro-Moreno, P. Hoet, L. Gonzalez, P. Dubruel, and P. Troisfontaines. Eco-, geno- and human toxicology of bio-active nanoparticles for biomedical applications. *Toxicology*, 269(2-3):170–181, 2010.

[7] H. Cabral, K. Miyata, K. Osada, and K. Kataoka. Block copolymer micelles in nanomedicine applications. *Chemical Reviews*, 118(14):6844–6892, 2018.

[8] C. J. Huang and F. C. Chang. Polypeptide diblock copolymers: Syntheses and properties of poly(n-isopropylacrylamide)-b-polylysine. *Macromolecules*, 41(19):7041–7052, 2008.

[9] J. G. Li, T. Wang, D. L. Wu, X. Q. Zhang, J. T. Yan, S. Du, Y. F. Guo, J. T. Wang, and A. Zhang. Stimuli-responsive zwitterionic block copolypeptides: Poly(n-isopropylacrylamide)-block-poly(lysine-co-glutamic acid). *Biomacromolecules*, 9(10):2670–2676, 2008.

[10] L. S. Nair and C. T. Laurencin. Biodegradable polymers as biomaterials. *Progress in Polymer Science*, 32(8-9):762–798, 2007.

[11] M. A. Ward and T. K. Georgiou. Thermoresponsive polymers for biomedical applications. *Polymers*, 3(3):1215–1242, 2011.

[12] J. C. Fu, H. M. Fares, and J. B. Schlenoff. Ion-pairing strength in polyelectrolyte complexes. *Macromolecules*, 50(3):1066–1074, 2017.

[13] M. Dompé, M. Vahditi, F. van Ligten, F. J. Cedano-Serrano, D. Hourdet, C. Creton, M. Zanetti, P. Bracco, T. Kodger, and M. Kamperman. Let the water go: strategies to increase the polymer concentration in pnipam-functionalized complex coacervates. 2019.

[14] R. Chollakup, W. Smitthipong, C. D. Eisenbach, and M. Tirrell. Phase behavior and coacervation of aqueous poly(acrylic acid)-poly(allylamine) solutions. *Macromolecules*, 43(5):2518–2528, 2010.

[15] J. van der Gucht, E. Spruijt, M. Lemmers, and M. A. C. Stuart. Polyelectrolyte complexes: Bulk phases and colloidal systems. *Journal of Colloid and Interface Science*, 361(2):407–422, 2011.

[16] M. Tekaat, D. Butergerds, M. Schonhoff, A. Fery, and C. Cramer. Scaling properties of the shear modulus of polyelectrolyte complex coacervates: a time-ph superposition principle. *Physical Chemistry Chemical Physics*, 17(35):22552–22556, 2015.

[17] T. Akagi, K. Watanabe, H. Kim, and M. Akashi. Stabilization of polyion complex nanoparticles composed of poly(amino acid) using hydrophobic interactions. *Langmuir*, 26(4):2406–2413, 2010.

[18] E. Spruijt, A. H. Westphal, J. W. Borst, M. A. C. Stuart, and J. van der Gucht. Binodal compositions of polyeletrolyte complexes. *Macromolecules*, 43(15):6476–6484, 2010.

[19] M. Dompé, F. J. Cedano-Serrano, O. Heckert, N. van den Heuvel, J. Van der Gucht, Y. Tran, D. Hourdet, C. Creton, and M. Kamperman. Thermoresponsive complex coacervate-based underwater adhesive. *Advanced Materials*, page 1808179, 2019.

[20] Q. Zhao, D. W. Lee, B. K. Ahn, S. Seo, Y. Kaufman, J. N. Israelachvili, and J. H. Waite. Underwater contact adhesion and microarchitecture in polyelectrolyte complexes actuated by solvent exchange. *Nature Materials*, 15(4):407–+, 2016.

[21] X. L. Zhao, W. G. Liu, D. Y. Chen, X. Z. Lin, and W. W. Lu. Effect of block order of aba- and bab-type nipaam/hema triblock copolymers on thermoresponsive behavior of solutions. *Macromolecular Chemistry and Physics*, 208(16):1773–1781, 2007.

[22] S. S. Heddleson, D. D. Hamann, and D. R. Lineback. The dahlquist criterion - applicability of a rheological criterion to the loss of pressure-sensitive tack in flour-water dough. *Cereal Chemistry*, 70(6):744–748, 1993.

[23] D. W. R. Balkenende, S. M. Winkler, and P. B. Messersmith. Marine-inspired polymers in medical adhesion. *European Polymer Journal*, 116:134–143, 2019.

[24] L. P. Bre, Y. Zheng, A. P. Pego, and W. X. Wang. Taking tissue adhesives to the future: from traditional synthetic to new biomimetic approaches. *Biomaterials Science*, 1(3):239–253, 2013.

[25] A. Lauto, D. Mawad, and L. J. R. Foster. Adhesive biomaterials for tissue reconstruction. *Journal of Chemical Technology and Biotechnology*, 83(4):464–472, 2008.

[26] M. Mehdizadeh and J. Yang. Design strategies and applications of tissue bioadhesives. *Macromolecular Bioscience*, 13(3):271–288, 2013.

[27] R. Pinnaratip, M. S. A. Bhuiyan, K. Meyers, R. M. Rajachar, and B. P. Lee. Multifunctional biomedical adhesives. *Advanced Healthcare Materials*, 8(11), 2019.

[28] W. Z. Zhu, Y. J. Chuah, and D. A. Wang. Bioadhesives for internal medical applications: A review. *Acta Biomaterialia*, 74:1–16, 2018.

[29] Y. Lee, C. J. Xu, M. Sebastin, A. Lee, N. Holwell, C. V. Xu, D. M. Nieves, L. Y. Mu, R. S. Langer, C. P. Lin, and J. M. Karp. Bioinspired nanoparticulate medical glues for minimally invasive tissue repair. *Advanced Healthcare Materials*, 4(16):2587–2596, 2015.

[30] P. K. Forooshani and B. P. Lee. Recent approaches in designing bioadhesive materials inspired by mussel adhesive protein. *Journal of Polymer Science Part a-Polymer Chemistry*, 55(1):9–33, 2017.

[31] A. S. Hoffman. Hydrogels for biomedical applications. *Advanced Drug Delivery Reviews*, 64:18–23, 2012.

[32] M. Kamimura, J. O. Kim, A. V. Kabanov, T. K. Bronich, and Y. Nagasaki. Block ionomer complexes of peg-block-poly(4-vinylbenzylphosphonate) and cationic surfactants as highly stable, ph responsive drug delivery system. *Journal of Controlled Release*, 160(3):486–494, 2012.

[33] N. Rapoport. Physical stimuli-responsive polymeric micelles for anti-cancer drug delivery. *Progress in Polymer Science*, 32(8-9):962–990, 2007.

[34] I. K. Voets, P. M. Moll, A. Aqil, C. Jerome, C. Detrembleur, P. de Waard, A. de Keizer, and M. A. C. Stuart. Temperature responsive complex coacervate core micelles with a peo and pnipaam corona. *Journal of Physical Chemistry B*, 112(35):10833–10840, 2008.

[35] H. Hamedi, S. Moradi, S. M. Hudson, and A. E. Tonelli. Chitosan based hydrogels and their applications for drug delivery in wound dressings: A review. *Carbohydrate Polymers*, 199:445–460, 2018.

[36] H. J. Kwon, K. Yasuda, J. P. Gong, and Y. Ohmiya. Polyelectrolyte hydrogels for replacement and regeneration of biological tissues. *Macromolecular Research*, 22(3):227–235, 2014.

[37] K. M. Jin and Y. H. Kim. Injectable, thermo-reversible and complex coacervate combination gels for protein drug delivery. *Journal of Controlled Release*, 127(3):249–256, 2008.

[38] X. Meng, F. Tian, J. Yang, C. N. He, N. Xing, and F. Li. Chitosan and alginate polyelectrolyte complex membranes and their properties for wound dressing application. *Journal of Materials Science-Materials in Medicine*, 21(5):1751–1759, 2010.

[39] A. V. Kabanov and S. V. Vinogradov. Nanogels as pharmaceutical carriers: Finite networks of infinite capabilities. *Angewandte Chemie-International Edition*, 48(30):5418–5429, 2009.

[40] C. Keplinger, J. Y. Sun, C. C. Foo, P. Rothemund, G. M. Whitesides, and Z. G. Suo. Stretchable, transparent, ionic conductors. *Science*, 341(6149):984–987, 2013.

[41] J. Y. Sun, C. Keplinger, G. M. Whitesides, and Z. G. Suo. Ionic skin. *Advanced Materials*, 26(45):7608–7614, 2014.

[42] S. Ilyas, J. de Grooth, K. Nijmeijer, and W. M. de Vos. Multifunctional polyelectrolyte multilayers as nanofiltration membranes and as sacrificial layers for easy membrane cleaning. *Journal of Colloid and Interface Science*, 446:386–393, 2015.

[43] K. D. Kelly, H. M. Fares, S. Abou Shaheen, and J. B. Schlenoff. Intrinsic properties of polyelectrolyte multilayer membranes: Erasing the memory of the interface. *Langmuir*, 34(13):3874–3883, 2018.

[44] D. Wandera, S. R. Wickramasinghe, and S. M. Husson. Stimuli-responsive membranes. *Journal of Membrane Science*, 357(1-2):6–35, 2010.

Summary

For wound closure, adhesives provide many advantages over the use of sutures. However, adhesives are not yet common practice in internal medicine, due to limited adhesive properties in wet conditions, **Chapter 1**. In this thesis, we developed bio-inspired temperature responsive polyelectrolytes that can be applied as underwater adhesive, and may serve as biomedical adhesive as well.

A thorough understanding of natural underwater adhesives is needed for biomimicry and, therefore, we reviewed the adhesion mechanisms by sandcastle worms and mussels, **Chapter 2**. Sandcastle worms are marine organisms that build protective shells from minerals found in their surroundings, which are stuck together by adhesive proteins. Before secretion, these proteins are stored in granules in which anionic and cationic macromolecules are combined. Upon combining oppositely charged macromolecules, complex coacervation occurs, which explains the fluidic, yet concentrated, character of the packaged proteins. Mussels adhere through byssal threads and the two proteins closest to the surface are rich in the amino acid *L*-3,4-dihydroxyphenylalanine (DOPA). Therefore, DOPA is believed to be an adhesion promotor through a versatility of chemical interactions. Moreover, oxidation of DOPA can lead to covalent bonding, which can be used to solidify adhesives. Accordingly, DOPA is often used in the development of underwater adhesives.

In literature, several examples can be found of adhesives based on electrostatic interactions, which are composed of either recombinant proteins or synthetic polymers. From those articles, we extracted common features important for optimizing adhesive properties, **Chapter 2**. First, complexation between oppositely charged molecules improves adhesion, because significantly weaker adhesion is obtained when only one of the charged molecules is used. Moreover, multiple charged groups per molecule seem to result in materials with more powerful adhesive properties, than molecules that carry just one unit of charge. Furthermore, the adhesive strength of charged materials is improved upon the addition of catechol groups, such as DOPA, and even further enhanced by oxidation of DOPA after application to the surface. Finally, the inclusion of metal ions for metal coordination, or a second covalent network were also shown to increase the adhesive strength of complex coacervate based materials.

The adhesive proteins of sandcastle worms contain large amounts of oppositely

charged and hydrophobic amino acids, and only limited amounts of DOPA. Therefore, we investigated adhesives based on electrostatic and hydrophobic interactions. The electrostatic interactions originate from oppositely charged polyelectrolytes (polyions) that form fluidic complex coacervates which enable easy application and a large adhesive interface. Solidification of the adhesive is achieved by introducing a thermo-responsive polymer with a lower critical solution temperature (LCST). In aqueous solution, this polymer is soluble at low temperatures, but becomes insoluble upon exceeding the LCST, because hydrophobic interactions become more dominant. As a result, temperature responsive polyelectrolyte complexes gel upon temperature increase.

The temperature responsive polyelectrolytes were prepared by reversible addition fragmentation chain-transfer (RAFT) polymerization, **Chapter 3**. Poly(*N*-isopropylacrylamide)-*b*-poly(acrylic acid)-*b*-poly(*N*-isopropylacrylamide) (PNIPAM-*b*-PAA-*b*-PNIPAM) was prepared by deprotection of PNIPAM-*b*-poly(*tert*-butyl acrylate)-*b*-PNIPAM, through a novel deprotection method to obtain complete removal of the *tert*-butyl groups, yielding anionic AA only. Two polymers with either 20 or 80 mole% NIPAM and a M_w/M_n of ≈1.6 were prepared successfully. Moreover, we investigated the synthesis of the cationic PNIPAM-*b*-poly(dimethylaminoethyl methacrylate)-*b*-PNIPAM (PNIPAM-*b*-PDMAEMA-*b*-PNIPAM). The chain transfer agent and cationic PDMAEMA precursor were successfully synthesized and purified. However, it remained unclear whether extension with temperature responsive NIPAM succeeded. As a result, further investigations are required and we proceeded with commercially available polyactions.

Micelles are formed by mixing PNIPAM-*b*-PAA-*b*-PNIPAM and PNIPAM-*b*-PDMAEMA, with low PNIPAM contents, in aqueous solutions with various NaCl concentrations, **Chapter 4**. At low salt, the anionic PAA and cationic PDMAEMA form a complex and become insoluble, while PNIPAM has a temperature dependent solubility. Consequently, complex coacervate core micelles (C3M) with a PNIPAM corona were formed at low temperatures, while the polymers aggregate above the LCST. At high NaCl concentrations, however, the polyelectrolytes are soluble at room temperature because complexation is prevented by salt. Moreover, PNIPAM is salted out and therefore insoluble at any investigated temperature. Accordingly, a PNIPAM core micelle with a polyelectrolyte corona is formed at low temperatures. Upon heating, complex coacervation reoccurs and the polymers aggregate.

Temperature responsive polyelectrolyte complexes (TERPOC) are prepared in **Chapter 5**, by mixing PNIPAM-*b*-PAA-*b*-PNIPAM and PDMAEMA at various polymer and NaCl concentrations. At low temperatures, concentrated solutions with C3Ms were obtained, whereas heating caused gelation. The resulting TERPOCs are strong, turbid, but somewhat brittle gels because of the high PNIPAM content. Upon gelation, the sample volume is preserved, which is likely caused by the polyelectrolytes, e.g. by forming water pockets. Moreover, charge neutralization by PDMAEMA is required to retrieve strong gels. Furthermore, the strength of the TERPOC and the gelation temperature, T_{gel}, can be adjusted by altering the salt or polymer concentration. Consequently, the toughest TERPOC was obtained at high salt and polymer

concentrations. However, a maximum work of adhesion, W_{adh}, was achieved for a submerged TERPOC with a lower salt concentration because of a higher T_{gel}. The W_{adh} was comparable to many other underwater adhesives, and therefore TERPOCs are a promising element for underwater adhesives.

It is expected that guanidinium thiocyanate, GndSCN, improves the polymer solubility compared to NaCl, as GndSCN is more weakly hydrated. Therefore, we compared TERPOCs with GndSCN and NaCl, in **Chapter 6**. Indeed, a higher T_{gel} and lower $c_{s,cr}$ were observed for GndSCN containing samples which resulted in clear ordered phase symmetries. The TERPOCs adapted a lamellar morphology below $c_{s,cr}$, while cylinders seemed present above $c_{s,cr}$. Moreover, considerably lower moduli and peak strains were found, which may be caused by the weaker electrostatic and hydrophobic interactions. Accordingly, varying the salt type is an easy tool to adjust the properties of TERPOCs which is important for adhesive development.

It was shown that materials with solely electrostatic and hydrophobic interactions can be used as underwater adhesive. To further improve the adhesive properties, it is important to lower the water content, while maintaining the deformability upon application, **Chapter 7**. This can be achieved by extrusion, by introducing more hydrophobic electrolytes, or by adding hydrophobic moieties into the polymer. Moreover, it can be interesting to introduce more molecular interactions, such as π- π, cation-π, or metal coordination, which can be realized by incorporating aromatic or catechol groups, such as DOPA. In addition, solidification by lowering the salt concentration after application can be explored. Over all, we believe that TERPOCs are a good candidate for the development of underwater adhesives.

Samenvatting

Op het gebied van wonddichting bieden lijmen veel voordelen ten opzichte van hechtingen. Echter, tot op heden zijn lijmen nog niet veelgebruikt in de interne geneeskunde, als gevolg van de beperkte kleefkracht in vochtige omstandigheden, **Hoofdstuk 1**. In dit proefschrift, beschrijven we door de natuur geïnspireerde temperatuurresponsieve geladen polymeren die toegepast kunnen worden als onderwaterlijm, en zouden kunnen dienen als biomedische lijm.

Een gedegen begrip van natuurlijke onderwaterlijmen is nodig voor biomimetica en daarom bespreken we de plakstrategieën van borstelwormen en mossels, **Hoofdstuk 2**. Borstelwormen zijn zeedieren die een beschermende huls bouwen van mineralen die zij vinden in hun omgeving. De mineralen worden aan elkaar gelijmd met behulp van plakkerige eiwitten, die voor gebruik worden opgeslagen in kleine pakketjes. In deze pakketjes worden negatief en positief geladen macromoleculen samengevoegd, wat leidt tot complexvorming en geconcentreerde maar vloeibare eiwitoplossingen. Mossels, daarentegen, gebruiken byssusdraden om zichzelf vast te plakken aan oppervlakken. De byssusdraden zijn opgebouwd uit grofweg vijf eiwitten die elk een bepaalde positie in de draad hebben. Aan het oppervlak bevinden zich twee eiwitten met een hoog gehalte van het aminozuur L-3,4-dihydroxyphenylalanine (DOPA). Er bestaat een sterk vermoeden dat DOPA een belangrijke rol speelt bij het bereiken van een grote plakkracht, omdat DOPA veel verschillende moleculaire interacties aan kan gaan. Bovendien kan DOPA geoxideerd worden, wat leidt tot sterke covalente bindingen en het uitharden van lijm. Als gevolg van deze veelzijdigheid wordt DOPA vaak gebruikt in de ontwikkeling van onderwaterlijmen.

In de literatuur worden verschillende lijmen gerapporteerd die gebaseerd zijn op elektrostatische interacties en bestaan uit recombinante eiwitten of synthetische polymeren. Met behulp van deze artikelen hebben we een aantal algemene kenmerken vastgesteld die belangrijk zijn bij het vergroten van de kleefkracht in water, **Hoofdstuk 2**. Allereerst wordt de adhesie verbeterd door het gebruik van complexen met tegenovergesteld geladen moleculen en verdere verbetering wordt bereikt als het molecuul meerdere ladingen bevat, in plaats van slechts één lading. Daarnaast kan de kleefkracht verbeterd worden door het gebruik van catecholen, zoals DOPA. De hoogste kleefkracht werd gerapporteerd als DOPA geoxideerd werd nadat de lijm aangebracht

was op het oppervlak. Ten slotte kan de kleefkracht van lijmen met elektrostatische interacties verbeterd worden door het gebruik van metaalionen voor metaal coördinatieverbindingen, of door het gebruik van twee polymeernetwerken.

De plakkerige eiwitten van borstelwormen bevatten grote hoeveelheden tegenovergesteld geladen en hydrofobe aminozuren, maar slechts een beperkte hoeveelheid DOPA. Om deze reden ontwikkelen we een lijm die gebaseerd is op elektrostatische en hydrofobe (waterafstotende) interacties. De elektrostatische interacties worden gevormd door tegenovergesteld geladen polyelektrolyten (geladen polymeren) die een vloeibaar complex coacervaat vormen. De vorming van dit complex zorgt voor een gemakkelijke aanbrenging van de lijm en een groot contactoppervlak. De lijm wordt uitgehard met behulp van een temperatuurresponsief polymeer wat aan het geladen polymeer is vastgemaakt. Het responsieve polymeer heeft een lagere kritische oplossingstemperatuur (LCST) wat betekent dat het polymeer oplosbaar is in water bij lage temperaturen, maar onoplosbaar wordt als de temperatuur toeneemt en de LCST overschreden wordt. Als gevolg van dit gedrag vormen temperatuurresponsieve polyelektrolyt complexen gels bij het verhogen van de temperatuur.

De temperatuur responsieve polyelektrolyten worden gesynthetiseerd met behulp van de polymerisatie methode RAFT (reversibele additie fragmentatie keten-overdracht) om nauwkeurig gedefinieerde polymeren te verkrijgen, **Hoofdstuk 3**. Het negatief geladen blok-copolymeer poly(N-isopropylacrylamide)-b-poly(acrylzuur)-b-poly(N-isopropylacrylamide) (PNIPAM-b-PAA-b-PNIPAM) wordt gemaakt door het ontschermen van PNIPAM-b-poly(*tert*-butylacrylaat)-b-PNIPAM met behulp van een nieuw uitgevonden ontschermingsmethode. Deze methode garandeert dat alle hydrofobe butylgroepen verwijderd worden en alleen hydrofiel acrylzuur overblijft, wat belangrijk is voor toepassingen in water. We synthetiseerden twee negatief geladen polymeren met 20 en 80 % van het temperatuurresponsieve PNIPAM. Daarnaast hebben we de synthese van het positief geladen blok-copolymeer PNIPAM-b-poly(dimethylaminoethyl methacrylaat)-b-PNIPAM (PNIPAM-b-PDMAEMA-b-PNIPAM) onderzocht. Het ketenoverdracht molecuul en het positief geladen homopolymeer PDMAEMA konden succesvol gesynthetiseerd en opgezuiverd worden. Echter, het bleef onduidelijk of de verlenging van PDMAEMA met het temperatuurresponsieve PNIPAM plaatsvond. Om deze reden is vervolg onderzoek noodzakelijk en is verder onderzoek uitgevoerd met commercieel verkrijgbaar positief geladen polymeren.

Het mengen van waterige keukenzoutoplossingen van PNIPAM-b-PAA-b-PNIPAM en PNIPAM-b-PDMAEMA met een lage PNIPAM hoeveelheid resulteert in de vorming van micellen, **Hoofdstuk 4**. Bij een lage zout concentratie vormen het negatief geladen PAA en positief geladen PDMAEMA een complex coacervaat wat onoplosbaar is, terwijl PNIPAM een temperatuur afhankelijke oplosbaarheid heeft. Zodoende worden bij lage temperaturen micellen gevormd met een complex coacervaat kern (C3M) en een PNIPAM schil. De polymeren aggregeren (worden onoplosbaar) als de temperatuur verhoogd wordt tot boven de LCST. Bij hoge zout concentraties, daarentegen, zijn de geladen polymeren oplosbaar bij kamertemperatuur omdat complexvorming voorkomen wordt door het zout. Bovendien zorgt

het zout ervoor dat de PNIPAM onoplosbaar is bij alle onderzochte temperaturen. Zodoende ontstaat bij kamertemperatuur een omgekeerde C3M micel met een PNIPAM kern en een polyelektrolyt schil. Bij het verhogen van de temperatuur vormen de polyelektrolyten alsnog complexen en de polymeren aggregeren.

Temperatuurresponsieve polyelektrolyt complexen (TERPOC) worden gemaakt door PNIPAM-*b*-PAA-*b*-PNIPAM en PDMAEMA te mengen bij verschillende polymeer en keukenzoutconcentraties, **Hoofdstuk 5**. Bij lage temperaturen worden geconcentreerde oplossingen met C3M micellen gevonden en verhitting leidt tot gelvorming. Deze gels, die we TERPOC noemen, zijn sterk, troebel en ietwat bros door de hoge PNIPAM hoeveelheid. Bij de gelvorming behoudt de polymeeroplossing zijn volume, wat waarschijnlijk veroorzaakt wordt door de aanwezigheid van de polyelektrolyten. Bovendien is ladingsneutralisatie door PDMAEMA noodzakelijk om sterke gelen te vormen. De sterkte van de gelen en de gelvormingstemperatuur, T_{gel}, worden beïnvloed door de zout en polymeer concentratie. De sterkste TERPOC wordt gevonden bij een hoge zout en polymeer concentratie. Echter, de grootste kleefarbeid onderwater werd gevonden voor een monster met een lagere zoutconcentratie en T_{gel}. De kleefarbeid is vergelijkbaar met andere gerapporteerde onderwaterlijmen en daarom vormen TERPOCS een veelbelovende basis voor onderwaterlijmen.

Naast keukenzout hebben we ook het zout guanidinium thiocyanaat, GndSCN, gebruikt om TERPOCS te maken, omdat we verwachtten dat GndSCN de oplosbaarheid van de polymeren zou verhogen in vergelijking met keukenzout, **Hoofdstuk 6**. Als gevolg van de verbeterde oplosbaarheid vonden we een verhoogde T_{gel} en een verlaagde kritische zout concentratie, $c_{s,cr}$, waarboven polyelektrolyt complexvorming niet meer optreedt. Deze verandering leidde tot goed geordende en gescheiden fasen van PNIPAM en polyelektrolyt. Bij zoutconcentraties onder $c_{s,cr}$ vonden we lamellen, terwijl cilinders gevonden werden bij hogere zoutconcentraties. Bovendien werden de TERPOCS zwakker en brosser door zwakkere interacties tussen de polymeren. Zodoende is het veranderen van de zoutsoort een gemakkelijke manier om de eigenschappen van een TERPOC te veranderen, wat belangrijk is in de ontwikkeling van lijmen.

In dit proefschrift hebben we aangetoond dat materialen met louter elektrostatische en hydrofobe interacties gebruikt kunnen worden als onderwaterlijm. Om de kleefeigenschappen verder te verbeteren is het belangrijk om het watergehalte van de TERPOCS te verlagen, terwijl de vervorming van de lijm bij het aanbrengen onverminderd blijft, **Hoofdstuk 7**. Dit doel kan bereikt worden door extrusie, het gebruiken van hydrofobere elektrolyten, of door hydrofobe groepen in het polymeer te introduceren. Daarnaast kan het interessant zijn om ook andere moleculaire interacties te introduceren, zoals π-π, kation-π, of metaal coördinatieverbindingen, met behulp van catecholen zoals DOPA. Daarbij is het interessant om uitharding van de TERPOCS door het verlagen van de zoutconcentratie na het aanbrengen van de lijm te onderzoeken. In zijn geheel genomen zijn wij van mening dat TERPOCS een veelbelovende basis vormen voor het ontwikkelen van onderwaterlijmen.

LIST OF PUBLICATIONS

This thesis:

- <u>Ilse A. van Hees</u>, Anton H. Hofman, Marco Dompé, Jasper van der Gucht and Marleen Kamperman, **Temperature responsive polyelectrolyte complexes for bio-inspired underwater adhesion**, *in preparation*

- <u>Ilse A. van Hees</u>, Piet J.M. Swinkels, Remco G. Fokkink, Aldrik H. Velders, Ilja K. Voets, Jasper van der Gucht and Marleen Kamperman, **Self-assembly of oppositely charged polyelectrolyte block copolymers containing short thermoresponsive blocks**, *Polymer Chemistry*, **10**, 3127 (2019)
  DOI: 10.1039/c9py00250b

- Anton H. Hofman, <u>Ilse A. van Hees</u>, Juan Yang and Marleen Kamperman, **Bioinspired underwater adhesives by using the supramolecular toolbox**, *Advanced Materials*, **30**, 1704640 (2018)
  DOI: 10.1039/c9py00250b

Other work:

- Alexei D. Filippov, <u>Ilse A. van Hees</u>, Remco Fokkink, Ilja K. Voets and Marleen Kamperman, **Rapid and quantitative de-*tert*-butylation for poly(acrylic acid) block copolymers and influence on relaxation of thermoassociated transient networks**, *Macromolecules*, **51**, 8316 (2018)
  DOI: 10.1021/acs.macromol.8b01440

- Juan Yang, Małgorzata K. Włodarczyk-Biegun, Alexei Filippov, Sabine Akerboom, Marco Dompé, <u>Ilse A. van Hees</u>, Merve Mocan and Marleen Kamperman, **Functional polymeric materials inspired by geckos, mussels and spider silk**, *Macromolecular Chemistry and Physics*, **219**, 1800051 (2018)
  DOI: 10.1002/macp.201800051

- Małgorzata K. Włodarczyk-Biegun, Cornelis J. Slingerland, Marc W.T. Werten, <u>Ilse A. van Hees</u>, Frits A. de Wolf, Renko de Vries, Martien A. Cohen Stuart and Marleen Kamperman, **Heparin as a bundler in a self-assembled fibrous network of functionalized protein-based polymers**, *Biomacromolecules*, **17**

About the Author

Ilse Adriënne van Hees was born on the 20th of January 1991 in Schagen, the Netherlands, and attended the Murmellius Gymnasium in Alkmaar where she graduated in 2009. Afterwards, she started the study Molecular Life Sciences at Wageningen University and specialized in Physical Chemistry.

During the master, she worked on a thesis under the supervision of Małgorzata Włodarczyk-Biegun and Marleen Kamperman. Made out of artificial proteins, gels for bone scaffolding were characterized by atomic force microscopy and rheology. In the right conditions, the proteins self-assemble into fibres, resulting in the formation of a brittle hydrogel. It was investigated whether the addition of calcium nanoparticles could improve the strength of the gels by providing additional crosslinks to the protein fibres. After the thesis, Ilse went to the United Kingdom for an internship in an industrial R&D and investigated the stability of laundry liquids, by performing enzyme activity essays. In 2015, she received her Master diploma.

In May 2015, Ilse started as a PhD candidate in the group of Physical Chemistry and Soft Matter. Under supervision of Prof. dr. Marleen Kamperman and Prof. dr. Jasper van der Gucht, she investigated the properties of temperature responsive polyelectrolyte complexes. This thesis presents the outcomes of the research.

Acknowledgements

During my master thesis, Marleen received her NWO VIDI grant and started to look for students to work on the "Sticky when wet" project. She appreciated the cooperation during the master project and invited me to apply. However, she also stressed that I should look carefully at the project, to see if the topic really suited me. So, I looked through the proposal, searched for other vacancies and decided that this was the nicest topic; A project about the relation between molecular interactions and material properties was exactly what I was looking for, as well as a science group with a good social atmosphere. There was only one minor part that I was not experienced in, synthesis. However, we expected that the synthesis of the polymers was going to be quick and easy, so we were good to go.

Marleen, we were only slightly off with our estimation that the polymer synthesis would be finished in a year. However, we learned a lot and persisted in striving for temperature responsive polycations till time no longer allowed us. Thank you for your relaxed, positive and open attitude. You always saw the light at the end of the tunnel, made sure that we learned what we needed, and that we were doing fine. When I was struggling with the synthesis, you suggested to combine it with other activities such as the design competition for primary schools. These activities kept me going and were a welcome change to the synthesis experiments. I hope that many more students will be able to work with you and that you keep enjoying to bring science to the public.

Jasper, thanks for your quick feedback to manuscripts. When I send one with the message that the actual deadline for submission was within 24 hours you corrected the manuscript as soon as you could. Also, when we needed an appointment to discuss rheology or scattering data, you made sure that there was time for us. I also like to thank you for your presence in the adhesion meetings, even when we extensively discussed syntheses, you were there.

Marco, *Anton* and *Aljosha*, it was a pleasure to work with you on the underwater adhesives project. Working in a team makes it so much easier to discuss science in depth, to solve issues, and understand the system quickly. I greatly enjoyed the lunches, dinners, and conferences, as well as our visits to the ESRF in Grenoble where *Remco* joined also. Anton, without your help I could not have reached this quality of polymer synthesis, thank you for thinking along. Moreover many students contributed to our

research; *Mariska*, *Piet*, *Olaf*, *Sjoerd*, and many more, it was a pleasure to work with you.

While working in the lab, there are plenty of opportunities to talk and we discussed many things, from cars, to houses, to Dutch words. Firstly I worked in lab *1010* at the Dreijen and later in *7070* and *6063* in Helix. In each lab I had a great time, thanks guys! *Diane*, you have been a lab buddy almost all the way through my PhD. Thanks for the good conversations and lets drive a truck once more! Additionally, I like to thank my office mates *Merve*, *Inge*, *Lucille*, and *Anton* for a good time. Sorry if I distracted you too much and keep enjoying the good views from our office.

Leonie and *Mara*, you are the golden people of the secretariat. Thanks for all the tea- and lunchtimes, good conversations, listening ears, and awesome defense slots. *Bert*, thanks for the dark chocolates and the longest Sinterklaas poem I ever received.

Frans thanks for the extensive thinking and discussions about propositions, SAXS data, and micelle formation. I hope that you will keep taking the time to think along with students and that the micellization model will be used in the future.

Hanne, thanks for co-organizing crowded Sinterklaas games with pizza and thanks to *Sven* and *Dana* for co-organizing the company visits. *René*, *Peter*, *Wolf*, *Dirk*, and many others, thanks for the teaching experience and the nice anecdotes that originate from these days. *Joanne*, thanks for being there for tea and outdoor lunches in summer, as well as for the LaTeX help. Last but not least, thanks to everyone else that I worked with at PCC for a great atmosphere and enjoyable lunches and teatimes.

Studying for a doctorate is a challenging and wobbly journey where you learn to deal with many challenges. This journey cannot be completed without the support of the people around you, which does not only include colleagues. *Rianne*, *Joëlle*, *Joanne*, *Hanne*, *Marleen*, *Andrea* and *Nadine*, thanks for your listening ears. You were a support during the challenges that I faced, even when it was already getting late. *Birgit*, *Maria*, and *Esther* thanks for the nice weekends out and fun activities that were always a good distraction. *Karin*, *Jackie*, *Herma* and *Marcel*, your classes at the Bongerd were a necessary, fun and relaxing activity that kept me going during the years. Additionally, I could not do without my weekly choir rehearsal that made me sing the next day also. Thanks to the people of the *WSKOV* and *WKK*, and in special to *Lisette*, *Emma*, *Marthe*, *Wilma*, *Daniëlle*, *Wierc* and *Mijke*.

Naast mijn vrienden mag ik natuurlijk ook familie niet vergeten. Met velen van jullie heb ik de afgelopen jaren gesproken over het reilen en zeilen van mijn PhD. Dank jullie wel voor jullie luisterend oor en ik hoop dat jullie iets begrepen hebben van mijn uitleg over het onderzoek. *Inge*, jou wil ik in het bijzonder bedanken voor het mooie en professionele ontwerp van de kaft en uitnodiging.

Pap en *mam*, jullie hebben mij geleerd om hard te werken en niet op te geven. Mede dankzij die instelling heb ik dit project tot een einde kunnen brengen. Ik ben er dankbaar voor dat ik dit moment met jullie kan delen en hoop dat we nog vele leuke momenten samen mogen meemaken.

Lars, zonder jouw steun was het me niet gelukt. Ik kwam soms gefrustreerd of gestresst thuis en jij gaf me alle ruimte die ik nodig had. Ik kijk uit naar de toekomst en hoop dat we nog veel meer mooie momenten samen mogen delen.

Overview of completed training activities

Discipline specific activities:

Han sur Lesse Winterschool (HSL Winterschool)	Han sur Lesse (B)	2016
RPK-A (PTN)	Utrecht	2016
CHAINS 2016 (NWO)†	Veldhoven	2016
CHAINS 2017 (NWO)†	Veldhoven	2017
CHAINS 2018 (NWO)†	Veldhoven	2018
Physics @ FOM (NWO/FOM)	Veldhoven	2016
Dutch Polymer Days (PTN)†	Lunteren	2016
Dutch Polymer Days (PTN)†	Lunteren	2017
Dutch Polymer Days (PTN)‡	Lunteren	2018
Dutch Polymer Days (PTN)†	Lunteren	2019
Research School Adhesion (ESPCI)	Paris (F)	2017
Scattering course (TU/e)	Eindhoven	2016
GRC&GRS Bioinspired Materials†	Les Diablerets (S)	2018

General courses

Essentials in scientific writing (WGS)	Wageningen	2015
PhD competence assessment (WGS)	Wageningen	2015
Photoshop and Illustrator cursus (MolMed)	Rotterdam	2015
Data Management Planning (WGS)	Wageningen	2015
VLAG PhD week (VLAG)	Soest	2016
Orientation on Teaching for PhD students (WGS)	Wageningen	2016
Teaching and supervising thesis students (WGS)	Wageningen	2017
Scientific writing Wageningen (WGS)	Wageningen	2017
Course Career Perspectives (WGS)	Wageningen	2018

‡ oral presentation   † poster presentation

Optionals

Journal club (PCC)	Wageningen	2015-2018
PhD trip Wageningen (PCC)	United Kingdom	2015
Workmeetings (PCC)	Wageningen	2015-2019
Seminars (PCC)	Wageningen	2015-2019
Research proposal (VLAG)	Wageningen	2015